Theses and Dissertations

8-2012

# Investigations of Protein-Lipid Interactions in Model Membranes: Influence of Aromatic Anchoring Residues and Buried Polar Residues

Nick Gleason
*University of Arkansas, Fayetteville*

Follow this and additional works at: http://scholarworks.uark.edu/etd

Part of the Biochemistry Commons, and the Biophysics Commons

## Recommended Citation

INVESTIGATIONS OF PROTEIN-LIPID INTERACTIONS IN MODEL MEMBRANES:
INFLUENCE OF AROMATIC ANCHORING RESIDUES AND BURIED POLAR RESIDUES

INVESTIGATIONS OF PROTEIN-LIPID INTERACTIONS IN MODEL MEMBRANES:
INFLUENCE OF AROMATIC ANCHORING RESIDUES AND BURIED POLAR RESIDUES


A dissertation submitted in partial fulfillment
of the requirements for the degree of
Doctor of Philosophy in Chemistry


By


Nicholas James Gleason
University of Central Arkansas
Bachelor of Science in Chemistry, 2007


August 2012
University of Arkansas

**ABSTRACT**

To investigate in detail the interactions between transmembrane proteins and the lipid bilayers in which they are constituted, designed model peptides with selective isotopic labels were synthesized and analyzed by means of solid-state deuterium NMR spectroscopy. Starting from the well-characterized model peptide GWALP23, acetyl-GGALW(LA)$_6$LWLAGA-amide, several Trp to Tyr mutations were compared to evaluate their respective interfacial anchoring abilities. It was found that Tyr, substituted on either or both termini, can effectively anchor the transmembrane α-helix, which then adopts a similar transmembrane topology in a range of bilayer thicknesses. Nevertheless, a consistent ~10° shift in tilt direction (helix rotation) is observed when a Tyr is substituted for Trp and found to be terminal-dependent (i.e. in opposite direction on each end). The fluorescence emission spectra from the single remaining Trp residue in Y$^5$GWALP23 and Y$^{19}$GWALP23 indicate that W$^5$ is buried more deeply in the bilayer than is W$^{19}$.

Using Y$^5$GWALP23 as a host, the influence of Lys was examined at positions 12 and 14 in various lipid bilayer thicknesses. Y$^5$GWALP23-K14 incorporates well into both thin and thick bilayers. It influences the peptide's orientation by increasing the tilt magnitude (4-9°) and altering the tilt direction (60-95°). In contrast, the L12K mutant yields multiple low-intensity peaks in $^2$H NMR spectra, recorded in DOPC, indicative of multi-state behavior. Nevertheless, the peptide orients well and adopts a large tilt angle (30°) in the thinner bilayers of DLPC. Y$^5$GWALP23-K12 in DOPC is observed to titrate at high pH to a neutral form that is well aligned in an orientation that is very similar to that of the host peptide without lysine. Titration of Y$^5$GWALP23-K14 reveals a pK$_a$ of 6.2 in DOPC at 50 °C and different transmembrane orientations when the peptides charged lysine, neutral lysine or no lysine are compared.

When Glu is added adjacent to a lysine, significantly improved NMR spectra and a stable transmembrane orientation are observed for $Y^5$GWALP23-($K^{12}$, $E^{13}$). $Y^5$GWALP23-K14 experiences a small change in orientation with Glu-15 addition, but interestingly titrates much like the peptide with K14 alone. Placement of a Glu residue (E13) near R12 also improves spectra quality, especially at higher pH. It appears a stabilizing ion-pair may in some instances "rescue" the K12 or R12 peptide from its multi-state behavior in DOPC. The individual ionization states of paired ionizable residues have yet to be determined.

This dissertation is approved for recommendation
to the Graduate Council.


Dissertation Director:


_____

Dr. Roger E. Koeppe II


Dissertation Committee:


_____

Dr. Paul Adams


_____

Dr. Dan Davis


_____

Dr. Suresh Kumar Krishnaswamy Thallapuranam


_____

Dr. David Paul

**DISSERTATION DUPLICATION RELEASE**

I hereby authorize the University of Arkansas Libraries to duplicate this dissertation when needed for research and/or scholarship.

Agreed _____

*Nicholas J. Gleason*

Refused _____

*Nicholas J. Gleason*

**ACKNOWLEDGEMENTS**

**DEDICATION**

      I dedicate this dissertation to my wife and best friend Jamie Gleason who has been far beyond supportive and encouraging to me throughout the entirety of this work.  I also dedicate this work to our fantastic daughter Loralei Dove Gleason who was born during the time of this graduate work (April 21$^{st}$, 2011) and provided a great catalyst for me to finish (…in a timely manner).

**TABLE OF CONTENTS**

**LIST OF THE ORIGINAL PAPERS**

Gleason, N. J., Vostrikov, V. V., Greathouse, D. V., Grant, C. V., Opella, S. J., and Koeppe, R. E. 2nd. (2012) Tyrosine Replacing Tryptophan as an Anchor in GWALP Peptides. *Biochemistry 51*, 2044-2053.

**INTRODUCTION**

Due to the heterogeneous nature of a biological membrane, populated by a multitude of

protein and lipid variants, there are a number of complexities involved in examining membrane

proteins in detail. The lipid bilayer has shown its ability to alter protein shape and function in a

variety of fashions, for example glucose transport activity in red blood cells has been shown to

have a dependence on lipid composition (Carruthers et al. 1984). Furthermore, rhodopsin's

photochemical function as well as the enzymatic activity of cytochrome c oxidase are also

affected by such things as bilayer curvature, elasticity and thickness (Brown et al. 1994;

Montecucco et al. 1982). Concurrently, membrane proteins can have dramatic effects on the

bilayer itself (Killian et al. 1992; Yang et al. 1996; Killian et al. 1996; Hong et al. 2004; Moe et

al. 2005). The large number of simultaneously contributing factors necessitates less complex

model systems that can used systematically to evaluate the various interactions involved. To

more precisely observe lipid bilayer contributions, samples can be studied in membranes

composed of synthetic lipids of unique head group, chain length, and degree of unsaturation,

which then can be varied to examine their differing effects. Many membrane proteins consist of

multiple spans through the bilayer that invoke additional protein-protein interactions and forces

beyond purely protein-lipid interactions. To overcome these extra protein contributions, small α-

helical peptides that possess only a single-membrane-span can be used. WALP model peptides,

of the form acetyl-GWWA(LA)$_n$LWWA-amide, were some of the earliest model peptide systems

in use and have been studied extensively for evaluating peptide-lipid interactions and the general

rules that govern them (e.g. hydrophobic matching) (Killian et al. 1996; de Planque et al. 1999;

van der Wel et al. 2002). The α-helical WALP peptide consists of a hydrophobic core of a

repeating Leu-Ala sequence that is flanked by two tryptophan residues on each end that have a

preference for the water/lipid interfacial region of the bilayer.  Further development of this system yielded GWALP23, acetyl-GGALW(LA)$_6$LWLAGA-amide, which possesses the same hydrophobic thickness of WALP19, but with only a single Trp residue on each end (Vostrikov et al. 2008). The peptide demonstrates much greater sensitivity to the lipid bilayer and has been useful in elucidating the importance of "anchoring" residues and illustrates well the effects of hydrophobic matching (Vostrikov and Koeppe 2011a).  Throughout the entirety of this dissertation, the model peptide GWALP23 serves as the framework for which further peptide-lipid interactions have been studied.

Solid-state deuterium NMR spectra can be recorded effectively using samples of $^2$H-labeled peptides incorporated into lipid bilayers that are able to be specifically oriented with respect to an external magnetic field.  Oriented glass plate samples provide a common method for bilayer alignment that can be achieved by means of macroscopic insertion of a sealed, hydrated sample of parallel plates into the NMR probe.  More recently, magnetically-aligned bicelles (bilayered micelles) have become a common method for orienting bilayer membranes for solid-state NMR experiments (Tjandra and Bax 1997; De Angelis et al. 2004).  Oriented bicelles are composed of a minimum of two lipid lengths, including a longer phospholipid as well as a shorter phospholipid. While the longer phospholipid, in greater abundance, forms a bilayer, the shorter phospholipid caps off the circumference to form a discoid-like structure.  A common formula includes a DMPC:DHPC mixture in a 3.2:1 mol:mol ratio.  DHPC is analogues to DMPC, but with only short six-carbon fatty acid tails.  While bicelles offer the advantages of rather facile preparation, greater sample hydration and realistic membrane curvature, they are limited by the small selection of available lipid formulations with which to work.  The first chapter of my dissertation describes the creation and optimization of a three-component DLPC-

based bicelle system to further expand the range of workable bicelle systems available for solid-state NMR experiments. Mixed combinations of short lipids were tested via solid-state $^{31}$P NMR in combination with DLPC to explore a range of lipid lengths, molar ratios and temperature to optimize a formula for best alignment. GWALP23, having been previously characterized in DLPC using oriented glass plate samples, was incorporated into the test DLPC bicelles for comparison purposes.

WALP peptide systems have relied heavily on the excellent anchoring capabilities of the amphipathic aromatic tryptophan residue. While there is a known enrichment of tryptophan at the lipid interfacial regions of single-span transmembrane proteins (Landolt-Marticorena et al. 1993), it is also true for tyrosine, though to a smaller extent on the N-terminal of transmembrane helices. Starting with framework of the GWALP23 sequence, the second chapter of this dissertation describes the influence of a Trp to Tyr replacement near the N-terminal upon the helix anchoring in a range of lipid bilayer membranes. Furthermore, a transmembrane GWALP-like model peptide containing a single tryptophan is desirable for the novel ability to provide quantitative steady-state fluorescence measurements over native GWALP23, which possesses two such fluorophores. Assessment of the Y$^5$GWALP23's orientation was conducted by means of solid-state $^2$H NMR spectroscopy and additionally $^{15}$N/$^1$H high resolution separate local field NMR spectroscopy (SAMPI4, similar to PISEMA) with the aid of collaborators. It was striking to observe close agreement in overall peptide orientation between GWALP23 and Y$^5$GWALP23, with only minimal deviations, particularly a small change in helix tilt direction. In addition, a double-Tyr mutant, Y$^{4,5}$GWALP23, was evaluated and found by solid-state $^2$H NMR to exhibit dramatically increased dynamics averaging of the NMR resonances, compared to the single anchored Trp or Tyr peptides.

Side chain dihedral angles in an α-helix do not project perpendicularly from the peptide backbone or the helix axis. Instead the $C_\alpha$-$C_\beta$ bonds project toward the N-terminus (van der Wel et al. 2002). This feature leads to asymmetric positioning of the anchoring indole rings in GWALP23 and it has been shown that they adopt differing arrangements, in which the C-terminal Trp indole ring rotates to point its polar nitrogen moiety toward the aqueous phase (Vostrikov and Koeppe 2011a). Indeed, while it has also been observed that Trp is heavily populated at both interfaces of single-span α-helices, tyrosine is to some extent less populated at the C-terminus (Landolt-Marticorena et al. 1993). To address any terminal bias in the anchoring residues, comparisons of the $Y^5GW^{19}ALP23$ and $Y^{19}GW^5ALP23$ peptides are the subject of chapter 3 in this dissertation. Again by the use of solid-state $^2H$ and $^{15}N$ NMR methods, $Y^{19}GW^5ALP23$ and $Y^5GW^{19}ALP23$ are seen to adopt similar tilt angles in a range of lipid bilayers of different thicknesses. Interestingly, Y5 and Y19 each cause an ~ 10° change in the GWALP23 helix tilt direction, but in opposite directions. These differences appear to cancel out in $GY^{5,19}ALP23$, which is exclusively anchored by Tyr residues and shows interesting properties nearly identical to the native GWALP23. Additionally, the consistently lower $^2H$ signals, and a tighter PISA-wheel for $Y^{19}GW^5ALP23$, indicate that the Y19 peptides may be undergoing greater extents of dynamics as compared to the W19-anchored peptides.

While GWALP-like peptides have allowed for valuable insight into the properties of helix-anchoring residues, the peptide family was then used for the study of polar, charged residues within the non-polar bilayer. Ionizable residues found incorporated within the transmembrane segments of membrane proteins have gained recent interest, particularly in terms of quantifying the energetic cost of potentially burying them (Hessa et al. 2005; Dorairaj et al. 2007). While the hydrophobic core of a helix is obviously depleted in the number of these polar

residues, since they introduce an energetic penalty by their presence, there are still many examples of individual ionizable residues that apparently are "buried" within a lipid bilayer membrane. For example, the voltage sensor domain of voltage-gated potassium channels possesses several arginine residues and reorients based on membrane potential to facilitate channel gating. A discrepancy still exists between theoretical and experimental estimates of the cost of forcing an Arg into the center of the bilayer (with estimates ranging from 5-25 kcal/mol) (MacCallum et al. 2008; Moon et al. 2011). As another example, a heavily conserved lysine is essential for certain integrin proteins to form larger complexes and promote signaling. This buried Lys is thought to snorkel towards the interfacial region and impart a helix tilt that is crucial for binding of the other subunits (Kim et al. 2011).

The designed GWALP23 peptide is advantageously poised for investigations of the effects of placing polar residues in the bilayer because GWALP23 serves as a well-behaving and well characterized host framework for addressing the influence of guest residues fundamentally. Specifically, lysine was introduced into GWALP23 and $Y^5$GWALP23 host peptides and examined by solid-state NMR methods, for which the results are discussed in the fourth chapter of this dissertation. Recently, the effects of inserting Arg into a DOPC bilayer were probed using GWALP23 as a host (Vostrikov et al. 2010b). When Arg was positioned away from the center (GWALP23-R14, ~ 3 Å from helix midpoint) it only showed a 10° change in helix tilt, with a larger effect on the azimuthal rotation. But when Arg was placed at the center of the helix (GWALP23-R12), the peptide produced multiple low-intensity signals in $^2$H NMR that are indicative of multi-state behavior, including a surface-bound population. The comparable study of lysine has produced similar results, with GWALP23-K14 being well-oriented with greater tilt magnitudes and a relatively large change in the helix azimuthal rotation (compared to the host

without lysine). Much like the Arg-12 peptide, Lys-12 appears unoriented in thicker DOPC bilayers. But in contrast to Arg-12, Lys-12 is observed to titrate at high pH and adopt a defined orientation that is highly similar to host alone. Lys-14 also titrates at high pH and at pH 8.2 is found to be less tilted, but maintains its shifted azimuthal rotation from the host. Further titration of Lys-14 demonstrated a two-state system in equilibrium and in fast-exchange on the NMR time-scale and allowed for the construction of a titration curve. The decreased $pK_a$ of the Lys $\varepsilon$-$NH_3^+$ group surrounded by a lipid environment was determined to be 6.2 at experimental conditions and is comparable to previous estimates by MD simulations (MacCallum et al. 2008). The GWALP23 system therefore provides a unique approach of a direct titration of an ionizable residue in a lipid-exposed environment.

The position-dependent behavior of Lys and Arg in GWALP-like peptides is certainly interesting in that a 3 Å change in the location can determine the peptide's behavior. While titration to high pH was one method of peptide "rescue" of Lys-12, the placement of an adjacent anionic residue was also able to stabilize the peptide by some ion-pairing interaction. The fifth chapter of this dissertation discusses the viability of investigating ion-pair interactions within the bilayer by strategically placing a counter-ion near one of the previously characterized Lys or Arg residues on the helix. Ion-pair interactions are commonly found in soluble proteins and in some instances have been found to increase stability when salt-bridges are found in the hydrophobic protein core (Hendsch and Tidor 1994). Due to the low dielectric constant of the bilayer, there is an expected amplification in the intensity of these ion-pair interactions. This has been previously observed experimentally, for example with results showing much stronger interactions in octanol than in water (Wimley et al. 1996). It has also been seen that the formation of stable salt bridges is highly dependent on the proximity and geometry of the two interacting counter-ions (Kumar

and Nussinov 1999). To address this issue, we have constructed peptide variants that would be candidates for a possible ion-pair interaction, including an $i$ to $(i + 1)$ set-up with glutamic acid placed directly adjacent in the sequence on the same helical turn, or an $i$ to $(i + 4)$ strategy with the prospective counter-ion placed on the next helix turn. The Y$^5$GWALP23 12K, 13E mutant was in fact shown to "rescue" the previously unoriented Lys-12 peptide in DOPC. Lys-14 was also affected by the presence of an adjacent Glu-15. In contrast, a 12K, 16E peptide showed no improvement. Interestingly though, both Lys-12 and Lys-14 peptides with adjacent Glu appeared nearly identical at high pH to their respective peptides without Glu present. Arg-12 was also improved with Glu-13 and to some extent with Glu-16. Both Arg/Glu peptides were sensitive to pH, with the most pronounced improvement being Y$^5$GWALP23 12R, 13E at pH 8.2 and possessing an orientation much like the 12K, 13E analogue.

Membrane proteins are certainly complex due to the heterogeneous lipid bilayer in which they reside and often present challenges in their examination. Nevertheless, throughout this dissertation we demonstrate the unique ability of synthetic membrane peptides to illuminate some of the important fundamental interactions that arise between membrane proteins and the lipid bilayer. While some of the forces can be masked by the entirety of a larger membrane protein system, when isolated from other factors, the individual contributions to the collective whole can be investigated.

## References

Brown, M.F. (1994) Modulation of rhodopsin function by properties of the membrane bilayer. Chem. Phys. Lipids 73, 159-180.

Carruthers, A. and Melchior, D. L. (1984) Human Erythrocyte Hexose Transporter Activity Is Governed by Bilayer Lipid Composition in Reconstituted Vesicles. *Biochemistry 23*, 6901-6911.

De Angelis, A. A., Nevzorov, A. A., Park, S. H., Howell, S. C., Mrse, A. A., and Opella, S. J. (2004) High-Resolution NMR Spectroscopy of Membrane Proteins in Aligned Bicelles. *J. Am. Chem. Soc. 126*, 15340-15341.

de Planque, M. R., Kruijtzer, J. A., Liskamp, R. M., Marsh, D., Greathouse, D. V., Koeppe, R. E. 2nd, de Kruijff, B., and Killian, J. A. (1999) Different membrane anchoring positions of tryptophan and lysine in synthetic transmembrane alpha-helical peptides. *J. Biol. Chem. 274*, 20839-20846.

Dorairaj, S. and Allen, T. W. (2007) On the thermodynamic stability of a charged arginine side chain in a transmembrane helix. *Proc. Natl. Acad. Sci. U. S. A. 104*, 4943-4948.

Hendsch, Z. S. and Tidor, B. (1994) Do salt bridges stabilize proteins? A continuum electrostatic analysis. *Protein Sci. 3*, 211-226.

Hessa, T., Kim, H., Bihlmaier, K., Lundin, C., Boekel, J., Andersson, H., Nilsson, I., White, W. H., and von Heijne, G. (2005) Recognition of transmembrane helices by the endoplasmic reticulum translocon. *Nature 433*, 377-381.

Hong, H. and Tamm, L. K. (2004) Elastic coupling of integral membrane protein stability to lipid bilayer forces. *Proc. Natl. Acad. Sci. U. S. A. 101*, 4065-4070.

Killian, J. A., Taylor, M. J., and Koeppe, R. E. 2nd (1992) Orientation of the valine-1 side chain of the gramicidin transmembrane channel and implications for channel functioning. A $^2$H NMR study. *Biochemistry 31*, 11283-11290.

Killian, J. A., Salemink, I., de Planque, M. R., Lindblom, G., Koeppe, R. E. 2nd, and Greathouse, D. V. (1996) Induction of nonbilayer structures in diacylphosphatidylcholine model membranes by transmembrane alpha-helical peptides: importance of hydrophobic mismatch and proposed role of tryptophans. *Biochemistry 35*, 1037-1045.

Kim, C., Schmidt, T., Cho, E., Ye, F., Ulmer, T. S., and Ginsberg, M. H. (2011) Basic amino-acid side chains regulate transmembrane integrin signalling. *Nature 481*, 209-213.

Kumar, S. and Nussinov, R. (1999) Salt Bridge Stability in Monomeric Proteins. *J. Mol. Biol. 293*, 1241-1255.

Landolt-Marticorena, C., Williams, K. A., Deber, C. M., and Reithmeier, R. A. (1993) Non-random distribution of amino acids in the transmembrane segments of human type I single span membrane proteins. *J. Mol. Biol. 229*, 602-608.

MacCallum, J. L., Bennett, W. F., and Tieleman, D. P. (2008). Distribution of Amino Acids in a Lipid Bilayer from Computer Simulations. *Biophys. J. 94*, 3393-3404.

Moe, P. and Blount, P. (2005) Assessment of potential stimuli for mechano-dependent gating of MscL: effects of pressure, tension, and lipid headgroups. *Biochemistry 44*, 12239-12244.

Montecucco, C., Smith, G. A., Dabbeni-sala, F., Johannsson, A., and Bisson, R. (1982) Bilayer thickness and enzymatic activity in the mitochondrial cytochrome c oxidase and ATPase complex. *FEBS. Lett. 144,* 145-148.

Moon, C. P. and Fleming, K. G. (2011) Side chain hydrophobicity scale derived from transmembrane protein folding into lipid bilayers. *Proc. Natl. Acad. Sci. U. S. A. 108*, 10174-10177.

Tjandra, N. and Bax, A. (1997) Direct Measurement of Distances and Angles in Biomolecules by NMR in a Dilute Liquid Crystalline Medium. *Science 278*, 1111-1114.

van der Wel, P. C., Strandberg, E., Killian, J. A., and Koeppe, R. E. 2nd (2002) Geometry and intrinsic tilt of a tryptophan-anchored transmembrane alpha-helix determined by $^2$H NMR. *Biophys. J. 83*, 1479-1488.

Vostrikov, V. V., Grant, C. V., Daily, A. E., Opella, S. J., and Koeppe, R. E. 2nd (2008) Comparison of "Polarization inversion with spin exchange at magic angle" and "geometric analysis of labeled alanines" methods for transmembrane helix alignment. *J. Am. Chem. Soc. 130*, 12584-12585.

Vostrikov, V. V., Hall, B. A., Greathouse, D. V., Koeppe, R. E. 2nd, and Sansom, M. S. P. (2010b) Changes in Transmembrane Helix Alignment by Arginine Residues Revealed by Solid-State NMR Experiments and Coarse-Grained MD Simulations. *J. Am. Chem. Soc. 132*, 5803–5811.

Vostrikov, V. V. and Koeppe, R. E. 2nd (2011a) Response of GWALP Transmembrane Peptides to Changes in the Tryptophan Anchor Positions. *Biochemistry 50*, 7522-7535.

Wimley, W. C., Gawrisch, K., Creamer, T. P., and White, S. H. (1996) Direct measurement of salt-bridge solvation energies using a peptide model system: Implications for protein stability. *Biochemistry 93*, 2985-2990.

Yang, F. Y. and Hwang, F. (1996) Effect of non-bilayer lipids on the activity of membrane enzymes. *Chem. Phys. Lipids 81*. 197-202.

# CHAPTER 1

## Development of Magnetically Aligned DLPC Bicelles for the Investigation of Peptide-Lipid Interactions

### 1.1 Abstract

Magnetically-oriented lipid bicelles offer alternative modes of the study of membrane peptides by solid-state $^2$H NMR as compared to traditional mechanically-oriented glass plate model membranes. Since their discovery, the significant disadvantage of using bicelles as a model membrane system has been the lack of variety among the choices lipid systems available for use, with the majority of bicelle publications having utilized DMPC/DHPC (C12:0/C6:0) bicelles. We have investigated the creation and optimization of magnetically-oriented DLPC (C12:0) bicelles for use in solid-state NMR studies. Solid-state $^{31}$P NMR was employed to measure bilayer alignment as several variable parameters were adjusted, such as lipid composition and temperature. A final formula of DLPC/DHPC/D5PC 13.3/1/3 (long to short lipid = 3.3) was deduced and optimal alignment was held at 30 °C. The transmembrane model peptide GWALP23 (acetyl-GGALW(LA)$_6$LWLAGA-ethanolamide), labeled with deuterated alanines, was incorporated into both glass plate samples and the new DLPC bicelle formulation. $^2$H NMR quadrupolar splittings were measured in each model membrane and were found to be largely in agreement. Initial samples also allowed for the performance of solid-state $^{15}$N NMR spectroscopy, providing valuable $^{15}$N chemical shifts from labeled amide groups in the peptide's backbone.

## 1.2 Introduction

In recent years, magnetically oriented bicelles (bilayered micelles) have been used to reconstitute membrane proteins and found useful for solid-state NMR experiments. An early bicelle experiment involving membrane proteins used dilute aligned bicelles as an anisotropic medium for measuring residual dipolar interactions for protein structure determination (Tjandra and Bax 1997). As opposed to oriented plate samples which mechanically align the lipid bilayer with the magnetic field, bicelles spontaneously orient themselves with the bilayer normal perpendicular to the applied magnetic field ($\beta = 90°$). The spontaneous alignment stems from a small negative anisotropy of the magnetic susceptibility tensor, $\chi$, of the lipid acyl chains (Sakurai et al. 1980; Scholz et al. 1984). In the large bicelle configuration of lipids, the combined magnetic anisotropy from all the lipid acyl chains packed into the ordered bilayer constitutes a cooperative interaction that is enough to overcome typical Brownian motion resulting by thermal energy (Marcotte et al. 2005; Sanders et al. 1993). It has also been shown that bicelles can be flipped 90° from their native orientation with respect to the magnetic field by the addition of lanthanide ions, to achieve a $\beta = 0°$ alignment (Prosser et al. 1996). $^2$H NMR quadrupolar splittings obtained in a $\beta = 0°$ alignment with lanthanide are expected to be twice as large as $\beta = 90°$ splittings, due to a $3/2(\cos^2 \beta - 1)$ factor.

Potential advantages of using bicelles over oriented samples include reduced sample preparation time and greater assurance of bilayer alignment. Bicelle samples also have greater hydration levels and potentially can better mimic membranes with inherent surface curvature. Using previously dried down solvent-free lipids, typical bicelle samples can be prepared in less than six hours as compared to multiple days or weeks for oriented glass plate samples, which also entail more tedious sample preparation steps. As opposed to some other model membrane

systems such as micelles, bicelles furthermore conserve the biological activity of membrane proteins, as found for examples with diacylglycerol kinase (Czerski et al. 2000)**.**  The limiting factor regarding sample stability of bicelles involves the rate of hydrolysis of the ester bond in the short-chain phospholipid.  This can be overcome by using synthetic ether-analog phospholipids instead, where bicelle samples can be safely stored for months under refrigeration.

Bicelles consist of a mixture of lipids often containing one long phospholipid (of the desired biophysically relevant lipid-type) and one shorter phospholipid.  Upon hydration, the long-chain lipid component forms a planar lipid bilayer while the short-chain lipids cap the edges, forming a "disc."  Depending on the lipid composition, alignable bicelles are formed roughly between 25º and 45 °C, as opposed to other possible isotropic or lamellar lipid phases (Triba et al. 2005).

DMPC/DHPC and POPC (C16:0, C18:1)/DHPC bicelles are the most commonly used systems to date, as optimized protocols have been developed for their formation and application. Small fractions of DMPG (di-C14:0 phosphatidylglycerol) have also been incorporated into DMPC bicelles to impart a negatively charged lipid surface if desired.  Though some formulas for DLPC bicelles have been reported, none are routinely used or contain entirely phospholipids; a universal protocol has not been established for DLPC (Wang et al. 1998; Whiles et al. 2002). Addition of DLPC bicelles would allow a wider approach to the investigation of peptide-lipid interactions with these bicelle model membranes.  After a suitable DLPC bicelle formula was deduced, the well characterized model peptide GWALP23 (Ac-GGALW(LA)$_6$LWLAGA-NH$_2$) was used for comparison to other oriented bilayer systems in place.

## 1.3 Materials and Methods

### Solid Phase Synthesis of $^2$H-Labeled Peptides

Model peptides with isotopic labels for insertion and examination into novel bicelles were synthesized as followed. Commercial L-alanine-d$_4$ from Cambridge Isotope Laboratories (Andover, MA) was modified with an Fmoc group, as described previously (Thomas et al. 2009), and recrystallized from ethyl acetate:hexane, 80:20.  NMR spectra ($^1$H) were used to confirm successful Fmoc-Ala-d$_4$ synthesis.  Fmoc-L-Ala-$^{15}$N and Fmoc-L-Leu-$^{15}$N were purchased from Cambridge.  Other amino acids and "WANG" resin were purchased from NovaBiochem (San Diego, CA).  All peptides were synthesized on a 0.1 mmol scale using "FastMoc™" methods and a model 433A synthesizer from Applied Biosystems by Life Technologies (Foster City, CA). Typically, two deuterated alanines of differing isotope abundances were incorporated into each synthesized peptide.  Selected precursors for deuterated residues therefore contained either 100% Fmoc-L-Ala-d$_4$ or 60% Fmoc-L-Ala-d$_4$ with 40% non-deuterated Fmoc-L-Ala.  Some peptides were synthesized without deuterium, but with 100% abundance of $^{15}$N in selected residues.  The final residue on each peptide was acetyl-Gly to yield a blocked, neutral N-terminal.

Completed synthesis product resin was cleaved using an ethanolamine protocol which produces a neutral C-terminal. Ten mL of a dichloromethane:ethanolalmine mixture (4/1) was added to the resin and allowed to react for 48 hours on an orbital shaker.  The resulting solution containing the dissolved peptide is filtered through a glass filter and is followed by multiples rinses of dichlormethane followed by 2,2,2-trifluoroethanol.  Solution is then reduced in volume by rotoevaporation and is added to ~ 100 mL doubly deionized Milli-Q™ water allowing for the peptide to precipitate out overnight.  Solution with solid peptide is centrifuged at 24,000 g for

two hours and supernatant is removed. Peptide is then dried on ultra-low pressure vacuum system.

MALDI-TOF mass spectrometry was used to confirm peptide molecular mass. Peptide purity was examined by reversed-phase HPLC with 280 nm detection, using a 4.6 x 50 mm Zorbax SB-C8 column packed with 3.5 μm octyl-silica (Agilent Technologies, Santa Clara, CA), operated at 1 mL/min using a methanol/water gradient from 85% to 99% methanol (with 0.1% TFA) over five min and generally showed >90-95% purity. Peptide quantities were measured by means of UV absorbance at 280 nm, using molar extinction coefficients of 5,600 $M^{-1}$ $cm^{-1}$ for each Trp.

## Solid-state $^2$H and $^{31}$P NMR Spectroscopy

Magnetically-oriented bicelles for solid-state NMR spectroscopy (1/60 - 1/80, peptide/total lipid) were prepared using DLPC (or DLPC-ether) in combination with short-chain phosphatidylcholine lipids ranging C4:0 to C7:0 and varying "q" value (mol long lipid/ total mol short lipids) from Avanti Polar Lipids (Alabaster, AL), in a total volume of 175 μL deuterium-depleted water (Cambridge). Peptide and DLPC were mixed and then dried under nitrogen flow and ultra-low pressure vacuum for 48 hours to remove all trace organic solvent. Peptide/Short lipid films were hydrated using 100 μL water, and DLPC with 75 μL water. After the contents of two separate vials were soluble, the peptide/short lipid solution was transferred to the DLPC solution. Contents were cycled between 0 °C and 45 °C several times, with intermittent vortexing, until the solution remained clear when cold. Interestingly, in contrast to normal DMPC bicelles which are more viscous at higher temperatures and fluid at low temperatures, DLPC bicelles must be heated to allow fluid transfer to a 5 mm NMR tube. The tube is then sealed.

Solid-state ^{31}P NMR experiments were performed on a 300 MHz Bruker Avance spectrometer with broadband ^{1}H decoupling. Samples were allowed to equilibrate in the magnet for at least 15 minutes before starting and allowed another 15 minutes between runs for temperature equilibration when needed. Between 128 and 256 free induction decays were gathered for each ^{31}P NMR run.

^{2}H NMR spectra of bicelles were recorded at 30 ˚C using on a Bruker Avance 300 spectrometer, utilizing a quadrupolar echo pulse sequence (Davis et al. 1976) with 90 ms recycle delay, 3.2 μs pulse length and 115 μs echo delay. Between 0.6 and 1.5 million scans were accumulated during each ^{2}H NMR experiment. An exponential weighting function with 100 Hz line broadening was applied prior to Fourier transformation.

Mechanically-aligned samples for solid-state NMR spectroscopy (1/40 - 1/80, peptide/lipid) were prepared using DLPC lipids from Avanti Polar Lipids (Alabaster, AL), and deuterium-depleted water (Cambridge; 45% w/w hydration), as described previously (Thomas et al. 2009). Bilayer alignment within each sample was confirmed using ^{31}P NMR at 50 ˚C on a Bruker Avance 300 spectrometer (Billerica, MA) at both $\beta = 0°$ (bilayer normal parallel to magnetic field) and $\beta = 90°$ macroscopic sample orientations deuterium NMR spectra of glass plate samples were recorded at 50 ˚C using both sample orientations on a Bruker Avance 300 spectrometer, utilizing a quadrupolar echo pulse sequence (Davis et al. 1976) with 90 ms recycle delay, 3.2 μs pulse length and 115 μs echo delay. Between 0.6 and 1.5 million scans were accumulated during each ^{2}H NMR experiment. An exponential weighting function with 100 Hz line broadening was applied prior to Fourier transformation.

**$^2$H NMR Data Analysis**

The analysis using semi-static peptide dynamics involves a principal order parameter $S_{zz}$ to estimate overall peptide motion with respect to an apparent average peptide orientation. These calculations are based on the GALA analysis, as previously described (van der Wel et al. 2002; Strandberg et al. 2004; Strandberg et al. 2009). A grid search is performed using $\tau$, $\rho$ and $S_{zz}$ as variable parameters and locates the global RMSD minimum. The analysis considers the $^2$H quadrupolar splittings for the isotope-labeled residues based on ideal $\alpha$-helix geometry. Because of the native $\beta = 90°$ alignment of the bicelles, only $\beta = 90°$ signals were considered in this particular analysis (including oriented samples).

## 1.4 Results

^{31}P NMR was used to optimize the bicelle formulation, and bicelle integrity was discerned by noting the sharpness of the major resonance and the resolution between the peaks. Initial DLPC bicelle trials varied the short-chain lipid using a q value of 3.3 as a starting point. Poor results were immediately noticed for the lipids C7:0 and C4:0 with DLPC, which appeared macroscopically opaque at a range of temperatures and contained only isotropic and no bilayer phase as was seen by ^{31}P NMR and were not further pursued. Dipentanoyl-PC (C5:0; D5PC) and DHPC bicelles both produced well-aligned bicelles with D5PC giving slightly sharper resonance. A combination of the two short-chain lipids was then attempted in different ratios. DHPC/D5PC in 3:1, 1:1, and 1:3 DLPC bicelles were created with 1:3 DHPC/D5PC giving the best spectrum (*Figure 1*). The q value was then scanned in 0.1 to 0.2 increments from q = 2.8 to 3.8 with q = 3.3 yielding the sharpest resonances (*Figure 2*). A formula using DLPC/(DHPC/D5PC) (1:3) and q = 3.3 was decided upon for use in studying transmembrane peptides in a DLPC bilayer. Additionally, variations in temperature also showed better DLPC bicelle alignment at 30 °C as opposed to 35 °C for DMPC bicelles (*Figure 3*). Typical DLPC bicelle ^{31}P NMR spectra produce three signals that appear to correspond to their mole ratio in peak magnitude. The DLPC phospholipid peak is observed furthest shifted from 0 ppm indicating the greatest lipid order (~ -18 ppm) followed by chemical shifts of -11 and -13 ppm for D5PC and DHPC, respectively.

GWALP23, having previously been characterized in DLPC in oriented glass plates (Vostrikov et al. 2008) was incorporated into the novel DLPC bicelles for comparison. A broadening of the ^{31}P NMR signals was experienced with the incorporation of peptide, but this is also known to occur in oriented plate samples as well (*Figure 4*). Quadrupolar splittings of

deuterated alanines in DLPC bicelles varied between 0.9 and 12.0 kHz and were comparable to DLPC glass plate samples (*Table 1*). A side-by-side comparison of oriented glass plates and bicelles can be seen in *Figure 5*. While the observed quadrupolar splittings are relatively unchanged, there is a significant loss of signal intensity and most samples required more than double the number of typical $^2$H NMR scans. There is also a noticeable increase in line widths and larger isotropic peaks. Despite the decrease in spectral quality of the bicelles, a variable-$S_{zz}$ analysis demonstrates agreement of GWALP23 in the two aligned DLPC bilayer systems with similar fits to tilt magnitude (17°-18°) and direction (305°-311°), also observed in the quadrupolar wave plot (*Table 2, Figure 6*).

Further use of this DLPC bicelle formula enabled the recording of solid-state $^{15}$N NMR chemical shifts of $^{15}$N-labeled Y$^5$GWALP23 peptide (*Figure 7*), to be later described (see Chapter 2).

## 1.5 Discussion

Previous DLPC bicelles had been prepared in several different manners using either DHPC or CHAPSO, a zwitterionic cholic acid detergent, as the capping component (Whiles et al. 2002). Since no proven protocol had been established for DLPC bicelles, we employed ^{31}P NMR to optimize the conditions for a novel DLPC bicelle system. DLPC lipid-only samples were prepared similarly to DMPC bicelles using small-chain lipid component, q-value, and temperature as variables. With a changing bilayer hydrocarbon length (from common DMPC/DHPC bicelles), it was expected that the short phospholipid component would also need to be modified to maintain a preferential discoidal model that would align magnetically. Considering that going from DMPC to DLPC results in the loss of two carbons from each half of the bilayer, it was understandable that the short lipid would also need to be reduced in length, but the extent was unknown. After less-than-satisfactory results using a pure two-lipid system (DLPC with either DHPC or D5PC), the idea of mixing multiple capping lipids arose. The greatest observed alignment of DLPC, as seen by ^{31}P NMR, occurs with a 3:1 D5PC/DHPC ratio and a q value of 3.3. Interestingly, the capping lipids appear to adopt differing degrees of order within the bicelle as seen by the three unique ^{31}P NMR resonances. DHPC is ~ 2 ppm farther from an isotropic signal than is D5PC and may possibly fall between the DLPC plane and the D5PC capping perpendicular to the bilayer.

A dramatic difference between DMPC and DLPC bicelles is their temperature-dependent phases. While a solution of DMPC bicelles is uniquely viscous at warm temperatures and fluid at lower temperatures, these DLPC bicelles adopt the opposite behavior and are more fluid at elevated temperatures.

19

DLPC bicelles, with incorporated GWALP23, were able to adequately produce a similar set of quadrupolar splittings to that of oriented glass plates and resulted in a similar solution for the peptide orientation by the GALA method. However, despite this positive result and significantly easier sample preparation, there appear to be drawbacks in the DLPC bicelle system that make glass plates currently more useful for solid-state $^2$H NMR studies. Firstly, bicelle samples are only able to incorporate less than one-half the amount of peptide of our glass plate samples, resulting in a reduced $^2$H signal intensity. The lower amount of isotopic label typically then requires about double the number of scans in the $^2$H NMR spectrometer. The large excess of scans consequentially results in the build-up of a near-isotropic peak that is likely a contribution from the lipids that can make resolving signals less straight-forward in scenarios with small quadrupolar splittings. Nevertheless, the DLPC bicelles have already proven useful in gaining complementary $^{15}$N NMR data on Y$^5$GWALP23 and offer a useful addition to the bicelle formula library.

## 1.6 Acknowledgments

## 1.7 References

Czerski, L. and Sanders, C. R. 2nd (2000) Functionality of a Membrane Protein in Bicelles. *Anal. Biochem. 284*, 327-333.

Davis, J. H., Jeffrey, K. R., Bloom, M., Valic, M. I., and Higgs, T. P. (1976) Quadrupolar echo deuteron magnetic resonance spectroscopy in ordered hydrocarbon chains. *Chem. Phys. Lett. 42*, 390-394.

Marcotte, I. and Auger, M. (2005) Bicelles as Model Membranes for Solid and Solution-State NMR Studies of Membrane Peptides and Proteins. *Concepts Magn. Reson. 24*, 17-37.

Prosser, R. S., Hunt, S. A., DiNatale, J. A., and Vold, R. R. (1996) Magnetically Aligned Membrane Model Systems with Positive Order Parameter: Switching the Sign of $S_{zz}$ with Paramagnetic Ions. *J. Am. Chem. Soc. 118*, 269-270.

Sakurai, I., Kawamura, Y., Ikegami, A., and Iwayanagi, S. (1980) Magneto-orientation of lecithin crystals. *Proc. Natl. Acad. Sci. U. S. A. 77*, 7232-7236.

Sanders, C. R. 2nd, Schaff, J. E., and Prestegard, J. H. (1993) Orientational behavior of phosphatidylcholine bilayers in the presence of aromatic amphiphiles and a magnetic field. *Biophys. J. 64*, 1069-1080.

Scholz, F., Boroske, E., and Helfrich, W. (1984) Magnetic anisotropy of lecithin membranes. A new anisotropy susceptometer. *Biophys. J. 45*, 589-92.

Strandberg, E., Ozdirekcan, S., Rijkers, D. T., van der Wel, P. C., Koeppe, R. E. 2nd, Liskamp, R. M., and Killian, J. A. (2004) Tilt angles of transmembrane model peptides in oriented and non-oriented lipid bilayers as determined by ^{2}H solid-state NMR. *Biophys. J. 86*, 3709-3721.

Strandberg, E., Esteban-Martin, S., Salgado, J., and Ulrich, A. S. (2009) Orientation and dynamics of peptides in membranes calculated from ^{2}H-NMR data. *Biophys. J. 96*, 3223-3232.

Thomas, R., Vostrikov, V. V., Greathouse, D. V., and Koeppe, R. E. 2nd (2009) Influence of proline upon the folding and geometry of the WALP19 transmembrane peptide. *Biochemistry 48*, 11883-11891.

Tjandra, N. and Bax, A. (1997) Direct Measurement of Distances and Angles in Biomolecules by NMR in a Dilute Liquid Crystalline Medium. *Science 278*, 1111-1114.

Triba, M. N., Warschawski, D. E., and Devaux, P. F. (2005) Reinvestigation by Phosphorus NMR of Lipid Distribution in Bicelles. *Biophys. J. 88*, 1887-1901.

van der Wel, P. C., Strandberg, E., Killian, J. A., and Koeppe, R. E. 2nd (2002) Geometry and intrinsic tilt of a tryptophan-anchored transmembrane alpha-helix determined by $^{2}$H NMR. *Biophys. J. 83*, 1479-1488.

Vostrikov, V. V., Grant, C. V., Daily, A. E., Opella, S. J., and Koeppe, R. E. 2nd (2008) Comparison of "Polarization inversion with spin exchange at magic angle" and "geometric analysis of labeled alanines" methods for transmembrane helix alignment. *J. Am. Chem. Soc. 130*, 12584-12585.

Wang, H., Eberstadt. M., Olejniczak, E. T., Meadows, R. P., and Fesik, S. W. (1998) A liquid crystalline medium for measuring residual dipolar couplings over a wide range of temperatures. *J. Biomol. NMR. 12*, 443-446.

Whiles, J. A., Glover, K. J., Vold, R. R., and Komives, E. A. (2002) Methods for studying transmembrane peptides in bicelles: consequences of hydrophobic mismatch and peptide sequence. *J. Magn. Resn. 158*, 149-156.

**1.8 Tables**

*Table 1.* Observed $^2$H NMR quadrupolar splittings[a] for GWALP23 incorporated into DLPC glass plates[b] and DLPC bicelles, in kHz.

|  | DLPC bilayer | |
|---|---|---|
| Ala-d$_4$ | Plates | Bicelles |
| 7 | 13.0 | 12.0 |
| 9 | 11.0 | 10.5 |
| 11 | 12.1 | 11.8 |
| 13 | 5.2 | 7.0 |
| 15 | 11.0 | 11.6 |
| 17 | 1.4 | 0.9 |

[a]Quadrupolar splittings are reported in kHz for only the $\beta = 90°$ sample orientation

[b]Values for GWALP23 in DLPC from Vostrikov et al. 2008.

24

*Table 2*. Semi-static GALA analysis[a] of GWALP23 in DLPC oriented glass plates and bicelles.

| DLPC | $\tau$ | $\rho$ | $S_{zz}$ | RMSD |
|---|---|---|---|---|
| Plates | 17.3° | 305° | 0.75 | 1.8 kHz |
| Bicelles | 18.0° | 311° | 0.71 | 1.4 kHz |

[a]Calculations based on six Ala methyl $^2H$ quadrupolar splittings at the $\beta$ = 90° orientation.

## 1.9 Figures

*Figure 1.* Optimization of DLPC bicelles by varying the short phospholipid component and monitored by solid-state ^{31}P NMR. All bicelles use a q-value of 3.3. DLPC/(DHPC/D5PC) (1:3) was selected.
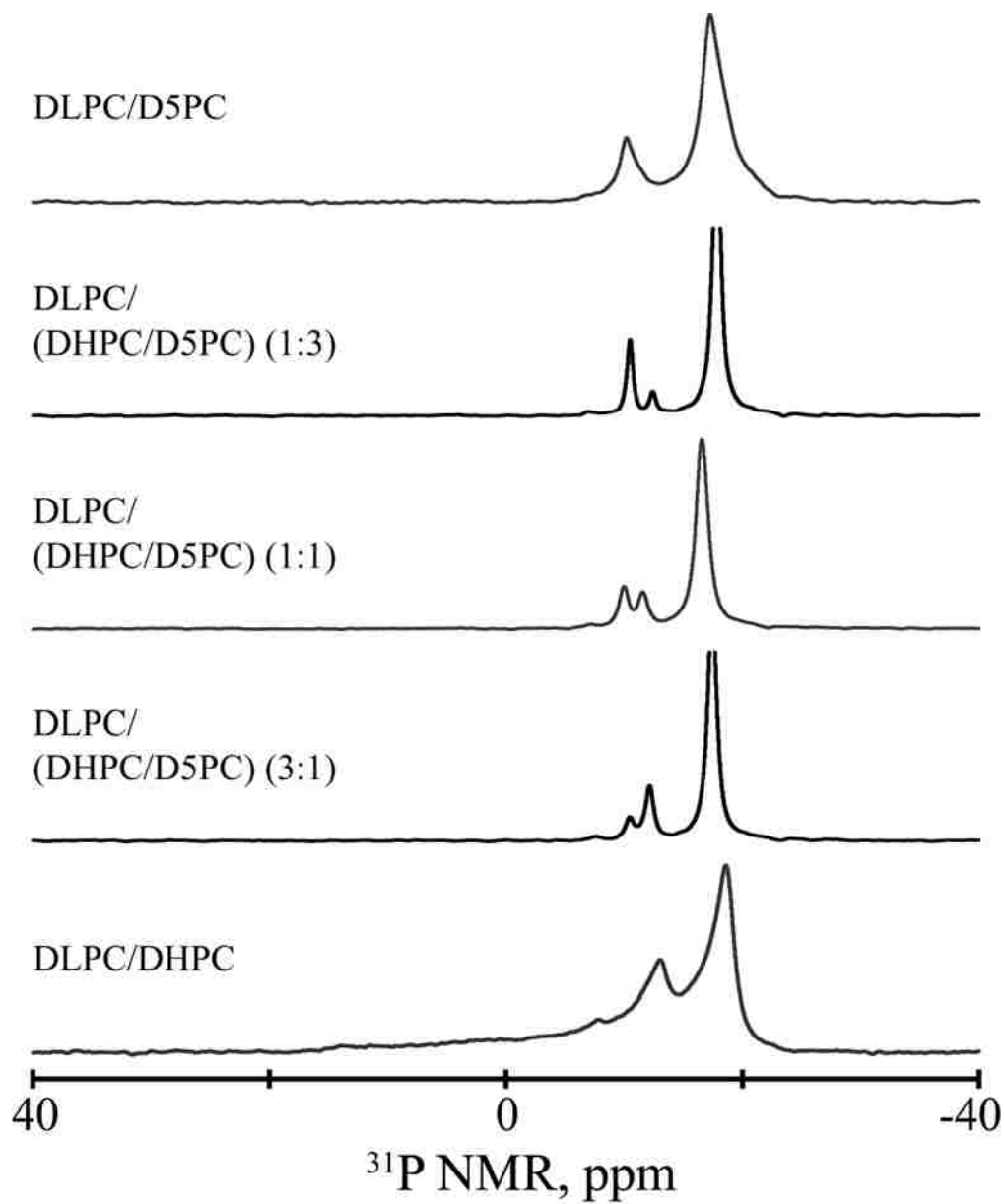
*Figure 2.* Optimization of DLPC bicelles by varying the q-value (ratio of long to short lipid) and monitored by solid-state $^{31}$P NMR. A q value of 3.3 was selected.
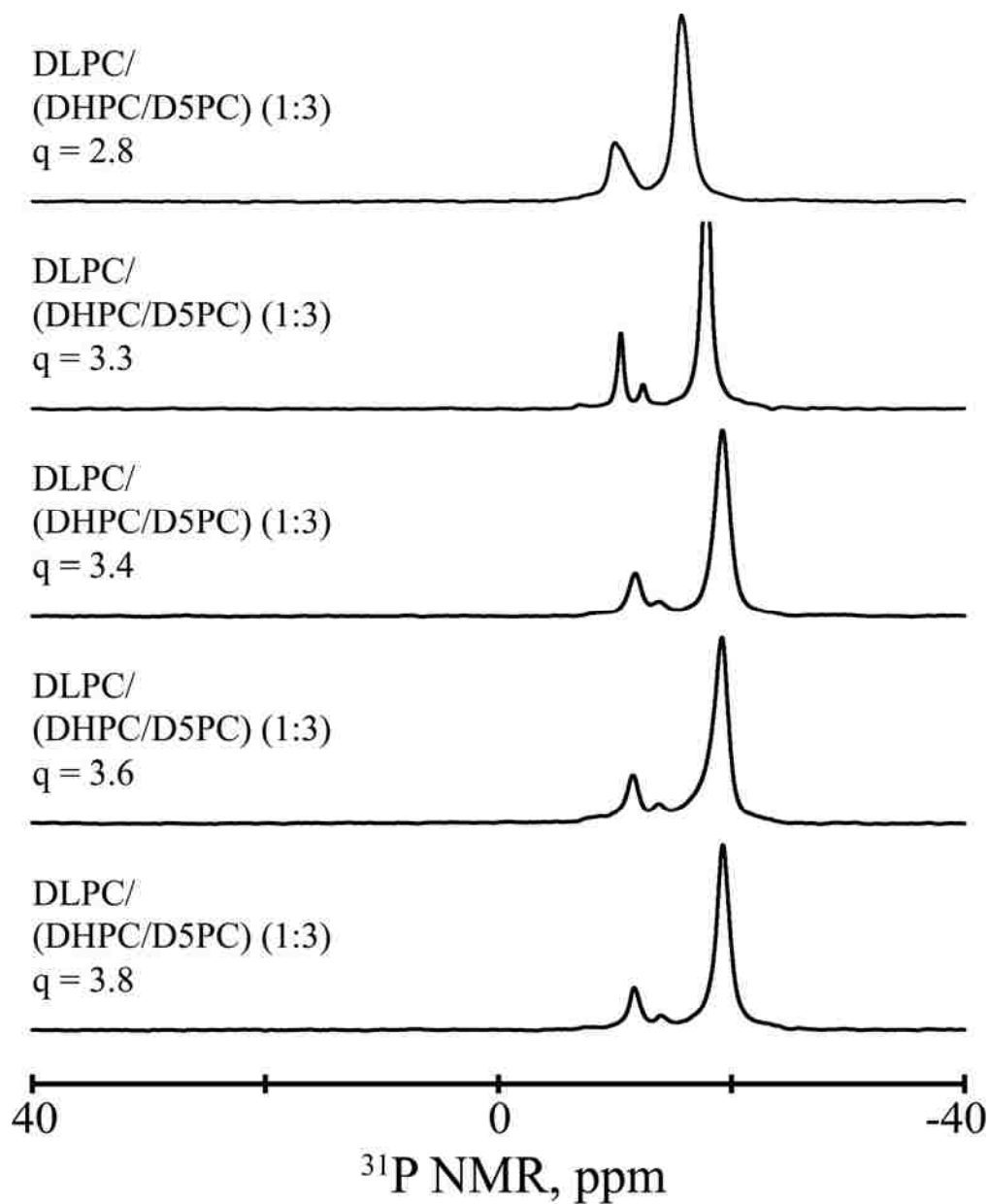
*Figure 3.* Optimization of DLPC bicelles by varying temperature and monitored by solid-state ^{31}P NMR. Shown bicelle spectra contains GWALP23 1:60 peptide/lipid.  A temperature of 30 °C was selected.
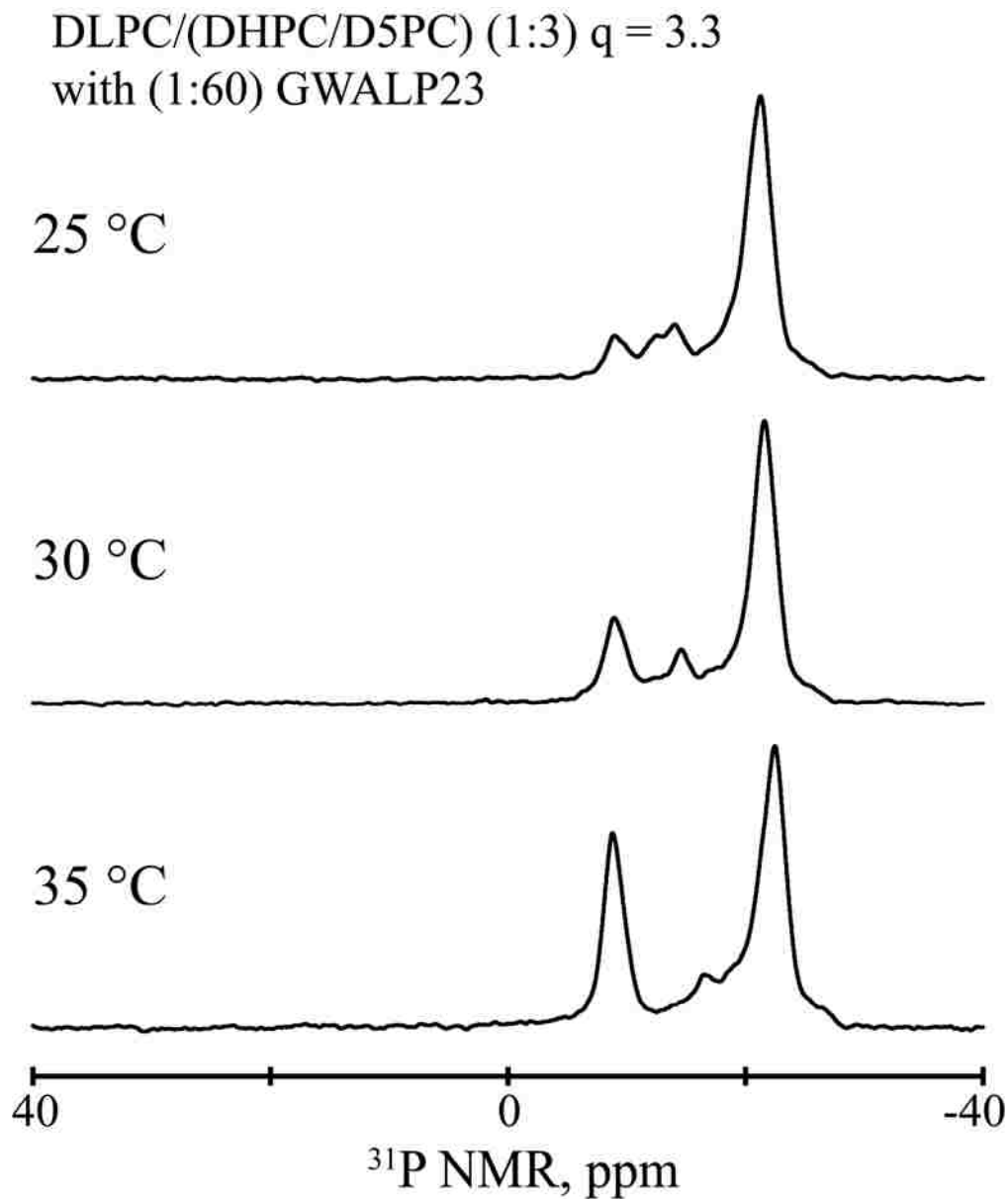
*Figure 4.* Solid-state ^{31}P NMR comparison of DLPC bicelles and DLPC glass plates containing peptide, GWALP23 1:60 peptide/lipid.



## DLPC bilayer with GWALP23 (P/L 1:60)

Bicelle; 30 °C

Glass plates; 50 °C

40        0        -40

^{31}P NMR, ppm
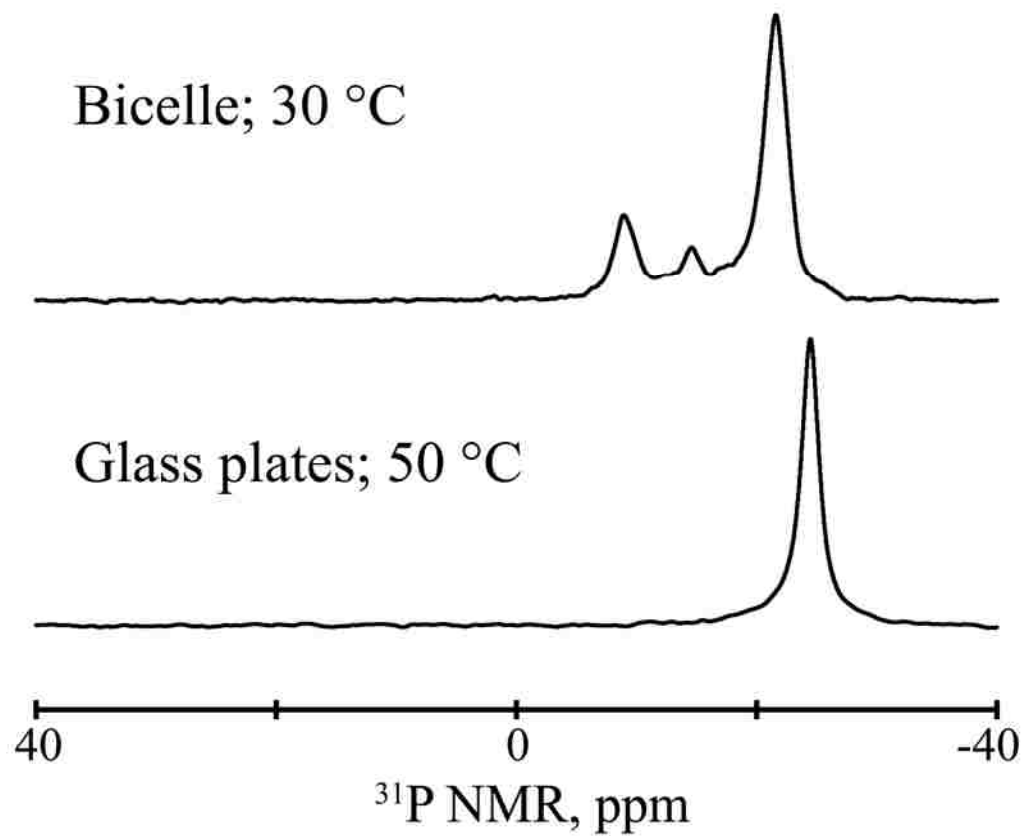
*Figure 5.* Solid-state $^2$H NMR of GWALP23 with Ala-d$_4$ labels compared in DLPC glass plates (top) and magnetically-oriented DLPC bicelles (bottom).
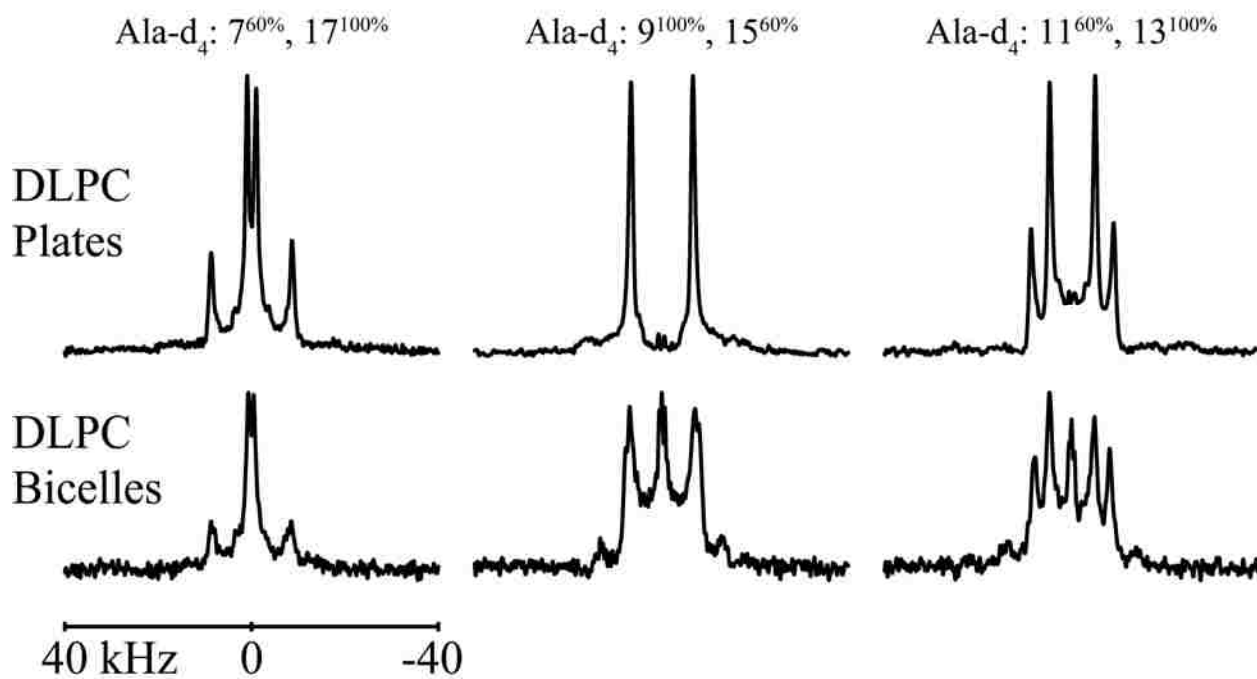
*Figure 6.* GALA semi-static analysis of Ala-d$_4$ quadrupolar splittings using variable S$_{zz}$ (see van der Wel et al. 2002). Quadrupolar wave plots are shown for GWALP23 in DLPC bicelles (red circles) and DLPC oriented glass plates (black square). Fitted curves represent theoretical $\Delta \nu_q$ values for orientations corresponding to best-fit values of $\tau$ and $\rho$.
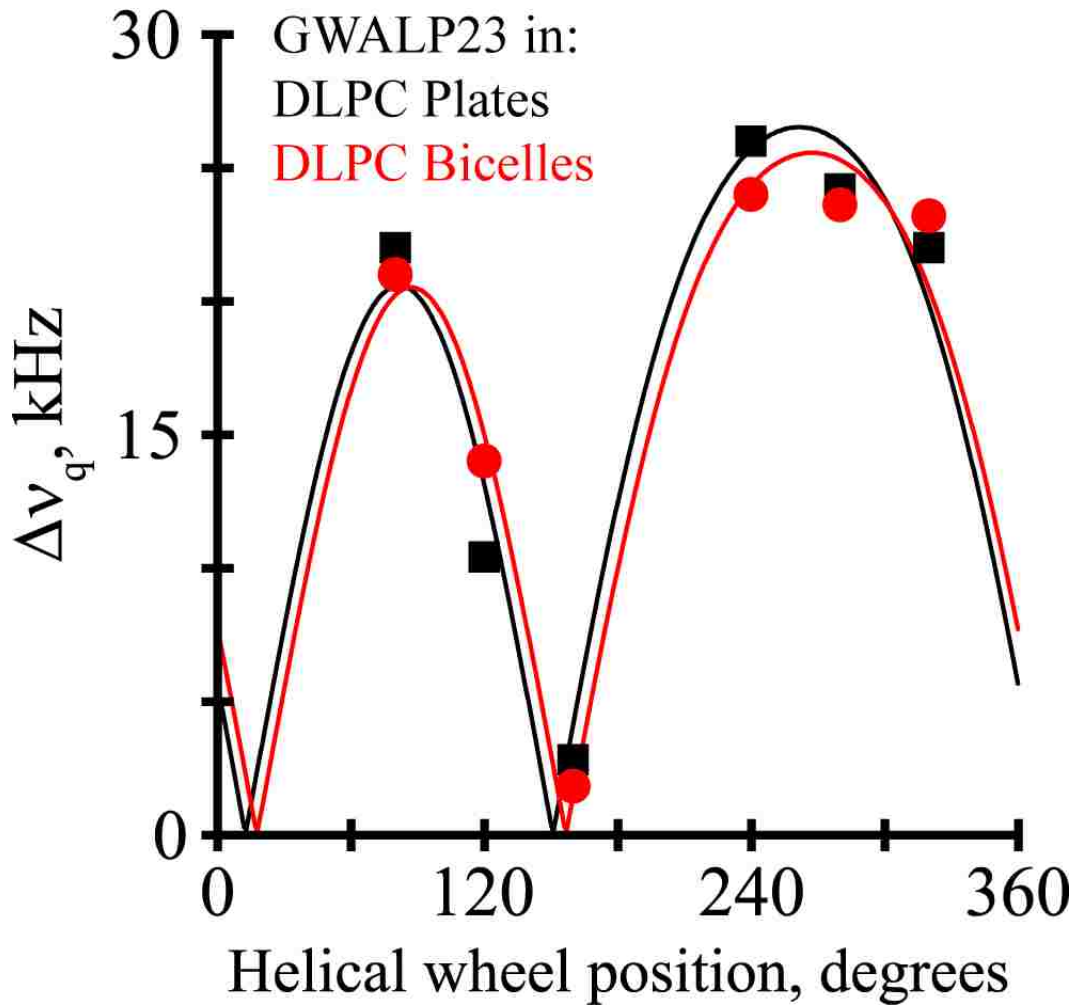
*Figure 7.* Solid-state $^{15}$N NMR of Y$^5$GWALP23 in DLPC bicelles (bottom, red) compared to Y$^5$GWALP23 in DMPC/DHPC bicelles (top, black).
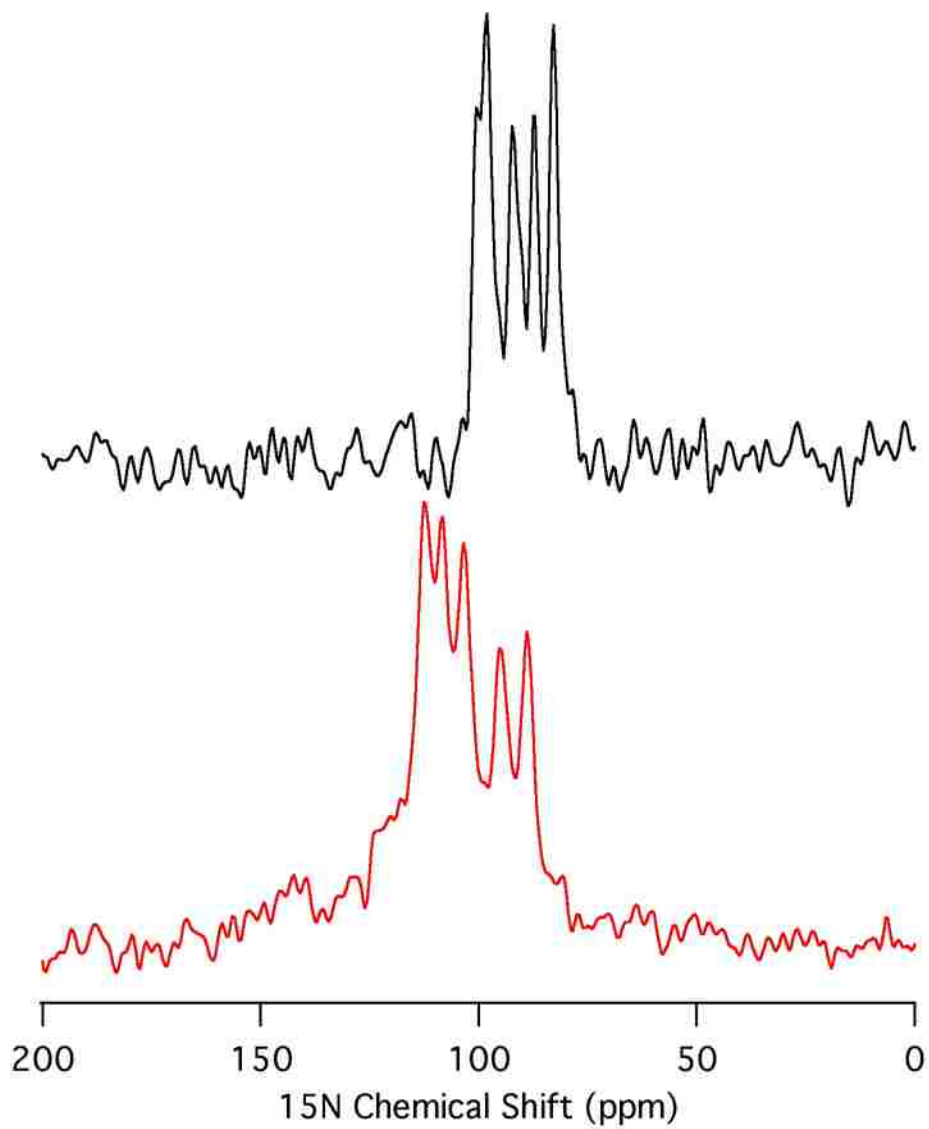
**CHAPTER 2**

**Tyrosine Replacing Tryptophan as an Anchor in GWALP Peptides**

**2.1 Abstract**

Synthetic model peptides have proven useful for examining fundamental peptide-lipid interactions. A frequently employed peptide design consists of a hydrophobic core of Leu-Ala residues with polar or aromatic amino acids flanking each side at the interfacial positions, which serve to "anchor" a specific transmembrane orientation. For example, WALP family peptides (acetyl-GWW(LA)$_n$LWWA-[ethanol]amide), anchored by four Trp residues, have received particular attention in both experimental and theoretical studies. A recent modification proved successful in reducing the number of Trp anchors to only one near each end of the peptide. The resulting GWALP23 (acetyl-GGALW$^5$(LA)$_6$LW$^{19}$LAGA-[ethanol]amide) displays reduced dynamics and greater sensitivity to lipid-peptide hydrophobic mismatch than traditional WALP peptides. We have further modified GWALP23 to incorporate a single tyrosine, replacing W$^5$ with Y$^5$. The resulting peptide, Y$^5$GWALP23 (acetyl-GGALY$^5$(LA)$_6$LW$^{19}$LAGA-amide) has a single Trp residue that is sensitive to fluorescence experiments. By incorporating specific $^2$H and $^{15}$N labels in the core sequence of Y$^5$GWALP23, we were able to use solid-state NMR spectroscopy to examine the peptide orientation in hydrated lipid bilayer membranes. The peptide orients well in membranes, and gives well defined $^2$H quadrupolar splittings and $^{15}$N/$^1$H

dipolar couplings throughout the core helical sequence between the aromatic residues.  The substitution of $Y^5$ for $W^5$ has remarkably little influence on the tilt or dynamics of GWALP23 in bilayer membranes of the phospholipids DOPC, DMPC or DLPC.  A second analogue of the peptide with one Trp and two Tyr anchors, $Y^{4,5}$GWALP23, is generally less responsive to the bilayer thickness and exhibits lower apparent tilt angles with evidence of more extensive dynamics.  In general, the peptide behavior with multiple Tyr anchors appears to be quite similar to the situation when multiple Trp anchors are present, as in the original WALP series of model peptides.

## 2.2. Introduction

Because characterizing the structures and functional properties of membrane proteins is generally a more complicated task than for aqueous soluble proteins, synthetic model membrane peptides have proven to be valuable for discerning fundamental principles that govern protein-lipid interactions. These chemically well-defined peptide systems offer opportunities for examining direct lipid interactions by placing limits upon external factors such as multiple transmembrane helices, large steric effects or interactions in oligomers. One of the first such peptide sequences was acetyl-KK(L)$_{24}$KK-amide (Davis et al. 1982; Davis et al. 1983). This sequence was chosen because it consists of a hydrophobic poly-leucine α-helix that was expected to associate with the acyl chains in a lipid bilayer membrane flanked on the ends by two hydrophilic, charged lysine residues that are expected to be soluble in the aqueous environment adjacent to the membrane. In this and other model membrane-spanning peptides, the N- and C-termini generally are capped to render them uncharged. Later peptide models incorporated an interior helical (Leu-Ala)$_n$ core sequence, which resulted in a lower overall hydrophobicity and an increased sensitivity to the identities of the lipids that compose the bilayer (Zhang et al. 1995).

A survey of type I single-span membrane proteins revealed a non-random distribution of the aromatic Trp, Tyr and Phe residues (Landolt-Marticorena et al. 1993). These aromatic residues are typically located near the aqueous-lipid interface where they are believed to act as anchors to help position the transmembrane helix within the bilayer (Schiffer et al. 1992). Other experiments with gramicidin A revealed that the Trp preference for the membrane interfacial region promotes lipid H$_{II}$ phase formation (Killian et al. 1989), as well as assembly of dimeric gramicidin channels in lipid bilayer membranes (O'Connell et al. 1990). WALP peptides (acetyl-GWWA(LA)$_n$LWWA-[ethanol]amide) incorporating multiple Trp anchors and the helical,

hydrophobic repeating Leu-Ala core sequence induced lipid phase changes, similar to gramicidin A, as a function of lipid-peptide hydrophobic mismatch (Killian et al. 1996). Later the four Trp anchor residues were mutated to various other aromatic or charged residues (Tyr, Phe, Lys, Arg, or His) to monitor the importance of the anchor's chemical and physical properties (de Planque et al. 1999; de Planque et al. 2002). These model peptides helped to describe the properties, such as peptide-dependent lipid phase behavior and lipid ordering, caused by the hydrophobic mismatch. In 2002, it was reported that WALP peptides have a characteristic non-zero tilt with respect to a lipid bilayer normal (van der Wel et al. 2002); on theoretical grounds the fundamental tilt subsequently was attributed to the entropy of precession about the bilayer normal (Lee and Im 2008). The ability to decrease the number of anchor residues has been demonstrated with (acetyl-GGALW(LA)6LWLAGA-[ethanol]amide), which possesses only one Trp anchor near each of the termini (Vostrikov et al. 2008). The tryptophans in GWALP23 flank a hydrophobic Leu-Ala core of the same length as that of WALP19 (Killian et al. 1996; van der Wel et al. 2002). With fewer anchor residues, it becomes easier to assess the roles of each of them. For example, the measured 2H quadrupolar splittings and apparent tilt angle of GWALP23 in lipid bilayers are much more responsive than those of WALP19 or WALP23 to the lipid hydrophobic thickness (Vostrikov et al. 2010a). Furthermore, the average tilt direction of GWALP23 remains essentially constant in lipid bilayers of different thickness (Vostrikov et al. 2010a). These results suggest that the four Trp anchors in the original WALP series of peptides are so dominating that they induce significant peptide dynamics, and variations in the tilt direction (Vostrikov et al. 2010a), while resisting significant changes to the magnitude of the apparent average tilt angle, even in cases where the bilayer thickness changes.

A further step beyond GWALP23 would be to replace one of the two remaining tryptophans with another chemically different anchoring residue. An advantage of such an approach would be to open a window for fluorescence experiments involving the single remaining Trp residue. To this end, we have investigated the influence of a single Trp to Tyr replacement upon GWALP23. The choice of tyrosine is based upon our preference to retain an aromatic residue and an uncharged "host" peptide (in preparation for future experiments that could investigate the introduction of a variety of "guest" charged residues within a parent peptide). We have synthesized a new peptide $Y^5GW^{19}ALP23$ (acetyl-GGALY(LA)$_6$LWLAGA-amide) and have incorporated deuterated alanine residues and 15N-labeled residues in selected sequence positions for analysis by solid-state NMR. Using circular dichroism spectroscopy, solid-state $^2H$ NMR spectroscopy with "Geometric Analysis of Labeled Alanines" (GALA) (van der Wel et al. 2002), and solid-state $^{15}N/^1H$ high resolution separate local field NMR spectroscopy (Marassi and Opella 2000; Wang et al. 2000), we have characterized the properties of $Y^5GW^{19}ALP23$ in lipid bilayer membranes of DOPC, DMPC and DLPC. Additionally, we incorporated a second tyrosine to form $Y^{4,5}GW^{19}ALP23$ and compared the orientation and dynamics of the "double-tyrosine" anchored peptide with those of $Y^5GW^{19}ALP23$ in the three different lipid bilayer membranes.

Knowledge of the orientations and dynamics of model transmembrane helices is significant for understanding principles that undergird not only the structure and function of membrane proteins in general but also the mechanisms of signaling (Hall et al. 2011; Kirchberg et al. 2011). To this end, it is important to have robust model systems that will establish a vigorous framework for such understanding.

## 2.3 Materials and Methods

### Solid Phase Synthesis of $^2$H-Labeled Peptides

Commercial L-alanine-$d_4$ from Cambridge Isotope Laboratories (Andover, MA) was modified with an Fmoc group, as described previously (Thomas et al. 2009), and recrystallized from ethyl acetate:hexane, 80:20. NMR spectra ($^1$H) were used to confirm successful Fmoc-Ala-$d_4$ synthesis. Fmoc-L-Ala-$^{15}$N and Fmoc-L-Leu-$^{15}$N were purchased from Cambridge. Other protected amino acids and acid-labile "Rink" amide resin were purchased from NovaBiochem (San Diego, CA). All peptides were synthesized on a 0.1 mmol scale using "FastMoc™" methods and a model 433A synthesizer from Applied Biosystems by Life Technologies (Foster City, CA). Typically, two deuterated alanines of differing isotope abundances were incorporated into each synthesized peptide. Selected precursors for deuterated residues therefore contained either 100% Fmoc-L-Ala-$d_4$ or 60% Fmoc-L-Ala-$d_4$ with 40% non-deuterated Fmoc-L-Ala. Some peptides were synthesized without deuterium, but with 100% abundance of $^{15}$N in selected residues. The final residue on each peptide was acetyl-Gly to yield a blocked, neutral N-terminal.

A peptide cleavage solution was prepared containing 85% trifluoroacetic acid (TFA) and 5% each (v/v or w/v) of triisopropylsilane, water, and phenol. TFA cleavage from "Rink" resin in 2 mL volume (2-3 h at 22 °C) leads to a neutral, amidated C-terminal. Peptides were precipitated by adding the TFA solution to 25 volumes of cold 50/50 MtBE/hexane. Peptides were collected by centrifugation, washed multiple times with MtBE/hexane, and lyophilized multiple times from (1:1) acetonitrile/water to remove residual TFA. MALDI-TOF mass spectrometry was used to confirm peptide molecular mass (*Figure S1* in Supplementary Material). Peptide purity was examined by reversed-phase HPLC with 280 nm detection, using a

4.6 x 50 mm Zorbax SB-C8 column packed with 3.5 μm octyl-silica (Agilent Technologies, Santa Clara, CA), operated at 1 mL/min using a methanol/water gradient from 85% to 99% methanol (with 0.1% TFA) over five min (*Figure S2* in Supplementary Material). Peptide amounts were measured by means of UV absorbance at 280 nm, using molar extinction coefficients of 5,600 $M^{-1}$ $cm^{-1}$ for each Trp and 1,490 $M^{-1}$ $cm^{-1}$ for each Tyr residue in the peptide (Pace et al. 1995). Solvents were of the highest available purity. Water was doubly deionized Milli-Q™ water.

## $^2$H NMR Spectroscopy using Oriented Bilayer samples

Mechanically aligned samples for solid-state NMR spectroscopy (1/60, peptide/lipid) were prepared using DOPC, DMPC or DLPC lipids from Avanti Polar Lipids (Alabaster, AL), and deuterium-depleted water (Cambridge; 45% w/w hydration), as described previously (Thomas et al. 2009). Bilayer alignment within each sample was confirmed using $^{31}$P NMR at 50 ˚C on a Bruker Avance 300 spectrometer (Billerica, MA) at both β = 0˚ (bilayer normal parallel to magnetic field) and β = 90˚ macroscopic sample orientations (*Figure S3* in Supplementary Material). Deuterium NMR spectra were recorded at 50 ˚C using both sample orientations on a Bruker Avance 300 spectrometer, utilizing a quadrupolar echo pulse sequence (Davis et al. 1976) with 90 ms recycle delay, 3.2 μs pulse length and 115 μs echo delay. Between 0.6 and 1.5 million scans were accumulated during each $^2$H NMR experiment. An exponential weighting function with 100 Hz line broadening was applied prior to Fourier transformation.

## $^{15}$N NMR Spectroscopy using Magnetically Oriented Bicelles

Magnetically oriented bicelles for solid-state $^{15}$N NMR spectroscopy (1/80, peptide/total lipid) were prepared using DMPC-ether and DHPC-ether lipids (3.2/1.0, mol/mol; "q" value)

from Avanti Polar Lipids (Alabaster, AL), in a total volume of 175 μL deuterium-depleted water (Cambridge). Peptide and DHPC-ether were mixed and then dried under nitrogen flow and vacuum to remove organic solvent. Separate samples of the separate DMPC-ether lipid also were prepared in aliquots and dried. Peptide/DHPC-ether films were hydrated using 100 μL water, and DMPC-ether with 75 μL water. After the contents of two separate vials were soluble, the peptide/DHPC-ether solution was transferred to the DMPC-ether solution. Contents were cycled between 0 °C and 45 °C several times, with intermittent vortexing, until the solution remained clear when cold. While still cold, the bicelle sample solution was transferred to a 5 mm NMR tube and sealed.

For ^{15}N-based SAMPI4 experiments (in the same family of pulse sequences as PISEMA), GWALP23 and Y[5]GWALP23 enriched in ^{15}N leucine and alanine were synthesized (five labels, residues 13-17). [15]N chemical shifts and [15]N-^{1}H dipolar coupling values were recorded using 500 MHz Bruker Avance and Varian Inova spectrometers and established pulse sequences (Marassi and Opella 2000; Wu et al. 1994; Nevzorov and Opella 2003; Cook and Opella 2010). Solid-state NMR high resolution separated local field SAMPI4 experiments (Nevzorov and Opella 2007) were performed using a 1 ms CP contact time, RF field strengths of approximately 50 kHz; 54 t1 points were acquired using 8.0 ms of acquisition time in the direct (t2) dimension and a 7.5 s recycle delay. The sample temperature was maintained at 42 °C, just below a critical temperature for structural transformation of DMPC/DHPC bicelle samples (Triba et al. 2005). We have found that the peptide order parameter is essentially unchanged between DMPC/DHPC bicelles at 42 °C and bilayer plate samples at 50 °C (Vostrikov et al. 2011b), where the spectral quality often improves for the plate samples (van der Wel et al. 2007). Attempts were made also to construct DLPC-based "bicelles" using DLPC-ether, DHPC-ether, and dipentanoyl-PC

(13.3/3/1) with peptide incorporated at 1/80 (peptide/DLPC; mol/mol) (Gleason et al. 2009). Unfortunately, we were unable to resolve the $^{15}$N/$^1$H dipolar couplings or assign the $^{15}$N chemical shift frequencies for such samples using the $^{15}$N-based SAMPI4 experiments.

**Data Analysis**

Combinations of $^2$H quadrupolar splittings and $^{15}$N/$^1$H dipolar coupling frequencies, individually or together, and in some cases along with $^{15}$N chemical shift values, were used to calculate the orientations of the peptide helix in the bilayers. Data uncertainty was estimated to be within ±0.5 kHz based on duplicate samples and measurements using different orientations of glass slide samples (Vostrikov et al. 2011b). We performed calculations both with a semi-static model and with a more dynamic model that incorporates Gaussian distributions for the tilt and direction of tilt (Strandberg et al. 2009). The detailed strategy for combined $^2$H and $^{15}$N/$^1$H analysis has been described (Vostrikov et al. 2011b).

The analysis using semi-static peptide dynamics involves a principal order parameter $S_{zz}$ to estimate overall peptide motion with respect to an apparent average peptide orientation. These calculations are based on the GALA analysis, as previously described (van der Wel et al. 2002; Strandberg et al. 2009; Strandberg, et al. 2004). For samples in DMPC, we incorporate also $^{15}$N/$^1$H dipolar coupling and $^{15}$N chemical shift values obtained from SAMPI4 spectra, to determine a best fit to the experimental data (Nevzorov et al. 2004). These calculations are performed using helix tilt $\tau$, rotation $\rho$ about the helix axis and a principal order parameter $S_{zz}$ as variable parameters. The analysis takes into account the $^2$H quadrupolar splittings and/or $^{15}$N/$^1$H dipolar coupling frequencies and $^{15}$N chemical shifts for the isotope-labeled residues based on ideal α-helix geometry.

To proceed beyond a semi-static model, we performed calculations that take into account more complex peptide dynamics, in which $\sigma_\tau$ and $\sigma_\rho$ relate to the widths of Gaussian distributions for the peptide tilt and rotation (Strandberg et al. 2009). In this analysis, a principal order parameter $S_{zz}$ is fixed at 0.88 to reflect isotropic fluctuations; and further anisotropic variations in $\tau$ and $\rho$ are permitted. A best-fit RMSD to observed dipolar and quadrupolar couplings, and $^{15}$N chemical shift values, is based upon the parameters $\tau_o$, $\rho_o$, $\sigma_\tau$ and $\sigma_\rho$., following (Strandberg et al. 2009). Fixed parameters in the analysis included chemical shift tensor components ($\sigma_{11}$, $\sigma_{22}$, $\sigma_{33}$) of (64, 77, 224) ppm, as reported for model dipeptides (Saito et al. 2010) and small proteins (Bechinger et al. 2011); a coupling constant of 10.22 kHz (based on an NH bond length of 1.06 Å) (Ketchem et al. 1996; Tian et al. 2003); and the angle $\varepsilon_{//}$ (14°) between the peptide helix axis and the N-H bond. In the combined analysis, equal weights were assigned to the $^2$H methyl quadrupolar couplings, $^{15}$N/$^1$H dipolar coupling frequencies, and the $^{15}$N chemical shift frequencies. Further details are described in (Vostrikov et al. 2011b) and (Vostrikov et al. 2011a).

### CD Spectroscopy

Small lipid vesicles incorporating 125 nM peptide and 7.5 μM lipid (1/60) were prepared by sonication in unbuffered water. An average of ten scans was recorded on a Jasco (Easton, MD) J710 CD spectropolarimeter, using a 1 mm cell path length, 1.0 nm bandwidth, 0.1 nm slit and a scan speed of 20 nm/min.

### Steady-state Fluorescence Spectroscopy

Vesicle solutions with 1/60 peptide/lipid for fluorescence experiments were prepared by dilution, 1/20 with water, of the samples prepared previously for CD spectroscopy (above). Samples were excited at 280 nm or 295 nm with a 5 nm excitation slit, and emission spectra

were recorded between 300 and 420 nm with a 5 nm emission slit using a Hitachi F-2500 fluorescence spectrophotometer. The spectra from five scans were averaged.

**2.4 Results**

Synthetic WALP peptides as well as analogues such as GWALP23 possess primarily α-helical character that is typical of transmembrane segments, and is expected from the repeating Leu-Ala core residues, which possess a propensity for forming helices. When the $L^4W^5$ sequence of GWALP23 is replaced with $L^4Y^5$ or $Y^4Y^5$, the resulting peptides have "single" or "double" Tyr anchors N-terminal to the core (Leu-Ala)$_n$ sequence. Circular dichroism spectra for such peptides in lipid bilayer membranes demonstrate equal or slightly reduced α-helical character when the Tyr anchor(s) are present, compared to GWALP23 (*Figure 2*). In particular, the presence of $Y^4$ as a second "anchor" residue seems to have little influence on the CD spectrum or the magnitudes of the peaks that characterize α-helices. Importantly, both the $Y^5$ and $Y^{4,5}$ derivatives maintain primarily an α-helical backbone structure. With sample formulation being vesicles for the CD spectra, stacked bilayers for the $^2H$ NMR spectra and bicelles for the $^{15}N/^1H$ NMR spectra, we believe that the core domains of the peptides are helical in all of the lipid membrane environments. Indeed, the $^2H$ resonances show agreement between bicelles and bilayers (Vostrikov et al. 2011b), and follow a helical pattern for the core alanines, while also illustrating helix unwinding in the vicinity of $A^3$ and $A^{21}$, outside of the central core sequence (Vostrikov et al. 2010a).

Further information was obtained from oriented lipid bilayer samples that included the $^2H$-labeled Tyr-containing peptides at a peptide:lipid molar ratio of 1:60. For such samples, $^{31}P$ NMR spectra confirmed that the bilayers were well aligned with respect to the magnetic field (Supporting Information, *Figure S3*). For the β = 90° sample orientation, a strong single $^{31}P$ resonance was observed at ~ -24 ppm (with the precise chemical shift frequency varying from -22.4 ppm to -26.3 ppm in the DLPC, DMPC and DOPC lipid bilayer membranes). When

samples were oriented at $\beta = 0°$, a strong peak at $\sim +18$ ppm was observed as well as small amounts of unoriented lipids that comprised a minor peak around -24 ppm.

The $^2$H NMR spectra display the two expected pairs of resonances corresponding to the quadrupolar splittings from the two labeled Ala methyl side chains in each peptide. *Figure 3* includes the spectra for alanines 7 and 17 in GWALP23, Y$^5$GWALP23, and Y$^{4,5}$GWALP23, each incorporated in DLPC, DMPC and DOPC bilayer membranes. The spectra for the other labeled alanines are included as supplemental material (*Figures S4-S5*). In rare cases, single sets of broad peaks were observed due to spectral overlap arising from similar $^2$H quadrupolar splittings from the two alanines. When the plate samples are turned from the $\beta = 0°$ orientation to $\beta = 90°$, the quadrupolar splittings are found to be reduced by a factor of two. The appearance of sharp resonances with half-magnitude quadrupolar splittings at $\beta = 90°$ illustrates that the peptides undergo fast axial rotational diffusion about the bilayer normal on the NMR timescale (Killian et al. 1992). It should be noted that the fast rotational averaging about the precession axis (bilayer normal) is distinct from averaging about the helix axis which, if complete, could average all of the $^2$H Ala signals to a common value (van der Wel et al. 2002), contrary to what is observed.

Y$^5$GWALP23 produced a relatively large range of $^2$H quadrupolar splitting magnitudes, from 8 kHz up to 30 kHz in DLPC (*Table 2*), suggesting a significant tilt of the peptide helix with respect to the bilayer normal. Somewhat smaller ranges of 4-23 kHz and 1-17 kHz were observed for Y$^5$GWALP23 in DMPC and DOPC, respectively. It is also noteworthy that the quadrupolar splittings for Y$^5$GWALP23 are in each case within 0.1 to 4 kHz of the corresponding Ala CD$_3$ signals in GWALP23 (Vostrikov et al. 2010a), suggesting that the Y$^5$ and W$^5$ peptides may adopt similar membrane orientations.

In contrast, the double-anchored Y$^{4,5}$GWALP23 exhibits a much smaller range of quadrupolar splittings, varying only between 1 kHz and 12 kHz in all three lipid bilayers (*Table 2*). The signals from Y$^{4,5}$GWALP23 do not appear to be similar to those from GWALP23 or Y$^5$GWALP23 in any of the lipid systems. Additionally, the range of quadrupolar splitting frequencies for Y$^{4,5}$GWALP23 remains approximately the same in each type of lipid bilayer membrane, regardless of the bilayer thickness. The quadrupolar splitting magnitudes for each of the six core alanine methyl side chains in Y$^5$GWALP23 and Y$^{4,5}$GWALP23 are listed in *Table 2* for each of the DLPC, DMPC and DOPC bilayer membrane environments.

Additional orientation information was derived from $^{15}$N-based SAMPI4 experiments that utilized magnetically aligned peptide-containing bicelles composed of the ether analogues of DMPC and DHPC (q=3.2:1, mol:mol). In these experiments, similar ranges are observed for the $^{15}$N chemical shift frequencies of residues 13-17 in GWALP23 (85 ppm to 100.7 ppm) and Y$^5$GWALP23 (84 ppm to 101 ppm; see *Table 3*). While the corresponding $^{15}$N/$^1$H dipolar coupling frequencies also are very similar, the ones for Y$^5$GWALP23 are slightly yet systematically smaller in magnitude (0.2 kHz to 0.5 kHz) than those for GWALP23, resulting in a SAMPI4 spectrum that appears to be somewhat below that of GWALP23 (*Figure 4*).

For Y$^5$GWALP23 in DMPC, we utilized a combined analysis of available data from $^2$H and $^{15}$N solid-state NMR experiments (Vostrikov et al. 2011b), using Gaussian as well as semi-static treatments of the dynamics. For the DMPC environment, we have a large collection of six $^2$H-Ala methyl quadrupolar splitting magnitudes, together with the $^{15}$N chemical shift frequencies and $^{15}$N/$^1$H dipolar coupling frequencies from residues 13-17 (*Figure 3-4; Tables 2-3*), giving a total of 16 restraints. For the DLPC environment, we calculated Gaussian and semi-static fits to

the dynamics using the six $^2$H-Ala methyl quadrupolar splittings from macroscopically oriented DLPC bilayers (*Table 2; Figure 3*).

The fits from the combined analysis of the $^2$H and $^{15}$N/$^1$H NMR data are quite good, with only minor discrepancies between the independent data sets (*Figure 5*; see Discussion). Importantly, the overall RMSD values of about 1.2 kHz (*Table 4*) from the combined fits are consistent with the uncertainty of the experimental measurements and suggest no over-fitting of the data. The quadrupolar and dipolar wave plots (*Figure 5A, B*) appear similar for the Gaussian and semi-static analysis methods, with data points close to the analytical curves that result from the combined analysis. Taken together, the independent measurements and the overall agreement lend confidence to the deduced molecular orientations and dynamics for the transmembrane peptides. The influence of the dynamics is evident from the ~10° smaller best-fit $\tau_o$ for the semi-static as opposed to the Gaussian analysis (*Figure 5C*). As has been characterized for other derivatives of GWALP23 (Vostrikov and Koeppe 2011a), four closely spaced minima are observed for the best-fit values of ($\sigma_\tau$, $\sigma_\rho$) (*Figure 5D*), with each minimum giving similar estimates for $\tau_o$ and $\rho_o$.

The dynamics as well as the average orientation of Y$^5$GWALP23 and GWALP23 are very similar in DMPC bilayers, regardless of whether Gaussian or semi-static approximations are employed to represent the peptide dynamics (*Table 4*). In DMPC, the Y5 and W5 peptides show similar small $\sigma_\tau$ values (5°-10°) and similar moderate to large $\sigma_\rho$ values (65°-70°). The apparent tilt angles for the two peptides in DMPC also are nearly identical; namely $\tau_o$ for both the Y5 and W5 peptides is about 21° based on the Gaussian analysis, or about 10° smaller ("apparent" tilt magnitude) when using the semi-static analysis (which ignores $\sigma_\rho$; *Table 4*). Again comparing

anchor residue Y5 to W5, the direction of peptide tilt $\rho_o$ differs consistently by about 10° (*Table 4*), regardless of the method of analysis, or whether the host lipid bilayer is DMPC or DLPC.

In DLPC, the dynamics and average orientation of Y[5]GWALP23 and GWALP23 are also very similar (*Table 4*). In these cases the Gaussian and semi-static fits to the dynamics, based on six ^{2}H quadrupolar splittings for each, yield similar $\tau_o$ values (about 21°). The Gaussian parameters in DLPC are modest, about 15° for $\sigma_\tau$ and about 30 for $\sigma_\rho$. Notably the helix properties do not vary when W5 is changed to Y5 in the GWALP23 framework in DLPC.

In DOPC bilayers, semi-static calculations performed using six ^{2}H quadrupolar splittings yield apparent tilt angles of about 6° for both Y[5]GWALP23 and GWALP23 (*Table 5*). The overall trends are similar for both peptides, with the apparent tilt angles being smaller in DOPC than in DMPC. The direction of tilt $\rho_o$ increases marginally and in parallel by about 5° from DLPC to DMPC, and by about 10° from DMPC to DOPC (*Table 5*), for both GWALP23 and Y[5]GWALP23. Notably, therefore, the rotation of Y[5]GWALP23 about its helix axis, ranging from about 295° in DLPC to 311° in DOPC, relative to the reference Cα of G[1] (van der Wel et al. 2002), is approximately a constant 10° less than that of GWALP23 in each lipid. The Tyr- and Trp-anchored peptide Y[5]GWALP23, indeed, is found to behave very similarly to the original GWALP23 in possessing an adjustable tilt that is sensitive to the lipid membrane thickness. *Figures 6A* and *7A* illustrate the rather similar $\rho_o$ values for Y[5]GWALP23 in bilayers of different thickness, along with the $\tau_o$ values that increase as the bilayer becomes thinner.

When a second tyrosine residue is introduced, in addition to the single Trp near the C-terminus, Y[4,5]GWALP23 is found to behave quite differently from GWALP23 and Y[5]GWALP23, as indicated first of all by the smaller range of observed ^{2}H quadrupolar splittings (*Figure 2*). Based on precedents with WALP23, and with the related peptide acetyl-

GWALW(LA)$_6$LWLAWA-[ethanol]amide (WWALP23), the rather narrow range of $^2$H quadrupolar splittings strongly suggests increased motional averaging of the $^2$H signals (Vostrikov et al. 2010a; Vostrikov et al. 2011b; Ozdirekcan et al. 2007; Esteban-Martin and Salgado 2007). Both the semi-static fit (with $S_{zz}$ of 0.66) and the Gaussian fit (with $\sigma_\tau$ of 27°) indicate a regime of high dynamics for Y$^{4,5}$GWALP23 in DLPC (*Table 4*). In the other lipids, consistently low apparent $\tau_o$ values, together with apparent $\rho_o$ values that diverge from bilayer to bilayer (*Figures 6B, 7B; Table 5*), again suggest highly dynamic behavior. Indeed the trends for Y$^{4,5}$GWALP23 mirror those that have been observed previously for WALP23 (Strandberg et al. 2004) and WWALP23 (Vostrikov and Koeppe 2011a). Also WALP19 is seen to be highly dynamic (large $\sigma_\rho$ value) in DLPC (Strandberg et al. 2012), although a model-dependent analysis (in which $\sigma_\tau$ is set to zero) suggests that $\sigma_\rho$ may become low under conditions of negative mismatch (Strandberg et al. 2012).

An added advantage of Y$^5$GWALP23 is the presence of only a single Trp residue, whose emission $\lambda_{max}$ should be unambiguously sensitive to the polarity of the environment of the single indole ring (Ren et al. 1997). It is within this context important to confirm that the fluorescence emission from Y$^5$GWALP23 is characteristic of interfacial tryptophan. Indeed, when Y$^5$GWALP23 and Y$^{4,5}$GWALP23 are excited at 295 nm, so as to minimize the contributions from the tyrosines, their emission spectra closely overlap that of GWALP23 (*Figure 8*), with $\lambda_{max}$ being about 335 nm for each peptide. The results suggest similar interfacial locations for the Trp residue(s) in all three peptides. When the excitation wavelength is 280 nm, contributions from the Tyr residue(s) are evident (*Figure S6* of the Supporting Information). (The Tyr fluorescence emission [at 306 nm], unlike the case of Trp, is not dependent on environment polarity.) The spectra in *Figure 8* moreover suggest that fluorescence from Y$^5$GWALP23,

excited at 295 nm, can serve as an effective probe for potential helix (center-of-mass) translation with respect to the bilayer midplane under the influence of guest residues. For example, when a guest arginine is introduced at position 14 in GWALP23, such helix translation by about 3 Å has been predicted by coarse-grained molecular dynamics simulations (Vostrikov et al. 2010b), but has not yet been observed experimentally.

## 2.5 Discussion

How many Trp residues are needed to maintain a defined orientation, with moderate to low dynamics, and minimal aggregation, for a transmembrane helical domain relative to an interface between water and the interior of a lipid bilayer membrane? Gramicidin channels have eight tryptophans (O'Connell et al. 1990), while the original WALP peptides employ only four tryptophans (Killian et al. 1996). With the introduction of GWALP23 (Vostrikov et al. 2008), we found that as few as two Trp residues can define a preferred orientation for a transmembrane α-helix (Vostrikov et al. 2010a). Now with the replacement of W5 by Y5, we learn that one interfacial Trp and one interfacial Tyr can confer a stable transmembrane orientation for Y$^5$GWALP23. Remarkably, the extent of dynamic averaging of the NMR resonances is *less* when only two Trps—or one Trp and one Tyr—are present than when more than two interfacial aromatic residues are present. In particular, the dynamic averaging is very extensive, and involves especially large values of $\sigma_\rho$, when four Trps (WALP23 and WWALP23; (Vostrikov et al. 2010a)) or one Trp with two Tyr (Y$^{4,5}$GWALP23; this work) provide the interfacial anchoring. Aspects of the data analysis and of the consequences of tyrosine substitutions for the orientation and dynamics of GWALP23 will be discussed in turn.

We took advantage of the combined and simultaneous analysis of $^2$H quadrupolar splittings, $^{15}$N chemical shifts and $^{15}$N/$^1$H dipolar couplings for Y$^5$GWALP23 in DMPC. The combined goodness-of-fit is essentially the same for GWALP23 and Y$^5$GWALP23, giving RMSD values of about 1.2 kHz when 16 parameters are analyzed for either of the peptides in DMPC (*Table 4*). With smaller data sets involving only a single type of parameter, the apparent RMSD values are somewhat lower, typically near 0.6 kHz; yet the deduced values of $\tau_o$ and $\rho_o$

are essentially the same.  For example, semi-static analysis gives a ($\tau_o$, $\rho_o$) estimate of (10°, 300°) when the six $^2$H $\Delta\nu_q$ values are analyzed alone (*Table 5*), compared to (16°, 306°) for the set of five $^{15}$N chemical shifts and five $^{15}$N/$^1$H dipolar couplings, or (12°, 298°) when all sixteen data points are employed (*Table 4*).  As noted previously (Vostrikov et al. 2008), the independent solid-state NMR methods agree rather well.

GWALP23 and Y$^5$GWALP23 show similar orientations and dynamics in DLPC, DMPC and DOPC bilayer membranes (Tables 4-5).  Remarkably, either a single tyrosine or a single tryptophan at position 5 is sufficient to define the orientation of the N-terminal of the transmembrane peptide with respect to W19 as the sole anchor for the C-terminus.  For both peptides in DMPC, the Gaussian dynamic fits show small values of $\sigma_\tau$ (5°-10°) and moderate values of $\sigma_\rho$ (65°-70°) (Table 4).  Indeed, if one compares in detail the fits to the Gaussian dynamics in DMPC (*Figure 9*), the similar narrow distributions of $\tau$, and broad distributions of $\rho$, for the two peptides can be directly observed.  Notably, the most probable $\tau_o$ is identical for the two peptides (*Figure 9*), while the width of the $\tau$ distribution increases marginally when Y5 is present, leading to the small increase in $\sigma_\tau$ from ~5° to ~10° for Y$^5$GWALP23 (*Table 4*).  We performed Gaussian analysis also for the peptides in DLPC, using the $^2$H NMR data (*Table 4*).  Once again, the results for Y$^5$GWALP23 agree with those for GWALP23 itself.  In DLPC, the Gaussian and semi-static analyses return nearly equivalent values of $\tau_o$, in the range of 19°-23° for both peptides, and the ~10° offset in $\rho_o$ is maintained between W5 and Y5.  The Gaussian analyses indicate moderate values of about 30° for $\sigma_\rho$ and about 15° for $\sigma_\tau$ for GWALP23 and Y$^5$GWALP23 in DLPC (*Table 4*).  Importantly, apart from the 10° change in $\rho_o$, the Gaussian distributions remain essentially the same when the identity of residue five is modified from Trp to Tyr.

The semi-static fits to the $^2$H NMR data reveal similar apparent tilt angles for the W5 and Y5 peptides in DOPC, as well as in DMPC and DLPC (*Table 5*). In all three lipids, the main effect of Y5 is to alter the most probable direction of the peptide tilt $\rho_o$ by about 10° (*Tables 4-5*), a result which is independent of whether a semi-static or Gaussian analysis is used to estimate the dynamics. GWALP23 and Y$^5$GWALP23 exhibit, furthermore, less extensive motional averaging of their $^2$H and $^{15}$N resonances than WALP23 (Strandberg et al. 2009) or WWALP23 (Vostrikov et al. 2010a) in each of the lipid membranes. With this direct comparison of residues W5 and Y5 in GWALP23 now available, it would be of future interest to compare also the substitution of W19 with Y19.

To address the question of whether one or two Tyr residues would be preferable for defining a transmembrane helix orientation, we compared the properties of the Y5 and Y4,5 peptides. The comparison (Figures 6-7) indicates a loss of systematic behavior when Y4 is introduced alongside Y5. With Y4 present, the observed $^2$H $\Delta\nu_q$ magnitudes span only a small range in each lipid, $\rho_o$ becomes unpredictable in membranes of different thickness, and $\tau_o$ no longer scales with the bilayer thickness. Indeed, the dynamic properties of Y$^{4,5}$GWALP23, as revealed by $^2$H NMR, resemble those of WALP19 (van der Wel et al. 2002; Lee and Im 2008), W$^{(2,3,21,22)}$ALP23 (Strandberg et al. 2009; Strandberg et al. 2004; Monticelli et al. 2010; Holt et al. 2010), and W$^{2,22}$W$^{5,19}$ALP23 (Vostrikov et al. 2010a), all of which possess 4 Trp residues. It is nevertheless conceivable that also the loss of the hydrophobic L4 residue itself could contribute to the apparent changes in the peptide dynamics, a situation which could be checked by investigating the properties of the single-tyrosine mutant Y$^4$GWALP23 peptide. Regardless of such a possibility, the present results suggest that "extra" aromatic residues may compete with each other at the membrane interface.

The accumulated results to date indicate, concerning the preferred number of aromatic Trp or Tyr residues to anchor each end of a transmembrane helix, that "one is enough," and "two are too many." When $(W^5)$GWALP23 and $Y^5$GWALP23 are compared, the orientations and dynamic properties are found to be remarkably similar in three different lipid bilayer membranes; namely Tyr is found to define a preferred peptide orientation as effectively as Trp (at the N-terminal). (The relative anchoring potential of Tyr versus Trp has yet to be established at the C-terminal.) Importantly, including additional aromatic residues—whether one more tyrosine in $Y^{4,5}$GWALP23, or two more tryptophans (for example, in WALP23 or WWALP23)—markedly increases the extent of the peptide dynamics. It is plausible that the increased dynamic behavior may be due to competition among different aromatic residues for preferred positions with respect to the head groups of the lipid bilayer.

## 2.6 Acknowledgments

## 2.7 References

Bechinger, B., Resende, J. M., and Aisenbrey, C. (2011) The structural and topological analysis of membrane-associated polypeptides by oriented solid-state NMR spectroscopy: established concepts and novel developments. *Biophys. Chem. 153*, 115-125.

Cook, G. A. and Opella, S. J. (2010) NMR studies of p7 protein from hepatitis C virus. *Eur. Biophys. J. 39*, 1097-104.

Davis, J. H., Hodges, R. S., and Bloom, M. (1982) The Interaction between a Synthetic Amphiphilic Polypeptide and Lipids. *Biophys. J. 37*, 170-171.

Davis, J. H., Clare, M. D., Hodges, R. S., and Bloom, M. (1983) The Interaction between a Synthetic Amphiphilic Polypeptide and Lipids in a Bilayer Structure. *Biochemistry 22*, 5298-5305.

Davis, J. H., Jeffrey, K. R., Bloom, M., Valic, M. I., and Higgs, T. P. (1976) Quadrupolar echo deuteron magnetic resonance spectroscopy in ordered hydrocarbon chains. *Chem. Phys. Lett 42*, 390-394.

de Planque, M. R., Kruijtzer, J. A., Liskamp, R. M., Marsh, D., Greathouse, D. V., Koeppe, R. E. 2nd, de Kruijff, B., and Killian, J. A. (1999) Different membrane anchoring positions of tryptophan and lysine in synthetic transmembrane alpha-helical peptides. *J. Biol. Chem. 274*, 20839-20846.

de Planque, M. R. , Boots, J. W., Rijkers, D. T., Liskamp, R. M. , Greathouse, D. V., and Killian, J. A. (2002) The effects of hydrophobic mismatch between phosphatidylcholine bilayers and transmembrane alpha-helical peptides depend on the nature of interfacially exposed aromatic and charged residues. *Biochemistry 41*, 8396-8404.

DeLano, W. L. (2002) The PyMOL Molecular Graphics System.

Esteban-Martin, S. and Salgado, J. (2007) The dynamic orientation of membrane-bound peptides: bridging simulations and experiments. *Biophys. J. 93*, 4278-4288.

Gleason, N. J., Vostrikov, V. V., and Koeppe, R. E. 2nd (2009) Comparison of Mechanical and Magnetic Alignment of WALP-like Peptides for Solid-State NMR. *2009 Biophysical Society Meeting Abstracts.* Biophys. J. Supplement, 445a, Abstract, 2349-Pos.

Hall, B. A., Armitage, J. P., and Sansom, M. S. P. (2011) Transmembrane Helix Dynamics of Bacterial Chemoreceptors Supports a Piston Model of Signalling. *PLOS Comput. Biol. 7*, e1002204.

Holt, A., Rougier, L., Reat, V., Jolibois, F., Saurel, O., Czaplicki, J., Killian, J. A., and Milon, A. (2010) Order parameters of a transmembrane helix in a fluid bilayer: case study of a WALP peptide. *Biophys. J. 98*, 1864-1872.

Ketchem, R. R., Lee, K. C., Huo, S., and Cross, T. A. (1996) Macromolecular structural elucidation with solid-state NMR-derived orientational constraints. *J. Biomol. NMR 8*, 1-14.

Killian, J. A., Prasad, K. U., Urry, D. W., and de Kruijff, B. (1989) A mismatch between the length of gramicidin and the lipid acyl chains is a prerequisite for $H_{II}$ phase formation in phosphatidylcholine model membranes. *Biochim. Biophys. Acta. 978*, 341-345.

Killian, J. A., Taylor, M. J., and Koeppe, R. E. 2nd (1992) Orientation of the valine-1 side chain of the gramicidin transmembrane channel and implications for channel functioning. A $^{2}H$ NMR study. *Biochemistry 31*, 11283-11290.

Killian, J. A., Salemink, I., de Planque, M. R., Lindblom, G., Koeppe, R. E. 2nd, and Greathouse, D. V. (1996) Induction of nonbilayer structures in diacylphosphatidylcholine model membranes by transmembrane alpha-helical peptides: importance of hydrophobic mismatch and proposed role of tryptophans. *Biochemistry 35*, 1037-1045.

Kirchberg, K., Kim, T. Y., Moller, M., Skegro, D., Raju, G. D., Granzin, J., Buldt, G., Schlesinger, R., and Alexiev, U. (2011) Conformational dynamics of helix 8 in the GPCR rhodopsin controls arrestin activation in the desensitization process. *Proc. Natl. Acad. Sci., U.S.A.  108*, 18690-18695.

Landolt-Marticorena, C., Williams, K. A., Deber, C. M., and Reithmeier, R. A. (1993) Non-random distribution of amino acids in the transmembrane segments of human type I single span membrane proteins. *J. Mol. Biol. 229*, 602-608.

Lee, J. and Im, W. (2008) Transmembrane helix tilting: insights from calculating the potential of mean force. *Phys. Rev. Lett. 100*, 018103.

Marassi, F. M. and Opella, S. J. (2000) A solid-state NMR index of helical membrane protein structure and topology. *J. Magn. Reson. 144*, 150-155.

Monticelli, L., Tieleman, D. P., and Fuchs, P. F. (2010) Interpretation of $^{2}H$-NMR experiments on the orientation of the transmembrane helix WALP23 by computer simulations. *Biophys. J. 99*, 1455-1464.

Nevzorov, A. A. and Opella, S. J. (2003) A "magic sandwich" pulse sequence with reduced offset dependence for high-resolution separated local field spectroscopy. *J. Magn. Reson. 164*, 182-186.

Nevzorov, A. A., Mesleh, M. F., and Opella, S. J. (2004) Structure determination of aligned samples of membrane proteins by NMR spectroscopy. *Magn. Reson. Chem. 42*, 162-171.

Nevzorov, A. A. and Opella, S. J. (2007) Selective averaging for high-resolution solid-state NMR spectroscopy of aligned samples. *J. Magn. Reson. 185*, 59-70.

O'Connell, A. M., Koeppe, R. E. 2nd, and Andersen, O. S. (1990) Kinetics of gramicidin channel formation in lipid bilayers: transmembrane monomer association. *Science 250*, 1256-1259.

Ozdirekcan, S., Etchebest, C., Killian, J. A., and Fuchs, P. F. (2007) On the orientation of a designed transmembrane peptide: toward the right tilt angle? *J. Am. Chem. Soc. 129*, 15174-15181.

Pace, C. N., Vajdos, F., Fee, L., Grimsley, G., and Gray, T. (1995) How to measure and predict the molar absorption coefficient of a protein. *Protein Sci. 4*, 2411-23.

Pulay, P., Scherer, E. M., van der Wel, P. C., and Koeppe, R. E. 2nd (2005) Importance of tensor asymmetry for the analysis of $^2$H NMR spectra from deuterated aromatic rings. *J. Am. Chem. Soc. 127*, 17488-17493.

Ren, J., Lew, S., Wang, Z., and London, E. (1997) Transmembrane orientation of hydrophobic alpha-helices is regulated both by the relationship of helix length to bilayer thickness and by the cholesterol concentration. *Biochemistry 36*, 10213-10220.

Saito, H., Ando, I., and Ramamoorthy, A. (2010) Chemical shift tensor - the heart of NMR: Insights into biological aspects of proteins. *Prog. Nucl. Magn. Reson. Spectrosc. 57*, 181-228.

Schiffer, M., Chang, C. H., and Stevens, F. J. (1992) The functions of tryptophan residues in membrane proteins. *Protein Eng. 5*, 213-214.

Strandberg, E., Ozdirekcan, S., Rijkers, D. T., van der Wel, P. C., Koeppe, R. E. 2nd, Liskamp, R. M., and Killian, J. A. (2004) Tilt angles of transmembrane model peptides in oriented and non-oriented lipid bilayers as determined by $^2$H solid-state NMR. *Biophys. J. 86*, 3709-3721.

Strandberg, E., Esteban-Martin, S., Salgado, J., and Ulrich, A. S. (2009) Orientation and dynamics of peptides in membranes calculated from $^2$H-NMR data. *Biophys. J. 96*, 3223-3232.

Strandberg, E., Esteban-Martin, S., Ulrich, A. S., and Salgado, J. (2012) Hydrophobic mismatch of mobile transmembrane helices: Merging theory and experiments. *Biochim. Biophys. Acta. 1818*, 1242-1249.

Thomas, R., Vostrikov, V. V., Greathouse, D. V., and Koeppe, R. E. 2nd (2009) Influence of proline upon the folding and geometry of the WALP19 transmembrane peptide. *Biochemistry 48*, 11883-11891.

Tian, C., Gao, P. F., Pinto, L. H., Lamb, R. A., and Cross, T. A. (2003) Initial structural and dynamic characterization of the M2 protein transmembrane and amphipathic helices in lipid bilayers. *Protein Sci. 12*, 2597-2605.

Triba, M. N., Warschawski, D. E., and Devaux, P. F. (2005) Reinvestigation by Phosphorus NMR of Lipid Distribution in Bicelles. *Biophys. J. 88*, 1887-1901.

van der Wel, P. C., Strandberg, E., Killian, J. A., and Koeppe, R. E. 2nd (2002) Geometry and intrinsic tilt of a tryptophan-anchored transmembrane alpha-helix determined by $^2$H NMR. *Biophys. J. 83*, 1479-1488.

van der Wel, P. C. A., Reed, N. D., Greathouse, D. V., and Koeppe, R. E. 2nd (2007) Orientation and Motion of Tryptophan Interfacial Anchors in Membrane-Spanning Peptides. *Biochemistry 46*, 7514–7524.

Vostrikov, V. V., Grant, C. V., Daily, A. E., Opella, S. J., and Koeppe, R. E. 2nd (2008) Comparison of "Polarization inversion with spin exchange at magic angle" and "geometric analysis of labeled alanines" methods for transmembrane helix alignment. *J. Am. Chem. Soc. 130*, 12584-12585.

Vostrikov, V. V., Daily, A. E., Greathouse, D. V., and Koeppe, R. E. 2nd (2010a) Charged or aromatic anchor residue dependence of transmembrane peptide tilt. *J. Biol. Chem. 285*, 31723-31730.

Vostrikov, V. V., Hall, B. A., Greathouse, D. V., Koeppe, R. E. 2nd, and Sansom, M. S. P. (2010b) Changes in Transmembrane Helix Alignment by Arginine Residues Revealed by Solid-State NMR Experiments and Coarse-Grained MD Simulations. *J. Am. Chem. Soc. 132*, 5803–5811.

Vostrikov, V. V. and Koeppe, R. E. 2nd (2011a) Response of GWALP Transmembrane Peptides to Changes in the Tryptophan Anchor Positions. *Biochemistry 50*, 7522-7535.

Vostrikov, V. V., Grant, C. V., Opella, S. J., and Koeppe, R. E. 2nd (2011b) On the Combined Analysis of $^2$H and $^{15}$N/$^1$H Solid-State NMR Data for Determination of Transmembrane Peptide Orientation and Dynamics. *Biophys. J. 101*, 2939-2947.

Wang, J., Denny, J., Tian, C., Kim, S., Mo, Y., Kovacs, F., Song, Z., Nishimura, K., Gan, Z., Fu, R., Quine, J. R., and Cross, T. A. (2000) Imaging membrane protein helical wheels. *J. Magn. Reson. 144*, 162-167.

Wu, C. H., Ramamoorthy, A., and Opella, S. J. (1994) High-Resolution Heteronuclear Dipolar Solid-State NMR Spectroscopy. *J. Magn. Reson. A 109*, 270-272.

Zhang, Y. P., Lewis, R. N., Henry, G. D., Sykes, B. D., Hodges, R. S., and McElhaney, R. N. (1995) Peptide models of helical hydrophobic transmembrane segments of membrane proteins. 1. Studies of the conformation, intrabilayer orientation, and amide hydrogen exchangeability of Ac-$K_2$-$(LA)_{12}$-$K_2$-amide. *Biochemistry 34*, 2348-2361.

## 2.8 Tables

*Table 1.* Sequences of GWALP23 and related peptides[a]

| Name | Sequence |
|---|---|
| WALP23 | a-GWW$^3$LALALALALALALALALALWWA-e |
| WALP19 | a-GWW$^3$LALALALALALALWWA-e |
| GWALP23 | a-GGALW$^5$LALALALALALALWLAGA-e |
| Y$^5$GWALP23 | a-GGALY$^5$LALALALALALALWLAGA-amide |
| Y$^{4,5}$GWALP23 | a-GGAYY$^5$LALALALALALALWLAGA-amide |

[a]Abbreviations: "a" denotes "acetyl" and "e" denotes "ethanolamide."

*Table 2.* Observed $^2$H quadrupolar splittings[a] for GWALP23[b] and Tyr-based analogues in three lipids, in kHz.

| Residue | DLPC | | | DMPC | | | DOPC | | |
|---|---|---|---|---|---|---|---|---|---|
| | $W^{5,19}$ | $Y^5W^{19}$ | $Y^{4,5}W^{19}$ | $W^{5,19}$ | $Y^5W^{19}$ | $Y^{4,5}W^{19}$ | $W^{5,19}$ | $Y^5W^{19}$ | $Y^{4,5}W^{19}$ |
| 7 | 26.4 | 29.3 | 11.6 | 21.9 | 22.8 | 11.7 | 16.6 | 16.2 | 10.2 |
| 9 | 25.5 | 24.0 | 0.5 | 8.9 | 9.2 | 3.2 | 1.7 | 0.5 | 3.8 |
| 11 | 26.9 | 26.4 | 6.9 | 20.9 | 20.3 | 10.7 | 16.7 | 13.6 | 10.0 |
| 13 | 14.6 | 10.5 | 4.6 | 3.8 | 3.9 | 2.8 | 1.5 | 0.5 | 3.8 |
| 15 | 20.7 | 19.5 | 6.9 | 17.6 | 15.6 | 10.7 | 15.4 | 13.6 | 12.6 |
| 17 | 3.4 | 8.1 | 11.6 | 2.9 | 5.6 | 4.4 | 2.6 | 4.8 | 3.8 |

[a]Quadrupolar splittings are reported in kHz for the β = 0° sample orientation of GWALP23 (having W5 and W19), $Y^5$GWALP23, and $Y^{4,5}$GWALP23. Each value is an average of (the magnitude observed when β = 0°), and (twice the magnitude observed when β = 90°).

[b]Values for GWALP23 from (Vostrikov and Koeppe 2011a). The positions of the aromatic residues in the peptides are listed as $W^{5,19}$, $Y^5W^{19}$ and $Y^{4,5}W^{19}$.

*Table 3.* Dipolar couplings and $^{15}$N chemical shift values for peptide $^{15}$N/$^1$H groups[a]

| Residue | GWALP23 | | Y$^5$GWALP23 | |
| --- | --- | --- | --- | --- |
| | $^{15}$N, ppm | $^{15}$N/$^1$H, kHz | $^{15}$N, ppm | $^{15}$N/$^1$H, kHz |
| 13 | 101 | 3.0 | 101 | 2.8 |
| 14 | 87 | 2.4 | 88 | 2.0 |
| 15 | 85 | 3.4 | 84 | 2.9 |
| 16 | 94 | 3.8 | 93 | 3.4 |
| 17 | 97 | 2.8 | 99 | 2.5 |

[a]Values were measured in DMPC/DHPC bicelles and correspond to a $\beta = 90°$ sample orientation.

*Table 4.* Calculated orientations and dynamics of peptides in DMPC and DLPC[a]

| Peptide | Lipid | Model | $\tau_0$ | $\sigma_\tau$ | $\rho_0$ | $\sigma_\rho$ | $S_{zz}$ | RMSD (kHz) | n[b] |
|---|---|---|---|---|---|---|---|---|---|
| GWALP23 | DMPC | Gaussian | 21° | 5° | 306° | 70° | 0.88[c] | 1.1 | 16 |
| | DMPC | semi-static | 11° | n.a.[d] | 307° | n.a.[d] | 0.75 | 1.2 | 16 |
| Y[5]GWALP23 | DMPC | Gaussian | 21° | 9° | 298° | 66° | 0.88[c] | 1.2 | 16 |
| | DMPC | semi-static | 12° | n.a.[d] | 298° | n.a.[d] | 0.73 | 1.2 | 16 |
| GWALP23 | DLPC | Gaussian | 23° | 15° | 304° | 33° | 0.88[c] | 0.7 | 6 |
| | DLPC | semi-static | 21° | n.a.[d] | 305° | n.a.[d] | 0.71 | 0.7 | 6 |
| Y[5]GWALP23 | DLPC | Gaussian | 21° | 12° | 295° | 27° | 0.88[c] | 0.7 | 6 |
| | DLPC | semi-static | 19° | n.a.[d] | 295° | n.a.[d] | 0.78 | 0.7 | 6 |
| Y[4,5]GWALP23 | DLPC | Gaussian | 11° | 27° | 261° | 60° | 0.88[c] | 1.5 | 6 |
| | DLPC | semi-static | 5° | n.a.[d] | 260° | n.a.[d] | 0.66 | 1.6 | 6 |

[a]The Gaussian model for the dynamics uses a fixed principal order parameter $S_{zz}$ (Strandberg et al. 2009), representing the dynamic extent of (mis)alignment (angle $\alpha$) between the molecular $z$-axis and its average orientation, characterized by the time average $S_{zz} = \langle 3 \cos^2\alpha - 1 \rangle / 2$ (Pulay et al. 2005). Within this context, further motions can be characterized by the widths $\sigma_\tau$ and $\sigma_\rho$ of Gaussian distributions about the average values of tilt magnitude $\tau_0$ and tilt direction $\rho_0$ (Strandberg et al. 2009). An alternative semi-static analysis, using three parameters instead of four, determines the best fit (lowest RMSD, in kHz) as a function of $\tau_0$, $\rho_0$ and a variable $S_{zz}$.

[b]Number of data points (from Tables 2-3), identified as six ^{2}H methyl quadrupolar couplings, either alone or with five ^{15}N/^{1}H dipolar couplings and ^{15}N chemical shifts.

[c]Fixed value.

[d]Not applicable.

*Table 5.* Semi-static GALA analysis of GWALP23 and Tyr-anchored analogues[a]

| Aromatic residues | DLPC | | | | DMPC | | | | DOPC | | | |
|---|---|---|---|---|---|---|---|---|---|---|---|---|
| | $\tau^{o}$ | $\rho^{o}$ | $S_{zz}$ | RMSD (kHz) | $\tau^{o}$ | $\rho^{o}$ | $S_{zz}$ | RMSD (kHz) | $\tau^{o}$ | $\rho^{o}$ | $S_{zz}$ | RMSD (kHz) |
| [b]W[5,19] | 21° | 305° | 0.71 | 0.7 | 9° | 311° | 0.88 | 1.0 | 6° | 323° | 0.87 | 0.6 |
| Y[5]W[19] | 19° | 295° | 0.78 | 0.7 | 10° | 300° | 0.84 | 0.7 | 5° | 311° | 0.84 | 1.0 |
| Y[4,5]W[19] | 5° | 260° | 0.66 | 1.6 | 3° | 323° | 0.77 | 0.6 | 3° | 359° | 0.82 | 1.1 |

[a]Calculations based on six Ala methyl $^2$H quadrupolar splittings only.  The reduced $S_{zz}$ values, variable apparent $\rho_o$ values and low apparent $\tau_o$ values render Y[4,5]GWALP23 the outlier among this set of peptides.

[b]Values for GWALP23 from reference (Vostrikov et al. 2010a)

## 2.9 Figures

*Figure 1*. Representative models of GWALP23, $Y^5$GWALP23, and $Y^{4,5}$GWALP23 (left to right), showing the locations of aromatic side chains on a ribbon helix, drawn using PyMOL (Delano et al. 2002). The side chain orientations are arbitrary.
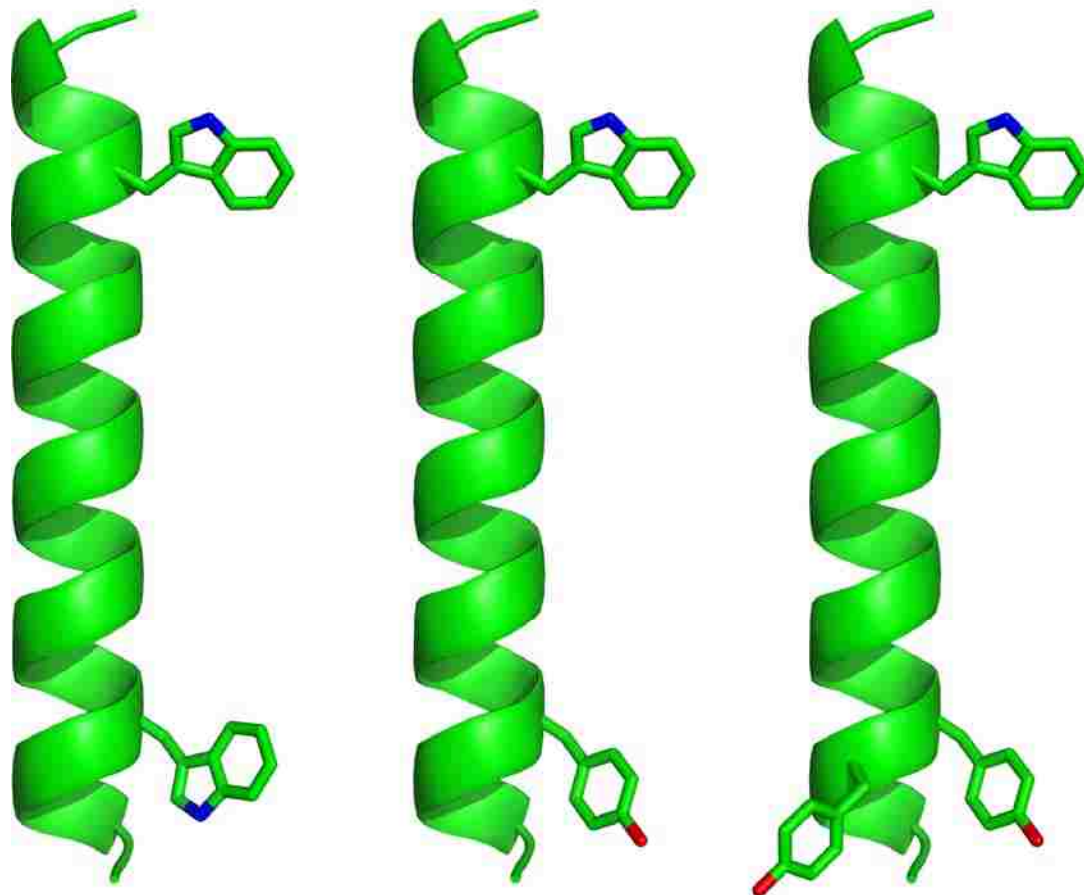
*Figure 2.* Circular dichroism spectra of GWALP23 (black), $Y^5$GWALP23 (blue) and $Y^{4,5}$GWALP23 (red) in DLPC vesicles.
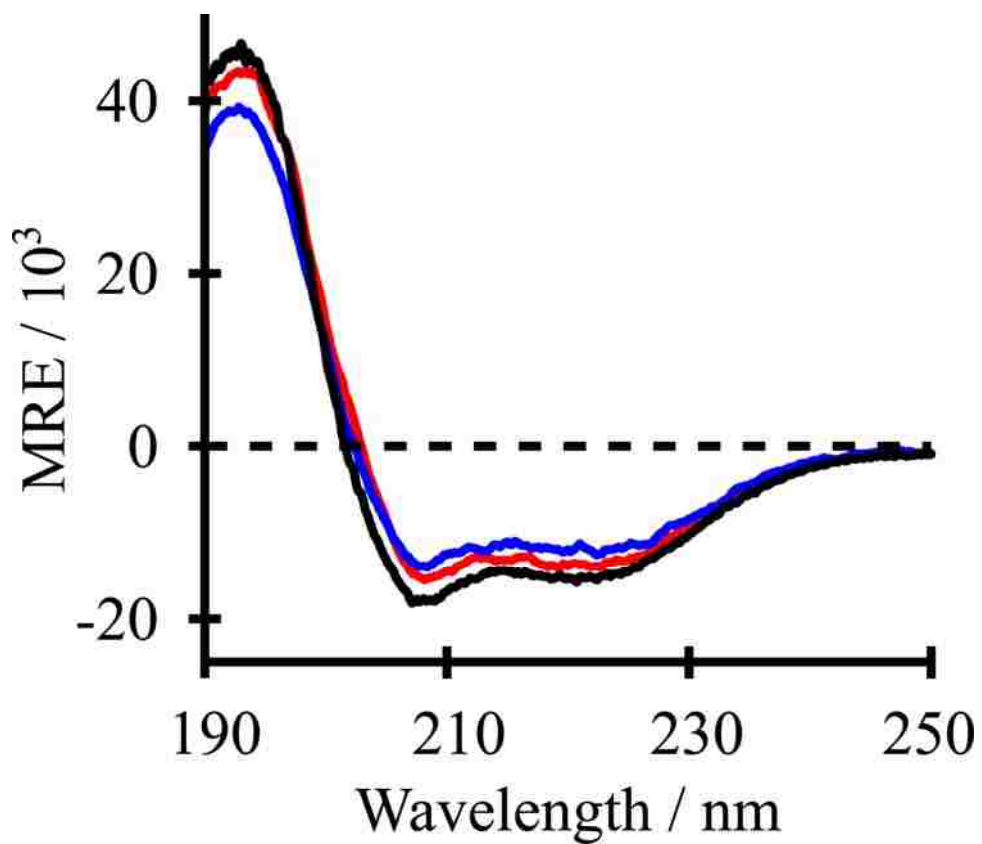
*Figure 3.* $^2$H NMR spectra of (top to bottom) GWALP23, Y$^5$GWALP23, and Y$^{4,5}$GWALP23, each labeled at Ala$^{17}$ (100% $^2$H) and Ala$^7$ (60% $^2$H), in hydrated oriented bilayers of DLPC, DMPC and DOPC. Peptide/lipid ratio, 1/60 (mol/mol); 50 °C; β = 90° sample orientation.
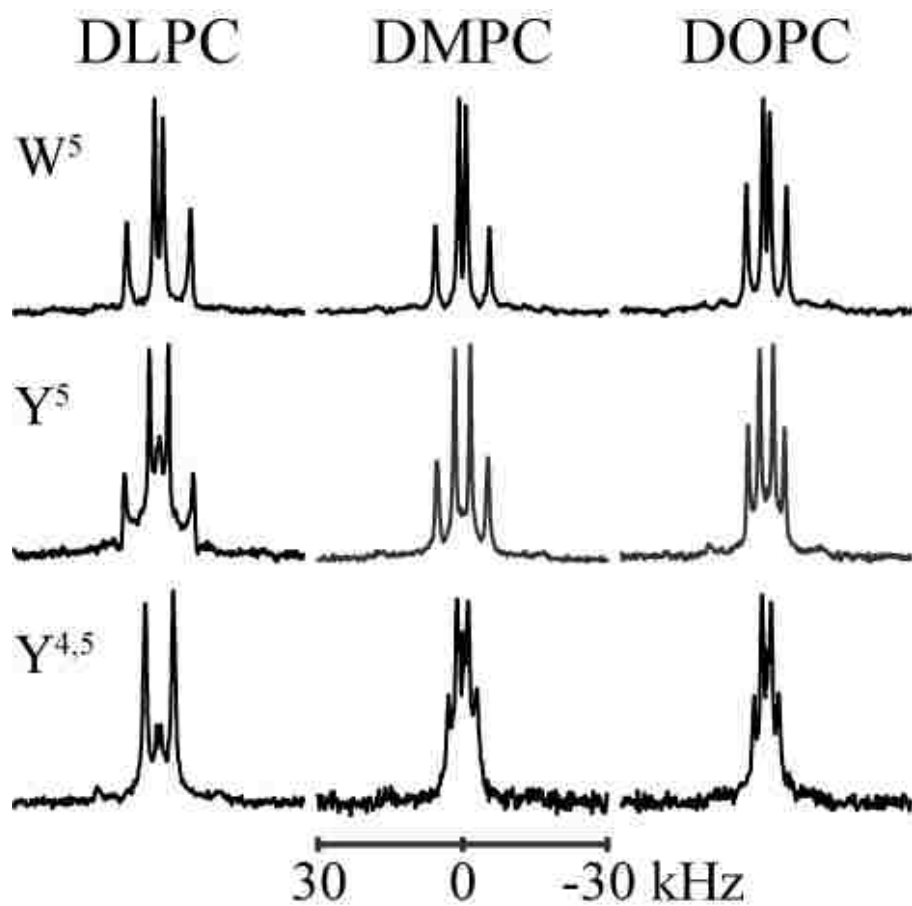
*Figure 4.* SAMPI4 spectra, with assignments, for GWALP23 (red) and $Y^5$GWALP23 (blue, with PISA wheel corresponding to the combined fit to $^{15}N$ and $^2H$ data, Table 4), each $^{15}N$ labeled in residues 13-17. Peptide/lipid ratio, 1/80 (mol/mol); 42 °C; bicelles of DMPC/DHPC (q = 3.2).
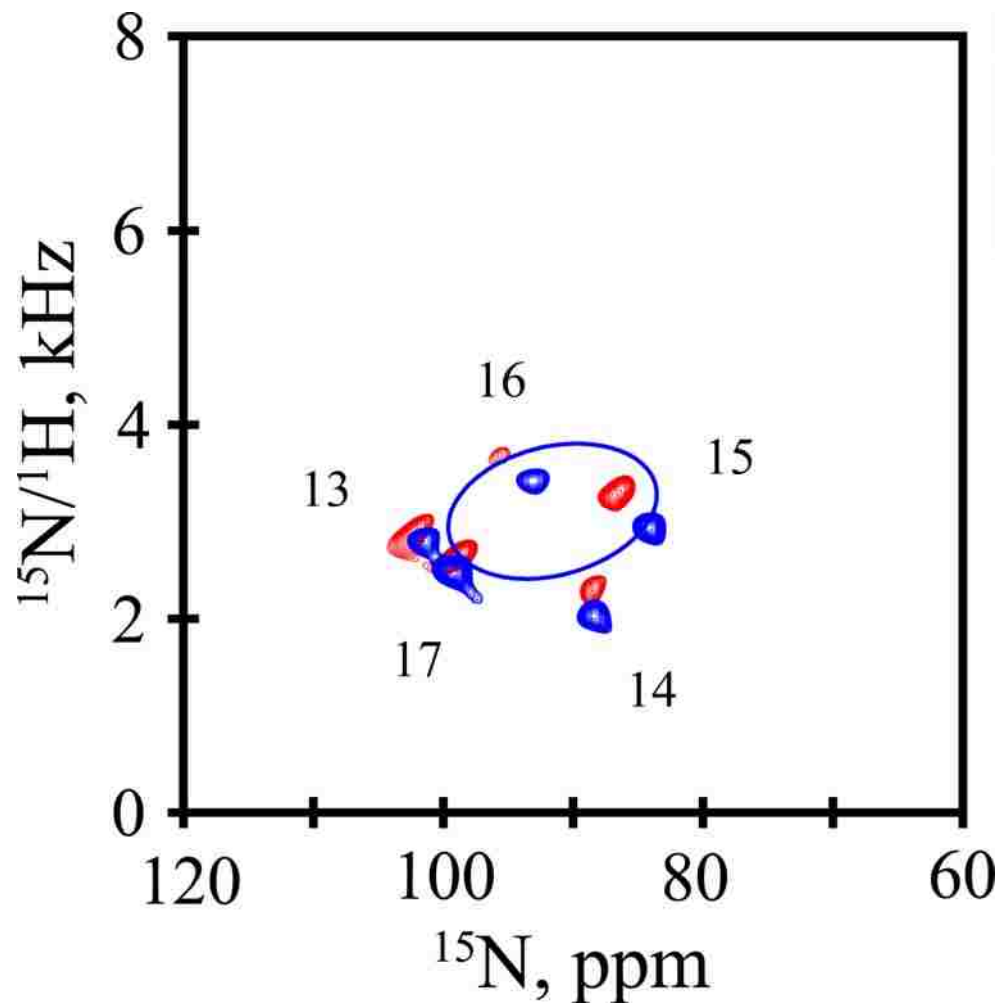
*Figure 5.* Combined $^{15}$N and $^{2}$H analysis for Y$^{5}$GWALP23 in DMPC.  A.  Quadrupolar waves from Gaussian dynamics (black curve) and semi-static (red curve) analysis.  B.  Dipolar waves from Gaussian (black curve) and semi-static (red curve) analysis.  C. RMSD ($\tau_o$ , $\rho_o$) graph for the Gaussian (black contours) and semi-static (red contours) analyses, contoured at 1.5, 2.0 and 2.5  kHz.  D. RMSD ($\sigma_\tau$ , $\sigma_\rho$) graph for the Gaussian dynamics analysis, contoured at 0.95, 1.15 and 1.35 kHz.
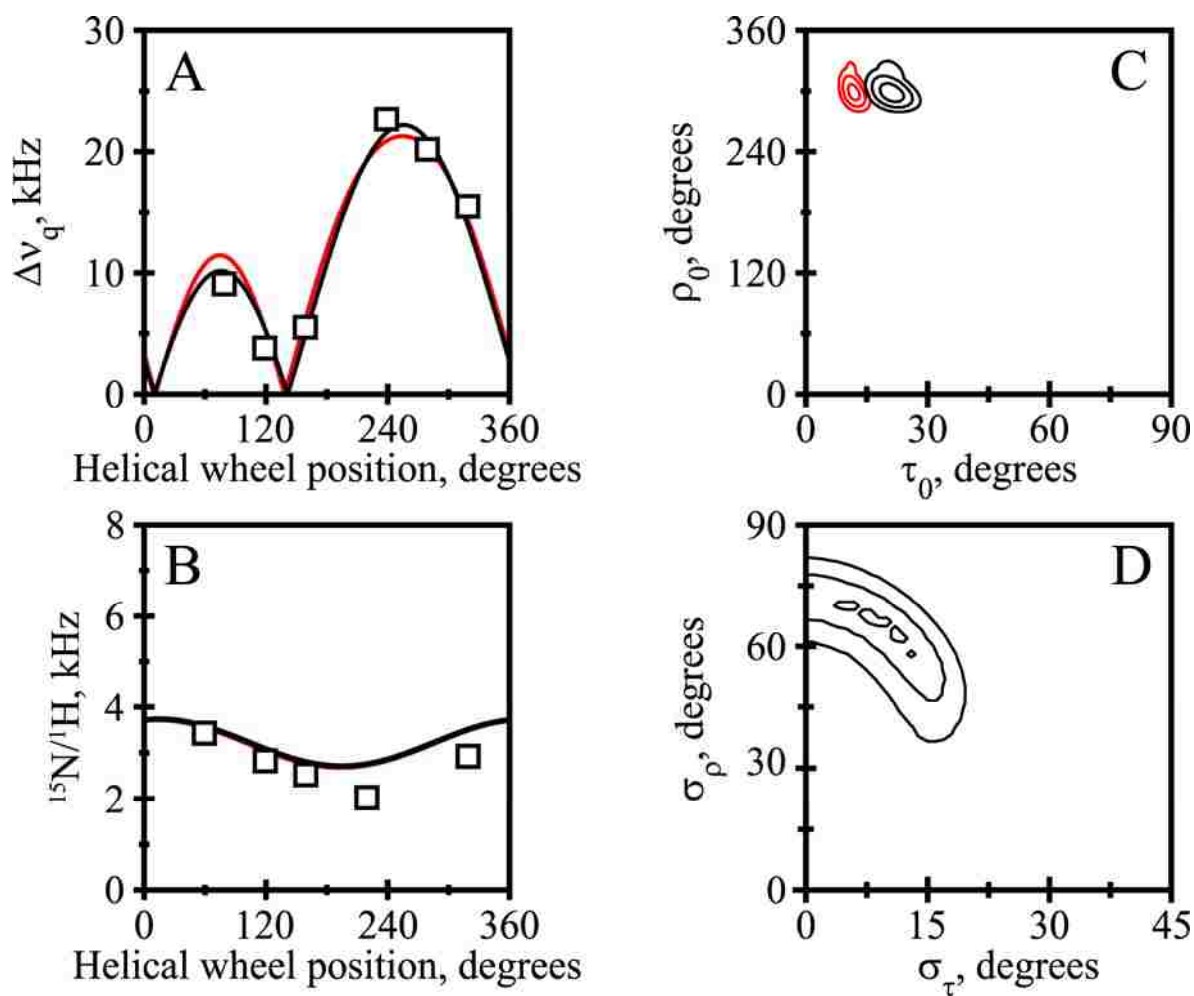
*Figure 6.* GALA semi-static analysis of Ala-d$_4$ quadrupolar splittings using variable S$_{zz}$ (see van der Wel et al. 2002). Quadrupolar wave plots are shown for Y$^5$GWALP23 (A) and Y$^{4,5}$GWALP23 (B) in oriented bilayers of DLPC (black squares), DMPC (red circles) and DOPC (blue triangles). Fitted curves represent theoretical $\Delta v_q$ values for orientations corresponding to best-fit values of $\tau_o$ and $\rho_o$.
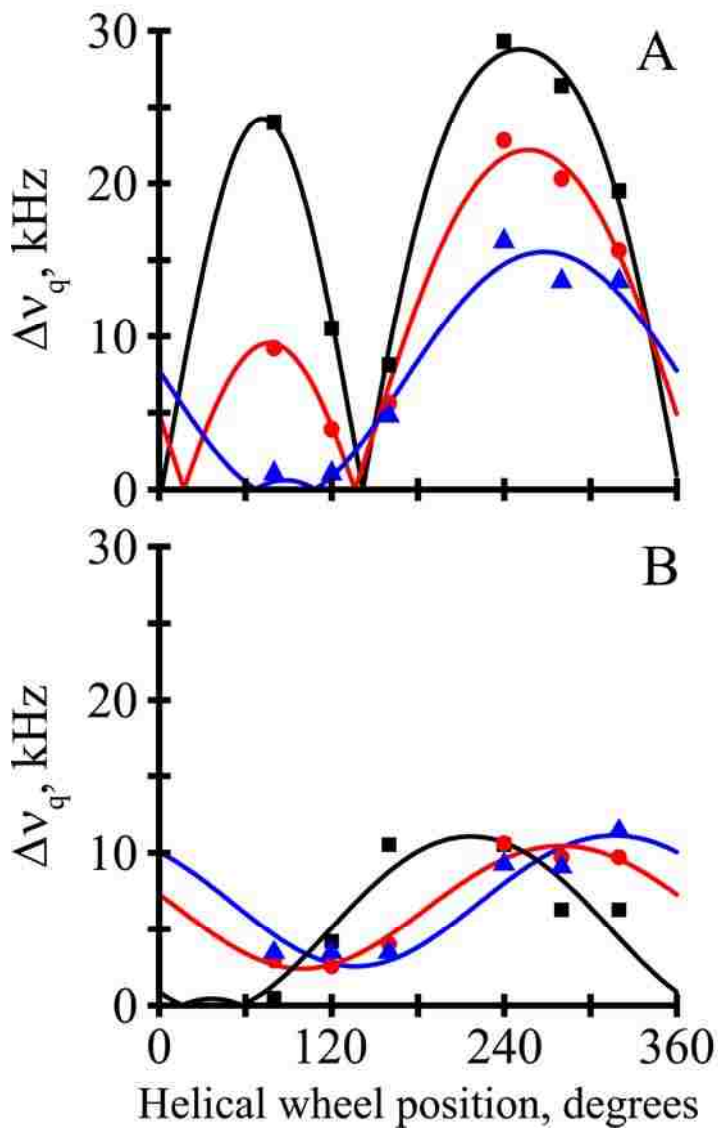
*Figure 7.* RMSD contour plots for apparent average tilt $\tau_o$ and rotation $\rho_o$ resulting from semi-static GALA analysis of $Y^5$GWALP23 (A) and $Y^{4,5}$GWALP23 (B) in DLPC (black), DMPC (red), and DOPC (blue). Contour levels are drawn at 1, 2, and 3 kHz.
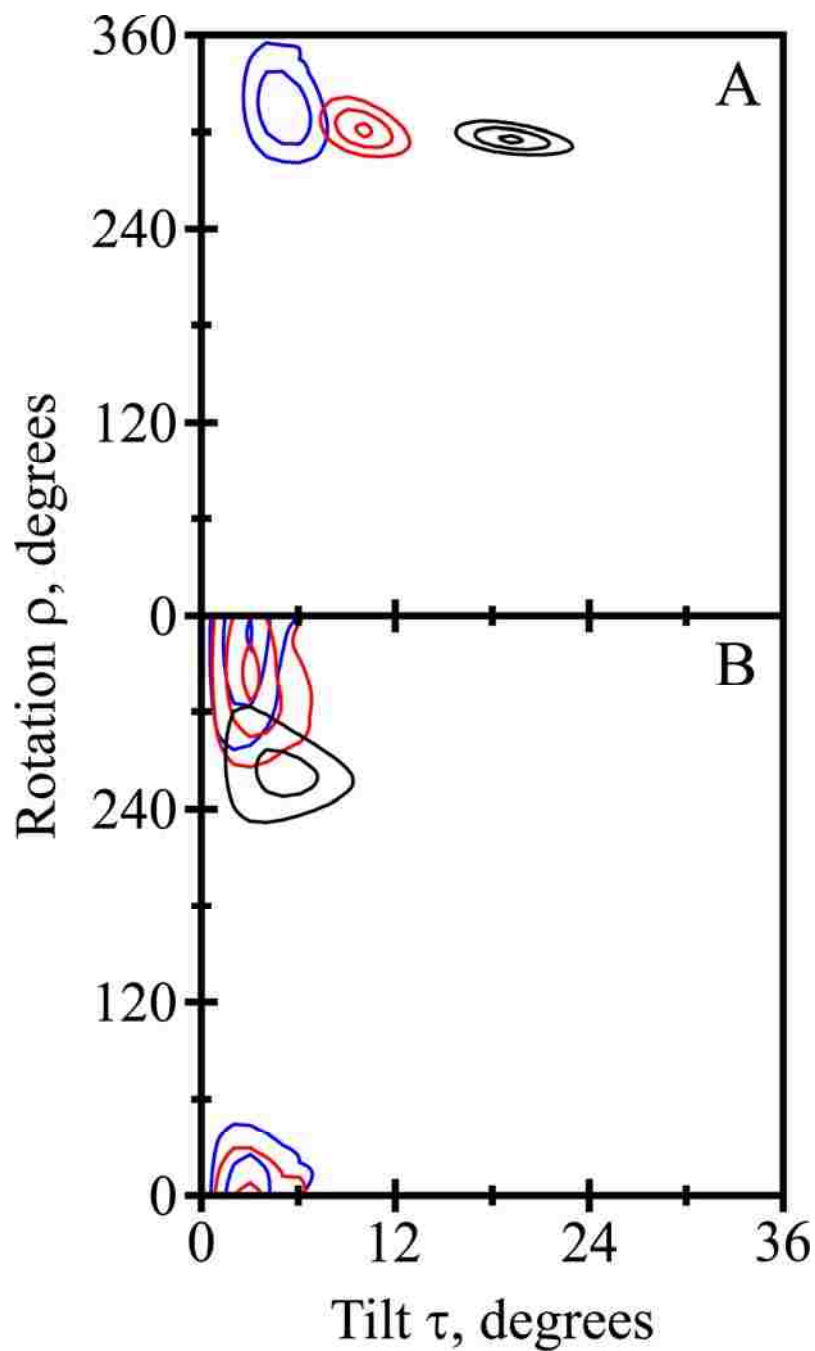
*Figure 8.* Steady-state fluorescence spectra of GWALP23 (black), Y[5]GWALP23 (blue) and Y[4,5]GWALP23 (red) in DLPC vesicles excited at 295 nm.
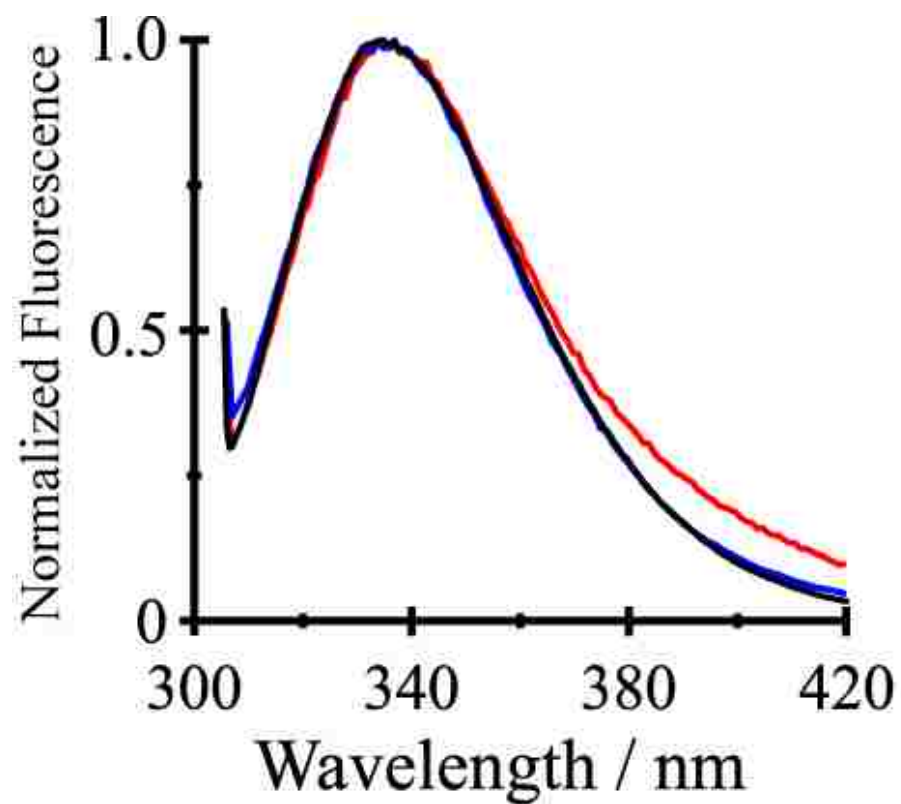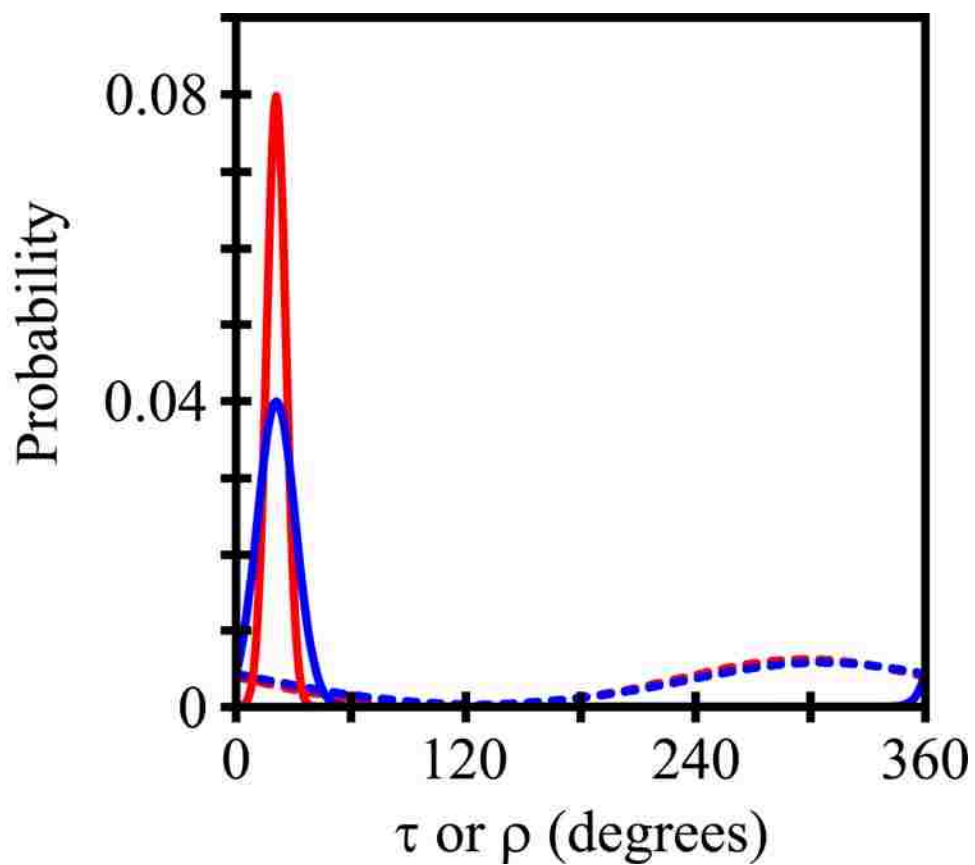
*Figure 9.* Curves to indicate the widths of the τ distributions (solid curves) and ρ distributions (dashed curves) for GWALP23 (red) and Y$^5$GWALP23 (blue), based on Gaussian dynamics analysis of combined GALA and SAMPI4 measurements for each peptide in DMPC.

**2.10 Supporting Information**

*Figure S1*. HPLC analysis of a purified Y$^5$GWALP23 peptide. Absorbance detection at 280 nm.
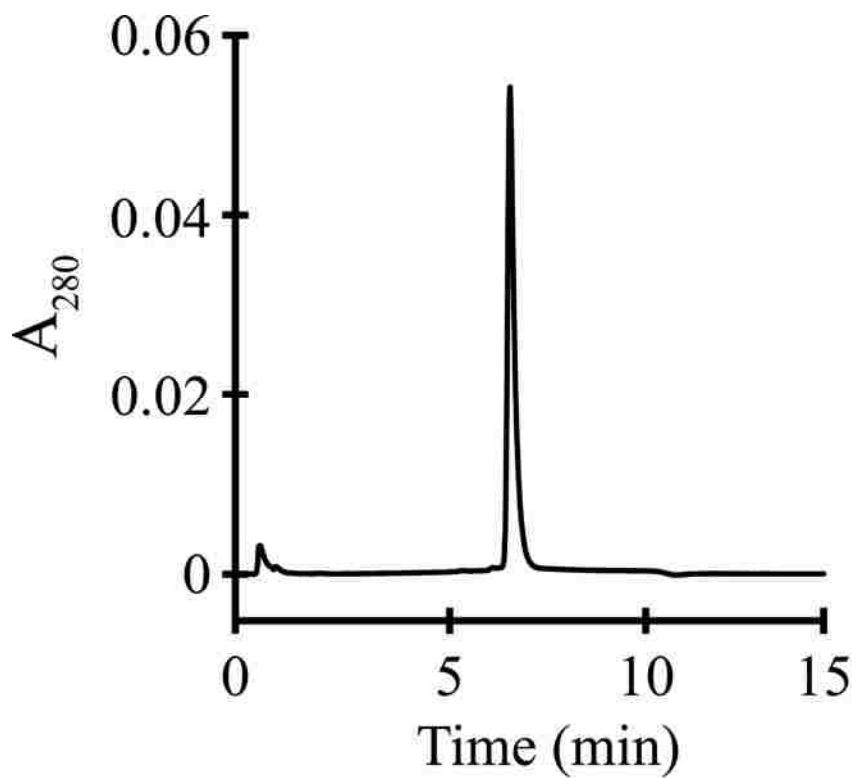
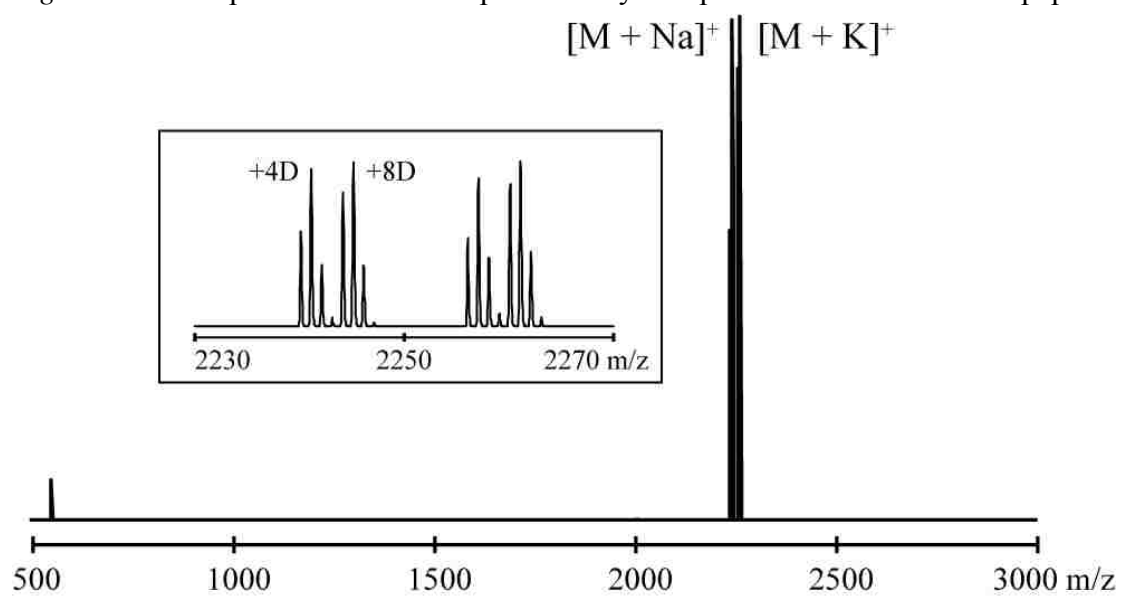*Figure S2.* Example MALDI-Mass spectrometry of a purified GWALP23-like peptide.



$[M + Na]^+$  $[M + K]^+$

+4D    +8D

2230    2250    2270 m/z

500    1000    1500    2000    2500    3000 m/z

*Figure S3.* Example ^{31}P NMR of Y[5]GWALP23 in DLPC oriented sample run at two macroscopically oriented alignments (labeled).

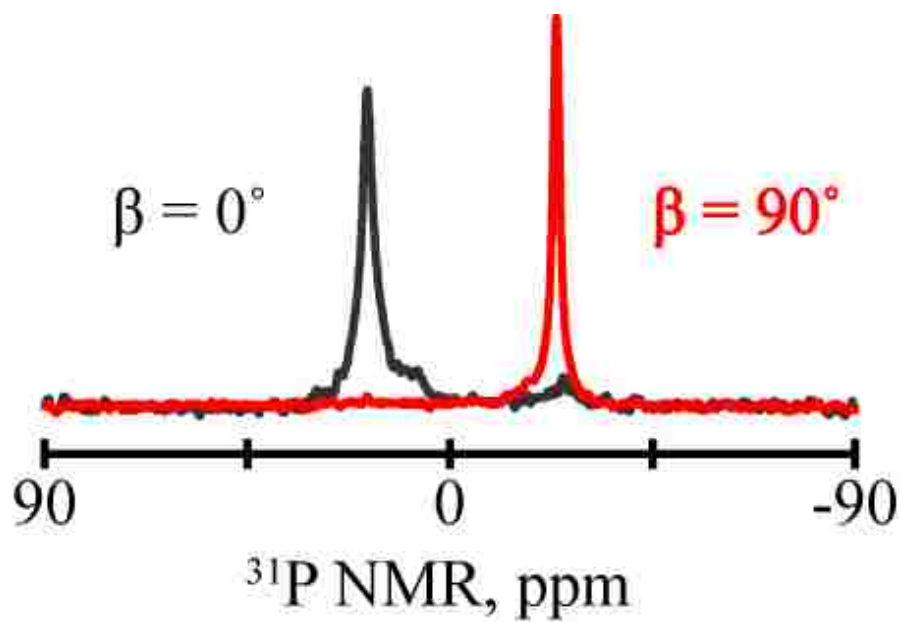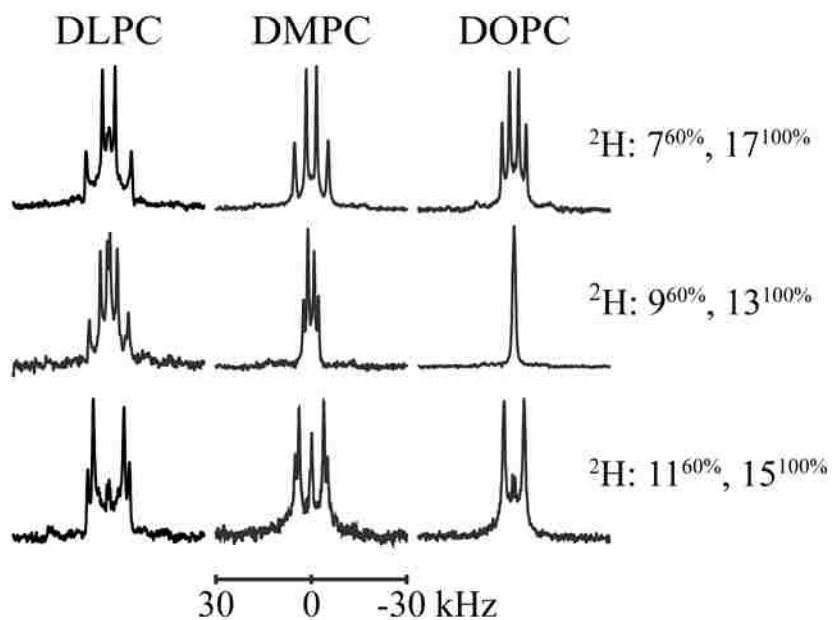*Figure S4.* $^2$H NMR of Y$^5$GWALP23 in lipids at β = 90° (top) and β = 0° (bottom)



Y$^5$GWALP23, β = 90°

DLPC    DMPC    DOPC

$^2$H: 7[60%], 17[100%]

$^2$H: 9[60%], 13[100%]

$^2$H: 11[60%], 15[100%]

30    0    -30 kHz

Y$^5$GWALP23, β = 0°

DLPC    DMPC    DOPC

$^2$H: 7[60%], 17[100%]

$^2$H: 9[60%], 13[100%]

$^2$H: 11[60%], 15[100%]

30    0    -30 kHz

77
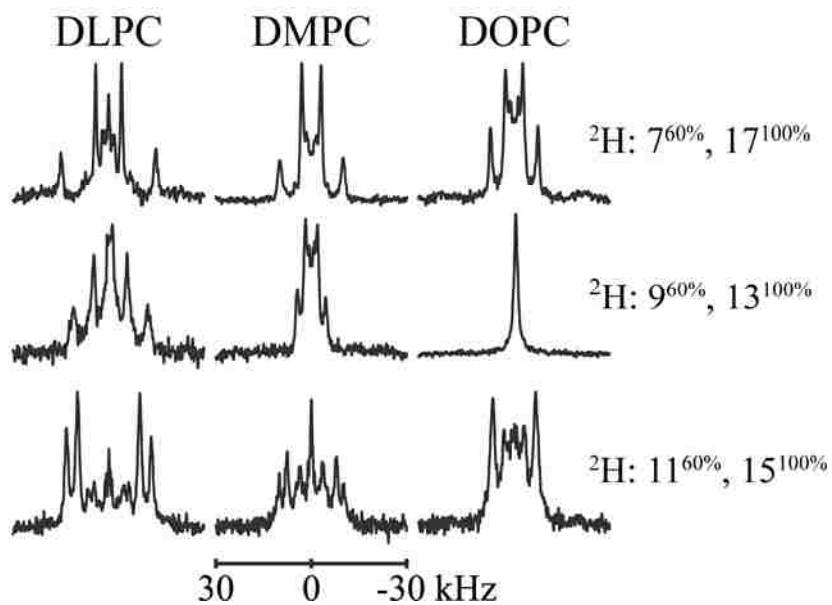
*Figure S5.* $^2$H NMR of Y$^{4,5}$GWALP23 in lipids at β = 90° (top) and β = 0° (bottom).



Y$^{4,5}$GWALP23, β = 90°

DLPC     DMPC     DOPC

$^2$H: 7$^{60\%}$, 17$^{100\%}$

$^2$H: 9$^{60\%}$, 13$^{100\%}$

$^2$H: 11$^{60\%}$, 15$^{100\%}$

30     0     -30 kHz

Y$^{4,5}$GWALP23, β = 0°

DLPC     DMPC     DOPC

$^2$H: 7$^{60\%}$, 17$^{100\%}$

$^2$H: 9$^{60\%}$, 13$^{100\%}$

$^2$H: 11$^{60\%}$, 15$^{100\%}$
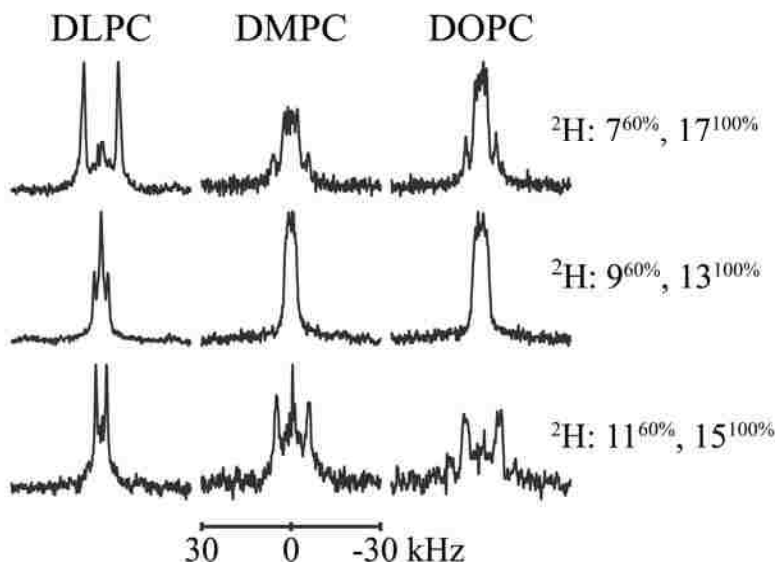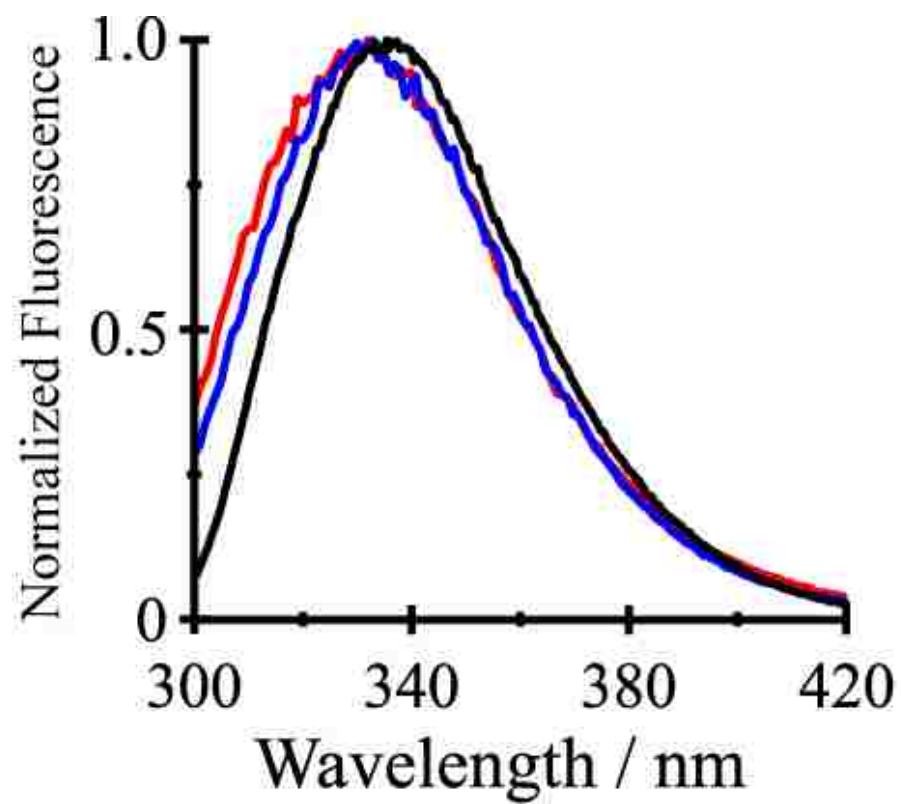
30     0     -30 kHz
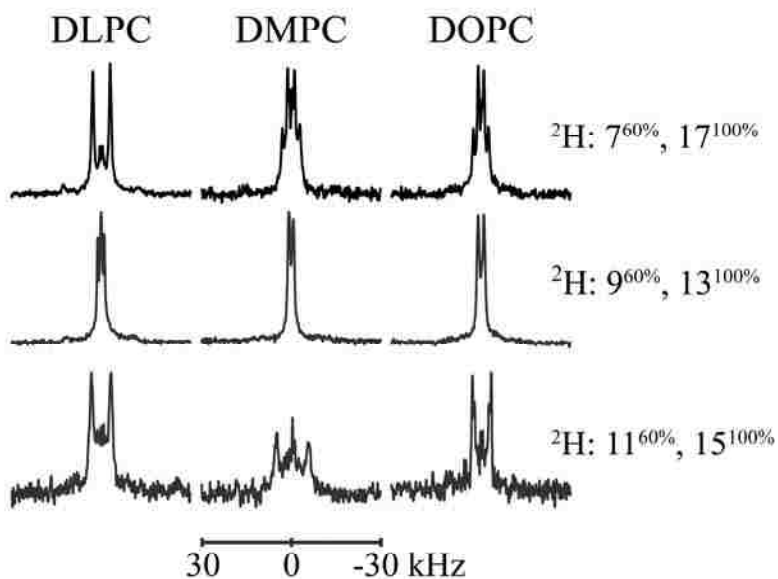
*Figure S6.* Fluorescence spectra of GWALP23 (black), $Y^5$GWALP23 (blue) and $Y^{4,5}$GWALP23 (red) excited @ 280 nm.

## 2.11 Copy Right Clearance Form

**Copyright Clearance Center**

**RightsLink®**

Home    Create Account    Help

**ACS Publications**
High quality High impact

**Title:** Tyrosine Replacing Tryptophan as an Anchor in GWALP Peptides

**Author:** Nicholas J. Gleason et al.

**Publication:** Biochemistry

**Publisher:** American Chemical Society

**Date:** Mar 1, 2012

Copyright © 2012, American Chemical Society

## PERMISSION/LICENSE IS GRANTED FOR YOUR ORDER AT NO CHARGE

This type of permission/license, instead of the standard Terms & Conditions, is sent to you because no fee is being charged for your order. Please note the following:

- Permission is granted for your request in both print and electronic formats.
- If figures and/or tables were requested, they may be adapted or used in part.
- Please print this page for your records and send a copy of it to your publisher/graduate school.
- Appropriate credit for the requested material should be given as follows: "Reprinted (adapted) with permission from (COMPLETE REFERENCE CITATION). Copyright (YEAR) American Chemical Society." Insert appropriate information in place of the capitalized words.
- One-time permission is granted only for the use specified in your request. No additional uses are granted (such as derivative works or other editions). For any other uses, please submit a new request.

BACK      CLOSE WINDOW

# CHAPTER 3

**Single Tryptophan and Tyrosine Comparisons in the N-terminal and C-terminal Interface Regions of GWALP Peptides**

## 3.1 Abstract

Hydrophobic membrane-spanning helices often are flanked by interfacial aromatic or charged residues. Several combinations of anchoring residues have been examined in model WALP-like peptides, which include a pair of like or unlike aromatic or charged residues on each side of a hydrophobic core helix. The peptides acetyl-GGALW$^5$(LA)$_6$LW$^{19}$LAGA-amide and acetyl-GGALY$^5$(LA)$_6$LW$^{19}$LAGA-amide, by contrast, include only a single aromatic residue on each side of the core helix. Compared to the pairs of interfacial aromatic residues, the single aromatic anchors confer markedly less dynamic averaging of the $^2$H and $^{15}$N solid-state NMR observables. It has been found that the substitution of Tyr for Trp near the N-terminus of GWALP23 causes essentially no change in the transmembrane helix tilt and only a 10° azimuthal rotation about the helix axis (Gleason et al. 2012). We now examine the results of Trp $\rightarrow$ Tyr substitution near the C-terminal, by changing W$^{19}$ to Y$^{19}$ in GWALP23, while retaining either W$^5$ or Y$^5$ near the N-terminal. Solid-state $^2$H and $^{15}$N NMR experiments show that Y$^{19}$GW$^5$ALP23 displays nearly identical magnitudes of peptide tilt as Y$^5$GW$^{19}$ALP23 and responds similarly to the changes in bilayer thickness from DLPC to DMPC to DOPC. Y$^{19}$ changes the azimuthal rotation ρ (about the helix axis) to a similar extent as Y$^5$, but in the opposite direction. When tyrosines are substituted for both tryptophans to yield GY$^{5,19}$ALP23, the helix tilt is again of comparable magnitude, and furthermore the preferred azimuthal rotation ρ is relatively unchanged from GWALP23.

**3.2 Introduction**

Membrane proteins present different challenges due to the presence of the heterogeneous lipid bilayer environment. The lipid bilayer membrane has the ability to alter protein dynamics, regulate enzymatic and transport activity, and influence other protein functions (Luo et al. 2009; Carruthers et al. 1984; Brown et al. 1994; Cybulski et al. 2010; Montecucco et al. 1982). Concurrently, membrane proteins can have noticeable effects on the bilayer itself, at times altering bilayer thickness, fluidity, curvature and even the lipid phase (Hong et al. 2004; Yang et al. 1996; Moe et al. 2005; Killian et al. 1996; Killian et al. 1992). With many variables acting simultaneously, it becomes important to understand how individual features contribute to the collective system. For better understanding the orientations and dynamic interactions between transmembrane helix segments and the lipid bilayer, model peptide sequences such as WALP-family peptides (Killian et al. 1996; van der Wel et al. 2002) and more recently GWALP23 (acetyl-GGALW$^5$(LA)$_6$LW$^{19}$AGA-amide) (Vostrikov et al. 2008; Vostrikov et al. 2010a) have been used to establish general rules and allow systematic approaches to properties such as hydrophobic matching and the importance of "anchoring" residues (de Planque et al. 1999; de Planque et al. 2002; Vostrikov and Koeppe 2011a).

Nevertheless, a number of contributing factors may govern the properties of even "simple" model peptides within the bilayer. For example, the peptide acetyl-G**R**ALW$^5$(LA)$_6$LW$^{19}$A**R**A-amide can be seen to increase systematically its tilt as the bilayer thins, to compensate for hydrophobic mismatch when the peptide contains a single Trp residue and a second charged residue within each membrane interface, flanking the core hydrophobic helix (Vostrikov et al. 2010a; Vostrikov and Koeppe 2011a). But upon addition of a second Trp near each terminal (replacing the **R** residues, above), the peptide dynamics increase dramatically

(Vostrikov and Koeppe 2011a), suggesting complex interfacial interactions for the aromatic residues.  Also the apparent loss of response to bilayer thickness suggests that hydrophobic "mismatch" may play a secondary role to the Trp-interface interactions as has been additionally observed in other model systems (de Planque et al. 2003).  Indeed, in the context of physiologically occurring transmembrane proteins, it has been confirmed through sequence surveys and statistical analysis that aromatic residues are preferentially found at the water-lipid interface regions (Landolt-Marticorena et al. 1993; Arkin and Brunger 1998; Ulmschneider et al. 2001).

Previously, we characterized the impact of changing the N-terminal $W^5$ anchor in GWALP23 to $Y^5$ and of introducing a second tyrosine to give the double-Tyr mutant $Y^{4,5}$GWALP23 (Gleason et al. 2012).  While the single $Y^5$ substitution yielded nearly identical peptide behavior (only an ~10° rotation about the helix axis), the $Y^{4,5}$ peptide experienced markedly increased dynamic averaging of NMR observables, behavior that was reminiscent of previous WALP sequences that incorporated multiple Trp anchors on both ends of the peptide.

To further assess the similarities and differences between Trp and Tyr as interfacial aromatic anchoring residues, we have substituted the $W^{19}$ with $Y^{19}$ in GWALP23, to obtain $Y^{19}GW^5$ALP23).  Within this context, one notes that the side chain torsion angles that promote interfacial hydrogen bonding will be different at the N- and C-terminals (van der Wel et al. 2007; Vostrikov and Koeppe 2011a).  Tyrosine terminal placement furthermore has been observed to be more common at the C-terminus in single-span transmembrane α-helices (Landolt-Marticorena et al. 1993).  In addition comparing the N- and C-terminal tyrosine placements, we examine the properties of  $GY^{5,19}$ALP23, in which both tryptophans of GWALP23 are replaced with tyrosine.

### 3.3 Materials and Methods

### Solid Phase Synthesis of $^2$H-Labeled Peptides

Commercial L-alanine-d$_4$ from Cambridge Isotope Laboratories (Andover, MA) was modified with an Fmoc group, as described previously (Thomas et al. 2009), and recrystallized from ethyl acetate:hexane, 80:20. NMR spectra ($^1$H) were used to confirm successful Fmoc-Ala-d$_4$ synthesis. Fmoc-L-Ala-$^{15}$N and Fmoc-L-Leu-$^{15}$N were purchased from Cambridge. Other protected amino acids and acid-labile "Rink" amide resin were purchased from NovaBiochem (San Diego, CA). All peptides were synthesized on a 0.1 mmol scale using "FastMoc™" methods and a model 433A synthesizer from Applied Biosystems by Life Technologies (Foster City, CA). Typically, two deuterated alanines of differing isotope abundances were incorporated into each synthesized peptide. Selected precursors for deuterated residues therefore contained either 100% Fmoc-L-Ala-d$_4$ or 60% Fmoc-L-Ala-d$_4$ with 40% non-deuterated Fmoc-L-Ala. Some peptides were synthesized without deuterium, but with 100% abundance of $^{15}$N in selected residues. The final residue on each peptide was acetyl-Gly to yield a blocked, neutral N-terminal.

A peptide cleavage solution was prepared containing 85% trifluoroacetic acid (TFA) and 5% each (v/v or w/v) of triisopropylsilane, water, and phenol. TFA cleavage from "Rink" resin in 2 mL volume (2-3 h at 22 °C) leads to a neutral, amidated C-terminal. Peptides were precipitated by adding the TFA solution to 25 volumes of cold 50/50 MtBE/hexane. Peptides were collected by centrifugation, washed multiple times with MtBE/hexane, and lyophilized multiple times from (1:1) acetonitrile/water to remove residual TFA. MALDI-TOF mass spectrometry was used to confirm peptide molecular mass (*Figure S1* in Supplementary Material). Peptide purity was examined by reversed-phase HPLC with 280 nm detection, using a

4.6 x 50 mm Zorbax SB-C8 column packed with 3.5 μm octyl-silica (Agilent Technologies, Santa Clara, CA), operated at 1 mL/min using a methanol/water gradient from 85% to 99% methanol (with 0.1% TFA) over five min (*Figure S2* in Supplementary Material). Peptide amounts were measured by means of UV absorbance at 280 nm, using molar extinction coefficients of 5,600 $M^{-1}$ $cm^{-1}$ for each Trp and 1,490 $M^{-1}$ $cm^{-1}$ for each Tyr residue in the peptide (Pace et al. 1995). Solvents were of the highest available purity. Water was doubly deionized Milli-Q™ water.

### $^{2}$H NMR Spectroscopy using Oriented Bilayer samples

Mechanically aligned samples for solid-state NMR spectroscopy (1/60, peptide/lipid) were prepared using DOPC, DMPC or DLPC lipids from Avanti Polar Lipids (Alabaster, AL), and deuterium-depleted water (Cambridge; 45% w/w hydration), as described previously (van der Wel et al. 2002). Bilayer alignment within each sample was confirmed using $^{31}$P NMR at 50 ˚C on a Bruker Avance 300 spectrometer (Billerica, MA) at both $\beta = 0°$ (bilayer normal parallel to magnetic field) and $\beta = 90°$ macroscopic sample orientations (*Figure S3* in Supplementary Material). Deuterium NMR spectra were recorded at 50 ˚C using both sample orientations on a Bruker Avance 300 spectrometer, utilizing a quadrupolar echo pulse sequence (Davis et al. 1976) with 90 ms recycle delay, 3.2 s pulse length and 115 s echo delay. Between 0.6 and 1.5 million scans were accumulated during each $^{2}$H NMR experiment. An exponential weighting function with 100 Hz line broadening was applied prior to Fourier transformation.

### $^{15}$N NMR Spectroscopy using Magnetically Oriented Bicelles

Magnetically oriented bicelles for solid-state $^{15}$N NMR spectroscopy (1/80, peptide/total lipid) were prepared using DMPC-ether and DHPC-ether lipids (3.2/1.0, mol/mol; "q" value) from Avanti Polar Lipids (Alabaster, AL), in a total volume of 175 μL deuterium-depleted water

(Cambridge).  Peptide and DHPC-ether were mixed and then dried under nitrogen flow and vacuum to remove organic solvent.  Separate samples of the separate DMPC-ether lipid also were prepared in aliquots and dried.  Peptide/DHPC-ether films were hydrated using 100 μL water, and DMPC-ether with 75 μL water. After the contents of two separate vials were soluble, the peptide/DHPC-ether solution was transferred to the DMPC-ether solution.  Contents were cycled between 0 °C and 45 °C several times, with intermittent vortexing, until the solution remained clear when cold.  While still cold, the bicelle sample solution was transferred to a 5 mm NMR tube and sealed.

For $^{15}$N-based SAMPI4 experiments (in the same family of pulse sequences as PISEMA), GWALP23 and Y$^5$GWALP23 enriched in $^{15}$N leucine and alanine were synthesized (five labels, residues 13-17). $^{15}$N chemical shifts and $^{15}$N-$^1$H dipolar coupling values were recorded using 500 MHz Bruker Avance and Varian Inova spectrometers and established pulse sequences (Marassi and Opella 2000; Wu et al. 1994; Nevzorov and Opella 2003).  Solid-state NMR high resolution separated local field SAMPI4 experiments (Nevzorov and Opella 2007) were performed using a 1 ms CP contact time, RF field strengths of approximately 50 kHz; 54 t1 points were acquired using 8.0 ms of acquisition time in the direct (t2) dimension and a 7.5 s recycle delay.  The sample temperature was maintained at 42 °C, just below a critical temperature for structural transformation of DMPC/DHPC bicelle samples (Triba et al. 2005).  We have found that the peptide order parameter is essentially unchanged between DMPC/DHPC bicelles at 42 °C and bilayer plate samples at 50 °C (Vostrikov et al. 2011b), where the spectral quality often improves for the plate samples (van der Wel et al. 2007).

**Data Analysis**

Combinations of $^2$H quadrupolar splittings and $^{15}$N/$^1$H dipolar coupling frequencies, individually or together, and in some cases along with $^{15}$N chemical shift values, were used to calculate the orientations of the peptide helix in the bilayers. Data uncertainty was estimated to be within ±0.5 kHz based on duplicate samples and measurements using different orientations of glass slide samples (Vostrikov et al. 2011b). We performed calculations both with a semi-static model and with a more dynamic model that incorporates Gaussian distributions for the tilt and direction of tilt (Strandberg et al. 2009). The detailed strategy for combined $^2$H and $^{15}$N/$^1$H analysis has been described (Vostrikov et al. 2011b).

The analysis using semi-static peptide dynamics involves a principal order parameter $S_{zz}$ to estimate overall peptide motion with respect to an apparent average peptide orientation. These calculations are based on the GALA analysis, as previously described (van der Wel et al. 2002; Strandberg et al. 2009; Strandberg et al. 2004). For samples in DMPC, we incorporate also $^{15}$N/$^1$H dipolar coupling and $^{15}$N chemical shift values obtained from SAMPI4 spectra, to determine a best fit to the experimental data (Nevzorov et al. 2004). These calculations are performed using helix tilt $\tau$, rotation $\rho$ about the helix axis and a principal order parameter $S_{zz}$ as variable parameters. The analysis takes into account the $^2$H quadrupolar splittings and/or $^{15}$N/$^1$H dipolar coupling frequencies and $^{15}$N chemical shifts for the isotope-labeled residues based on ideal $\alpha$-helix geometry.

To proceed beyond a semi-static model, we performed calculations that take into account more complex peptide dynamics, in which $\sigma_\tau$ and $\sigma_\rho$ relate to the widths of Gaussian distributions for the peptide tilt and rotation (Strandberg et al. 2009). In this analysis, a principal order parameter $S_{zz}$ is fixed at 0.88 to reflect isotropic fluctuations; and further anisotropic

87

variations in τ and ρ are permitted. A best-fit RMSD to observed dipolar and quadrupolar couplings, and $^{15}$N chemical shift values, is based upon the parameters $\tau_o$, $\rho_o$, $\sigma_\tau$ and $\sigma_\rho$., following (Strandberg et al. 2009). Fixed parameters in the analysis included chemical shift tensor components ($\sigma_{11}$, $\sigma_{22}$, $\sigma_{33}$) of (64, 77, 224) ppm, as reported for model dipeptides (Saito et al. 2010) and small proteins (Bechinger et al. 2011); a coupling constant of 10.22 kHz (based on an NH bond length of 1.06 Å) (Ketchem et al. 1996; Tian et al. 2003); and the angle $\varepsilon_{//}$ (14°) between the peptide helix axis and the N-H bond. In the combined analysis, equal weights were assigned to the $^{2}$H methyl quadrupolar couplings, $^{15}$N/$^{1}$H dipolar coupling frequencies, and the $^{15}$N chemical shift frequencies. Further details are described in (Vostrikov et al. 2011b) and (Vostrikov and Koeppe 2011a).

## CD Spectroscopy

Small lipid vesicles incorporating 125 nM peptide and 7.5 μM lipid (1/60) were prepared by sonication in unbuffered water. An average of ten scans was recorded on a Jasco (Easton, MD) J710 CD spectropolarimeter, using a 1 mm cell path length, 1.0 nm bandwidth, 0.1 nm slit and a scan speed of 20 nm/min.

## Steady-State Fluorescence Spectroscopy

Vesicle solutions with 1/60 peptide/lipid for fluorescence experiments were prepared by dilution, 1/20 with water, of the samples prepared previously for CD spectroscopy (above). Samples were excited at 280 nm or 295 nm with a 5 nm excitation slit, and emission spectra were recorded between 300 and 420 nm with a 5 nm emission slit using a Hitachi F-2500 fluorescence spectrophotometer. Tyrosine fluorescence contribution can be seen to be negligible by exciting at 295 nm (Supplemental *Figure S9*). The spectra from five to ten scans were averaged.

## 3.4 Results

The designed model peptides (*Table 1*, *Figure 1*) were synthesized successfully, and their identities and high levels of purity (> 95%) were confirmed by RP-HPLC and MALDI-TOF (*Figures S1* and *S2* of the Supporting Information). With the hydrophobic core of GWALP-like peptides consisting entirely of residues with a propensity for α-helix formation (Leu-Ala), a predominantly α-helix secondary structure is expected for the bilayer-incorporated peptides and is indeed confirmed by CD spectra. Mean residue ellipticity (MRE) profiles of each peptide were found in a variety of lipid thicknesses and generally found comparable, but slightly reduced from native GWALP23.

By using solid-state NMR methods and mechanically-aligned samples of peptides incorporated within hydrated lipid-bilayer membranes, one is able to deduce each peptide's average orientation and describe its dynamic properties, with respect to the lipid bilayer. Oriented glass plate samples were first analyzed by $^{31}$P NMR spectroscopy to confirm the alignment of the lipid bilayers. All presented peptide-lipid systems were found to be well-aligned as bilayers, with dominant $^{31}$P resonances at ~ -24 ppm at β = 90° macro-alignment and then ~ +18 ppm at β = 0° (with minimal amounts of unoriented material sometimes seen at ~ -24 ppm in the spectra recorded with β = 0°) (*Figure S3* of the Supporting Information).

Initial visual comparison of $^2$H NMR quadrupolar splittings (from labeled alanines) of novel Y$^{19}$GW$^5$ALP23 and GY$^{5,19}$ALP23 peptides to previous GWALP-like sequences show only minimal deviations in DLPC, DMPC, and DOPC bilayers from that of their precursors (*Figure 2*). This qualitative assessment of the new peptides already suggests that they may adopt similar orientations to that of GWALP23 and Y$^5$GWALP23, which each exhibited a progressively

89

increasing tilt with respect to the degree of hydrophobic mismatch. A small, but noticeable, decrease in experiment signal intensity was seen for the new peptides as compared to GWALP23 or even Y[5]GWALP23. Data was collected for both peptides at six alanine isotope labels located in the helix core (*Table 2*, Supporting Information *Figure S4* and *S5*) and a quadrupolar wave plot was constructed (*Figure 3*). The observed $^2$H quadrupolar splittings were then processed by the GALA analysis using a variable $S_{zz}$ approach using a grid search to screen for a lowest possible RMSD values using $\tau$, $\rho$, and $S_{zz}$ as variables.

The GALA results, listed in *Table 3* and illustrated in *Figure 4*, demonstrate that the hydrophobic helix anchored by Tyr on the C-terminus as well as the Y[5,19] anchored peptide adopt similar magnitudes of tilt, $\tau$, in all respective lipids with a similar scaling to hydrophobic mismatch from previous experiments. Minimal tilts of ~5° in the longer DOPC lipid were measured, followed by median tilts of 9° in DMPC, and larger tilts of ~19° in the shorter DLPC bilayer where greater hydrophobic mismatch occurs. Solution RMSD's were generally higher than that of GWALP or even Y[5]GWALP23 in DLPC, but within normal values for DMPC and DOPC. While the degree of tilt is again largely similar it can inferred from a slight phase shift in the quadrupolar wave plots that there is consistent change in the direction of tilt, $\rho$, for Y[19]GWALP23, especially when compared superimposed to Y[5]GWALP23 (Supplemental *Figure S6*). While it was previously seen that the W5Y mutation of GWALP23 resulted in a ~ -10° change in rotation in all tested lipids, in contrast a W19Y mutation displays a shift in the opposite direction to a similar magnitude. Furthermore, once the identity of both anchors has gone from tryptophan to tyrosine in Y[5,19]GALP23, the contributing Tyr influence appears to cancel out and the peptide rotation does not significantly change from that native GWALP23.

*Figure 5* displays the rho-dependence of anchoring residues in DLPC and a similar trend was exhibited in all tested lipids (Supplemental *Figure S7*).

[15]N-based SAMPI4 experiments were conducted on Y[19]GWALP23 in magnetically-aligned DMPC/DHPC bicelles (3.2:1 mol to mol; ether analogues). The peptide was labeled with ^{15}N in the Leu-Ala core at residues 13 through 17. The obtained PISA wheel (i.e. circle of resonances) is found nearly centered on previous Y[5]GWALP23 spectra, but with a tighter wheel pattern (*Figure 6*). [15]N chemical shift frequencies are found in a smaller range than previous GWALP23 or Y[5]GWALP23 spectra and were found between 89 and 98.3 ppm (*Table 4*) (compared to ~84 to 101 ppm). [15]N/^{1}H dipolar coupling frequencies also exhibited a diminished range from 2.3 to 3.1 kHz (*Table 4*).

With an increased number of NMR observables for Y[19]GWALP23 in DMPC we employed a combined analysis of available data that used a Gaussian treatment of peptide dynamics as well as a semi-static method (Vostrikov et al. 2011b; Vostrikov and Koeppe 2011a). Using quadrupolar splittings of six [2]H-Ala methyl groups, along with the ^{15}N chemical shift frequencies and ^{15}N/^{1}H dipolar coupling frequencies of five core residues, the analysis of 16 restraints produced a well fitting solution with low RMSD (1.1 kHz) (*Figure 7C*). As seen in the quadrupolar and dipolar wave plots (*Figure 7A* and *7B*), independent measurements agree on a orientation of $\tau_o$ of 24° and $\rho_o$ of 321° (*Table 5*). As seen in *Figure 7D*, Y[19]GWALP23 possesses similar dynamics in DMPC compared to GWALP23 and Y[5]GWALP23, but with a smaller $\sigma_\tau$ range of 2° and then a larger $\sigma_\rho$ of 77° (Supplemental *Figure S8*). Semi-static fits using all 16 restraints yield similar results to previous solutions using exclusively [2]H-Ala quadrupolar splittings (*Table 5*), but typically semi-static solutions did not fit the NMR observables as well as the solution using Gaussian dynamics.

Steady-state fluorescence experiments of $Y^{19}$GWALP23 in DOPC vesicles revealed a slightly less polar environment for the remaining Trp anchor when it is on the N-terminus. Indeed, the entire spectrum for $Y^{19}$GWALP23 in DOPC is blue-shifted about 3 nm compared to the spectrum for $Y^{5}$GWALP23 in DOPC (*Figure 8*). The environment surrounding $W^{5}$ is less polar than the environment surrounding $W^{19}$.

**3.5 Discussion**

The initial comparison of Trp versus Tyr anchoring properties was recently evaluated in GWALP-like peptides, in which the two aromatic residues were found to behave very similarly when exchanged on the N-terminus (Gleason et al. 2012). We have further analyzed the system by comparing N- versus C-terminal anchoring by the aromatic Trp and Tyr residues in the GWALP23 model peptide.

The patterns of obtained $^2$H NMR signals illustrated in the quadrupolar wave plots (wave magnitude and phase) in *Figure 3* possess similar characteristics to those of GWALP23 itself as well as Y$^5$GWALP23 (Gleason et al. 2012), which is suggestive of comparable orientations. As further seen by the variable-S$_{zz}$ GALA analysis, Y$^{19}$GWALP23 and GY$^{5,19}$ALP23 adopt a range of tilt magnitudes that are largely dependent on the extent of peptide/lipid hydrophobic mismatch, with greater degrees of tilt occurring in thinner bilayers. This systematic behavior in bilayers of different thickness, and the relatively low RMSD values of the solutions, similar to GWALP23 itself, illustrate peptides are less dynamic than those that possess more than two interfacial aromatic residues, such as WALP19 (van Der Wel et. al. 2002), WALP23 (Strandberg et al. 2004), WWALP23 (Vostrikov et al. 2011b) and Y$^{4,5}$GWALP23 (Gleason et al. 2012).

Though Tyr-19 anchored peptides appear less dynamic as compared to multi-aromatic containing peptides, it would appear they are slightly more dynamic than GWALP23 or even the N-terminally Tyr-anchored Y$^5$GWALP23. The first indication of increased dynamics is the relatively low $^2$H NMR signal intensity that was produced by Y$^{19}$GWALP23 and GY$^{5,19}$ALP23. Typically about 30-50% more scans were required for an equivalent signal-to-noise ratio. The $^{15}$N-based SAMPI4 experiments also demonstrate the increased dynamic averaging, which leads to a reduced diameter for the PISA-wheel of Y$^{19}$GWALP23 (*Figure 6*). In the previously

mentioned WWALP23, though the helix is tilted, that the resonances in the PISA-wheel collapse to a single point of overlapping resonances (Vostrikov and Koeppe 2011a; Vostrikov et al. 2011b). Indeed, the PISA wheel for $Y^{19}$GWALP23 is intermediate between the larger wheel for $Y^5$GWALP23 and the collapsed wheel for WWALP23 (Vostrikov et al. 2011b).

Further analysis of all solid-state NMR observables for $Y^{19}$GWALP23 in DMPC was performed using a combined analysis with explicit Gaussian dynamics that describes the peptide's orientation by means of probability distributions for the tilt magnitude and azimuthal rotation. This method was recently described in detail in (Vostrikov Grant et al. 2011) and has been applied also to $Y^5$GWALP23 (Gleason et al. 2012). Compared to $Y^5$GWALP23, $Y^{19}$GWALP23 displays a similar tilt magnitude, $\tau_0$, in DMPC, but a reduction in $\sigma_\tau$ is observed when moving Tyr from the N- to C-terminal (9° to 2°). This seemingly reduction in $\sigma_\tau$ may be explained by a very wide and shallow plateau of solutions with similar RMSD as $\sigma_\tau$ is varied (*Figure 7D*). While a global minimal with a $\sigma_\tau$ of 2° is obtained, a corresponding solution with $\sigma_\tau = 7°$ would only increase the RMSD by less than 0.03 kHz. Furthermore, due to the shallow solution field, a range of solutions with $\sigma_\tau$ between 0° and 13° all have RMSD within 0.03 kHz of the minimum value of 1.1 kHz.

In contrast, a rather steep and narrow range of solutions exists for $\sigma_\rho$. Looking at all solutions with RMSD less than 1.13 kHz, for a given $\sigma_\tau$, the $\sigma_\rho$ only ranges ± 3° indicating that the $\sigma_\rho$ is better defined than $\sigma_\tau$. The Gaussian distribution of the peptide's rotation (tilt direction) is centered around $\rho_0$ of 321° with a $\sigma_\rho$ of 77°. The larger $\sigma_\rho$ value, compared to $\sigma_\rho$ of 66° for the $Y^5$GWALP23 isomer, is indicative of the peptide's somewhat increased dynamic averaging of the NMR observables, as seen in the respective PISA wheels (*Figure 6*).

These experiments demonstrate the individual influence of interfacial aromatic anchoring residues on the helix tilt direction. Through a range of lipid bilayers, the peptides show consistent shifts in their azimuthal rotation demonstrating specific preferences that related to both the anchor group identity and location. It was previously seen that replacement of Trp-5 with Tyr-5 in GWALP23 produced a ~ 10° shift in azimuthal rotation. The current experiments now show that a change from Trp-19 to Tyr-19 in GWALP23 results in a similar shift in azimuthal rotation, but in the opposite direction. If the argument can be made that each single Trp residue, whether W5 or W19, dominates over Tyr at the other interface, then it would appear that $W^5$ and $W^{19}$ only differ ~ 20° in their rotational preferences, though residues 5 and 19 project 40° apart on a helical wheel.

One can imagine a scenario in which each interfacial aromatic residue is independently trying to influence the helix into an orientation that would best position itself with respect to the lipid head groups and enhance its own hydrogen bonding capabilities. This competition could lead to the high dynamic averaging observed with previous WALP peptides that have multiple aromatic groups, each attempting to fit itself favorably in the bilayer. Within this scenario of ongoing aromatic ring competition, it is known also that the Trp side chain does possess rotational freedom to adapt to a given environment and produce a favorable orientation of the indole (van der Wel et al. 2007). In a bilayer, the C-terminal Trp of any transmembrane peptide is expected to adjust its side chain $\chi 1$ and $\chi 2$ torsion angles so as to "flip" the indole ring in order to reorient the indole amino moiety toward the aqueous phase. This indole reorientation has in fact been observed both for WALP peptides (van der Wel et al. 2007) and for [2]H-labled Trp residues in GWALP23 (Vostrikov and Koeppe 2011a). It was also seen that as the GWALP23

95

helix adopted different orientations in different bilayers, the indole rings themselves also adjusted somewhat independently of the helix to produce an optimal ring placement.

This asymmetry of the C-terminal versus N-terminal anchoring residue placement in a transmembrane helix may be manifest in a physiological context. For examples, Type 1 single-span membrane helices show a preference for tyrosine at the C-terminal (Landolt-Marticorena et al. 1993). Additionally, further statistical analysis that also included polytopic proteins (those with multiple membrane-spanning helices) showed a small preference of Trp for the non-cytoplasmic side (Ulmschneider and Sansom 2001).

It is interesting that when both GWALP23 tryptophans are replaced with tyrosine, the peptide helix adopts a near-identical orientation. It would appear that the net residue contributions cancel out and that the radial placement of the anchoring residues is the predominant factor. Indeed, it was recently shown that azimuthal rotation changes as the radial positions of the anchoring Trp residues are varied in a pairwise fashion within GWALP23 (Vostrikov and Koeppe 2011a). While the chief rotation determinants, in the absence of charged residues, are the radial positions of single aromatic residues at each interface, Trp and Tyr differ by about 10° in their preferences for the helix rotation, such that the identities of the aromatic residues play a small, but important, additional role.

Steady-state fluorescence measurements of WALP and GWALP peptides produce emission spectra that reflect the sum of all present Trp fluorophores. Single Trp-anchored $Y^5$GWALP23 and $Y^{19}$GWALP23 peptides have the advantage of a single fluorescence reporter and potentially can provide more quantitative information about the local environment of the remaining Trp indole ring. The ~ 3 nm blue shift for W5 compared to W19, across the entire emission spectrum, is consistent with our understanding of the helix tilting in the bilayer. Given

that the GWALP23 tilts in the direction of its N-terminal Trp residue (with the C-terminal Trp being only 40° radially offset), W5 becomes further submerged into the non-polar bilayer, while W19 at the same time is more exposed to the aqueous phase by the tilting. The fluorescence emission spectra of $Y^{19}G\mathbf{W^5}ALP23$ and $Y^5G\mathbf{W^{19}}ALP23$ are in line with these conclusions.

## 3.6 Acknowledgments

## 3.7 References

Arkin, I. T. and Brunger, A. T. (1998) Statistical analysis of predicted transmembrane α-helices. *Biochim. Biophys. Acta. 1429*, 113-128.

Bechinger, B., Resende, J. M., and Aisenbrey, C. (2011) The structural and topological analysis of membrane-associated polypeptides by oriented solid-state NMR spectroscopy: established concepts and novel developments. *Biophys. Chem. 153*, 115-125.

Brown, M.F. (1994) Modulation of rhodopsin function by properties of the membrane bilayer. *Chem. Phys. Lipids 73,* 159-180.

Carruthers, A. and Melchior, D. L. (1984) Human Erythrocyte Hexose Transporter Activity Is Governed by Bilayer Lipid Composition in Reconstituted Vesicles. *Biochemistry 23*, 6901-6911.

Cybulski, L. E., Martin, M., Mansilla, M. C., Fernández, A., and de Mendoza, D. (2010) Membrane Thickness Cue for Cold Sensing in a Bacterium. *Current Biology 20*, 1539-1544.

Davis, J. H., Jeffrey, K. R., Bloom, M., Valic, M. I., and Higgs, T. P. (1976) Quadrupolar echo deuteron magnetic resonance spectroscopy in ordered hydrocarbon chains. *Chem. Phys. Lett 42*, 390-394.

de Planque, M. R., Kruijtzer, J. A., Liskamp, R. M., Marsh, D., Greathouse, D. V., Koeppe, R. E. 2nd, de Kruijff, B., and Killian, J. A. (1999) Different membrane anchoring positions of tryptophan and lysine in synthetic transmembrane alpha-helical peptides. *J. Biol. Chem. 274*, 20839-20846.

de Planque, M. R. , Boots, J. W., Rijkers, D. T., Liskamp, R. M. , Greathouse, D. V., and Killian, J. A. (2002) The effects of hydrophobic mismatch between phosphatidylcholine bilayers and transmembrane alpha-helical peptides depend on the nature of interfacially exposed aromatic and charged residues. *Biochemistry 41*, 8396-8404.

de Planque, M. R. R., Bonev, B. B., Demmers, J. A. A., Greathouse, D. V., Koeppe, R. E. 2nd, Separovic, F., Watts, A., and Killian, A. (2003) Interfacial Anchor Properties of Tryptophan Residues in Transmembrane Peptides Can Dominate over Hydrophobic Matching Effects in Peptide-Lipid Interactions. *Biochemistry 42*, 5341-5318.

DeLano, W. L. (2002) The PyMOL Molecular Graphics System.

Gleason, N. J., Vostrikov, V. V., Greathouse, D. V., Grant, C. V., Opella, S. J., and Koeppe, R. E. 2nd. (2012) Tyrosine Replacing Tryptophan as an Anchor in GWALP Peptides. *Biochemistry 51*, 2044-2053.

Hong, H. and Tamm, L. K. (2004) Elastic coupling of integral membrane protein stability to lipid bilayer forces. *Proc. Natl. Acad. Sci. U. S. A. 101*, 4065-4070.

Killian, J. A., Taylor, M. J., and Koeppe, R. E. 2nd (1992) Orientation of the valine-1 side chain of the gramicidin transmembrane channel and implications for channel functioning. A $^2$H NMR study. *Biochemistry 31*, 11283-11290.

Killian, J. A., Salemink, I., de Planque, M. R., Lindblom, G., Koeppe, R. E. 2nd, and Greathouse, D. V. (1996) Induction of nonbilayer structures in diacylphosphatidylcholine model membranes by transmembrane alpha-helical peptides: importance of hydrophobic mismatch and proposed role of tryptophans. *Biochemistry 35*, 1037-1045.

Landolt-Marticorena, C., Williams, K. A., Deber, C. M., and Reithmeier, R. A. (1993) Non-random distribution of amino acids in the transmembrane segments of human type I single span membrane proteins. *J. Mol. Biol. 229*, 602-608.

Luo, W., Cady, S. D., and Hong, M. (2009) Immobilization of the Influenza A M2 Transmembrane Peptide in Virus Envelope-Mimetic Lipid Membranes: A Solid-State NMR Investigation. *Biochemistry 48*, 6361-6368.

Marassi, F. M. and Opella, S. J. (2000) A solid-state NMR index of helical membrane protein structure and topology. *J. Magn. Reson. 144*, 150-155.

Moe, P. and Blount, P. (2005) Assessment of potential stimuli for mechano-dependent gating of MscL: effects of pressure, tension, and lipid headgroups. *Biochemistry 44*, 12239-12244.

Montecucco, C., Smith, G. A., Dabbeni-sala, F., Johannsson, A., and Bisson, R. (1982) Bilayer thickness and enzymatic activity in the mitochondrial cytochrome c oxidase and ATPase complex. *FEBS. Lett. 144,* 145-148.

Nevzorov, A. A. and Opella, S. J. (2003) A "magic sandwich" pulse sequence with reduced offset dependence for high-resolution separated local field spectroscopy. *J. Magn. Reson. 164*, 182-186.

Nevzorov, A. A., Mesleh, M. F., and Opella, S. J. (2004) Structure determination of aligned samples of membrane proteins by NMR spectroscopy. *Magn. Reson. Chem. 42*, 162-171.

Nevzorov, A. A. and Opella, S. J. (2007) Selective averaging for high-resolution solid-state NMR spectroscopy of aligned samples. *J. Magn. Reson. 185*, 59-70.

Pace, C. N., Vajdos, F., Fee, L., Grimsley, G., and Gray, T. (1995) How to measure and predict the molar absorption coefficient of a protein. *Protein Sci. 4*, 2411-23.

Saito, H., Ando, I., and Ramamoorthy, A. (2010) Chemical shift tensor - the heart of NMR: Insights into biological aspects of proteins. *Prog. Nucl. Magn. Reson. Spectrosc. 57*, 181-228.

Strandberg, E., Ozdirekcan, S., Rijkers, D. T., van der Wel, P. C., Koeppe, R. E. 2nd, Liskamp, R. M., and Killian, J. A. (2004) Tilt angles of transmembrane model peptides in oriented and non-oriented lipid bilayers as determined by $^2$H solid-state NMR. *Biophys. J. 86*, 3709-3721.

Strandberg, E., Esteban-Martin, S., Salgado, J., and Ulrich, A. S. (2009) Orientation and dynamics of peptides in membranes calculated from $^2$H-NMR data. *Biophys. J. 96*, 3223-3232.

Thomas, R., Vostrikov, V. V., Greathouse, D. V., and Koeppe, R. E. 2nd (2009) Influence of proline upon the folding and geometry of the WALP19 transmembrane peptide. *Biochemistry 48*, 11883-11891.

Triba, M. N., Warschawski, D. E., and Devaux, P. F. (2005) Reinvestigation by Phosphorus NMR of Lipid Distribution in Bicelles. *Biophys. J. 88*, 1887-1901.

Ulmschneider, M. B. and Sansom, M. P. (2001) Amino acid distributions in integral membrane protein structures. *Biochim. Biophys. Acta 1512*, 1-14.

van der Wel, P. C., Strandberg, E., Killian, J. A., and Koeppe, R. E. 2nd (2002) Geometry and intrinsic tilt of a tryptophan-anchored transmembrane alpha-helix determined by $^2$H NMR. *Biophys. J. 83*, 1479-1488.

van der Wel, P. C. A., Reed, N. D., Greathouse, D. V., and Koeppe, R. E. 2nd (2007) Orientation and Motion of Tryptophan Interfacial Anchors in Membrane-Spanning Peptides. *Biochemistry 46*, 7514–7524.

Vostrikov, V. V., Grant, C. V., Daily, A. E., Opella, S. J., and Koeppe, R. E. 2nd (2008) Comparison of "Polarization inversion with spin exchange at magic angle" and "geometric analysis of labeled alanines" methods for transmembrane helix alignment. *J. Am. Chem. Soc. 130*, 12584-12585.

Vostrikov, V. V., Daily, A. E., Greathouse, D. V., and Koeppe, R. E. 2nd (2010a) Charged or aromatic anchor residue dependence of transmembrane peptide tilt. *J. Biol. Chem. 285*, 31723-31730.

Vostrikov, V. V. and Koeppe, R. E. 2nd (2011a) Response of GWALP Transmembrane Peptides to Changes in the Tryptophan Anchor Positions. *Biochemistry 50*, 7522-7535.

Vostrikov, V. V., Grant, C. V., Opella, S. J., and Koeppe, R. E. 2nd (2011b) On the Combined Analysis of $^2$H and $^{15}$N/$^1$H Solid-State NMR Data for Determination of Transmembrane Peptide Orientation and Dynamics. *Biophys. J. 101*, 2939-2947.

Wu, C. H., Ramamoorthy, A., and Opella, S. J. (1994) High-Resolution Heteronuclear Dipolar Solid-State NMR Spectroscopy. *J. Magn. Reson. A 109*, 270-272.

Yang, F. Y. and Hwang, F. (1996) Effect of non-bilayer lipids on the activity of membrane enzymes. *Chem. Phys. Lipids 81*. 197-202.

**3.8 Tables**

*Table 1.* Sequences of GWALP23-like peptides[a]

| Name | Sequence |
|------|----------|
| GWALP23 | a-GGALW$^5$LALALALALALALW$^{19}$LAGA-e |
| Y$^5$GWALP23 | a-GGALY$^5$LALALALALALALW$^{19}$LAGA-amide |
| Y$^{19}$GWALP23 | a-GGALW$^5$LALALALALALALY$^{19}$LAGA-amide |
| Y$^{5,19}$GALP23 | a-GGALY$^5$LALALALALALALY$^{19}$LAGA-amide |

[a]Abbreviations: "a" denotes "acetyl" and "e" denotes "ethanolamide."

*Table 2.* Observed $^2$H quadrupolar splittings[a] for Tyr-based analogues of GWALP23 in three lipid bilayers.

| Ala-d$_4$ | DLPC | | | DMPC | | | DOPC | | |
|---|---|---|---|---|---|---|---|---|---|
| | [b]Y$^5$ | Y$^{19}$ | Y$^{5,19}$ | [b]Y$^5$ | Y$^{19}$ | Y$^{5,19}$ | [b]Y$^5$ | Y$^{19}$ | Y$^{5,19}$ |
| 7 | 29.3 | 25.6 | 18.8 | 20.6 | 20.1 | 19.2 | 15.1 | 14.2 | 13.9 |
| 9 | 24.0 | 20.9 | 18.0 | 9.2 | 8.0 | 7.5 | 0.5 | 0.5 | 0.5 |
| 11 | 26.4 | 23.2 | 20.1 | 20.3 | 20.5 | 19.4 | 13.0 | 14.9 | 14.0 |
| 13 | 10.5 | 14.8 | 9.7 | 3.9 | 7.2 | 4.2 | 0.5 | 0.5 | 0.5 |
| 15 | 19.5 | 19.6 | 18.9 | 15.6 | 20.2 | 15.9 | 13 | 14.9 | 14.0 |
| 17 | 8.1 | 0.8 | 4.2 | 6.3 | 0.5 | 3.4 | 5.5 | 1.0 | 3.9 |

[a]Quadrupolar splittings are reported in kHz for the β = 0° sample orientation of Y$^5$GWALP23, Y$^{19}$GWALP23, and Y$^{5,19}$GALP23.  Each value is an average of (the magnitude observed when β = 0°), and (twice the magnitude observed when β = 90°).

[b]Y$^5$GWALP23 values from (Gleason et al. 2012)

*Table 3.* Semi-static GALA analysis of GWALP23-like Tyr analogues[a]

| Peptide | DLPC | | | | DMPC | | | | DOPC | | | |
|---|---|---|---|---|---|---|---|---|---|---|---|---|
| | $\tau$ | $\rho$ | $S_{zz}$ | RMSD (kHz) | $\tau$ | $\rho$ | $S_{zz}$ | RMSD (kHz) | $\tau$ | $\rho$ | $S_{zz}$ | RMSD (kHz) |
| [b]$Y^5$ | 19° | 295° | 0.78 | 0.7 | 10° | 300° | 0.81 | 0.39 | 5° | 310° | 0.81 | 0.88 |
| $Y^{19}$ | 19° | 310° | 0.67 | 1.0 | 9° | 323° | 0.87 | 0.87 | 5° | 336° | 0.83 | 0.77 |
| $Y^{5,19}$ | 19° | 305° | 0.58 | 1.6 | 9° | 311° | 0.8 | 0.37 | 5° | 325° | 0.83 | 0.50 |

[a]Calculations based on six Ala methyl $^2$H quadrupolar splittings only.

[b]Values for $Y^5$GWALP23 from reference (Gleason et al. 2012).

*Table 4.* Dipolar couplings and $^{15}N$ chemical shift values for peptide's $^{15}N/^{1}H$ groups[a]

| Residue | Y[19]GWALP23 | |
| --- | --- | --- |
| | $^{15}N$, ppm | $^{15}N/^{1}H$, kHz |
| 13 | 98.2 | 2.9 |
| 14 | 91.4 | 2.3 |
| 15 | 89 | 2.7 |
| 16 | 90.9 | 3.1 |
| 17 | 98.3 | 2.6 |

[a]Samples were measured in magnetically-oriented DMPC/DHPC bicelles and correspond to a $\beta = 90°$ sample orientation.

*Table 5.* Calculated orientations and dynamics of peptides in DMPC[a]

| Peptide | Model | $\tau_0$ | $\sigma_\tau$ | $\rho_0$ | $\sigma_\rho$ | $S_{zz}$ | RMSD (kHz) | n[b] |
|---------|-------|----------|---------------|----------|---------------|----------|------------|------|
| GWALP23 | Gaussian | 21° | 5° | 306° | 70° | 0.88[c] | 1.1 | 16 |
|  | semi-static | 11° | n.a.[d] | 307° | n.a.[d] | 0.75 | 1.2 | 16 |
| Y[5]GWALP23 | Gaussian | 21° | 9° | 298° | 66° | 0.88[c] | 1.2 | 16 |
|  | semi-static | 12° | n.a.[d] | 298° | n.a.[d] | 0.73 | 1.2 | 16 |
| Y[19]GWALP23 | Gaussian | 24° | 2° | 321° | 77° | 0.88[c] | 1.1 | 16 |
|  | semi-static | 11° | n.a.[d] | 322° | n.a.[d] | 0.72 | 1.3 | 16 |

[a]The Gaussian model for the dynamics uses a fixed principal order parameter $S_{zz}$ (Strandberg et al. 2009), representing the dynamic extent of (mis)alignment (angle $\alpha$) between the molecular $z$-axis and its average orientation, characterized by the time average $S_{zz} = \langle 3 \cos^2\alpha - 1 \rangle/2$ (Pulay et al. 2005). Within this context, further motions can be characterized by the widths $\sigma_\tau$ and $\sigma_\rho$ of Gaussian distributions about the average values of tilt magnitude $\tau_0$ and tilt direction $\rho_0$ (Strandberg et al. 2009). An alternative semi-static analysis, using three parameters instead of four, determines the best fit (lowest RMSD, in kHz) as a function of $\tau_0$, $\rho_0$ and a variable $S_{zz}$.

[b]Number of data points (from Tables 2-3), identified as six $^2$H methyl quadrupolar couplings, either alone or with five $^{15}$N/$^1$H dipolar couplings and $^{15}$N chemical shifts.

[c]Fixed value.

[d]Not applicable.

## 3.9 Figures

*Figure 1*.  Representative models of GWALP23, Y[19]GWALP23 and GY[5,19]ALP23 (left to right), showing the locations of aromatic side chains on a ribbon helix, drawn using PyMOL (DeLano et al. 2002). The side chain orientations are arbitrary.
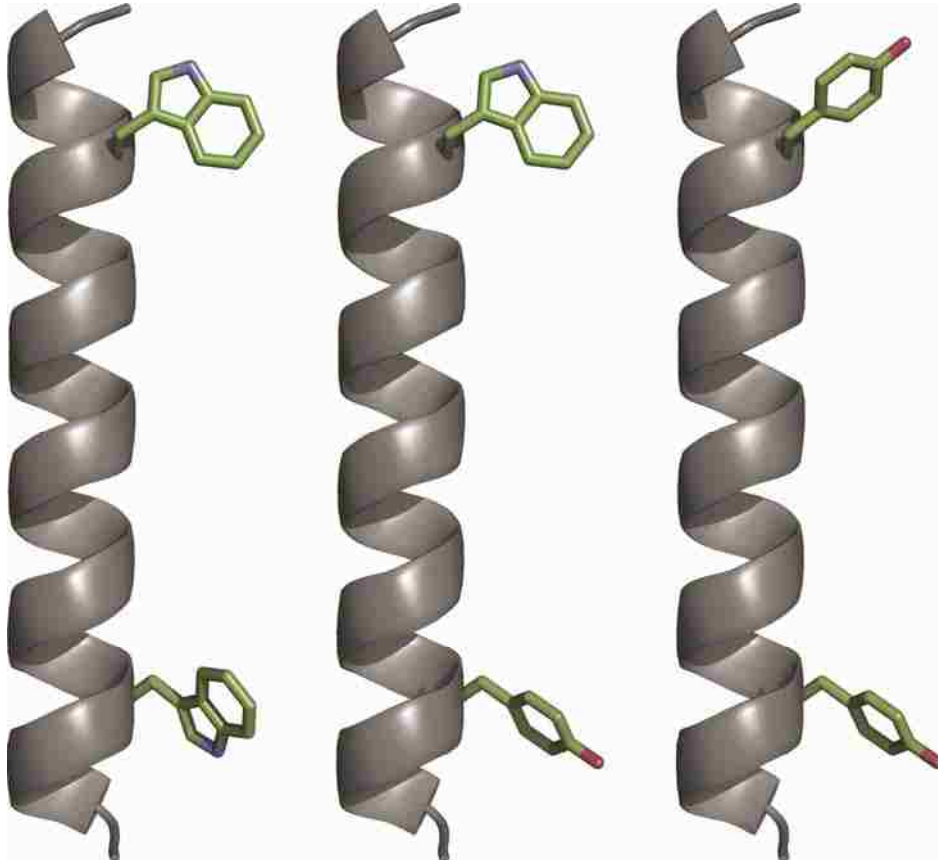
*Figure 2.* $^2$H NMR spectra of (top to bottom) Y$^{19}$GWALP23 and Y$^{5,19}$GALP23, each labeled at Ala$^{17}$ (100% $^2$H) and Ala$^7$ (60% $^2$H), in hydrated oriented bilayers of DLPC, DMPC and DOPC. Peptide/lipid ratio, 1/60 (mol/mol); 50 °C; β = 90° sample orientation. Complete spectra set of all Ala-d$_4$ labels included in Supplemental *Figure S4* and *S5*.
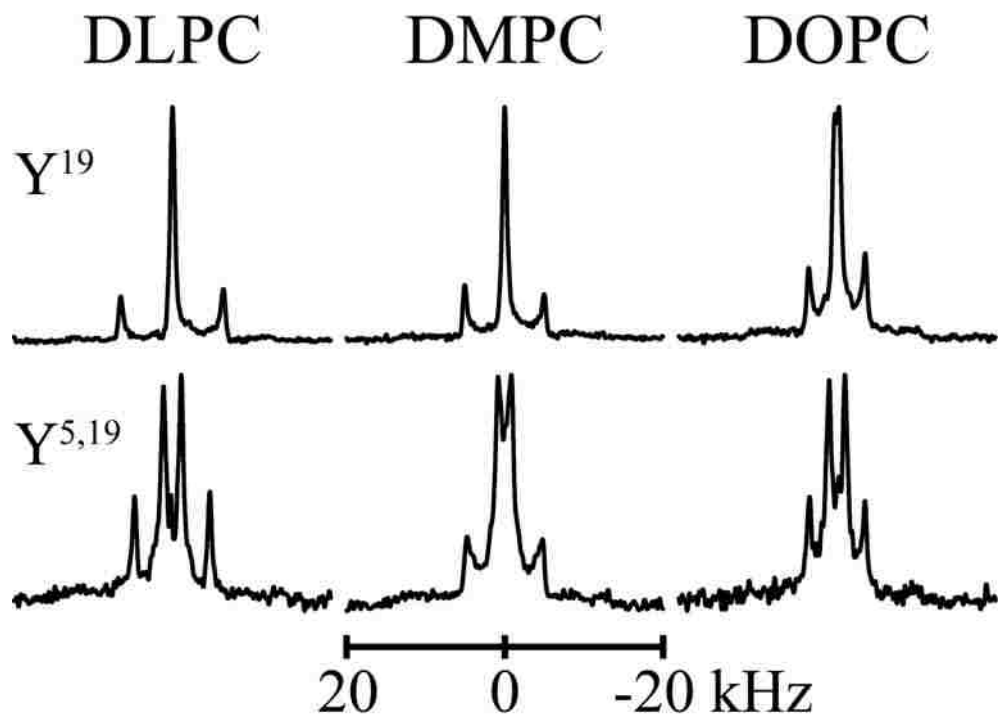
*Figure 3*. GALA semi-static analysis of Ala-d$_4$ quadrupolar splittings using variable S$_{zz}$ (see van der Wel et al. 2002). Quadrupolar wave plots are shown for Y[19]GWALP23 (A) and GY[5,19]ALP23 (B) in oriented bilayers of DLPC (black squares), DMPC (red circles) and DOPC (blue triangles). Fitted curves represent theoretical Δν$_q$ values for orientations corresponding to best-fit values of τ and ρ.
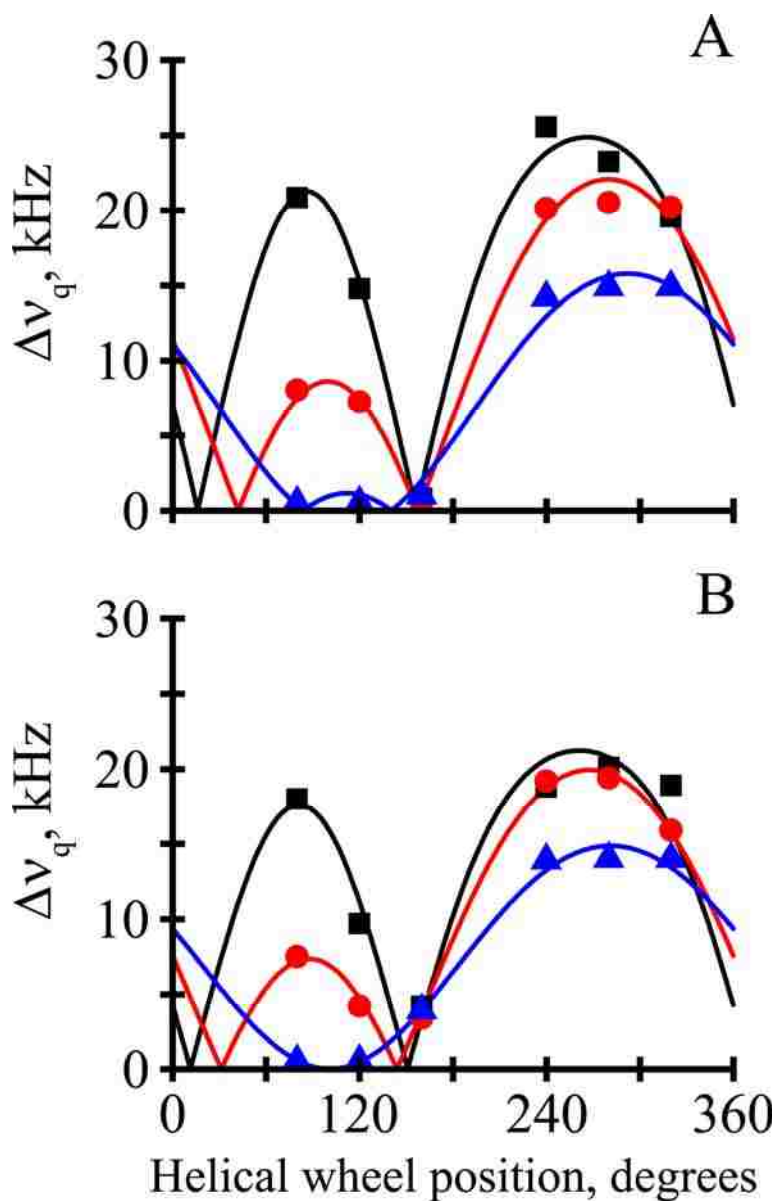
*Figure 4.* RMSD contour plots for apparent average tilt $\tau$ and rotation $\rho$ resulting from semi-static GALA analysis of Y[5]GWALP23 (A), Y[19]GWALP23 (B) and GY[5,19]ALP23 (C) in DLPC (black), DMPC (red), and DOPC (blue). Contour levels are 1 kHz with outside corresponding to 3 kHz.
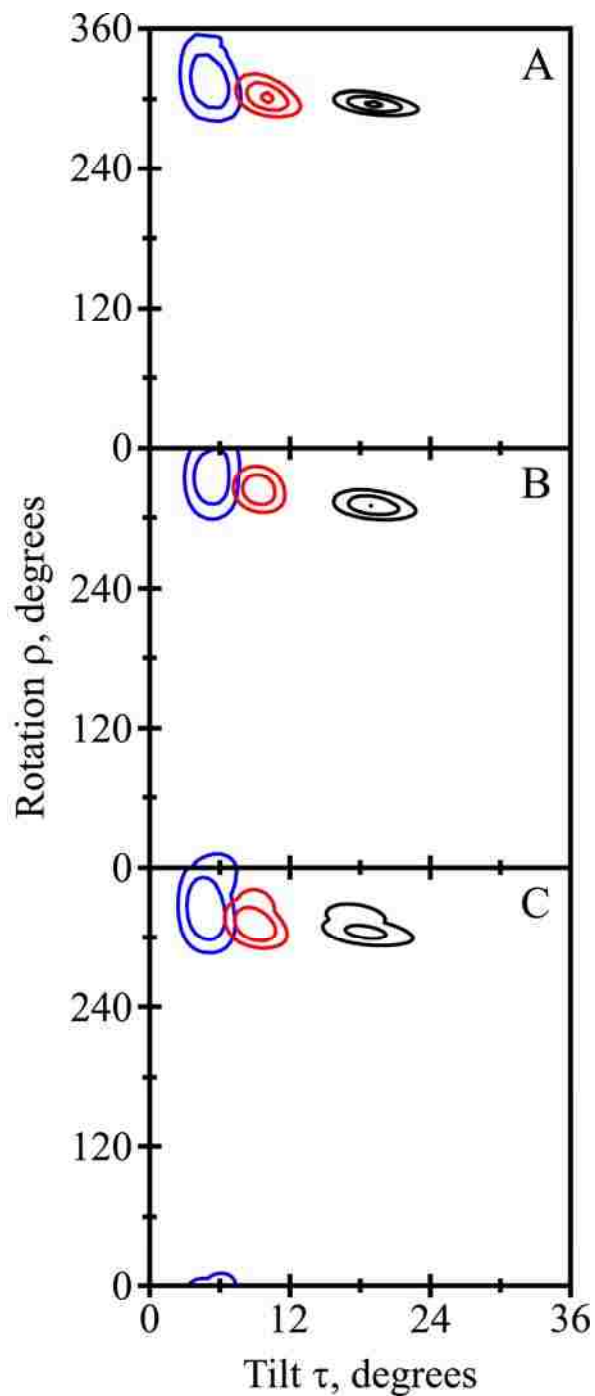
*Figure 5.* Rho-dependence of anchoring residues in DLPC. Radial positions of anchors are labeled in context to the tilt direction, rho.
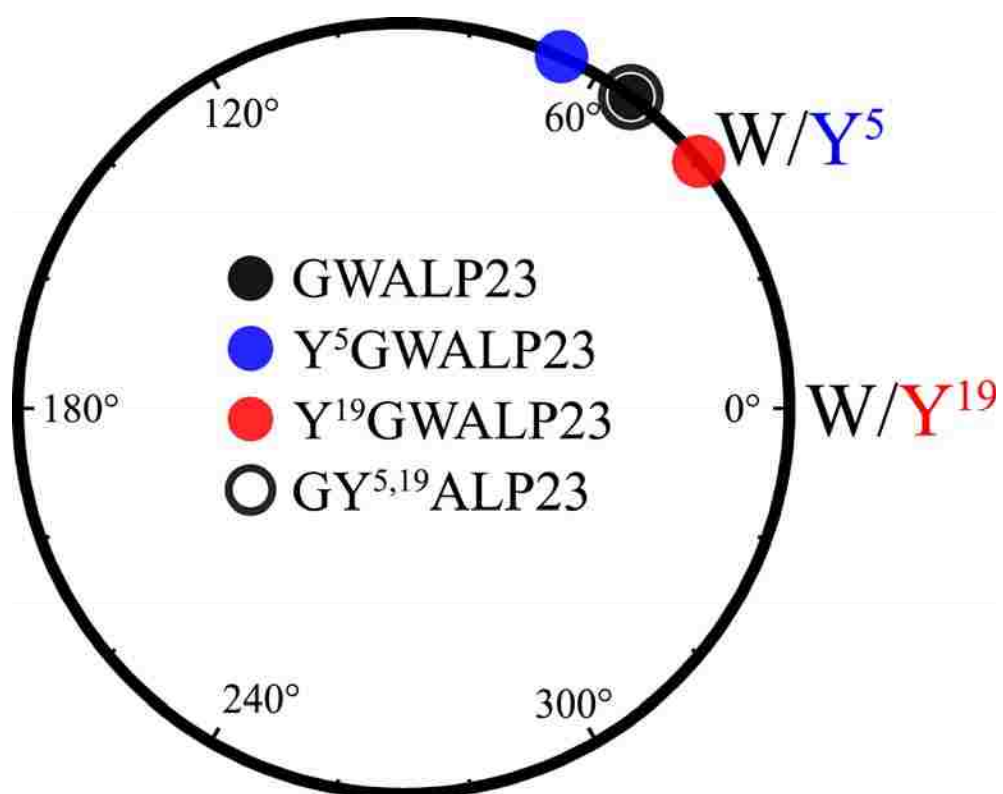
*Figure 6.* SAMPI4 spectra, with assignments, for Y[19]GWALP23 (red) and Y[5]GWALP23, each $^{15}N$ labeled in residues 13-17. Peptide/lipid ratio, 1/80 (mol/mol); 42 °C; bicelles of DMPC/DHPC (q = 3.2).
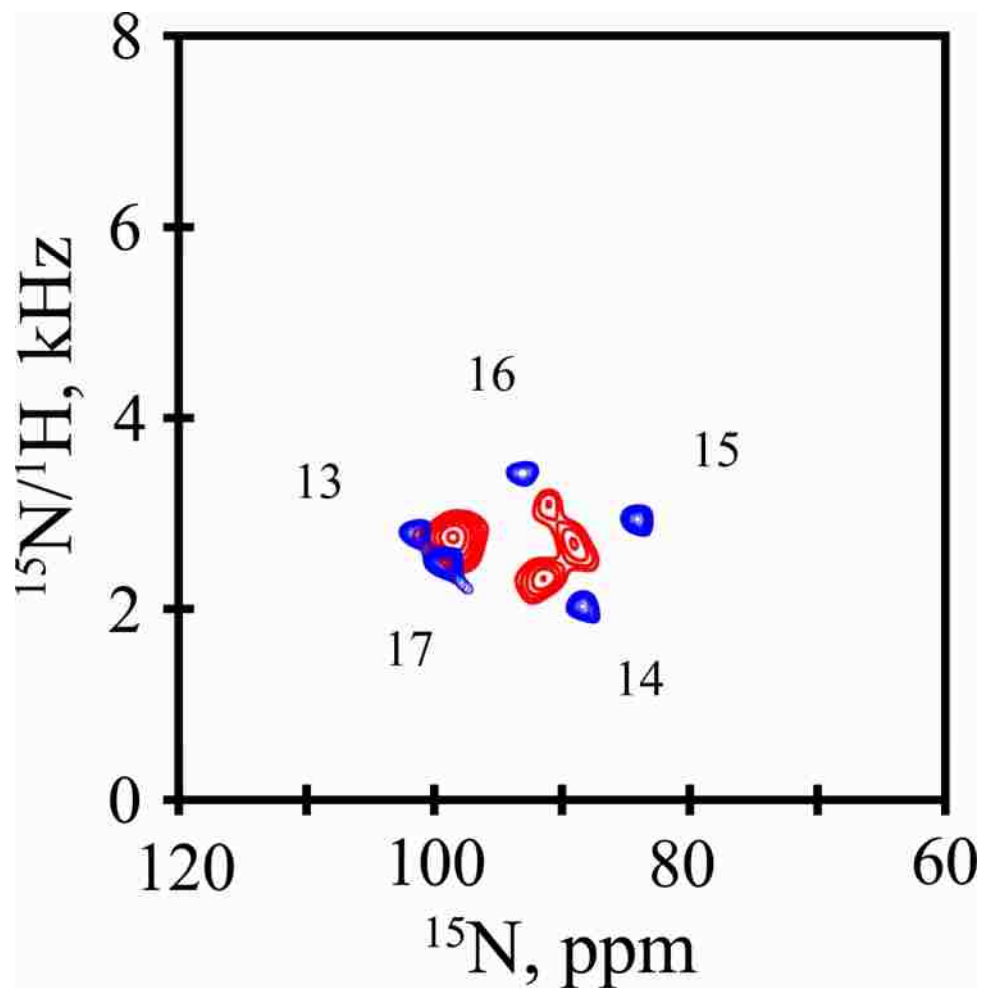
*Figure 7.* Combined $^{15}N$ and $^{2}H$ analysis for $Y^{19}GWALP23$ in DMPC. A. Quadrupolar waves from Gaussian dynamics (black curve) and semi-static (red curve) analysis. B. Dipolar waves from Gaussian (black curve) and semi-static (red curve) analysis. C. RMSD ($\tau_o$, $\rho_o$) graph for the Gaussian (black contours) and semi-static (red contours) analyses, contoured at 2 and 3 kHz. D. RMSD ($\sigma_\tau$, $\sigma_\rho$) graph for the Gaussian dynamics analysis, from 1.10 to 1.19 kHz in 0.03 kHz contours.
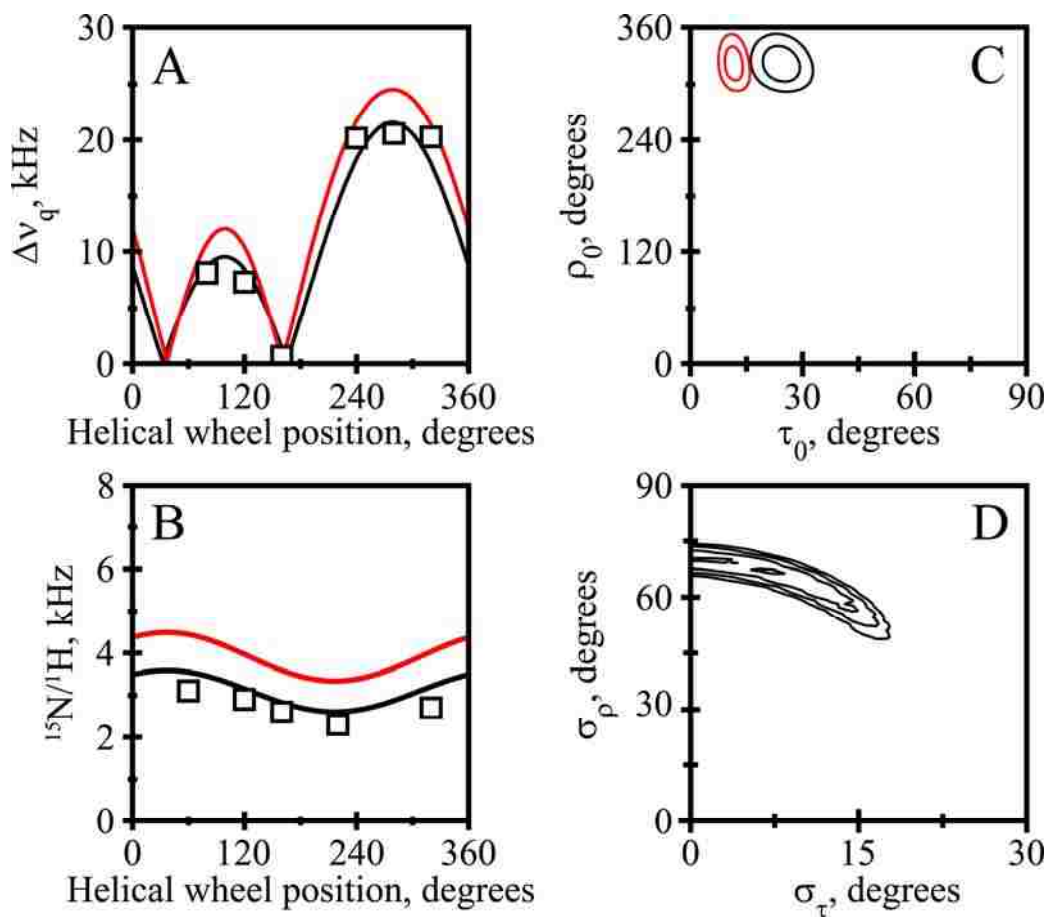
*Figure 8.* Steady-state fluorescence spectra of $Y^{19}$GWALP23 (black) and $Y^5$GWALP23 (red) in DOPC vesicles excited at 295 nm.
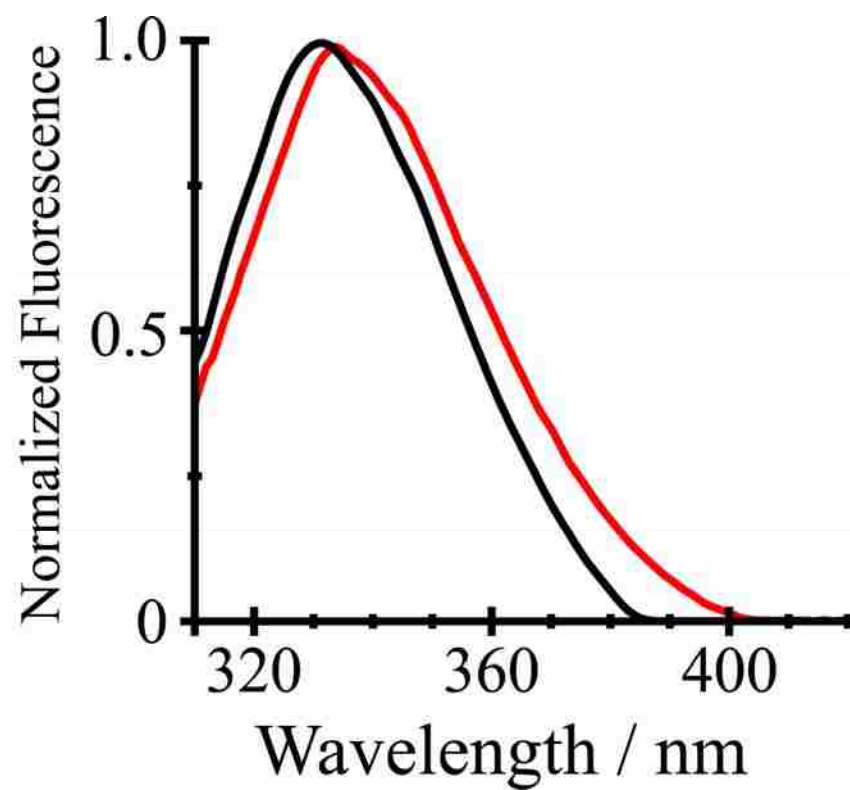
## 3.10 Supporting Information

*Figure S1.* Peptide identity confirmation by MALDI-TOF Mass spectrometry of a Y[19]GWALP23 peptide with two Ala-d₄ labels (50% and 100%)
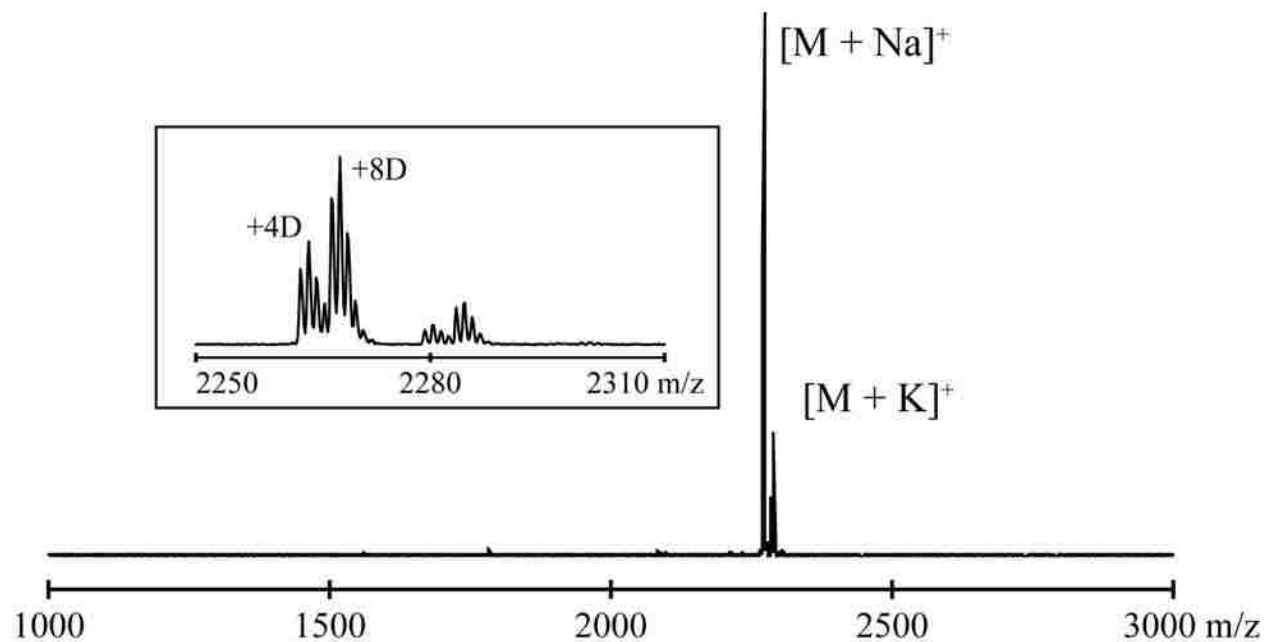
*Figure S2*. RP-HPLC analysis of GWALP23-like peptides for purity determination.  Absorbance measured at 280 nm.
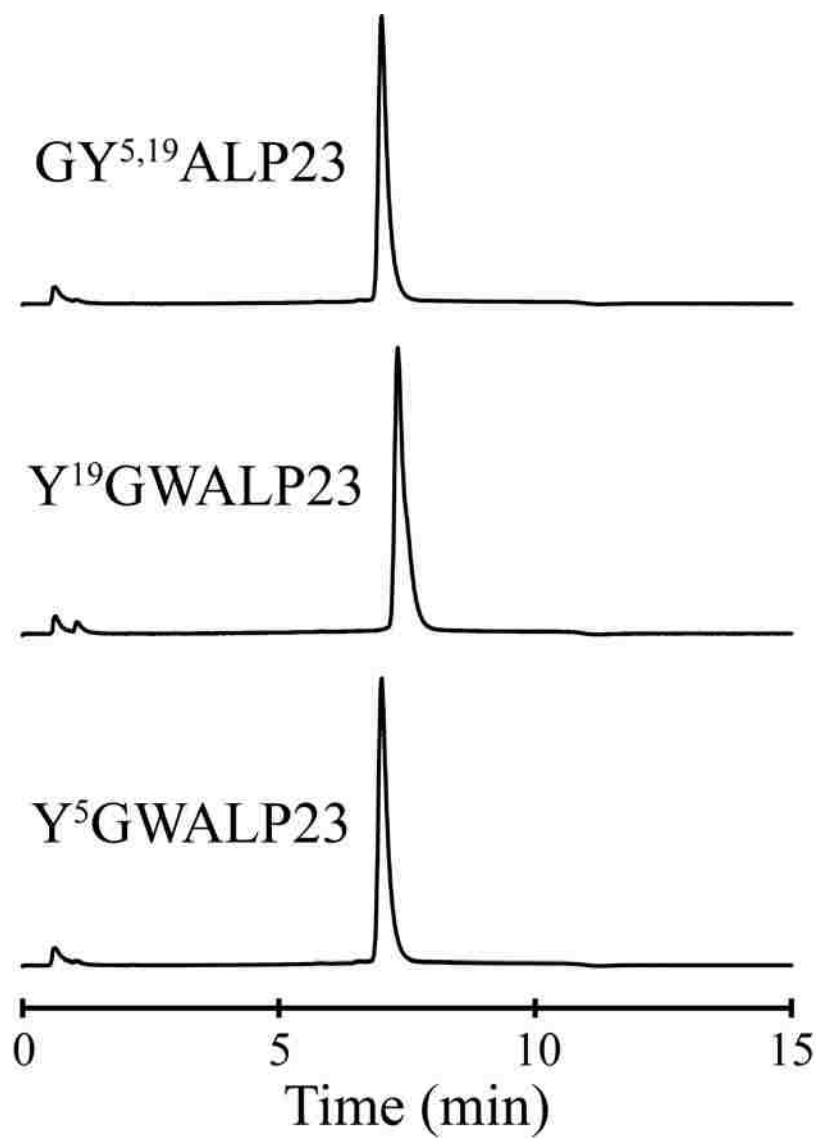


GY$^{5,19}$ALP23

Y$^{19}$GWALP23

Y$^{5}$GWALP23

Time (min)

*Figure S3.* Bilayer alignment confirmation of oriented samples by ^{31}P NMR. Y[19]GWALP23 shown in lipid at two macroscopically oriented alignments.
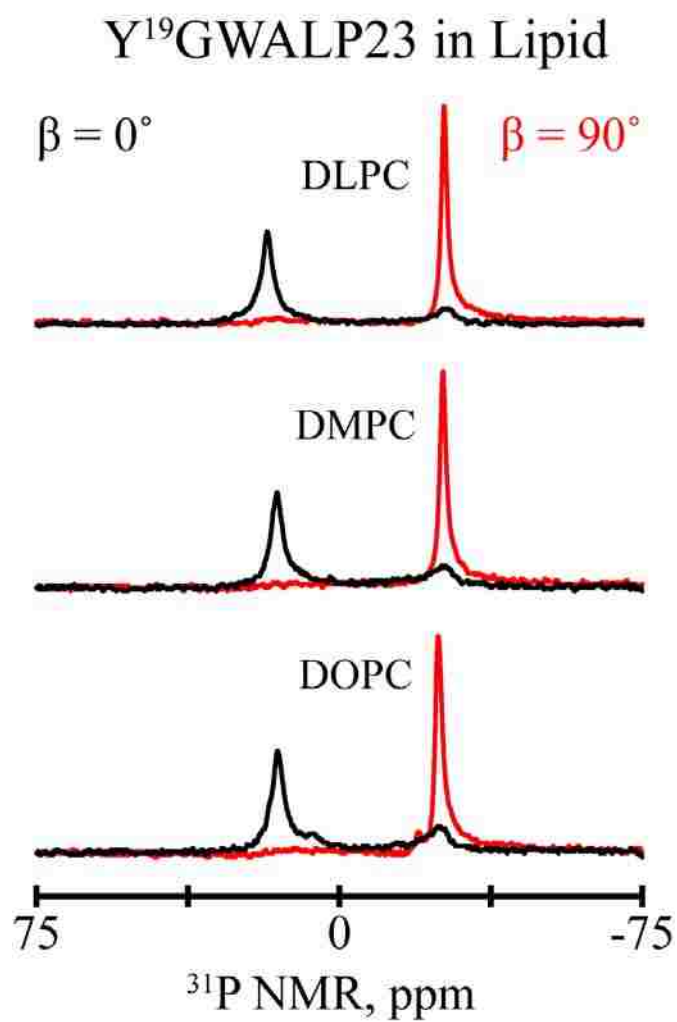


Y[19]GWALP23 in Lipid

$\beta = 0°$

$\beta = 90°$

DLPC

DMPC

DOPC

75    0    -75

^{31}P NMR, ppm

*Figure S4.* $^2$H NMR spectra for Y$^{19}$GWALP23 in lipids.



Y$^{19}$GWALP23, β = 90°

DLPC          DMPC          DOPC

$^2$H: 7$^{60\%}$, 17$^{100\%}$

$^2$H: 9$^{60\%}$, 13$^{100\%}$

$^2$H: 11$^{60\%}$, 15$^{100\%}$

30      0      -30 kHz

Y$^{19}$GWALP23, β = 0°

DLPC          DMPC          DOPC

$^2$H: 7$^{60\%}$, 17$^{100\%}$

$^2$H: 9$^{60\%}$, 13$^{100\%}$

$^2$H: 11$^{60\%}$, 15$^{100\%}$

30      0      -30 kHz

118
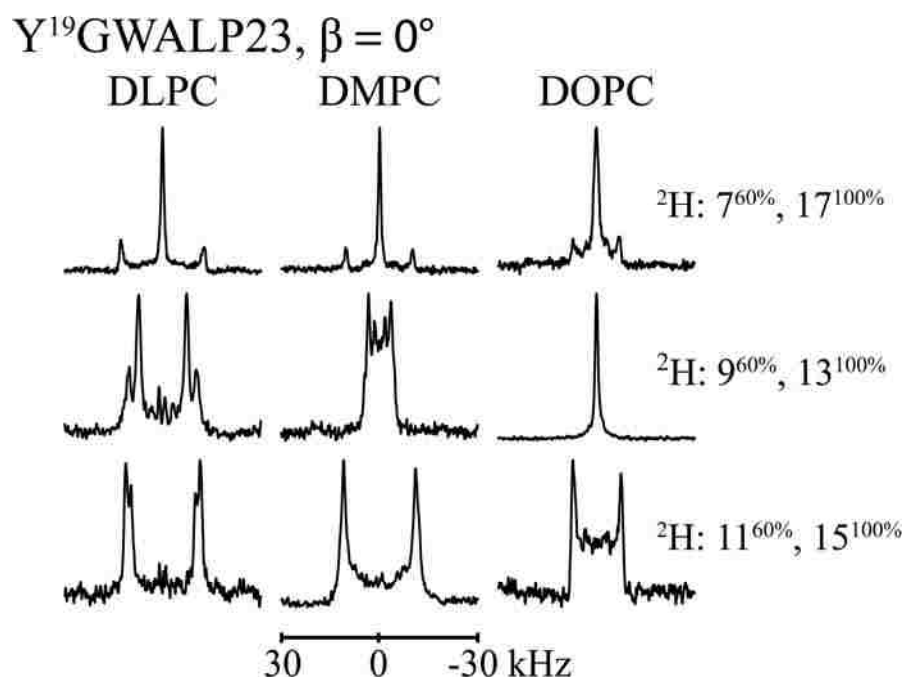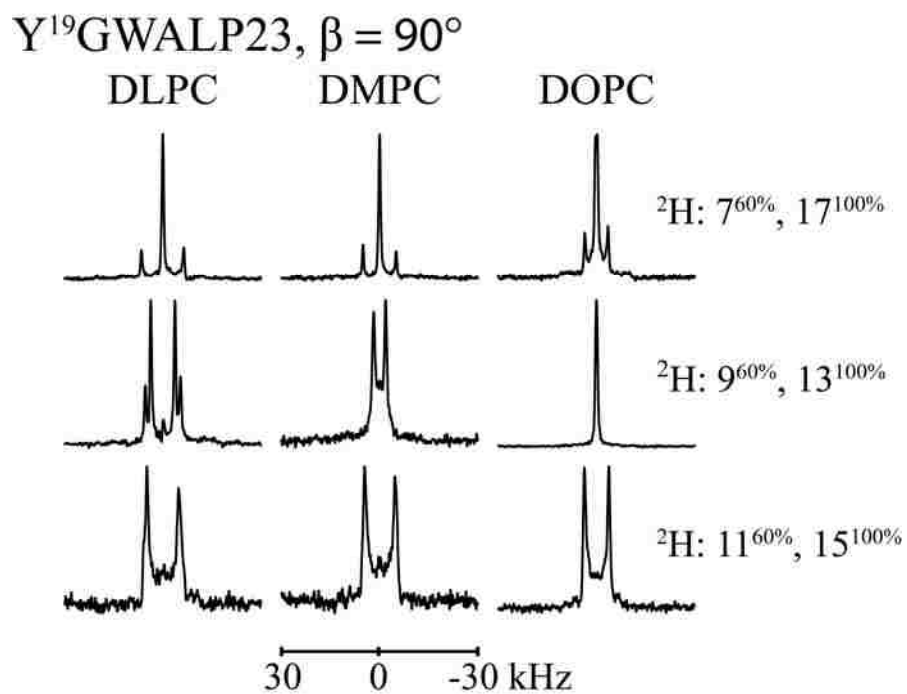
*Figure S5*. $^2$H NMR spectra for GY$^{5,19}$ALP23 in lipids.



Y$^{5,19}$GALP23, β = 90°

DLPC        DMPC        DOPC

$^2$H: 7$^{60\%}$, 17$^{100\%}$

$^2$H: 9$^{60\%}$, 13$^{100\%}$

$^2$H: 11$^{60\%}$, 15$^{100\%}$

30        0        -30 kHz

Y$^{5,19}$GALP23, β = 0°

DLPC        DMPC        DOPC

$^2$H: 7$^{60\%}$, 17$^{100\%}$

$^2$H: 9$^{60\%}$, 13$^{100\%}$

$^2$H: 11$^{60\%}$, 15$^{100\%}$

30        0        -30 kHz

119
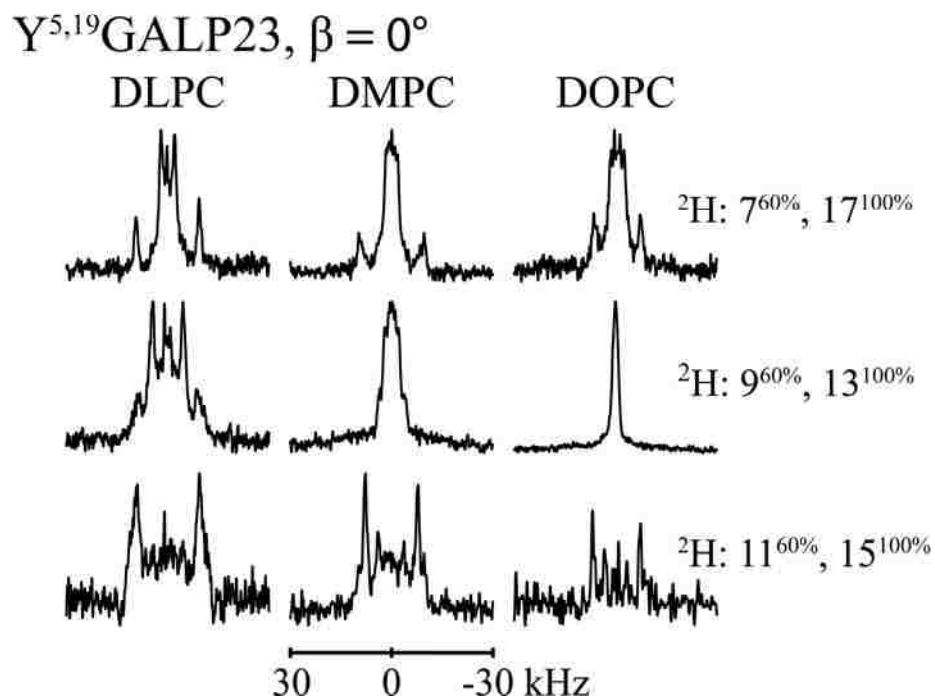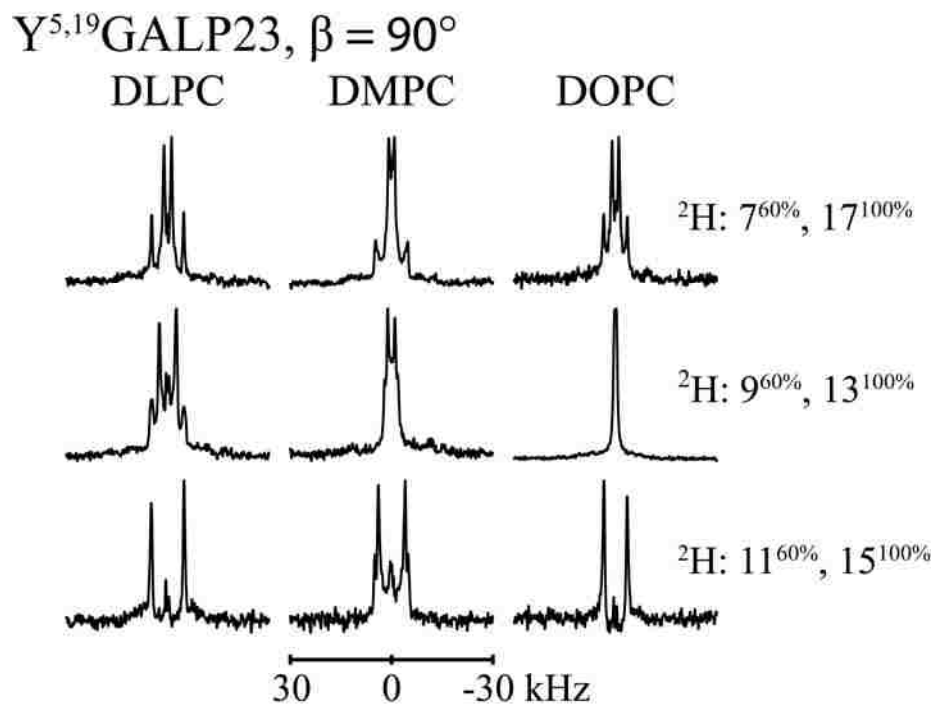
*Figure S6.* Comparison of Y[19]GWALP23 (black squares) and Y[5]GWALP23 (blue circles) quadrupolar wave plots in oriented DOPC bilayers.
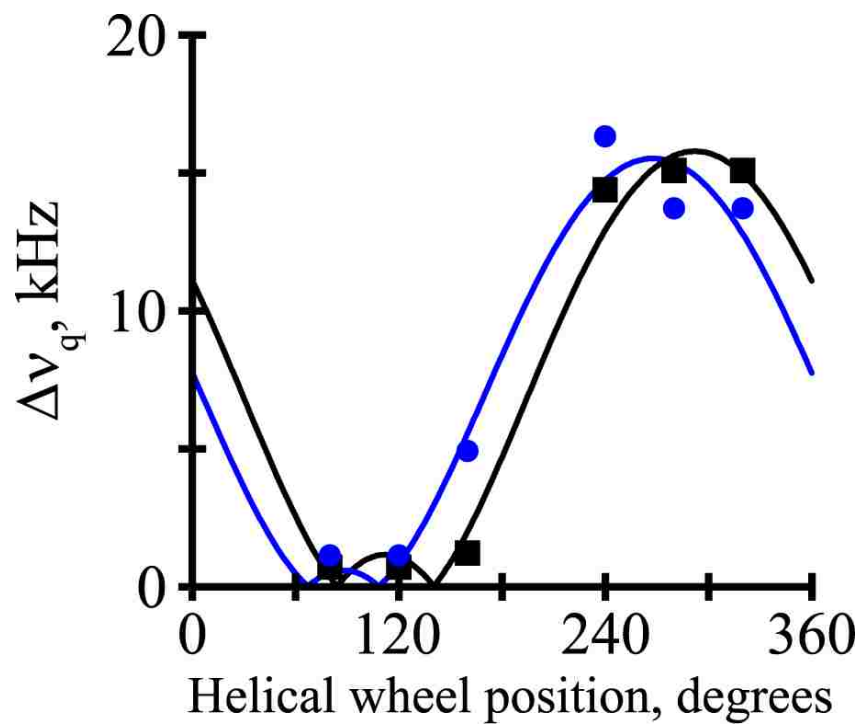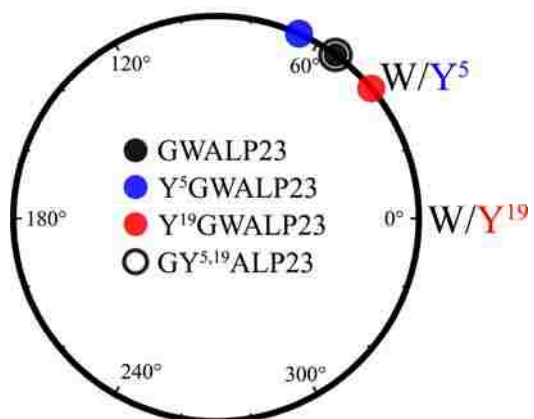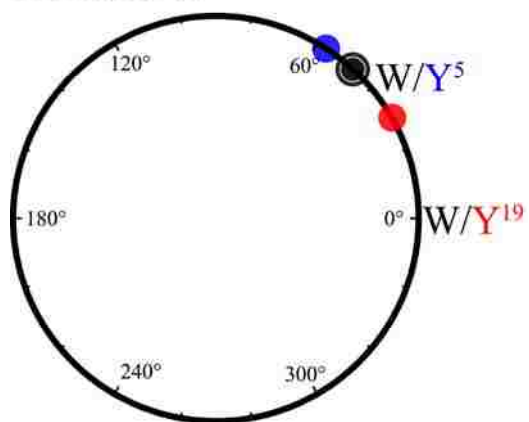
*Figure S7.* Rho-dependence of anchoring residues in lipids. Radial positions of anchors are shown in context to the tilt direction, rho.
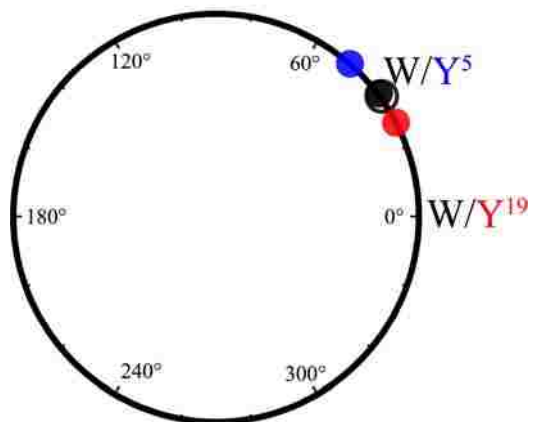
*Figure S8.* Azimuthal rotation of GWALP23 (black), $Y^5$GWALP23 (blue), and $Y^{19}$GWALP23 (red) in DMPC expressed with Gaussian dynamics ($\rho_0$, $\sigma_\rho$).
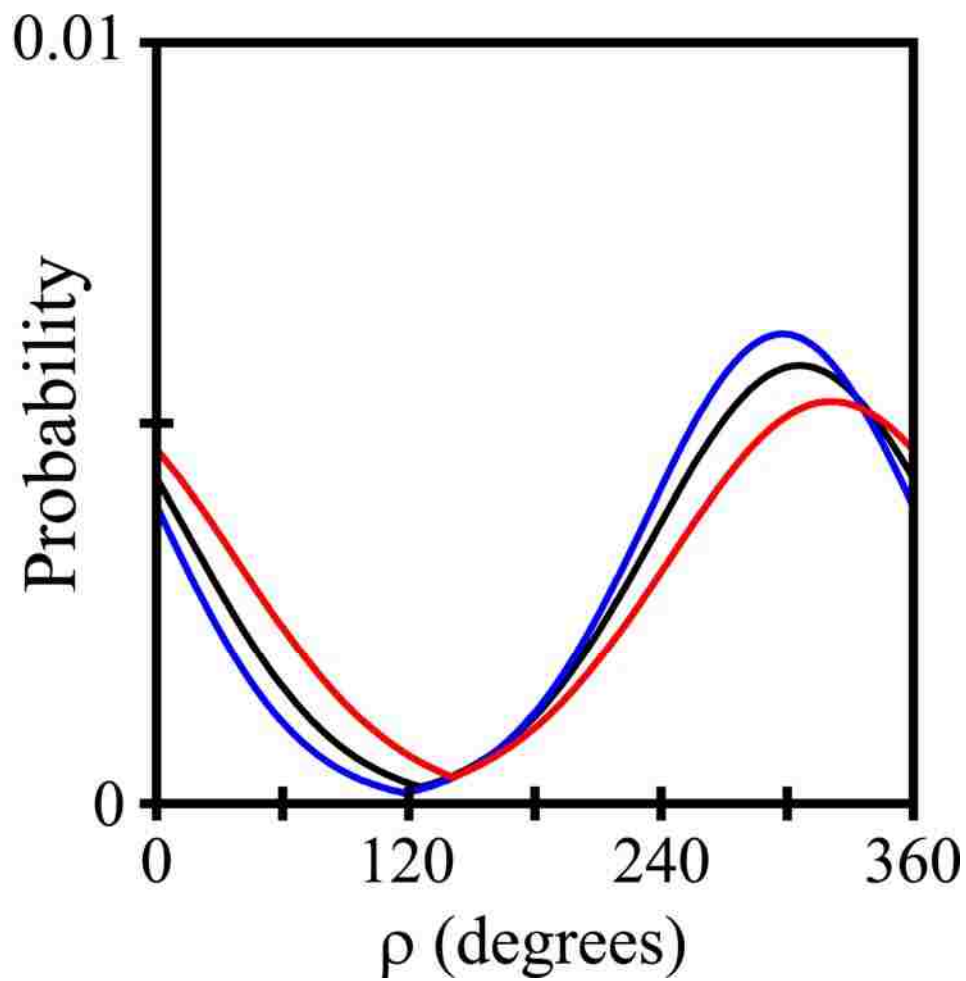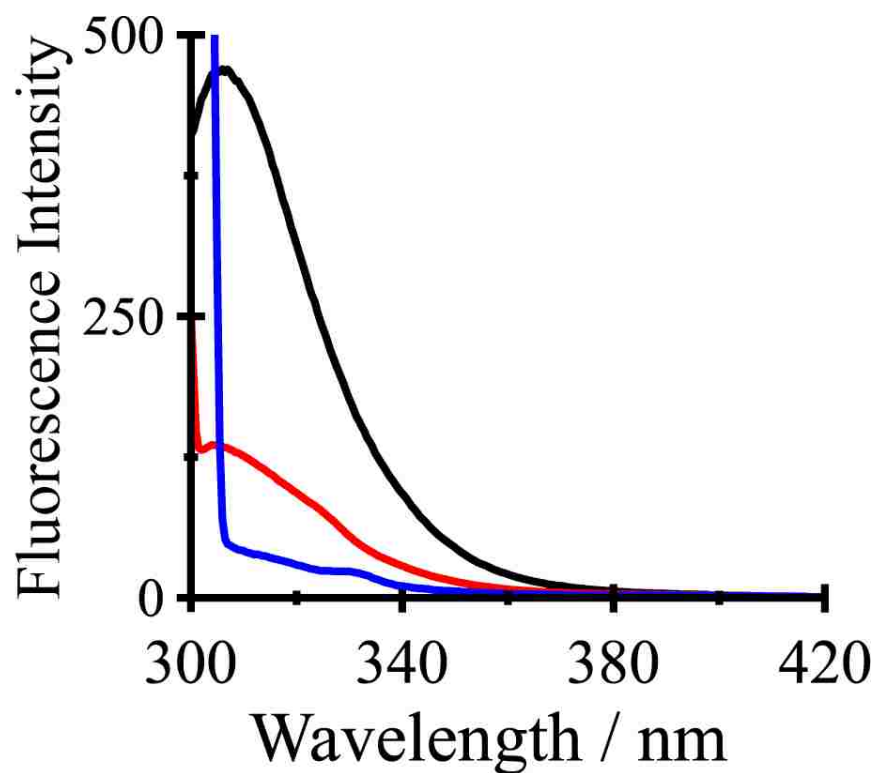
*Figure S9.* Fluorescence spectra of GY[5,19]ALP23 in DLPC excited at 280 nm (black), 290 nm (red) and 295 nm (blue).

**CHAPTER 4**

**Response of GWALP Transmembrane Peptides to Titration of a Buried Lysine Residue**

**4.1 Abstract**

Designed α-helical peptides such as GWALP23 serve as useful models for probing the influence of polar amino acids within a core transmembrane helical sequence. We incorporated lysine as a guest residue into the membrane-spanning host peptides GWALP23 and closely related Y[5]GWALP23 (acetyl-GGAL(W[5]/Y[5])LALALAL[12]AL[14]ALALW[19]LAGA-amide). Lysine was introduced at either position 12 or 14 of the host sequences, for which position 12 corresponds to the center. Solid-state NMR spectra of $^2$H-Ala residues in peptides incorporated into oriented lipid bilayer samples reveal that L14K mutant peptides adopt well-defined orientations in DOPC and DLPC. In each lipid membrane, the L14K substitution increases the helix tilt at neutral pH and is accompanied by a change in the helix azimuthal rotation angle (direction of tilt). The L12K substitution, on the other hand, reduces the $^2$H NMR spectral quality and lead to multiple unresolvable peaks of low intensity in water, particularly in the thicker DOPC, suggesting a lack of distinct orientation, as the system struggles to insert a charged lysine into the thicker bilayers. As the positively charged K12 amino group is titrated to higher pH values, nevertheless, the $^2$H NMR spectral quality improves in DOPC, and the K12 peptides adopt an average orientation nearly matching the one found for the host peptides GWALP23 and Y[5]GWALP23 (with L12). In similar fashion, titration of K14 to pH 8.2 at 50 °C, in any of the tested lipid bilayer membranes, results in a smaller helix tilt, again much closer to that observed for the L14 peptides without a polar guest residue, but retaining a significant azimuthal rotation difference. Additionally, the titration of K14 based on the pH dependence of

alanine methyl $^2$H quadrupolar splittings enabled the generation of a titration curve and an experimentally determined p$K_a$ of 6.2 at 50 °C (p$K_a$ of 6.8 at at 25 °C) for the $\varepsilon$-NH$_3^+$ of the Lys-14 side chain.

## 4.2 Introduction

Ionizable residues are often found in catalytic sites and can be essential for protein activity (Bartlett et al. 2002). Specifically, the basic residues lysine and arginine can be found in membrane proteins enriched at the interfacial region and are believed to assist in anchoring integral proteins (Landolt-Marticorena et al. 1993; de Planque et al. 1999; de Planque et al. 2002; Vostrikov et al. 2010a). In the hydrophobic core of transmembrane proteins, these highly polar amino acids are significantly depleted due to the energetic cost of burying them in the non-polar lipid environment. Nevertheless, though their membrane occupancy is diminished, in many proteins lysine and arginine can still be found present in the bilayer so one can presume a functional role must be present to necessitate the added energetic cost. For example, the transmembrane domains of integrin proteins possess conserved basic residues that are found essential for signaling regulation (Kim et al. 2011). Cell-penetrating peptides, though rich in lysine and arginine, are able to cross the large energy barrier of the hydrophobic bilayer while carrying other macromolecules by a process that is still largely not understood energetically (Eguchi et al. 2001; Su et al. 2009). The four-helix bundle voltage senor domain (VSD) of Voltage-gated potassium channels has been found to possess multiple arginine and lysine residues. It is believed they are present to allow the VSD to reposition based on membrane potential to open and close the channel (Dorairaj et al. 2007; Hessa et al. 2005). Debate is still ongoing as to how these charges shift to facilitate conformational changes, with chief argument involving the low probability of these charges, specifically Arg, to even enter the bilayer. Several MD simulations have estimated large energy barriers for moving Arg into the bilayer (14 - 17 kcal/mol) (Dorairaj et al. 2007; MacCallum et al. 2008) while some experiments have

shown a much more tolerable ~ 2 - 2.5 kcal/mol energy cost (Hessa et al. 2005; Moon et al. 2011).

Indeed, Coulombic interactions are intensified in the lipid bilayer as compared to aqueous solution due to the low dielectric medium and need to be addressed fundamentally. Model transmembrane systems such as GWALP23 (Vostrikov et al. 2008) and $Y^5$GWALP23 (Gleason et al. 2012) have been previously used to study various issues of integral proteins such as hydrophobic mismatch, transmembrane helix anchoring, and proline influence (Killian et al. 1996; van der Wel et al. 2002; Vostrikov et al. 2010; Vostrikov and Koeppe 2011a; Thomas et al. 2009). Recently, Arg influence on a transmembrane helix was probed using GWALP23 in a DOPC bilayer using solid-state $^2$H NMR (Vostrikov et al. 2010b). Positioning Arg somewhat away from the center of the bilayer (~ 3 Å on the helical backbone) yielded only relatively small changes to the helix as compared to the host alone with an increased tilt and azimuthal rotation that likely favors snorkeling of the guanidium group. In contrast, when Arg was placed at the center of the peptide helix (GWALP23-R12), the peptide exhibited multi-state behavior that was in slow-exchange on the NMR time scale as seen by multiple low-intensity broad quadrupolar splittings of $^2$H NMR.

Here we have conducted an analogous study of the positively charged lysine residue using GWALP23 and $Y^5$GWALP23 as the hosts (*Table 1*). The results demonstrate by $^2$H NMR that Lys-14, positioned near the center, behaves similar to Arg-14. Examination of the equivalent Lys-12 peptide also shows $^2$H NMR spectra suggestive of multi-state behavior, like R12. In contrast to R12, it was observed that Lys was able to titrate at high pH to produce well-oriented helix. Further titration of K14 between a protonated charged form and a neutral deprotonated form allowed for the creation of a titration curve to calculate the $pK_a$ of the lipid-

127

exposed $\varepsilon$-NH$_3^+$ Lys side chain. The experimental pK$_a$ of 6.8 (at 25 °C) is comparable to previous estimates by MD simulations (MacCallum et al. 2008).

## 4.3 Materials and Methods

### Solid Phase Synthesis of $^2$H-Labeled Peptides

Commercial L-alanine-$d_4$ from Cambridge Isotope Laboratories (Andover, MA) was modified with an Fmoc group, as described previously (Thomas et al. 2009), and recrystallized from ethyl acetate:hexane, 80:20. NMR spectra ($^1$H) were used to confirm successful Fmoc-Ala-$d_4$ synthesis. Other protected amino acids and acid-labile "Rink" amide resin were purchased from NovaBiochem (San Diego, CA). All peptides were synthesized on a 0.1 mmol scale using "FastMoc™" methods and a model 433A synthesizer from Applied Biosystems by Life Technologies (Foster City, CA). Typically, two deuterated alanines of differing isotope abundances were incorporated into each synthesized peptide. Selected precursors for deuterated residues therefore contained either 100% Fmoc-L-Ala-$d_4$ or 50% Fmoc-L-Ala-$d_4$ with 50% non-deuterated Fmoc-L-Ala. The final residue on each peptide was acetyl-Gly to yield a blocked, neutral N-terminal.

A peptide cleavage solution was prepared containing 85% trifluoroacetic acid (TFA) and 5% each (v/v or w/v) of triisopropylsilane, water, and phenol. TFA cleavage from "Rink" resin in 2 mL volume (2-3 h at 22 °C) leads to a neutral, amidated C-terminal. Peptides were precipitated by adding the TFA solution to 25 volumes of cold 50/50 MtBE/hexane. Peptides were collected by centrifugation, washed multiple times with MtBE/hexane and lyophilized from (1:1) acetonitrile/water. After lyophilization, crude peptide dissolved in TFE was purified via HPLC on a Zorbax Rx-C8 9.4 mm x 25 cm column packed with 5 μm octyl-silica (Agilent Technologies, Santa Clara, CA) with a typical gradient of 92-96% methanol/water (0.1% TFA) and a 1.7 mL/min. flow rate. Collected product is lyophilized multiple times to remove residual TFA. MALDI-TOF mass spectrometry was used to confirm peptide identity by molecular mass

(*Figure S1* in Supplementary Material).  Peptide purity was examined by reversed-phase HPLC (*Figure S2*) with 280 nm detection, using a 4.6 x 50 mm Zorbax SB-C8 column packed with 3.5 μm octyl-silica (Agilent Technologies, Santa Clara, CA), operated at 1 mL/min using a methanol/water gradient from 85% to 99% methanol (with 0.1% TFA) over five min.  Peptide quantity was calculated by means of UV absorbance at 280 nm, using molar extinction coefficients of 5,600 $M^{-1}$ $cm^{-1}$ for each Trp and 1,490 $M^{-1}$ $cm^{-1}$ for each Tyr residue in the peptide (Pace et al. 1995). Solvents were of the highest available purity.  Water was doubly deionized Milli-Q™ water.

### $^2$H NMR Spectroscopy using Oriented Bilayer samples

Mechanically aligned samples for solid-state NMR spectroscopy (1/40, peptide/lipid) were prepared using DOPC, DMPC, or DLPC lipids from Avanti Polar Lipids (Alabaster, AL), and deuterium-depleted water (Cambridge; 45% w/w hydration), as described previously (Thomas et al. 2009).  Bilayer alignment within each sample was confirmed using $^{31}$P NMR at 50 °C on a Bruker Avance 300 spectrometer (Billerica, MA) at both β = 0° (bilayer normal parallel to magnetic field) and β = 90° macroscopic sample orientations.  Deuterium NMR spectra were recorded at both sample orientations on a Bruker Avance 300 spectrometer, utilizing a quadrupolar echo pulse sequence (Davis et al. 1976) with 90 ms recycle delay, 3.2 μs pulse length and 115 μs echo delay.  Between 0.5 and 1.5 million scans were accumulated during each $^2$H NMR experiment.  An exponential weighting function with 100 Hz line broadening was applied prior to Fourier transformation.

Buffers for oriented samples were prepared at room temperature using vacuum-dried reagents and prepared in deuterium-depleted water. Buffers include: pH 4 Acetate buffer 50 mM (sodium acetate and acetic acid, Sigma, St. Louis, MO); pH 6 and 7 Tris-Bis buffers 50 mM

(EMD, Gibbstown, NJ); pH 7.5, 8, 8.5, and 9 Tris buffers 50 mM (Trizma® hydrochloride and Trizma® base, St. Louis, MO).

Due to the temperature-dependence of the $pK_a$ for various buffers, each buffer's pH (excluding Acetate buffer with a known negligible temperature-dependence) was measured at incremental temperatures between room temperature (23°) and 60° (Supplemental *Figure S7*) to account for the elevated temperature (50°) in which the $^2$H NMR samples were run. Trendlines were found to be highly linear for Tris and Tris-Bis buffers. d(pH)/dT values of -0.0306 and -0.019 were used for adjusting pH values of buffers Tris and Tris-Bis respectively for 50° for $^2$H NMR data interpretation.

### Data Analysis

The analysis using semi-static peptide dynamics involves a principal order parameter $S_{zz}$ to estimate overall peptide motion with respect to an apparent average peptide orientation. These calculations are based on the GALA analysis, as previously described (van der Wel et al. 2002; Strandberg et al. 2004; Strandberg et al. 2009). A grid search is performed using $\tau$, $\rho$ and $S_{zz}$ as variable parameters and locates the global RMSD minimum. The analysis considers the $^2$H quadrupolar splittings for the isotope-labeled residues based on ideal $\alpha$-helix geometry.

### CD Spectroscopy

Small lipid vesicles incorporating 125 nM peptide and 7.5 μM lipid (1/60) were prepared by sonication in unbuffered water. An average of ten scans was recorded on a Jasco (Easton, MD) J710 CD spectropolarimeter, using a 1 mm cell path length, 1.0 nm bandwidth, 0.1 nm slit and a scan speed of 20 nm/min.

**Steady-state Fluorescence Spectroscopy**

Vesicle solutions for fluorescence experiments were prepared the same as those for CD spectroscopy. Samples were excited at 280 nm or 295 nm with a 5 nm excitation slit, and emission spectra were recorded between 300 and 420 nm with a 5 nm emission slit using a Hitachi F-2500 fluorescence spectrophotometer. The spectra from five to thirty scans were averaged.

## 4.4 Results

Circular dichroism (CD) spectra indicate that all peptides retain the alpha-helical secondary structure upon the addition of lysine within the central core helix (Supplemental *Figure S3*). Characteristic CD spectra for alpha-helices were observed for both Lys-12 and Lys-14 peptides in small unilamellar lipid vesicles of DLPC, DMPC and DOPC. However, a reduction in mean-residue-ellipticity was observed for the Lys-12 peptide.

### $^2$H NMR spectra of peptides in $H_2O$

Solid-state $^2$H NMR spectra of the $^2$H-labeled alanines in the lysine-containing peptides incorporated into mechanically oriented glass plate samples yielded an assortment of results. Lys-14 peptides produced different, but well-defined, quadrupolar splittings in a range of lipid bilayer thicknesses (C12:0-C18:1), indicating that the peptide adopts a stable transmembrane orientation in each case (*Table 2*, Supplemental *Figure S2*). Further analysis by the semi-static GALA method reveals that in all lipid thicknesses the addition of Lys-14 increases the helix tilt (*Table 3*). In the case of negative hydrophobic mismatch found in DOPC, the magnitude of peptide tilt increases from 6° to 15°. In DMPC, where the hydrophobic length of bilayer and core are nearly equal, it is observed to increase the degree of tilt from 9° to 18°. In the positive hydrophobic mismatch situation of DLPC, GWALP23 increases to a smaller extent from 21° to 24° when Lys-14 is introduced. The direction of tilt ρ (also denoted rotation angle) of GWALP23, ~ 310°, is also significantly influenced by the addition of Lys-14. In DOPC a 95° rotational shift from 323° to 228° is observed (*Figure 5, Table 3*). In the shorter lipid system of DLPC we also find a shift to a lower rotation angle (246°) (*Table 3*).

In the case of Lys-12 peptides, there is a drastic decrease in $^2$H spectral quality (signal/noise decrease and peak broadening) as the bilayer lipid length increases from DLPC to

DOPC, to the point where individual quadrupolar splittings are no longer distinguishable (*Figure 3*). This trend is parallel to an analogous study observing Arg-12 in the bilayer, where CG MD simulations also illustrated multiple orientations for the peptide, including a surface-bound population in longer lipid bilayers (Vostrikov et al. 2010b). The $^2$H quadrupolar splittings reached a magnitude of ~ 29 kHz in DLPC suggesting a moderate helix tilt with respect to the bilayer normal. Discernable quadrupolar splittings were obtained for all six labeled Ala-d$_4$ residues in DLPC allowing for further analysis by the GALA method. When the NMR observables are fit to the variable-S$_{zz}$ GALA method, the peptide is shown to adopt a relatively dramatic tilt of ~30° (*Table 3*). The Lys-12 peptide is found to tilt in nearly the same direction (254°) as its Lys-14 analogue; tilting in a direction ~ 40° different from the host peptide.

**Titration of peptides**

Oriented samples of lysine-containing peptides were then created in bilayers at both acidic and basic conditions. Quadrupolar splittings and overall spectra quality went universally unchanged at pH 4 for both Lys-14 and Lys-12 in all lipids (*Figure 7* and *9*), suggesting that the Lys ε-amino group when hydrated with unbuffered water is also found in a protonated, charged state. When Lys-14 is hydrated at pH 8.2 in DLPC at 50 °C, no change in $^2$H NMR spectra was observed from water indicating that the ε-amino group had not reached the pK$_a$ threshold to titrate and remained protonated. (We note the temperature dependence of the buffer, such that pH 8.2 at 50 °C corresponds to pH 9.0 at 25 °C.) By contrast, Lys-12 in DLPC showed different patterns of quadrupolar splittings when at pH 8.2 and was found with a decreased tilt (23°) that is closer to the host peptide (19°), but with an azimuthal rotation much unchanged (*Table 3*).

When the Lys-12 peptides were incorporated into thicker DOPC bilayers and hydrated by pH 8.2 Tris buffer, the previously poor spectra were significantly improved to reveal well-

resolved quadrupolar splittings, indicating that the peptides were able to titrate and orient in the DOPC bilayer (*Figure 2*). Interestingly, it was determined that the peptide holds an orientation nearly identical to that of the host peptide, with a tilt $\tau$ of 5° and a rotation $\rho$ 308° that defines the direction of the tilt (*Table 3, Figure 4*). When Lys-14 is titrated to pH 8.2 in DOPC, the GALA analysis shows the peptide tilt decrease from 15° in water to 9° in buffer, but (unlike Lys-12) not quite back to the host peptide's tilt of 6° in DOPC (*Table 3, Figure 5*). Also unlike the titration of Lys-12, the direction of tilt remains 244°, in the vicinity of the charged peptide's direction, but not that of the host peptide.

Further incremental titration of GWALP23 L14K in DOPC between pH 4 and pH 8.2 using $^2$H NMR allowed for the direct determination of the p$K_a$ of the $\varepsilon$-amino group (*Figure 7*). *Figure 8* shows titration curves using a single Lys-14 peptide containing two Ala-$d_4$ labels; the results for the two curves using concurrent reporters agree upon a p$K_a$ of 6.2 at 50 °C. $^2$H NMR experiments were conducted at 50 °C and an observed temperature-dependent Lys p$K_a$ depression has been previously reported to be -.024 u/°C (Nagai et al. 2008). We therefore infer a p$K_a$ of 6.5 at 37 °C, or 6.8 at 25 °C.

Additional titration was carried out on Y$^5$GWALP23 L12K in a similar pH range. Unlike Lys-14, with two states (protonatated/unprotonated) that are well behaved and in fast-exchange on the NMR time scale, Lys-12 likely exhibits multi-state behavior when charged (potentially surface-bound) and no such migration of quadrupolar splittings is observed. In contrast, as the sample pH is lowered incrementally from 8.2, there is a progressive decrease in spectra quality (*Figure 9*) and a reduction in the heights of the primary peaks. However, even as signal/noise continues to decrease down to pH 6.5, the dominant QS's appear unmoved until no longer

distinguishable. Potentially, the pH dependence of the primary peak heights would be of interest to indicate a pseudo "titration" curve which could set an upper limit for the Lys-12 $pK_a$ value.

### Fluorescence Emission Spectroscopy

When excited at 295 nm, the Trp fluorescence either of the Y5 peptides is observed with $\lambda_{max}$ around 335 nm, regardless of the lipid environment or the presence of the charged or neutral lysine residue, indicating an expected interfacial positioning of the Trp[19] anchor in all cases (*Figure 10*). Addition of either Lys-12 or Lys-14 appears to broaden the emission peak, nevertheless. Titrated (neutral) Lys-12 at high pH in DOPC is modestly blue shifted, but the $\lambda_{max}$ is not identical to that of the host L12 peptide, as one might have assumed based on nearly identical helix orientations. Emission peaks of the Lys-containing peptides appear generally narrower at pH 9.

**4.5 Discussion**

To determine the properties and influence of a polar lysine residue in a hydrophobic bilayer, α-helical GWALP peptides were used as a transmembrane host into which a Lys guest residue was substituted at various positions. The effects of the Lys additions were gauged by the host peptide's adaptation from its native orientation in the bilayer. Peptide orientation was determined by a semi-static analysis of orientational-dependent Ala residues, labeled with deuterium, and analyzed by solid-state $^2$H NMR. Addition of lysine at position L14 was shown to increase helix tilt in DOPC and induce a large change in direction of tilt by nearly 100°. This newly described orientation demonstrates the peptide's attempt to allow the polar ε-NH$_3^+$ to snorkel further out of the bilayer. In the deduced orientation of GWALP23, the peptide tilts in the general direction of the N-terminal Trp-5 residue. In this scenario, Lys-14, found on the opposite side of the helix, would be extending further into the bilayer with great energetic cost. Instead, the peptide undergoes a rotation that, along with the added tilt, improves its ability to access more polar regions near the C-terminal. This reorientation to allow favorable snorkeling of the charged moiety is paralleled by the analogous study of GWALP23 Arg-14, for which additional CG-MD simulations also showed an accompanying 3 Å displacement of the peptide helix toward the C-terminal's lipid leaflet (Vostrikov et al. 2010b). This snorkeling effect has been previously seen for Lys and Arg residues (Chamberlain et al. 2004; Strandberg et al. 2003) and in some cases is found essential for function, such as in integrin β3, which with a conserved snorkeling Lys or Arg residue creates a necessary crossing angle for formation of a larger complex and for signal transduction (Kim et al. 2011).

In the shorter DLPC bilayer, the peptide also undergoes an increase in tilt magnitude with Lys-14 addition, but to a lesser extent. The difference likely occurs because the host peptide is

already significantly tilting in DLPC, on account of the hydrophobic mismatch. The already present tilt allows for some stabilization of the charge in DLPC while in DOPC it is forced to adopt a greater tilt exclusively on account of the added charge. Accompanying the increase in tilt magnitude again is a large shift in tilt direction, going further away from the radial positions of the anchoring residues of GWALP23. It has been previously shown that the anchoring residues of GWALP23-like peptides largely determine the tilt direction of the helix (Vostrikov and Koeppe 2011a), but the presence of Lys-14 appears to supersede the aromatic residue influence.

Similar to Lys-14, Lys-12 is also able to insert into the relatively short bilayer of DLPC and influence the helix. Lys-12 addition is distinguishable from that of Lys-14 in two important ways. The first obvious difference is that it is in the center of the peptide helix and thus would be found buried deeper into the bilayer in a transmembrane configuration. Secondly, as position 12 falls on the same face of the helix as the anchoring residues, position 14 is found 200° away as visualized in *Figure 1*. Given the extra 3 Å in distance that Lys-12 is closer to the helix center than Lys-14, these experiments demonstrate it requires greater extents of tilting to allow optimal placement of Lys12. In contrast, while azimuthal rotation still changes, it does so to a lesser degree, probably because K12 is on the same helix face as Y5 and W19. Given the peptide's orientation and favored side chain torsion angles on an $\alpha$-helix, the side chain is likely extending towards the lipid leaflet associated with the N-terminus, in contrast to Lys-14.

The observation of multi-state behavior of a peptide containing charged Lys-12 in DOPC was not unprecedented, as it had recently been seen also for Arg in the same experimental scheme (Vostrikov et al. 2010b). With the $pK_a$ of the $\varepsilon$-$NH_3^+$ being lower than that of the guanidium group, it was unknown whether this peptide would choose to deprotonate or remain

charged within a lipid bilayer, and then how it would act accordingly. Despite the lower $pK_a$ of Lys, several reasons why Arg might be able to enter the bilayer more easily than Lys have been put forth. In contrast to Lys with the entirety of its charge concentrated on a single atom, Arg's charge is delocalized via resonance, allowing for charge dispersion and a resulting lesser hydration. This leads to a decreased dehydration penalty for Arg to enter the bilayer (Harms et al. 2011; Mason et al. 2003). With regard to larger membrane proteins, Arg can participate in a larger number of stabilizing noncovalent interactions such as H-bonding, ion-pairs, $\pi$-cation (Borders et al. 1994; Waldburger et al. 1995; Wei et al. 2003). This is further illustrated by two recently constructed hydrophobicity scales that use thermodynamic cycling of mutants to generate changes in free energy upon protein insertion (Hessa et al. 2005; Moon et al. 2011). In both cases Lys is estimated to be energetically more costly to insert.

Nevertheless, Lys with its lower $pK_a$, stands the possibility to deprotonate over Arg and enter the hydrophobic core in its neural form. In water, the $pK_a$ of the $\varepsilon$-amino group of lysine is ~ 10.5. When submerged into the hydrophobic bilayer the $pK_a$ is expected to decrease to favor the neutral form. Additionally, the level of $pK_a$ depression is scaled by depth as the gradient of penetrating water diminishes farther into the bilayer (MacCallum et al. 2008; Vorobyov et al. 2010). Knowing that a charged Lys-14 can be buried, but not Lys-12 leads to the conclusion that at a specific depth the normally transmembrane host peptide is no longer able to "carry" the charge any farther into the bilayer. This would also be affected by the ability of the charged moiety to snorkel.

It was first observed that titration of Lys-12 in DOPC to pH 8.2 could in fact "rescue" the peptide from its previous multi-state behavior by deprotonating Lys, supporting the view that Lys was indeed still charged in previous unbuffered water samples. It was also surprising that

the neutral form appeared to adopt a state nearly identical to that of the host peptide, which would indicate that a neutral amino group in this case behaves essentially like the Leu residue it replaced.  However, this Leu $\rightarrow$ Lys$^0$ mutation is further illuminated by the titrations of Lys-12 in DLPC and Lys-14 in DOPC to their neutral forms, which are found to behave differently from the parent Leu peptide.  In both instances, when Lys$^+$ was titrated to Lys$^0$, the tilt magnitudes also decreased, closer to the $\tau$ of the host peptide, similar to Lys-12 in DOPC.  But the direction of tilt, $\rho$, did not return back to that of the native host, thus demonstrating that while a deprotonated Lys$^0$ no longer possesses a great need to tilt the peptide helix further (reduced snorkeling), it has a preferential orientation (due to its polarity) and still appears to have greater influence than the anchoring residues for defining $\rho$.

The gradual migration of $^2$H NMR signals of GWALP23 Lys-14 in DOPC during titration is observed because the two states (charged/uncharged) are both in transmembrane configurations and are in fast-exchange on the NMR time scale.  This results in averaged quadrupolar splittings that depend on the mole ratio of protonated/unprotonated states (seen to shift from one state at low pH to the other at high pH).  Spectra quality, nevertheless, is noticeably lower around the midpoint of the titration (We are unsure of the reason for this observation.) The two-state system allowed for direct pK$_a$ determination by titration and the inferred pK$_a$ is 6.8 at 25 °C (including a correction for the temperature dependence).  This reduction of nearly 4 pH units (from the pK$_a$ of Lys in aqueous buffer) is in substantial agreement with previous MD simulations, though our results suggests a greater pK$_a$ reduction at the given bilayer insertion depth, compared to the predictions from calculations (MacCallum et al. 2008).  A recent set of experiments by Chymes and Grosman 2011 estimated various Lys pK$_a$ values, also in the range of $6.5 - 7.5$ for a residue near the mouth of an ion channel, by means of

electrophysiological recordings of single-channel currents at different pH values. The advantage of GWALP23-K14 is that it allows for the direct examination of a Lys residue that is the only ionizable candidate and that is largely interacting with only the bilayer, without other contributing protein interactions that can be found in larger membrane proteins.

The extent of lowering of the Lys $pK_a$ is, again, dependent on the depth of insertion of the side chain into the bilayer. We estimate that in DOPC, Lys-14 is ~ 8 angstroms from the bilayer center. Lys-14 in the much thinner DLPC bilayer will be closer to the aqueous phase, and does not even begin to titrate by pH 8.2. Due to lipid susceptibility to degradation under basic conditions, we could not probe at higher pH values.

When the Lys-12 peptide was similarly evaluated in buffers spanning a range of pH's, as seen in *Figure 9,* it became apparent, going from high to low pH, that the well-behaved Lys$^0$ peptide is in exchange with the multi-state Lys$^+$ peptide. But in contrast to Lys-14 titration, the multiple states of the Lys$^+$ peptide are in slow-exchange on the NMR time scale, since the multiples states for Lys$^+$-12 likely include surface-bound orientations. Due to the lack of a single defined Lys$^+$-12 state in DOPC, we cannot calculate it's $pK_a$ since it is not an equilibrium two-state model. Nevertheless, the dominant QS's, though of lower intensity, do not shift their positions as the multi-state behavior increases (at lower pH) and we can estimate an upper limit of the $pK_a$ to be near 7 by comparing the reduction in signal intensity as the pH is lowered.

Most of the peptides examined fluoresce equally around 335 nm, regardless of the lipid environment of the side chain charge. Titrated Lys-12 in DOPC leads to a modest blue shift at high pH, but the spectrum is not quite identical to that of the host peptide, as might have been expected based on the nearly identical helix orientations. If a peptide is pivoting on the C-terminal tryptophan anchor to tilt (much like a hinge) due to a stronger interaction of W19 with

the interfacial region, over Y5, then only minor changes in $\lambda_{max}$ may be expected if Trp-19 is not significantly moved.

**4.6 Acknowledgments**

**4.7 References**

Bartlett, G.J., Porter, C. T., Borkakoti, N., and Thornton, J. M. (2002) Analysis of catalytic residues in enzyme active sites. *J. Mol. Biol. 324,* 105-121.

Borders, C. L., Broadwater, J. A., Bekeny, P. A., Salmon, J. E., Lee, A. S., Eldridge, A. M., and Pett, V. B. (1994) A structural role for arginine in proteins: Multiple hydrogen bonds to backbone carbonyl oxygens. *Protein Sci. 3*, 541-548.

Chamberlain, A. K., Lee, Y., Kim S., and Bowie, J. U. (2004) Snorkeling Preferences Foster an Amino Acid Composition Bias in Transmembrane Helices. *J. Mol. Biol. 339*, 471-479.

Chymes, G. D. and Grosman, C. (2011) Probing ion-channel pores one proton at a time. *Nature 438*, 975-980.

Davis, J. H., Jeffrey, K. R., Bloom, M., Valic, M. I., and Higgs, T. P. (1976) Quadrupolar echo deuteron magnetic resonance spectroscopy in ordered hydrocarbon chains. *Chem. Phys. Lett. 42*, 390-394.

de Planque, M. R., Kruijtzer, J. A., Liskamp, R. M., Marsh, D., Greathouse, D. V., Koeppe, R. E. 2nd, de Kruijff, B., and Killian, J. A. (1999) Different membrane anchoring positions of tryptophan and lysine in synthetic transmembrane alpha-helical peptides. *J. Biol. Chem. 274*, 20839-20846.

de Planque, M. R. , Boots, J. W., Rijkers, D. T., Liskamp, R. M. , Greathouse, D. V., and Killian, J. A. (2002) The effects of hydrophobic mismatch between phosphatidylcholine bilayers and transmembrane alpha-helical peptides depend on the nature of interfacially exposed aromatic and charged residues. *Biochemistry 41*, 8396-8404.

DeLano, W. L. (2002) The PyMOL Molecular Graphics System.

Dorairaj, S. and Allen, T. W. (2007) On the thermodynamic stability of a charged arginine side chain in a transmembrane helix. *Proc. Natl. Acad. Sci. U. S. A. 104*, 4943-4948.

Eguchi, A., Akuta, T., Okuyama, H., Senda, T., Yokoi, H., Inokuchi, H., Fujita, S., Hayakawa, T., Takeda, K., Hasegawa, M., and Nakanishi, M. (2001) Protein Transduction Domain of HIV-1 Tat Protein Promotes Efficient Delivery of DNA into Mammalian Cells. *J. Biol. Chem. 276*, 26204-26210.

Gleason, N. J., Vostrikov, V. V., Greathouse, D. V., Grant, C. V., Opella, S. J., and Koeppe, R. E. 2nd. (2012) Tyrosine Replacing Tryptophan as an Anchor in GWALP Peptides. *Biochemistry 51*, 2044-2053.

Harms, M. J., Schlesman, J. L., Sue, G. R., and Garica-Moreno, E. B. (2011) Arginine residues at internal positions in a protein are always charged. *Proc. Natl. Acad. Sci. U. S. A. 108*, 18954-18959.

Hessa, T., Kim, H., Bihlmaier, K., Lundin, C., Boekel, J., Andersson, H., Nilsson, I., White, W. H., and von Heijne, G. (2005) Recognition of transmembrane helices by the endoplasmic reticulum translocon. *Nature 433*, 377-381.

Killian, J. A., Salemink, I., de Planque, M. R., Lindblom, G., Koeppe, R. E. 2nd, and Greathouse, D. V. (1996) Induction of nonbilayer structures in diacylphosphatidylcholine model membranes by transmembrane alpha-helical peptides: importance of hydrophobic mismatch and proposed role of tryptophans. *Biochemistry 35*, 1037-1045.

Kim, C., Schmidt, T., Cho, E., Ye, F., Ulmer, T. S., and Ginsberg, M. H. (2011) Basic amino-acid side chains regulate transmembrane integrin signalling. *Nature 481*, 209-213.

Landolt-Marticorena, C., Williams, K. A., Deber, C. M., and Reithmeier, R. A. (1993) Non-random distribution of amino acids in the transmembrane segments of human type I single span membrane proteins. *J. Mol. Biol. 229*, 602-608.

MacCallum, J. L., Bennett, W. F., and Tieleman, D. P. (2008). Distribution of Amino Acids in a Lipid Bilayer from Computer Simulations. *Biophys. J. 94*, 3393-3404.

Mason, P. E., Neilson, G. W., Dempsey, C. E., Barnes, A. C., and Cruickshank, J. M. (2003) The hydration structure of guanidinium and thiocyanate ions:    Implications for protein stability in aqueous solution. *Proc. Natl. Acad. Sci. U. S. A. 100, 4557-4561.*

Moon, C. P. and Fleming, K. G. (2011) Side chain hydrophobicity scale derived from transmembrane protein folding into lipid bilayers. *Proc. Natl. Acad. Sci. U. S. A. 108*, 10174- 10177.

Nagai, H., Kuwabara, K., and Carta, G. (2008) Temperature Dependence of the Dissociation Constants of Several Amino Acids. *J. Chem. Eng. Data 53*, 619-627.

Pace, C. N., Vajdos, F., Fee, L., Grimsley, G., and Gray, T. (1995) How to measure and predict the molar absorption coefficient of a protein. *Protein Sci. 4*, 2411-23.

Strandberg, E. and Killian, J. A. (2003) Snorkeling of lysine side chains in transmembrane helices: how easy can it get? *FEBS Lett 544*, 69-73.

Su, Y., Doherty, T., Waring, A. J., Ruchala, P., and Hong, M. (2009) Roles of Arginine and Lysine Residues in the Translocation of a Cell-Penetrating Peptide from ^{13}C, ^{31}P, and ^{19}F Solid-State NMR. *Biochemistry 48*, 4587-4595.

Thomas, R., Vostrikov, V. V., Greathouse, D. V., and Koeppe, R. E. 2nd (2009) Influence of proline upon the folding and geometry of the WALP19 transmembrane peptide. *Biochemistry 48*, 11883-11891.

145

van der Wel, P. C., Strandberg, E., Killian, J. A., and Koeppe, R. E. 2nd (2002) Geometry and intrinsic tilt of a tryptophan-anchored transmembrane alpha-helix determined by $^2$H NMR. *Biophys. J. 83*, 1479-1488.

Vorobyov, I., Bekker, B., and Allen, T. W. (2010) Electrostatics of Deformable Lipid Membranes. *Biophys J. 98*, 2904-2913.

Vostrikov, V. V., Daily, A. E., Greathouse, D. V., and Koeppe, R. E. 2nd (2010a) Charged or aromatic anchor residue dependence of transmembrane peptide tilt. *J. Biol. Chem. 285*, 31723-31730.

Vostrikov, V. V., Hall, B. A., Greathouse, D. V., Koeppe, R. E. 2nd, and Sansom, M. S. P. (2010b) Changes in Transmembrane Helix Alignment by Arginine Residues Revealed by Solid-State NMR Experiments and Coarse-Grained MD Simulations. *J. Am. Chem. Soc. 132*, 5803–5811.

Vostrikov, V. V. and Koeppe, R. E. 2nd (2011a) Response of GWALP Transmembrane Peptides to Changes in the Tryptophan Anchor Positions. *Biochemistry 50*, 7522-7535.

Waldburger, C. D., Schildbach, J. F., and Sauer, R. T. (1995) Are Buried Salt Bridges Important for Protein Stability and Conformational Specificity. *Nature Structural Biology 2*, 122-128.

Wei, Y., Horng J. C., Vendel, A. C., Raleigh, D. P., and Lumb, K. J. (2003) Contribution to stability and folding of a buried polar residue at the CARM1 methylation site of the KIX domain of CBP. *Biochemistry 42*, 7044-7049.

## 4.8 Tables

*Table 1.* Sequences of $(Y^5)$GWALP23 and Lys containing peptides[a]

| Name | Sequence |
|------|----------|
| GWALP23 | a-GGALW$^5$LALALALALALALWLAGA-e |
| Y$^5$GWALP23 | a-GGALY$^5$LALALALALALALWLAGA-amide |
| GWALP23 L14K | a-GGALW$^5$LALALALAKALALWLAGA-e |
| Y$^5$GWALP23 L12K | a-GGALY$^5$LALALAKALALALWLAGA-amide |

[a]Abbreviations:  "a" denotes "acetyl" and "e" denotes "ethanolamide."

*Table 2*. Observed $^2$H quadrupolar splittings[a] for (Y$^5$)GWALP23 L12K or L14K in lipid bilayers.

| Ala-d$_4$ | DLPC | | | | DOPC | | | |
|---|---|---|---|---|---|---|---|---|
| | 14K H$_2$O | 14K pH 8.2 | 12K H$_2$O | 12K pH 8.2 | 14K H$_2$O | 14K pH 8.2 | 12K H$_2$O | 12K pH 8.2 |
| 7 | 29.0 | 28.6 | 29.0 | 29.8 | 20.2 | 19.2 | 27.0 | 16.3 |
| 9 | 9.7 | 8.8 | 16.0 | 19.1 | 3.2 | 1.0 | 3.2 | 1.1 |
| 11 | 19.4 | 20.0 | 22.9 | 21.9 | 8.4 | 11.4 | [b] | 14.4 |
| 13 | 16.1 | 14.6 | 11.6 | 5.5 | 19.7 | 11.4 | [b] | 1.3 |
| 15 | 6.3 | 7.7 | 1.2 | 6.2 | 10.5 | 1.0 | [b] | 12.9 |
| 17 | 33.3 | 32.2 | 27.6 | 20.8 | 29.8 | 18.2 | [b] | 5.0 |

[a]Quadrupolar splittings are reported in kHz for the $\beta = 0°$ sample orientation of GWALP23 L14K (14K) and Y$^5$GWALP23 L12K (12K). Each value is an average of (the magnitude observed when $\beta = 0°$), and (twice the magnitude observed when $\beta = 90°$).

[b]Indiscernible due to poor spectra

*Table 3.* Semi-static GALA analysis of (Y[5])GWALP23, L12K or L14K in lipid bilayers in water or pH 8.2 buffer[a]

| Peptide | DLPC | | | | DOPC | | | |
|---|---|---|---|---|---|---|---|---|
| | $\tau$ | $\rho$ | $S_{zz}$ | RMSD (kHz) | $\tau$ | $\rho$ | $S_{zz}$ | RMSD (kHz) |
| W[5 b] | 21° | 305° | 0.71 | 0.7 | 6° | 323° | 0.87 | 0.6 |
| Y[5 c] | 19° | 295° | 0.78 | 0.7 | 5° | 311° | 0.80 | 0.9 |
| W[5] 14K | 24° | 246° | 0.83 | 1.5 | 15° | 228° | 0.88 | 1.2 |
| W[5] 14K, pH 8.2 | 25° | 245° | 0.80 | 1.6 | 9° | 244° | 0.86 | 0.3 |
| Y[5] 12K | 30° | 254° | 0.71 | 0.5 | d | d | d | d |
| Y[5] 12K, pH 8.2 | 23° | 265° | 0.74 | 0.9 | 5° | 308° | 0.83 | 0.8 |

[a]Calculations based on six Ala methyl ^{2}H quadrupolar splittings only.

[b]Values for GWALP23 from reference (Vostrikov et al. 2010a).

[c]Values for Y5GWALP23 from reference (Gleason et al. 2012).

[d]Y[5]GWALP23 L12K does not produce suitable spectra in DOPC for analysis.

*Table 4.* Observed $^2$H NMR quadrupolar splittings[a] (kHz) of GWALP23 L14K in DOPC in various pH conditions at 50 °C.

| pH  | Ala-15-d$_4$ | Ala-17-d$_4$ |
|-----|--------------|--------------|
| 4.0 | -5.3         | 15.4         |
| 5.5 | -4.2         | 13.8         |
| 6.5 | -1.8         | 12.0         |
| 6.6 | -0.9[b]      | 10.7         |
| 7.2 | -0.9         | 10.1         |
| 7.7 | -0.7         | 9.4          |
| 8.2 | -0.5         | 9.2          |

[a]$\beta = 90°$

[b]Outlying data point; not included in pK$_a$ calculation.

**4.9 Figures**

*Figure 1*. Model representation of Y$^5$GWALP23 L14K (A) and Y$^5$GWALP23 L12K (B). Models drawn using PyMOL (DeLano et al. 2002). The side chain orientations are arbitrary.
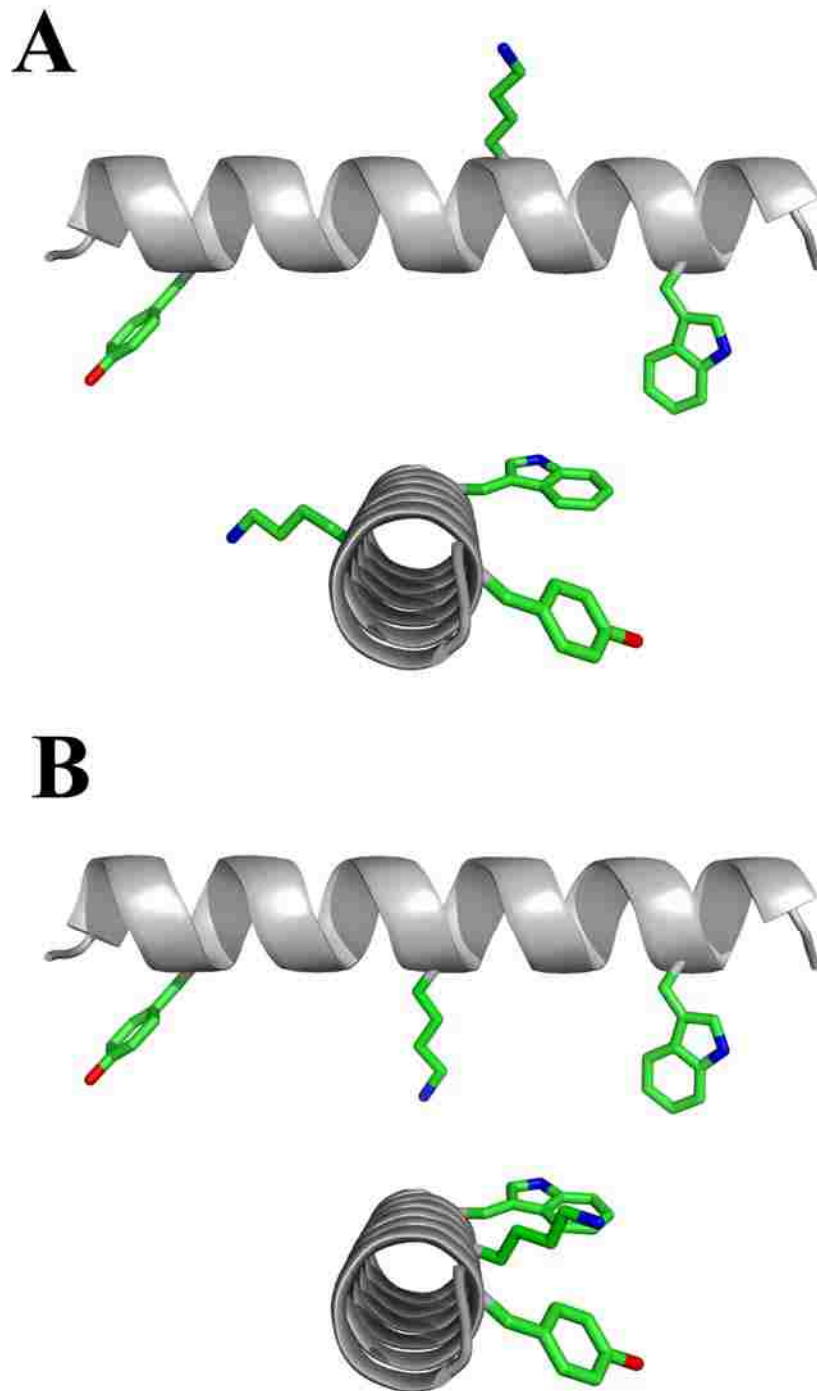
*Figure 2*. $^2$H NMR spectra of GWALP23 L14K (A) and Y$^5$GWALP23 L12K (B) in DOPC (1:40) oriented samples ($\beta$ = 90°) run at 50 °C. Samples hydrated with H$_2$O in left column and pH 8.2 Tris buffer in right column. Deuterated alanines labeled.
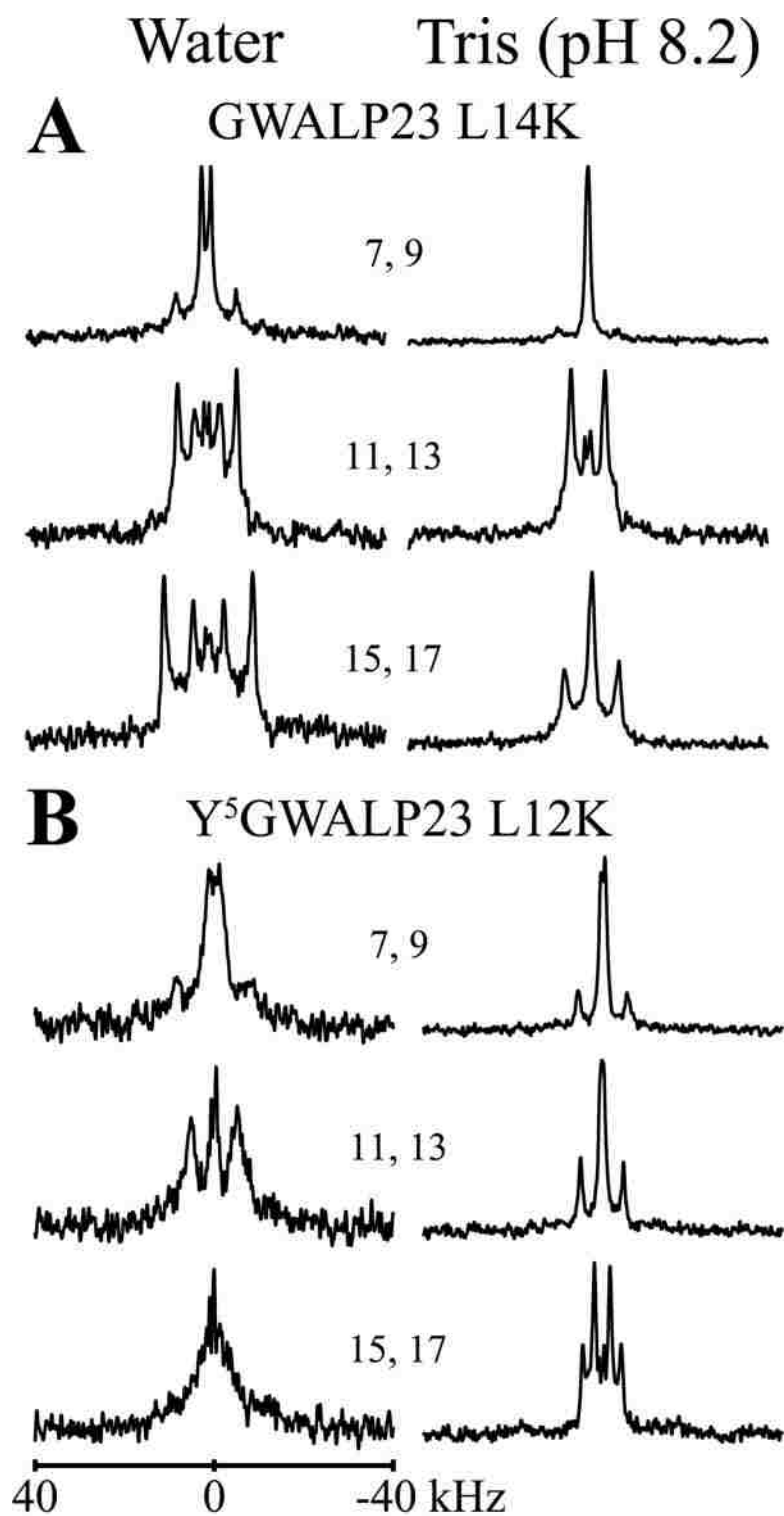
*Figure 3*. $^2$H NMR spectra of Y$^5$GWALP23 L12K in lipid; labeled at Ala$^{15}$ (60% $^2$H) and Ala$^{17}$ (100% $^2$H). β = 90°
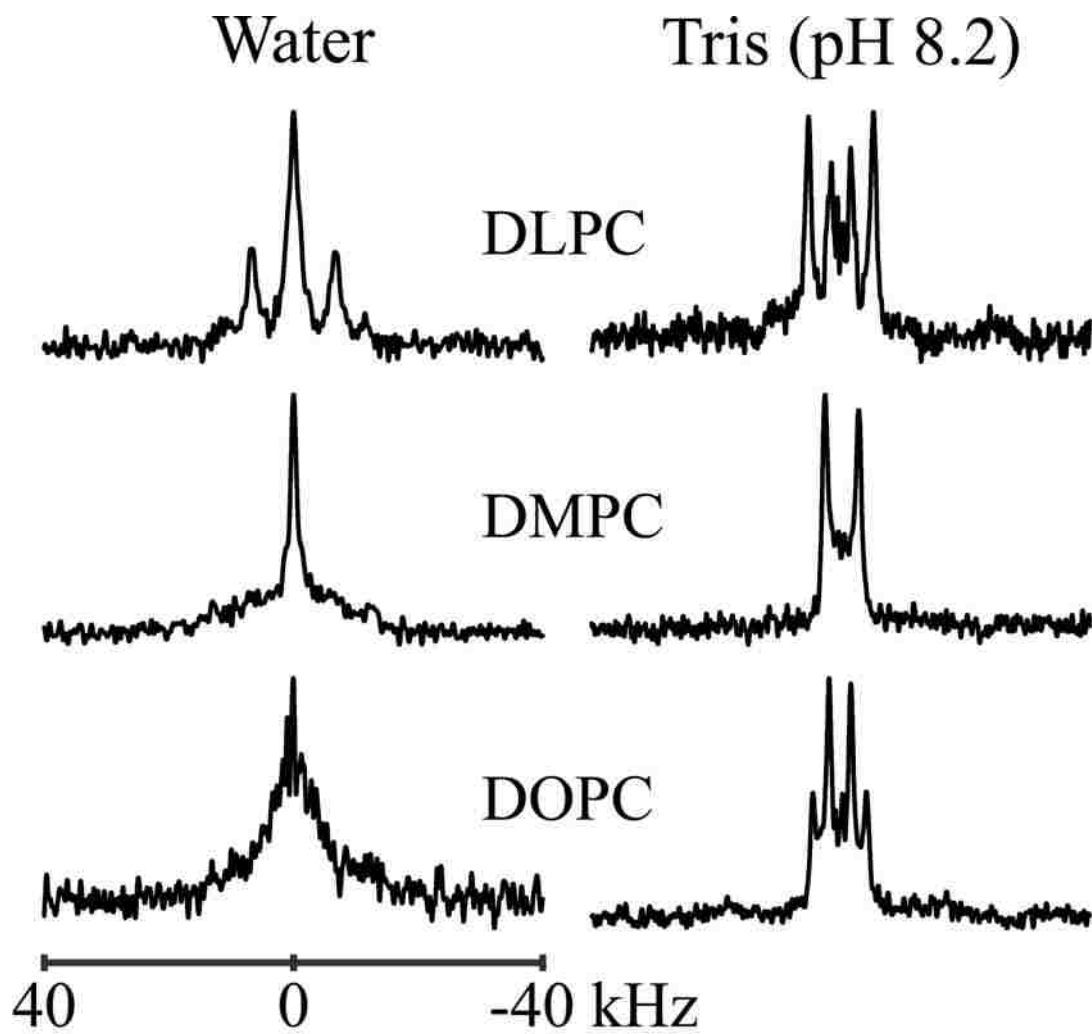
*Figure 4*.  GALA semi-static analysis of Ala-$d_4$ quadrupolar splittings using variable $S_{zz}$ (see van der Wel et al. 2002).  Quadrupolar wave plots are shown for $Y^5$GWALP23 L12K at pH 8.2 (blue triangles) and the host peptide in DOPC in $H_2O$ (black squares).  Fitted curves represent theoretical $\Delta v_q$ values for orientations corresponding to best-fit values of $\tau$ and $\rho$.
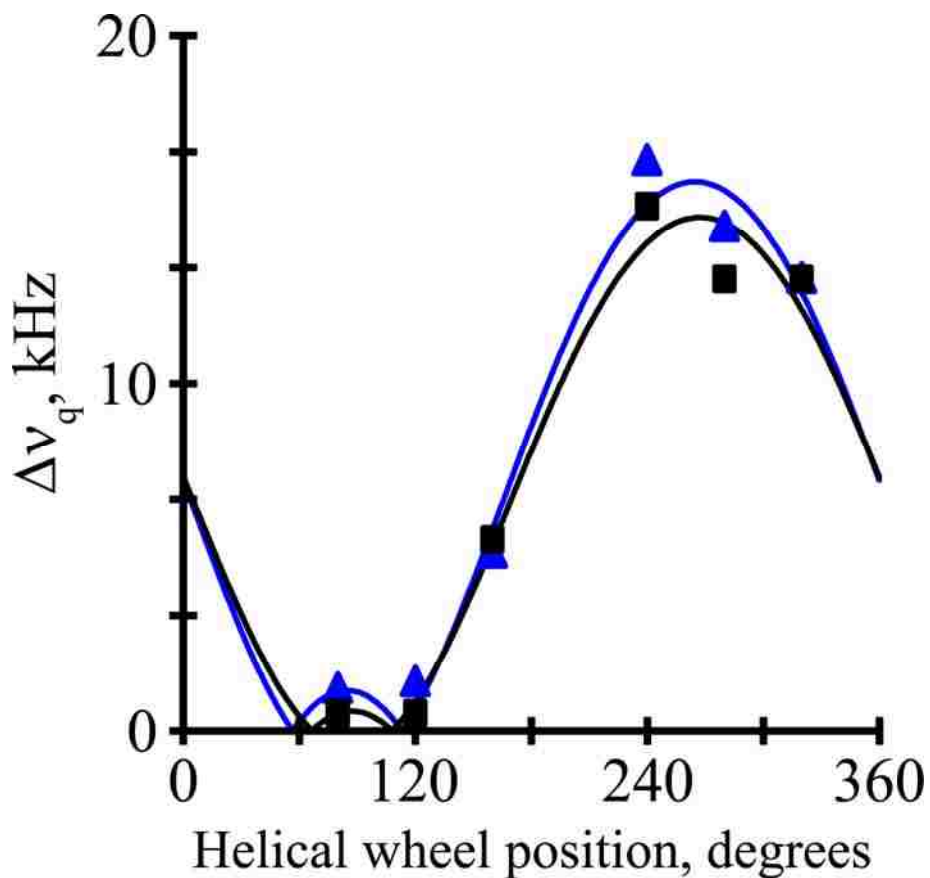
*Figure 5*. GALA semi-static analysis of Ala-d$_4$ quadrupolar splittings using variable S$_{zz}$ (see (van der Wel et al. 2002)). Quadrupolar wave plots are shown for GWALP23 L14K in DOPC in H$_2$O (red circles), at pH 8.2 (blue triangles) and the host peptide (black squares) in H$_2$O. Fitted curves represent theoretical $\Delta v_q$ values for orientations corresponding to best-fit values of $\tau$ and $\rho$.
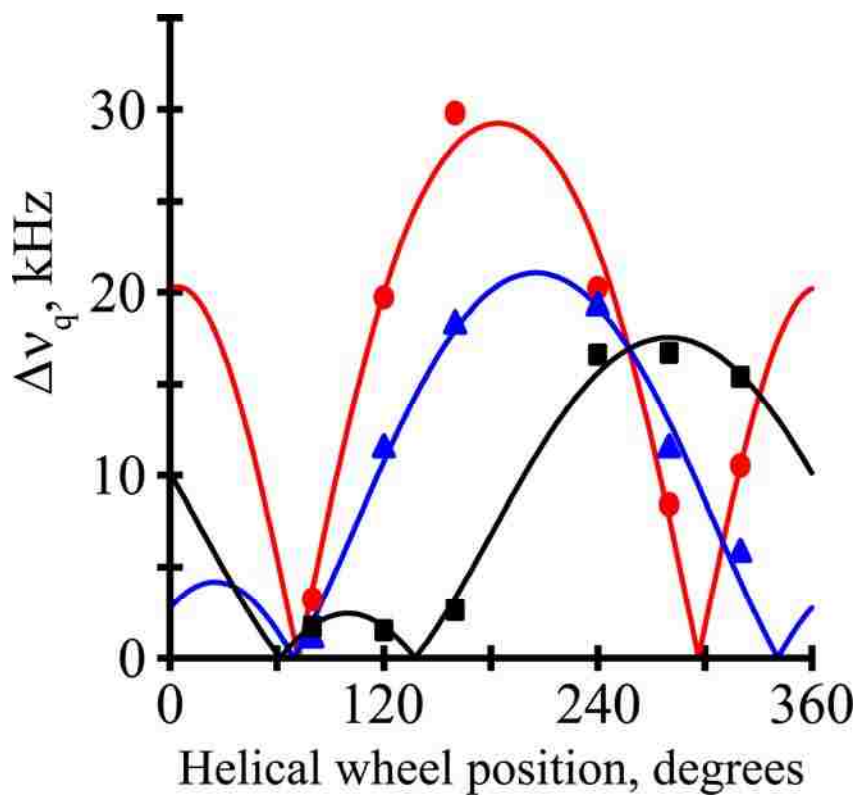
*Figure 6.* Polar plot of ρ and τ derived from semi-static GALA analysis for (Y[5])GWALP23 (black and grey), L14K (blue), and L12K (red) peptides in DOPC (A) and DLPC (B) with radial positions labeled of key residues. Open symbols depict orientation at pH 8.2. L14K/DOPC at pH 8.2 is unchanged from water hydration and is not shown.
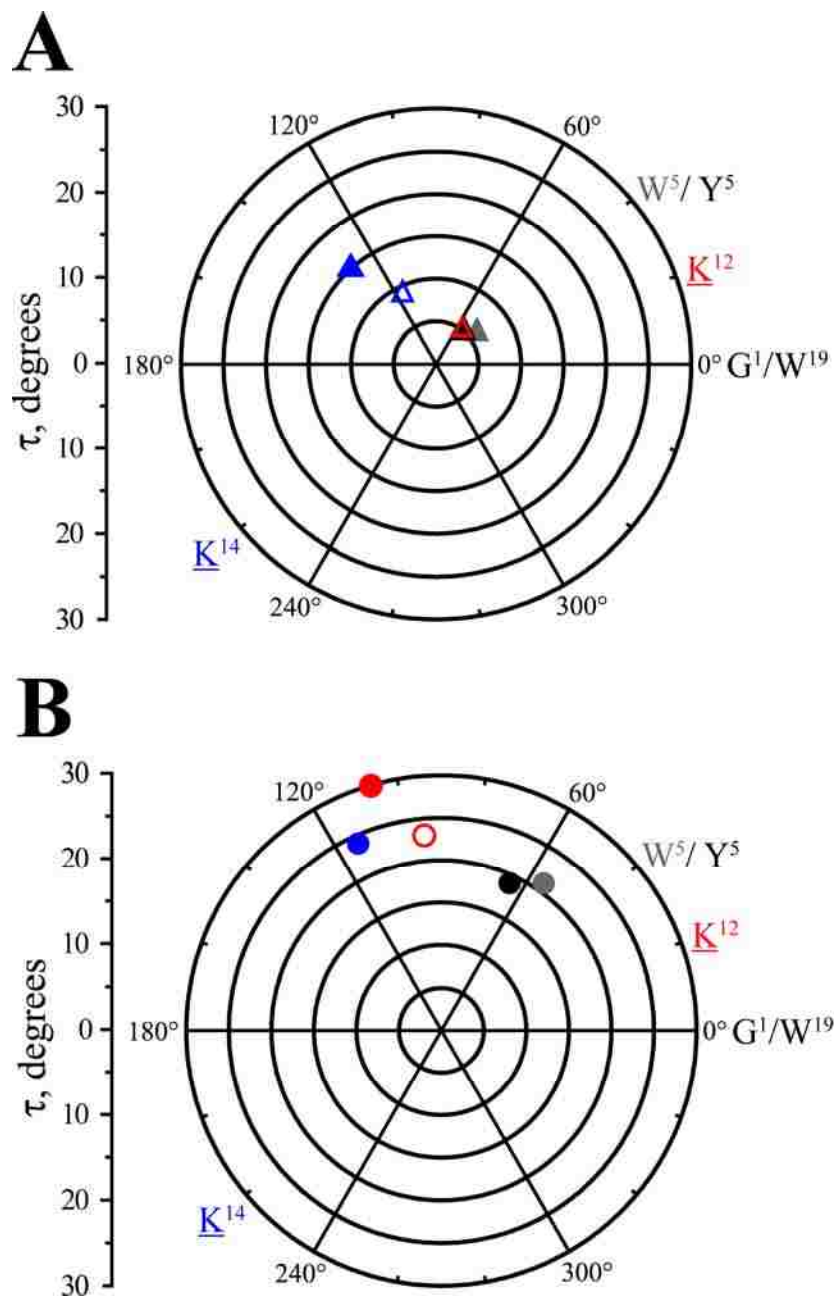
*Figure 7.* Titration observed in the $^2$H NMR spectra of GWALP23 L14K in DOPC (1:40) oriented samples run at 50 °C ($\beta = 90°$). Samples hydrated at various pH's labeled in figure. Deuterated alanines labeled.
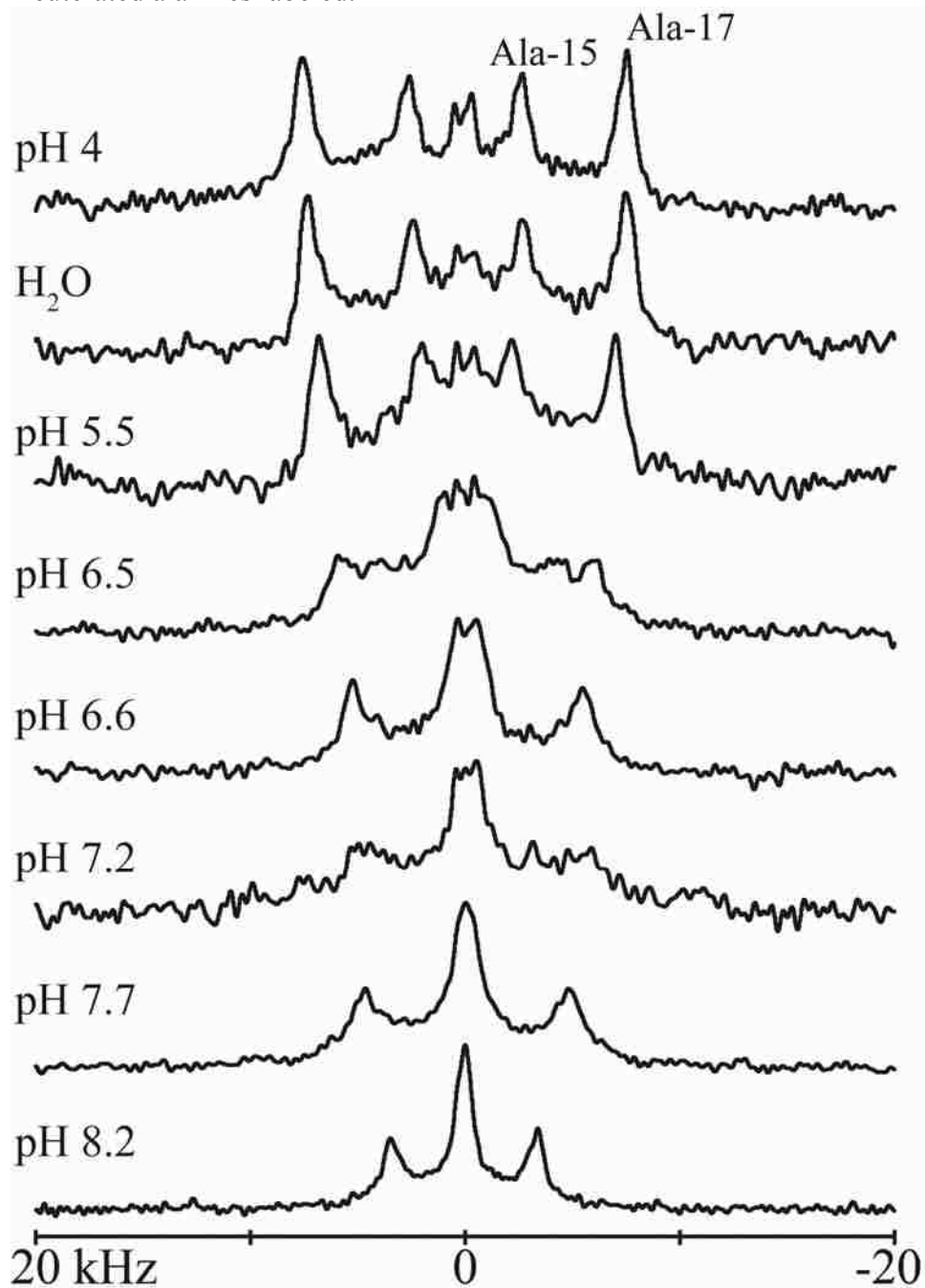
*Figure 8.* Titration Curves of GWALP23 L14K in DOPC using concurrent quadrupolar splittings ($\beta = 90°$) of Ala-15-$d_4$ and Ala-17-$d_4$ reporters indicate a p$K_a$ of 6.2 at 50 °C.
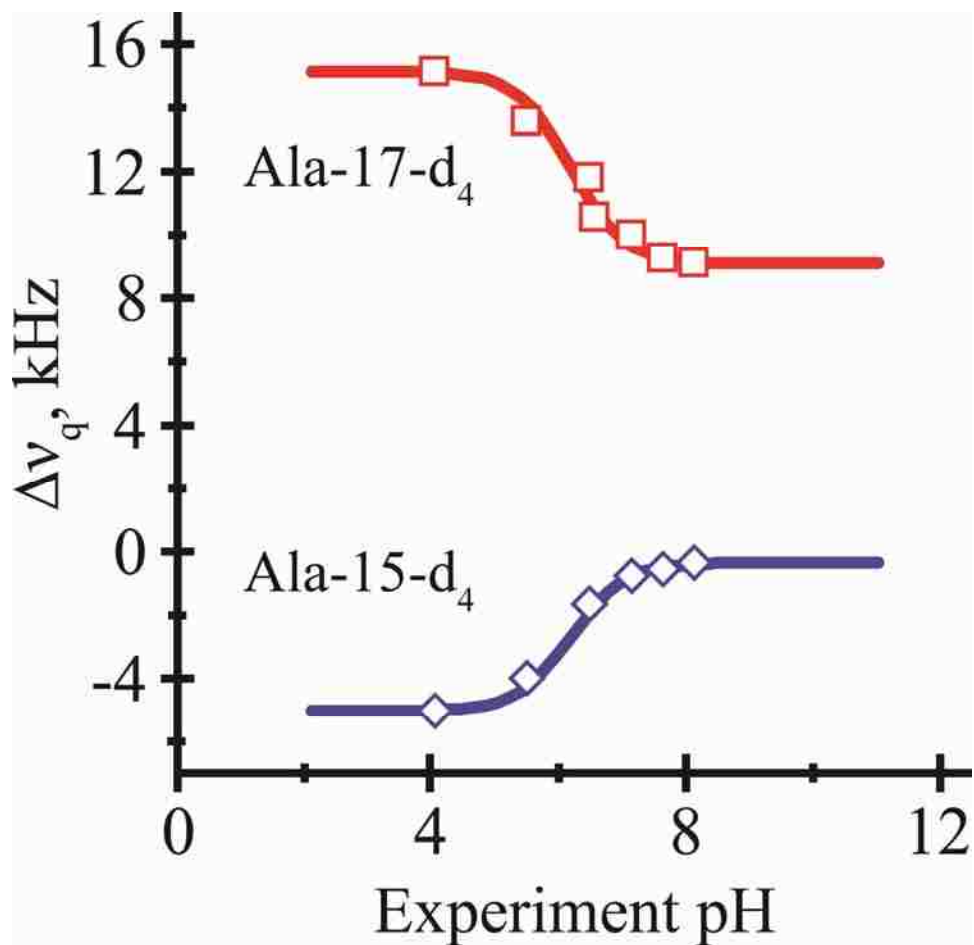
*Figure 9.* Titration observed in the $^2H$ NMR spectra of $Y^5$GWALP23 L12K in DOPC (1:40) oriented samples run at 50 °C ($\beta = 90°$). Labeled at $Ala^{15}$ (60% $^2H$) and $Ala^{17}$ (100% $^2H$). Samples hydrated at various pH conditions labeled in figure.
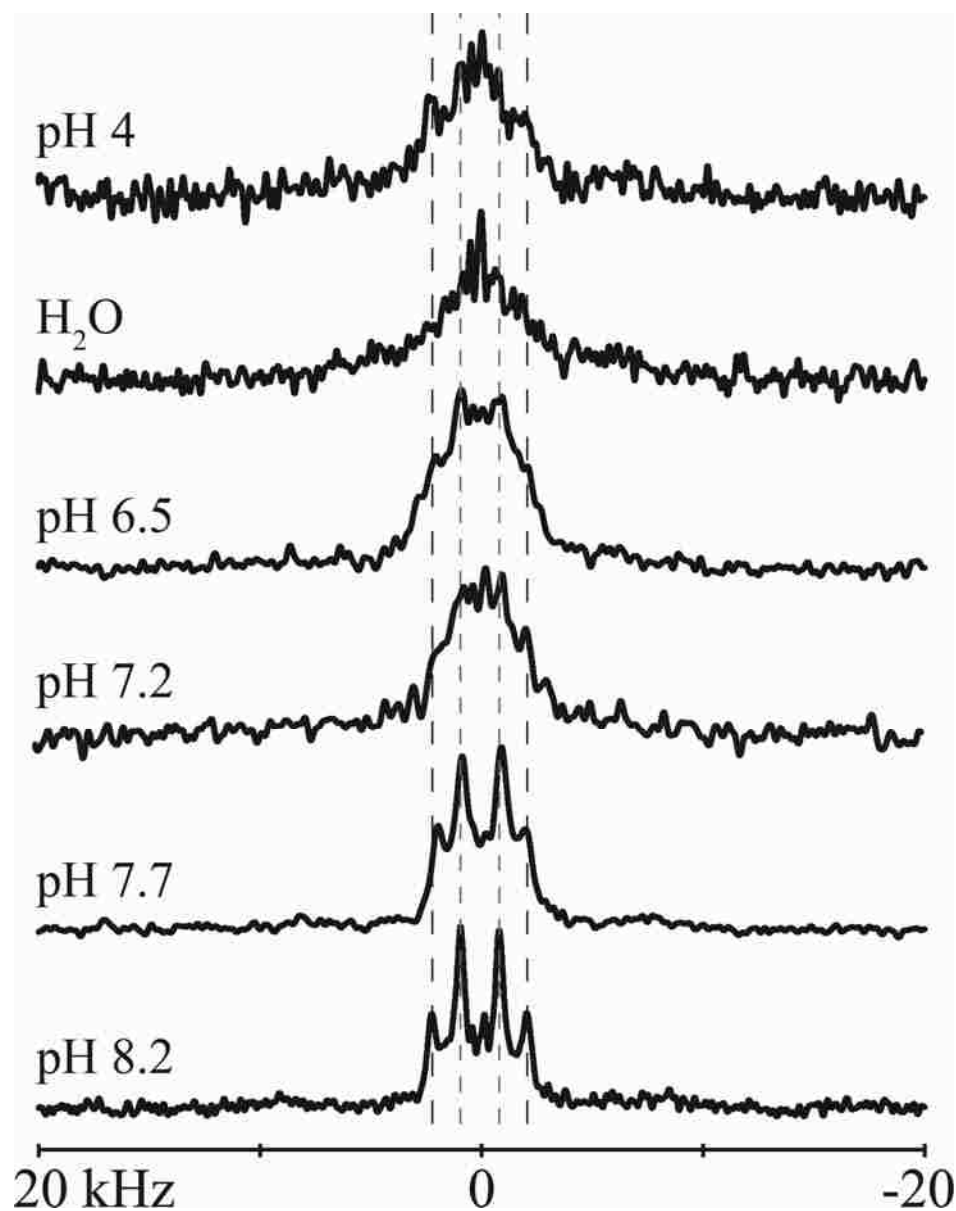
*Figure 10.* Fluorescence of Y$^5$GWALP23 L14K (A) and Y$^5$GWALP23 L12K (B) in DOPC vesicles. Samples excited at 295 nm.
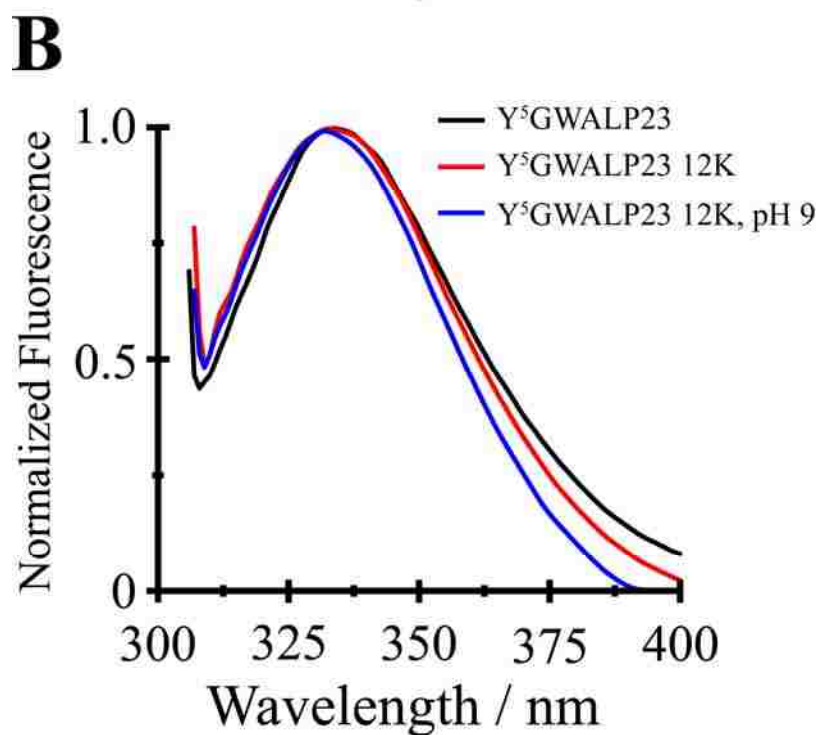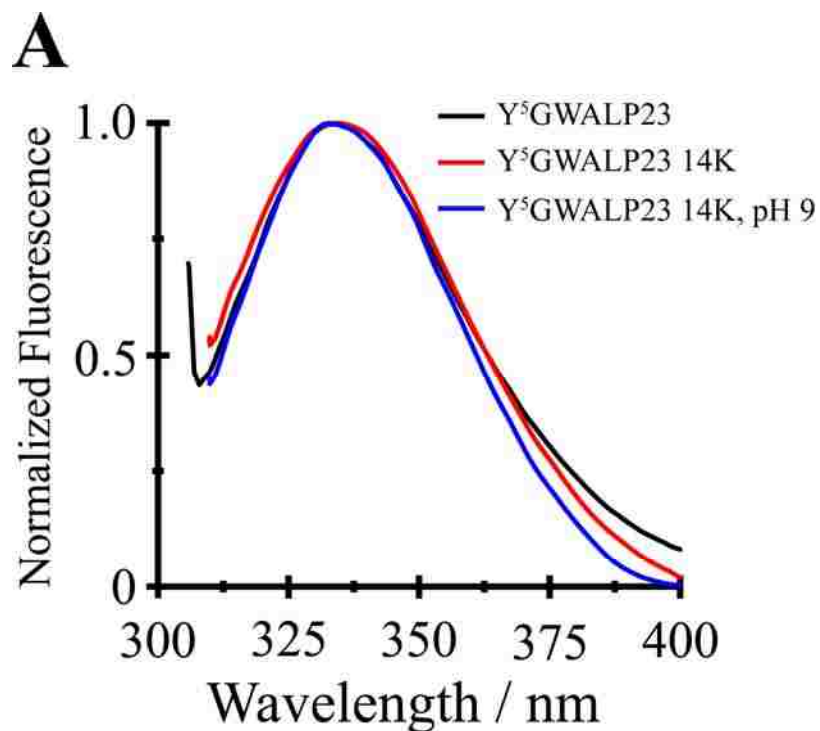
## 4.10 Supporting Information

*Figure S1*. Peptide identity confirmation by MALDI-TOF Mass spectrometry of a Y$^5$GWALP23 L12K peptide with two Ala-d$_4$ labels (50% and 100%).
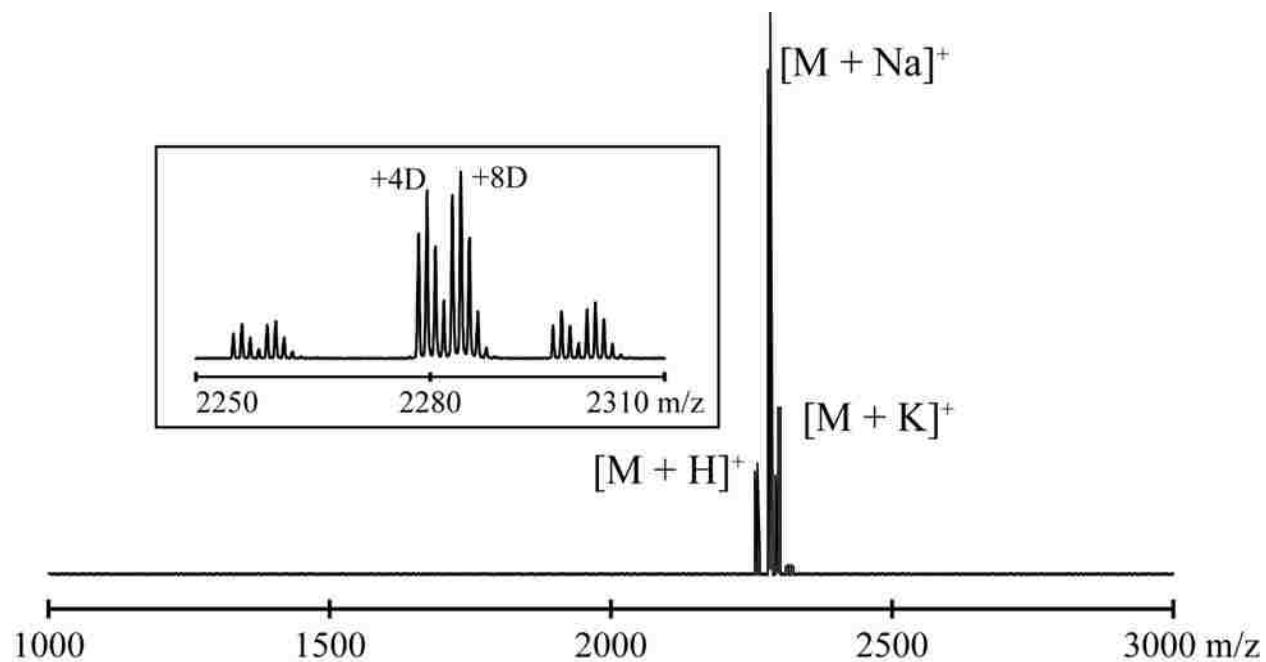
*Figure S2.* HPLC analysis of a Y[5]GWALP23 and Lys-12 analogue. Absorbance detection at 280 nm.
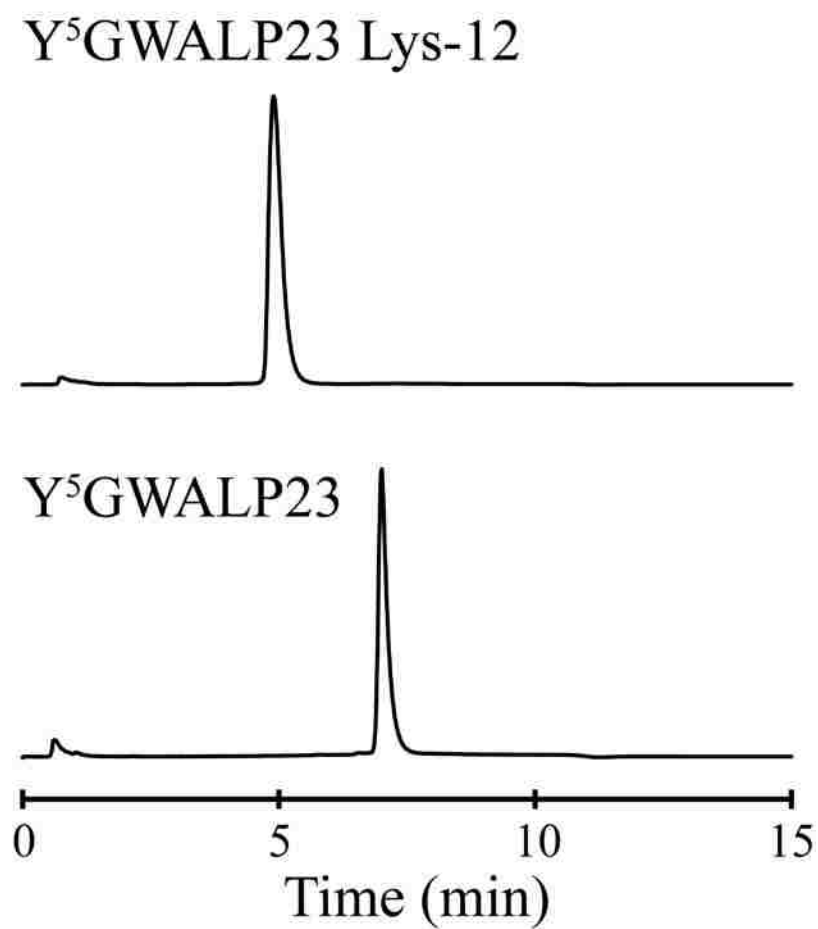
*Figure S3.* Circular dichroism spectra of peptides in DLPC vesicles (1:60).
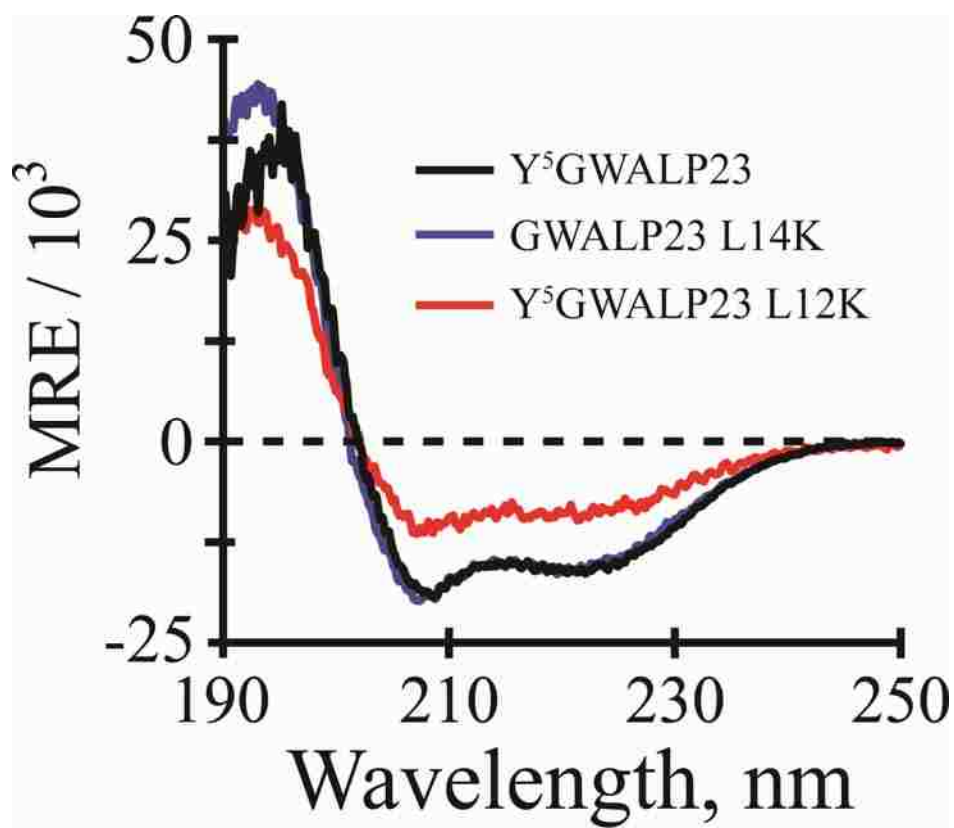
*Figure S4.* Bilayer alignment in oriented samples with peptides was determined by solid-state ^{31}P NMR. Shown in lipid at two macroscopically oriented alignments.
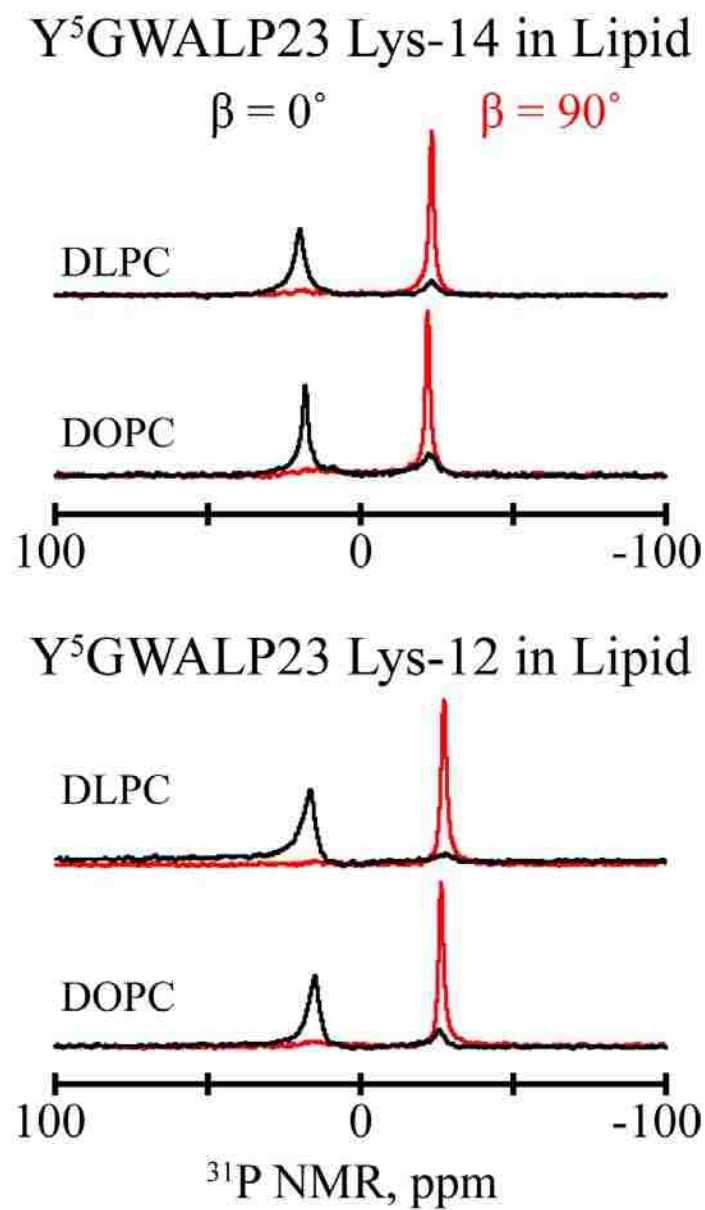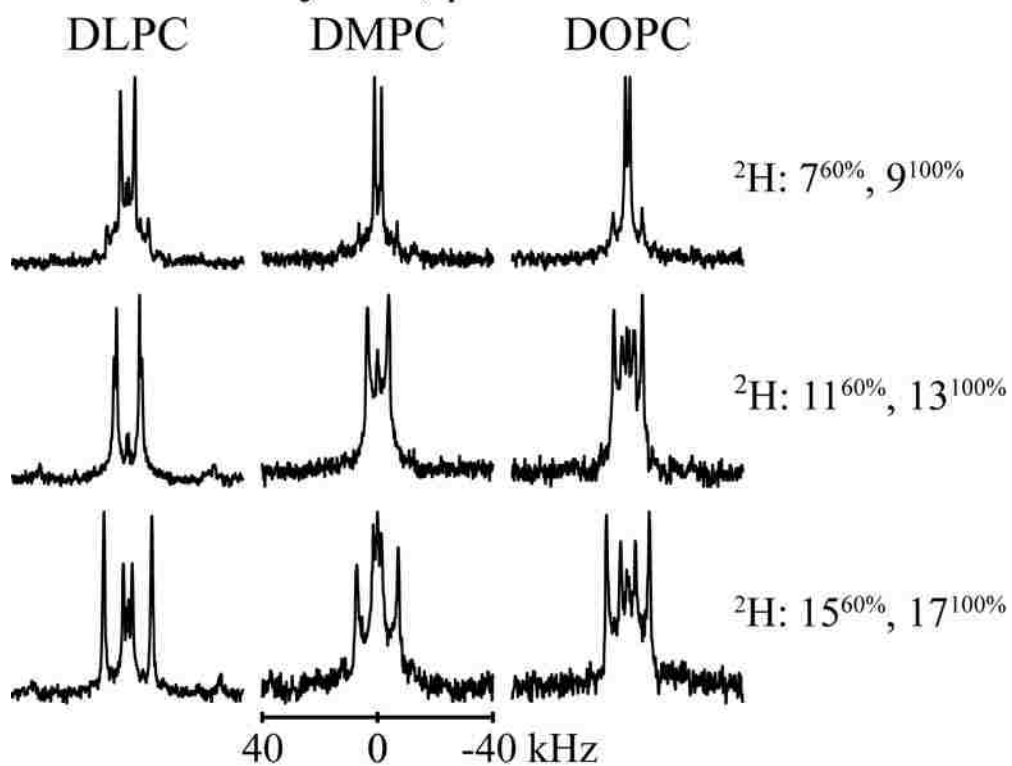


Y[5]GWALP23 Lys-14 in Lipid

$\beta = 0°$   $\beta = 90°$

DLPC

DOPC

100    0    -100

Y[5]GWALP23 Lys-12 in Lipid

DLPC

DOPC

100    0    -100

^{31}P NMR, ppm

*Figure S5.* $^2$H NMR spectra of GWALP23 L14K in lipid.

## GWALP23 Lys-14, β = 90°

DLPC          DMPC          DOPC

$^2$H: 7$^{60\%}$, 9$^{100\%}$

$^2$H: 11$^{60\%}$, 13$^{100\%}$

$^2$H: 15$^{60\%}$, 17$^{100\%}$

40        0      -40 kHz

## GWALP23 Lys-14, β = 0°

DLPC          DMPC          DOPC

$^2$H: 7$^{60\%}$, 9$^{100\%}$

$^2$H: 11$^{60\%}$, 13$^{100\%}$

$^2$H: 15$^{60\%}$, 17$^{100\%}$

40        0      -40 kHz
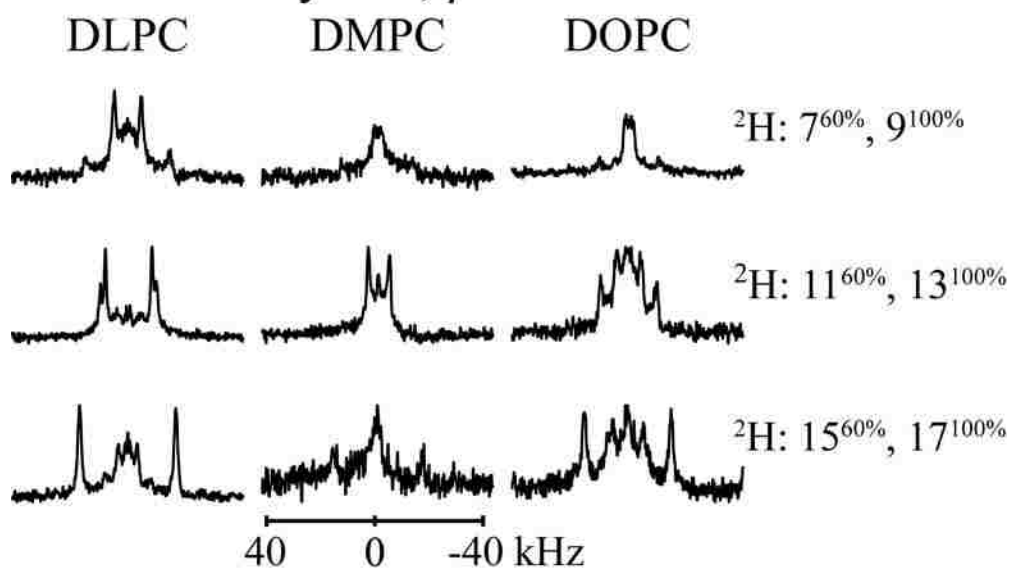
*Figure S6.* $^2$H NMR spectra of Y$^5$GWALP23 L12K in lipid.



Y$^5$GWALP23 Lys-12, $\beta = 90°$

DLPC  DMPC  DOPC

$^2$H: $7^{60\%}$, $9^{100\%}$

$^2$H: $11^{60\%}$, $13^{100\%}$

$^2$H: $15^{60\%}$, $17^{100\%}$

40    0    -40 kHz

Y$^5$GWALP23 Lys-12, $\beta = 0°$

DLPC  DMPC  DOPC

$^2$H: $7^{60\%}$, $9^{100\%}$

N/A    $^2$H: $11^{60\%}$, $13^{100\%}$

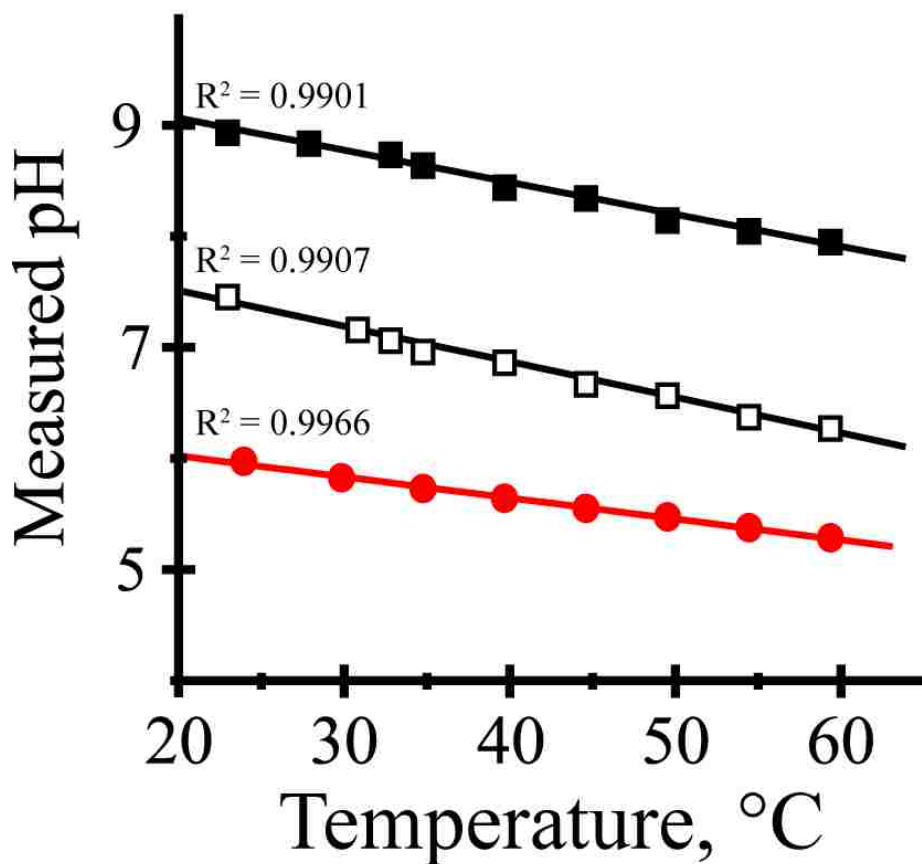$^2$H: $15^{60\%}$, $17^{100\%}$

40    0    -40 kHz

166
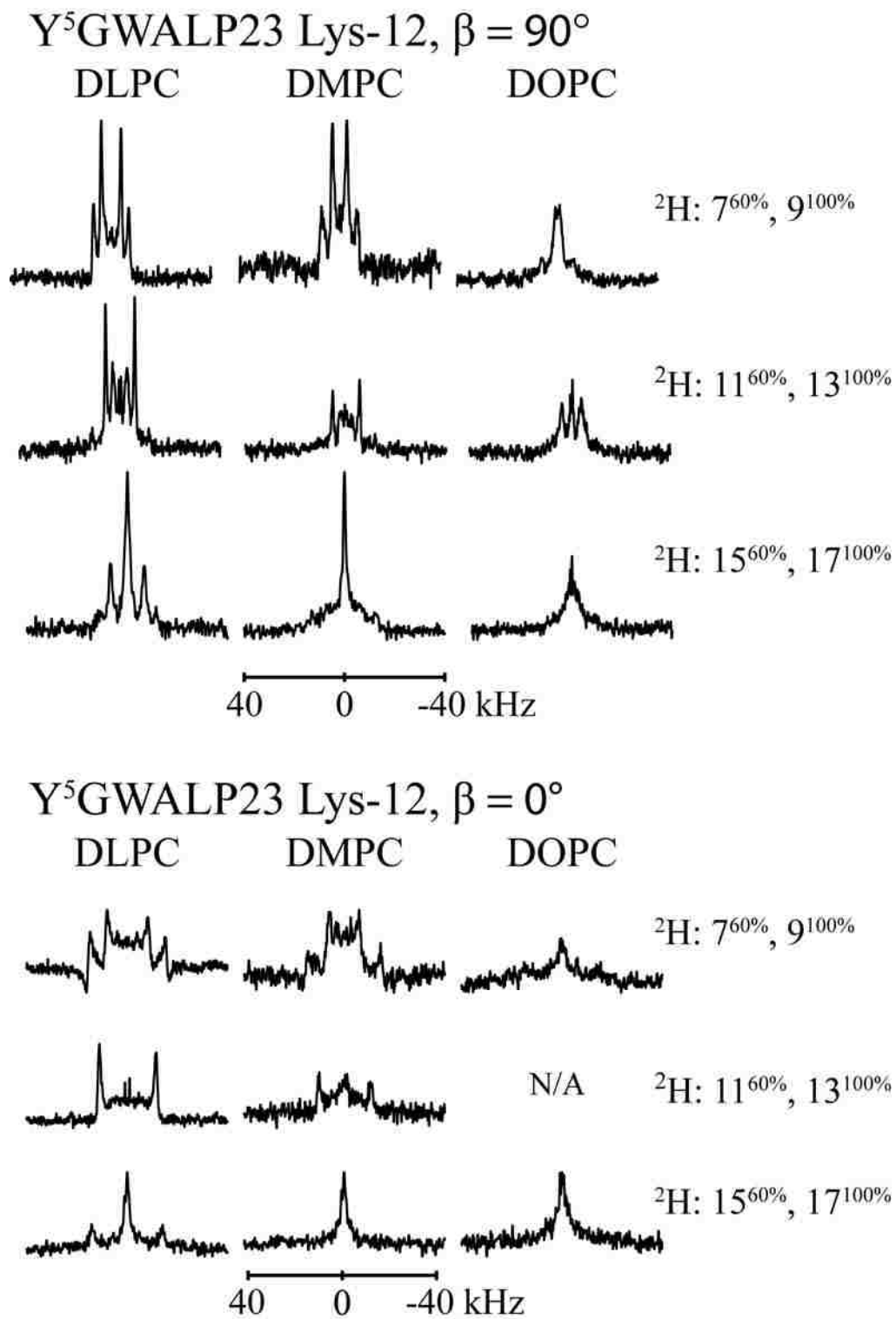
*Figure S7.* Buffer pH temperature-dependence[a] of pH 9 Tris buffer (black squares), pH 7.5 Tris buffer (open squares), and pH 6 Bis-tris (red circles). All buffers prepared at room temperature and 50 mM.



[a]Fitted trendlines correspond to -0.029 u/°C (Tris, pH 9), -0.0321 u/°C (Tris, pH 7.5), and -0.019 u/°C (Bis-tris, pH 6)

# CHAPTER 5

## Examination of Membrane-Buried Ion Pairs within GWALP23 Peptides

## 5.1 Abstract

Previous solid-state $^2$H NMR experiments have demonstrated the use of model peptides to examine the depth to which Lys or Arg can be inserted into a lipid bilayer (Dissertation chapter 4; Vostrikov et al. 2010). While GWALP23-R14 [acetyl-GGALWLALALALARALALWLAGA-amide] behaved well in DOPC membranes, the R12 analogue, with $^2$H-Ala labels, produced several broad $^2$H NMR peaks of low intensity, likely indicating multi-state behavior including a surface-bound population. The corresponding Lys analogues ((Y$^5$)GWALP23–K14 and –K12) exhibited similar position-dependent behavior; and furthermore could be titrated at high pH to yield states that more closely resemble those of the parent peptides. We now attempt to stabilize the bilayer-incorporated cationic residues by strategically placing an anionic residue (Glu) nearby, in hopes of either "rescuing" the X12 peptides with a stabilized ion pair or observing a noticeable change in the X14 peptide orientation in the bilayer due to an intra-helix salt bridge. Glutamic acid was placed either at position ($i$ + 1) or ($i$ + 4), with respect to Lys or Arg at position $i$, corresponding to either directly adjacent or proximal to the charged residue in the next helix turn. The addition of Glu-13 does in fact allow the Lys-12 peptide to orient in DOPC, but Glu-16 does not. Lys-14 was also influenced by Glu-15 insertion. Both Lys peptides with adjacent Glu appeared nearly identical at high pH to their Lys-only parents without Glu present. Arg-12 also appeared to be affected by the presence of either Glu-13 or 16. Both R12 peptides yielded better resolved NMR spectra at high pH, with E13 giving the most pronounced improvement at pH 8.2. Y$^5$GWALP23–(R12, E13) and –(K12, E13) behave similarly at pH 8.2.

**5.2 Introduction**

The Arg guanidino group is characterized by a high $pK_a$, due to resonance stabilization and a delocalized charge. The effects are sufficiently strong to inhibit the guanidium side chain from deprotonating even in nonpolar environments such as the interior of a lipid bilayer. Some investigators speculate that Arg will always be charged in a lipid environment and may even be able to withstand complete hydrocarbon isolation without deprotonating (Allen et al. 2008; Harms et al. 2011). Lysine, on the other hand, with a lower aqueous $pK_a$ has been readily observed in both charged and neutral forms, as its $pK_a$ can be lowered from about 10.5 in aqueous solution to the physiological pH range in non-polar environments (Stites et al. 1991). The highly polar and ionizable lysine and arginine residues show interesting position-dependence within GWALP-like peptides in the bilayer. While both residue insertions are well-behaved at ~ 3 Å from the helix center (L14), insertion at the middle (L12) produced dramatic changes in behavior with multiple low intensity peaks indicative of multi-state behavior (Dissertation chapter 4; Vostrikov et al. 2010). $Y^5$GWALP23 12K was able to recover from its multi-state behavior by neutralizing at high pH, unlike the Arg-12 analogue.

While titration to high pH was one method of peptide rescue for Lys-12, alternatively, the placement of an adjacent anionic residue was also pursued to see if a potentially stabilizing ion-pairing interaction could also favor a particular transmembrane helix orientation. Ion-pairs (or salt-bridges) are commonly found in soluble proteins and are not exclusive to their polar exterior. A large number of examples of these Coulombic interactions exist with varying strengths in the hydrophobic cores of proteins and in many cases improve the overall stability of the protein (Hendsch and Tidor 1994; Zhang et al. 2007). The low dielectric environment of hydrophobic

regions enhances these electrostatic ion-pair interactions, as has been observed experimentally by ion-pair titrations through water:octanol partitioning (Wimley et al. 1996).

To assess the viability of an intra-helix ion-pair interaction within the bilayer, we have strategically placed a counter-ion near one of the previously characterized Lys or Arg residues in GWALP23-like peptides. The proximity and geometry of paired counter-ions is very important regarding salt-bridge formation and stability (Kumar and Nussinov 1999). To address this issue, two peptide variants with different modes of interaction have been constructed to serve as candidates for a possible ion-pair interaction, including an $i$ to $(i + 1)$ strategy with glutamic acid placed directly adjacent in sequence or an $i$ to $(i + 4)$ placement with the anionic residue found on the same face of the helix on the next helix turn (*Table 1*). Ion-paring motifs are illustrated by models in *Figure 1*. The Y$^5$GWALP23 12K, 13E peptide was in fact shown to rescue the previously unoriented Lys-12 peptide in DOPC and Lys-14 was also affected by an adjacent Glu-15. When peptides were titrated to high pH, both Lys-12 and Lys-14 peptides with adjacent Glu residues appeared nearly identical to their respective parent peptides without Glu present. Arg-12 was also affected by Glu-13 and to a lesser extent by Glu-16. The most pronounced improvement in Arg-12 $^2$H NMR spectra was observed with Y$^5$GWALP23 12R, 13E at pH 8.2, which displayed an orientation much like the 12K, 13E analogue.

## 5.3 Materials and Methods
### Solid Phase Synthesis of $^2$H-Labeled Peptides

Commercial L-alanine-d$_4$ from Cambridge Isotope Laboratories (Andover, MA) was modified with an Fmoc group, as described previously (Thomas et al. 2009), and recrystallized from ethyl acetate:hexane, 80:20. NMR spectra ($^1$H) were used to confirm successful Fmoc-Ala-d$_4$ synthesis. Other protected amino acids and acid-labile "Rink" amide resin were purchased from NovaBiochem (San Diego, CA). All peptides were synthesized on a 0.1 mmol scale using "FastMoc™" methods and a model 433A synthesizer from Applied Biosystems by Life Technologies (Foster City, CA). Typically, two deuterated alanines of differing isotope abundances were incorporated into each synthesized peptide. Selected precursors for deuterated residues therefore contained either 100% Fmoc-L-Ala-d$_4$ or 50% Fmoc-L-Ala-d$_4$ with 50% non-deuterated Fmoc-L-Ala. The final residue on each peptide was acetyl-Gly to yield a blocked, neutral N-terminal.

A peptide cleavage solution was prepared containing 85% trifluoroacetic acid (TFA) and 5% each (v/v or w/v) of triisopropylsilane, water, and phenol. TFA cleavage from "Rink" resin in 2 mL volume (2-3 h at 22 °C) leads to a neutral, amidated C-terminal. Peptides were precipitated by adding the TFA solution to 25 volumes of cold 50/50 MtBE/hexane. Peptides were collected by centrifugation, washed multiple times with MtBE/hexane and lyophilized from (1:1) acetonitrile/water. After lyophilization, crude peptide dissolved in TFE was purified via HPLC on a Zorbax Rx-C8 9.4 mm x 25 cm column packed with 5 μm octyl-silica (Agilent Technologies, Santa Clara, CA) with a typical gradient of 92-96% methanol/water (0.1% TFA) and a 1.7 mL/min. flow rate. Collected product is lyophilized multiple times to remove residual TFA. MALDI-TOF mass spectrometry was used to confirm peptide identity by molecular mass

(*Figure S1* in Supplementary Material). Peptide purity was examined by reversed-phase HPLC with 280 nm detection, using a 4.6 x 50 mm Zorbax SB-C8 column packed with 3.5 μm octyl-silica (Agilent Technologies, Santa Clara, CA), operated at 1 mL/min using a methanol/water gradient from 85% to 99% methanol (with 0.1% TFA) over five min (*Figure S2* in Supplementary Material). Peptide quantity was calculated by means of UV absorbance at 280 nm, using molar extinction coefficients of 5,600 $M^{-1}$ $cm^{-1}$ for each Trp and 1,490 $M^{-1}$ $cm^{-1}$ for each Tyr residue in the peptide (Pace et al. 1995). Solvents were of the highest available purity. Water was doubly deionized Milli-Q™ water.

## $^2$H NMR Spectroscopy using Oriented Bilayer samples

Mechanically aligned samples for solid-state NMR spectroscopy (1/40, peptide/lipid) were prepared using DOPC or DLPC lipids from Avanti Polar Lipids (Alabaster, AL), and deuterium-depleted water (Cambridge; 45% w/w hydration), as described previously (Thomas et al. 2009). Bilayer alignment within each sample was confirmed using $^{31}$P NMR at 50 ˚C on a Bruker Avance 300 spectrometer (Billerica, MA) at both β = 0˚ (bilayer normal parallel to magnetic field) and β = 90˚ macroscopic sample orientations. Deuterium NMR spectra were recorded at both sample orientations on a Bruker Avance 300 spectrometer, utilizing a quadrupolar echo pulse sequence (Davis et al. 1996) with 90 ms recycle delay, 3.2 μs pulse length and 115 μs echo delay. Between 0.5 and 1.5 million scans were accumulated during each $^2$H NMR experiment. An exponential weighting function with 100 Hz line broadening was applied prior to Fourier transformation.

Buffers for oriented samples were prepared at room temperature using vacuum-dried reagents and prepared in deuterium-depleted water. Buffers include: pH 4 Acetate buffer 50 mM (sodium

acetate and acetic acid, Sigma, St. Louis, MO) and pH 9 Tris buffer 50 mM (Trizma[®] hydrochloride and Trizma[®] base, St. Louis, MO).

Due to the temperature-dependence of the $pK_a$ for various buffers, each buffer's pH (excluding acetate buffer with a known negligible temperature-dependence) was measured at incremental temperatures between room temperature (23°) and 60° (Dissertation chapter 4) to account for the elevated temperature (50°) in which the $^2$H NMR samples were run. Trendlines were found to be highly linear for Tris buffer. A d(pH)/dT value of -0.0306 was used for adjusting the pH value of Tris buffer for 50° for $^2$H NMR data interpretation.

## $^2$H NMR GALA Analysis

The analysis using semi-static peptide dynamics involves a principal order parameter $S_{zz}$ to estimate overall peptide motion with respect to an apparent average peptide orientation. These calculations are based on the GALA analysis, as previously described (van der Wel et al. 2002; Strandberg et al. 2004; Strandberg et al. 2009). These calculations are performed using $\tau$, $\rho$ and $S_{zz}$ as variable parameters and screen for the lowest RMSD. The analysis considers the $^2$H quadrupolar splittings (QS) for the isotope-labeled residues based on ideal $\alpha$-helix geometry.

173

**5.4 Results**

It was seen that Y$^5$GWALP23 Lys-12 and GWALP23 Arg-12 exhibit multi-state behavior in DOPC bilayer membranes (Dissertation chapter 4, Vostrikov et al. 2010). In an attempt to stabilize and maintain these energetically unfavorable charged groups within the bilayer membrane, an additional ionizable residue of opposite charge, glutamic acid, was placed adjacent to serve as a counter-ion. The $^2$H NMR spectra of Y$^5$GWALP23 K12, E13 in DOPC were immensely improved from over those observed when K12 alone was present in the absence of E13 (*Figure 2*). Moreover in DLPC, the *i* to (*i* + 1) configuration of complementary ionizable residues altered the orientation of a K12 peptide, as indicated by the changes in the QS's (*Figure 3*). In contrast, when an *i* to (*i* + 4) motif was used for the counter-ion placement, the spectra did not improve in DOPC (*Figure 2*). Furthermore, whereas the K12 peptide was previously behaving quite well in the thin DLPC bilayer, when E16 is present there appears a multi-state behavior, as indicated by $^2$H NMR spectra (*Figure 3*). A total of four QS's were obtained for Y$^5$GWALP23 K12, E13 in DLPC and DOPC (*Table 2*) and a variable-$S_{zz}$ analysis was applied to fit the orientational constraints and estimate the peptide's orientation within the bilayer (*Table 3*). In DOPC, the newly rescued helix with Lys-12 with Glu-13 possesses a tilt magnitude of 19° and azimuthal rotation of 268°, illustrated in *Figure 5*. In the thinner DLPC bilayer the helix also seems to orient quite similarly, but the precise orientation is at this time unclear due to some uncertainty in the NMR assignments. The two potential solutions: $\tau$ = [b]19° or [c]37° and $\rho$ = [b]282° or [c]285° are displayed in *Figure 5*. Both solutions provide some level of credibility, but also raise individual concerns that will be explored in the Discussion.

Y$^5$GWALP23 R12, E13 yielded spectra in DOPC that were somewhat improved over the peptide with R12 alone, but the $^2$H NMR spectrum still is not particularly "good" (compared to what would be expected for a single dominant helix orientation). The spectra for the corresponding *i* to (*i* + 4) peptide (Arg-12, Glu-16) also showed some signs of improvement, but not still was not particularly "good" (*Figure 8*). Equivalent samples were then prepared at pH 8.2, and improved spectra with altered QS's were observed (*Figure 8).* The spectra for the peptide with (Arg-12, Glu-13) were the most improved, so this peptide was additionally labeled and four QS's were obtained. Variable S$_{zz}$ GALA analysis reveals a helix orientation (*Figure 9*) close to that of the peptide having (Lys-12, Glu-13) at lower pH.

GWALP23 Lys-14 had previously shown to orient well in a range of lipids and was also subjected to an *i* to (*i* + 1) addition of Glu (*Figure 7*). The K14 peptide does appear slightly affected by the added Glu (E15), as shown in a quadrupolar wave plot of the $^2$H NMR QS's (*Figure 6*). The (K14, E15) peptide reorients with increased tilt magnitude of 21° ($\Delta\tau$ = +6°) and an azimuthal rotation of 253° ($\Delta\rho$ = +26°) when Glu-15 is added (*Table 3*).

Several pH experiments were performed of the Lys-containing peptides to help elucidate their potential ion-pairing interactions. Again, the already mentioned Arg-12, Glu-X peptides each appeared to be sensitive to the environmental pH, with improved NMR spectra resulting at higher pH. Concerning the (Lys-14, Glu-15) peptide with a potentially enhanced charged state by a stabilizing counter-ion, a change in its titration properties was somewhat expected from that of Lys-14 alone. Nevertheless, titration of the Lys-14, Glu-15 peptide to pH 8.2, yields the QS's appearing very similar to its Lys-only predecessor when titrated, and the QS's furthermore were identical at pH 4. In contrast, Y$^5$GWALP23 K12, E13 in DOPC bilayer remains largely unchanged at pH 8.2 as compared to when hydrated with unbuffered water (*Figure 8*). Though

at pH 4, while the dominant QS's still remain, albeit with lower intensities, the peptide does appear to show extra signals emerging, suggestive of an increasing population exhibiting multi-state behavior.  Again, though the dominant QS magnitudes are unchanging across the pH range, the general trend shows improvement of spectral quality as the pH increases.

**5.5 Discussion**

The previous observation of the multi-state Lys-12 peptide in DOPC being stabilized by neutralization at high pH is relatively straightforward to understand in that the system cannot incorporate the single charge ($\varepsilon$-NH$_3^+$), but can readily bury a deprotonated $\varepsilon$-NH$_2$ group. The alternative of stabilization by ion-pair interactions present new complexities for consideration. As these experiments are in fact only monitoring the isotopically labeled alanines and deducing peptide helix orientation within the bilayer, we are left to make educated predictions about the dynamics occurring in and between the present counter-ions in each case based on results. While the placement of counter-ions and their relative geometry has been shown to play a crucial role in the formation and stabilization of ion-pairs (Kumar and Nussinov 1999), we do not possess atomistic depictions of the side chain orientations that might definitely help to elucidate the interactions. Furthermore, titration experiments are complicated by the presence of two ionizable polar residues.

A separate study of glutamic acid alone substituted into Y$^5$GWALP23 was done and revealed only minor changes in QS's when Glu was introduced at position 12 or 14 (Supplemental *Figure S3*). A significant reduction in the $^2$H NMR spectra quality was nevertheless observed. Further analysis showed only minimal changes to the peptide helix orientation in response to E12 and a ~50 change in azimuthal rotation in response to E14 (Supplemental *Figure S4*), while maintaining the helix tilt magnitude. Recent titration experiments from our lab have shown improved spectra at low pH (2.5) and signal fall-off as pH is raised to 8.2 in DOPC likely, suggesting that the Glu residue is partially protonated in unbuffered water samples, but probably also in the midst of titration, with a small population of

the ionized form also present. These preliminary data suggest that the $pK_a$ of Glu-14 may be between 6 and 7.5.

Normally Lys and Glu exhibit $pK_a$'s ~ 6.5 units apart in aqueous solution. However, when subjected to the non-polar bilayer environment both $pK_a$'s shift to favor the neutral form. The Lys $pK_a$ was shown to be ~ 4 units lower in previous experiments with GWALP23-K14 (Dissertation, chapter 4). It is likely that the Glu $pK_a$, conversely, is about 2-4 units higher in the bilayer than in aqueous solution. Clearly, the $pK_a$'s of bilayer-incorporated Lys and Glu may nearly overlap or even reverse their relative positions. The apparent overlap of $pK_a$'s can lead to ambiguity of titration data and render it difficult to directly access the protonation state of each residue.

The vast improvement in the $^2$H NMR spectra when Glu-13 is added to the Lys$^+$-12 peptide in DOPC is certainly evidence of some charge stabilization. It is noteworthy that, in contrast to titrated Lys$^0$-12 peptide, which adopts a small tilt nearly identical to the host peptide, Y$^5$GWALP23 with the ion-pair retains a relatively large tilt (19°) in DOPC, which may be evidence that a charged ion pair is partially submerged in the bilayer. A stabilization of charges is further illustrated when the system is subjected to low or high pH. The lack of change of the QS's at pH 4 (despite a small reduction in spectral quality) may indicate the Glu $pK_a$ has shifted back towards its original value to retain the negatively charged state that is stabilized by the adjacent cationic residue. Furthermore, because we do not see a shift at pH 8.2 as well (only slight spectral improvement), it provides further evidence that the Lys $pK_a$ may have also shifted upwards to support a charged Lys$^+$ that is capable of a favorable ion-pair interaction, with the spectrum at pH 8.2 being improved by the now complete deprotonation of Glu.

Concerning this same Lys-12, Glu-13 peptide in DLPC, due to a rather limited data set and an assignment uncertainty, we were unable to definitively assign a single peptide orientation and instead display two potential solutions (*Figure 5*). In one scenario ($\tau = 19°$, $\rho = 282°$), the peptide appears to have adopted an orientation very similar to that in DOPC. This seeming lack of bilayer sensitivity would be interesting, but the unrealistically high $S_{zz}$ of 1.0 is puzzling (and without precedent). Attempts to manually hold $S_{zz}$ to lower values leads to solutions with significantly high RMSD values. Alternatively, a solution of ($\tau = 37°$, $\rho = 285°$) possesses a reasonable $S_{zz}$ of 0.65 that is similar to the peptide fits in DOPC, but displays an abnormally high tilt angle (again without precedent within the GWALP23 family). The presence of a large QS > 38 kHz lends some credibility to this solution, as a general trend is for larger QS's to indicate increased tilts. Additionally, this fit holds a lower RMSD than the previous, but both are within normal limits. The existing data set is limited by its small size (only four QS's) and by the uncertain assignments for Ala-7 and Ala-9. More data points and reconfirmation of the assignments are needed.

The particularly poor performance of Lys-12 with a Glu-16 placed in the *i* to (*i* + 4) confirmation fashion is of interest. My initial hypothesis, based on helix side chain modeling, expected this arrangement to allow for the two ionizable residue to exist in closer proximity to each other, more favorably than with the *i* to (*i* + 1) placement. The loss of a stable Lys$^+$-12 orientation in DLPC in the presence of Glu-16 demonstrates the complications arising from glutamic acid substitution, and suggests furthermore that the charged Lys$^+$-12 and Glu$^-$-16 groups may compete with each other in terms of each having different preferences for the tilted orientation of the transmembrane peptide. In similar fashion, the NMR solution structure of

another model peptide system also shows a greater propensity for $i$ to $(i + 1)$ ion-pair formation over the $i$ to $(i + 4)$ arrangement, albeit in a bent water-soluble $\alpha$-helix (Zhang et al. 2007).

The small change in the GWALP23 Lys$^+$-14 orientation in DLPC and DOPC upon the addition of Glu-15 also demonstrates its influence, but is relatively more difficult to characterize. Unlike with Lys-12, Glu-13 in DOPC; Lys-14, Glu-15 titrates at high pH and then curiously looks remarkably like the peptide with Lys$^0$-14 alone in DOPC. This lack of titration resistance seems to argue against an ion-pair interaction. Perhaps Glu-15 is independently, but additively, influencing the peptide's orientation along with Lys-14, but not actually interacting as a counter-ion. It is plausible that both of the (charged) residues may simply attempt to snorkel separately. The $i$ to $(i + 4)$ strategy has not yet been examined with Lys-14, considering that Glu-18 would likely be near the interface.

These seemingly divergent results of Lys-12 and Lys-14 with an $i$ to $(i + 1)$ Glu counter-ion demonstrate the importance of the residue locations and the bilayer depth for charge interactions. Indeed, the extent of water penetration could be important for the Lys-14 $\varepsilon$-NH$_3$$^+$, in that if water is available there may be little influence from a nearby Glu residue. Conceivably, nevertheless, Glu-15 may aid in creating a water defect and in "recruiting" water molecules that can be further utilized to stabilize Lys$^+$-14.

The stabilization of an Arg-12 peptide in DOPC was particularly interesting in that it appears to require both a high pH environment and the presence of Glu-13. Fortunately, the Arg experiments alleviate some of the uncertainties of side chain titrations because the guanidium group is expected to remain charged in all scenarios (Harms et al. 2011). Therefore the observed titration must be the deprotonation of glutamic acid. Obviously, the Arg interaction with a counter-ion would not be identical to that of Lys. Considering that Lys possesses its charge

concentrated on a single atom, it could therefore be expected to better "motivate" the adjacent Glu residue to deprotonate for an ion-pair interaction (resulting in a lower Glu $pK_a$). In contrast, the Arg charge is delocalized via resonance across the guanidium side chain. This dispersion of charge may result in lower influence on the adjacent Glu's protonation state and could therefore require a higher pH to produce a charged Glu⁻ residue that is capable of an ionic pair interaction.

In contrast to Lys-12, Glu-16; the $i$ to ($i$ + 4) approach of forming an ion-pair interaction showed some spectral improvement with (Arg-12, Glu-16) over the Arg-12 peptide alone in DOPC. (Spectral "improvement" generally will mean a greater tendency for the peptide helix to adopt one particular preferred orientation with respect to the lipid bilayer membrane). A single, and large, QS of 58.6 kHz is discernable in unbuffered water samples (*Figure 8*). However, this high value would seem to indicate a surface-bound peptide. (While it seems possible that the signal could result from the often elusive $C_\alpha$-D label, as they typically demonstrate much larger QS's (~ 50 - 115 kHz), it would be puzzling why the universally more intense, sharper and more readily observable $C_\beta$-$D_3$ signals would not be seen). If in fact the QS is indeed reporting the peptide's orientation as a $C_\beta$-$D_3$ signal, the result would suggest a minimum tilt of 40° up to an apparent surface-bound orientation of 75° (assuming a $S_{zz}$ of about 0.8).

In the titrated samples at pH 8.2, the (Arg-12, Glu-16) peptide produces a much more reasonable set of QS's (35 & 9 kHz for Ala-7 & Ala-9, respectively) that are typical of a moderately tilted transmembrane peptide. Nevertheless, spectral quality is overall poor as compared to the usual $^2$H NMR spectra of "well-behaving" peptide systems. Further experiments with more isotopic labels are needed.

## 5.6 Acknowledgments

## 5.7 References

Li, L., Vorobyov, I., MacKerell, A. D., and Allen, T. W. (2008) Is Arginine Charged in a Membrane? *Biophys. J. 94*, L11-L13.

DeLano, W. L. (2002) The PyMOL Molecular Graphics System.

Harms, M. J., Schlesman, J. L., Sue, G. R., and Garica-Moreno, E. B. (2011) Arginine residues at internal positions in a protein are always charged. *Proc. Natl. Acad. Sci. U. S. A. 108*, 18954-18959.

Hendsch, Z. S. and Tidor, B. (1994) Do salt bridges stabilize proteins? A continuum electrostatic analysis. *Protein Sci. 3*, 211-226.

Kumar, S. and Nussinov, R. (1999) Salt Bridge Stability in Monomeric Proteins. *J. Mol. Biol. 293*, 1241-1255.

Pace, C. N., Vajdos, F., Fee, L., Grimsley, G., and Gray, T. (1995) How to measure and predict the molar absorption coefficient of a protein. *Protein Sci. 4*, 2411-23.

Stites, W. E., Gittis, A. G., Lattman, E. E., and Shortle, D. (1991) In a staphylococcal nuclease mutant the side chain of a lysine replacing valine 66 is fully buried in the hydrophobic core. *J. Mol. Biol. 221*, 7–14.

Strandberg, E., Ozdirekcan, S., Rijkers, D. T., van der Wel, P. C., Koeppe, R. E. 2nd, Liskamp, R. M., and Killian, J. A. (2004) Tilt angles of transmembrane model peptides in oriented and non-oriented lipid bilayers as determined by ^{2}H solid-state NMR. *Biophys. J. 86*, 3709-3721.

Strandberg, E., Esteban-Martin, S., Salgado, J., and Ulrich, A. S. (2009) Orientation and dynamics of peptides in membranes calculated from ^{2}H-NMR data. *Biophys. J. 96*, 3223-3232.

Thomas, R., Vostrikov, V. V., Greathouse, D. V., and Koeppe, R. E. 2nd (2009) Influence of proline upon the folding and geometry of the WALP19 transmembrane peptide. *Biochemistry 48*, 11883-11891.

van der Wel, P. C., Strandberg, E., Killian, J. A., and Koeppe, R. E. 2nd (2002) Geometry and intrinsic tilt of a tryptophan-anchored transmembrane alpha-helix determined by ^{2}H NMR. *Biophys. J. 83*, 1479-1488.

Vostrikov, V. V., Hall, B. A., Greathouse, D. V., Koeppe, R. E. 2nd, and Sansom, M. S. P. (2010b) Changes in Transmembrane Helix Alignment by Arginine Residues Revealed by Solid-State NMR Experiments and Coarse-Grained MD Simulations. *J. Am. Chem. Soc. 132*, 5803–5811.

Wimley, W. C., Gawrisch, K., Creamer, T. P., and White, S. H. (1996) Direct measurement of salt-bridge solvation energies using a peptide model system: Implications for protein stability. *Biochemistry 93*, 2985-2990.

Zhang, L. and Morikis, D. (2007) Solution Structure of a Bent $\alpha$-Helix. *Biochemistry 46*, 12959-12967.

## 5.8 Tables

*Table 1.* Sequences of (Y[5])GWALP23 and Arg/Lys/Glu containing peptides[a]

| Name | Sequence |
|---|---|
| GWALP23 | a-GGALWLALALALALALALWLAGA-e |
| Y[5]GWALP23 | a-GGALYLALALALALALALWLAGA-amide |
| GWALP23 L14K | a-GGALWLALALALAKALALWLAGA-e |
| Y[5]GWALP23 L12K | a-GGALYLALALAKALALALWLAGA-amide |
| Y[5]GWALP23 L12R | a-GGALYLALALARALALALWLAGA-amide |
| Y[5]GWALP23 L12K, A13E | a-GGALYLALALAKELALALWLAGA-amide |
| Y[5]GWALP23 L12R, A13E | a-GGALYLALALARELALALWLAGA-amide |
| Y[5]GWALP23 L12K, L16E | a-GGALYLALALAKALAEALWLAGA-amide |
| Y[5]GWALP23 L12R, L16E | a-GGALYLALALARALAEALWLAGA-amide |
| Y[5]GWALP23 L14K, L15E | a-GGALYLALALALAKELALWLAGA-amide |

[a]Abbreviations:  "a" denotes "acetyl" and "e" denotes "ethanolamide."

*Table 2.* Observed $^2$H quadrupolar splittings[a] of Y$^5$GWALP23 (Arg-X or Lys-X) with Glu-X

| Ala-d4 | DLPC | | DOPC | | | |
|---|---|---|---|---|---|---|
| | K12, E13 H$_2$O | K14, E15 H$_2$O | K14, E15 H$_2$O | K12, E13 H$_2$O | K12, E13 pH 8.2 | R12, E13 pH 8.2 |
| 7 | 26.2[b] | 33.2 | 28.3 | 24.8 | 25.0 | 25.5 |
| 9 | 38.4[b] | 25.9 | 11.5 | 14.3 | 13.8 | 16.8 |
| 13 | c | 6.3 | 10.2 | c | c | c |
| 15 | 18.3 | c | c | 6.6 | 5.2 | 11.4 |
| 17 | 19.7 | 30.6 | 28.0 | 17.4 | 18.3 | 11.4 |

[a]Quadrupolar splittings are reported in kHz for the β = 0° sample orientation. Each value is an average of (the magnitude observed when β = 0°), and (twice the magnitude observed when β = 90°).

[b]Speculative assignments of Ala-7 and Ala-9 due to intensity swapping of 2H NMR peaks (see *Figure 4*).

[c]Data point not recorded due to lack of Alanine residue upon Glu substitution.

*Table 3*. Semi-static GALA analysis of Y$^5$GWALP23 peptides containing ion-pairs[a]

| | DLPC | | | DOPC | | | |
|---|---|---|---|---|---|---|---|
| | K12, E13 H$_2$O[b] | K12, E13 H$_2$O[b] | K14, E15 H$_2$O | K14, E15 H$_2$O | K12, E13 H$_2$O | K12, E13 pH 8.2 | R12, E13 pH 8.2 |
| τ | 19° | 37° | 28° | 21° | 19° | 19° | 17° |
| ρ | 282° | 285° | 263° | 253° | 268° | 265° | 284° |
| S$_{zz}$ | 1.00 | 0.65 | 0.85 | 0.80 | 0.69 | 0.69 | 0.71 |
| RMSD (kHz) | 1.03 | 0.13 | 1.25 | 1.18 | 0.11 | 0.09 | 0.68 |

[a]Calculations based on four Ala methyl $^2$H quadrupolar splittings only.

[b]Two potential solutions displayed of (K12, E13) peptide in DLPC due to indiscernible spectra assignments (*Figure 4*).

## 5.9 Figures

*Figure 1.* Model representations of potential ion pair motifs on an α-helix. *i* to (*i* + 4) demonstrated by Y$^5$GWALP23 Lys-12, Glu-16 (left) and *i* to (*i* + 1) as shown by Y$^5$GWALP23 Lys-12, Glu-13 (right). Models drawn using PyMOL (DeLano et al. 2002). The side chain orientations are hypothetically arranged for optimal interaction of counter-ions.
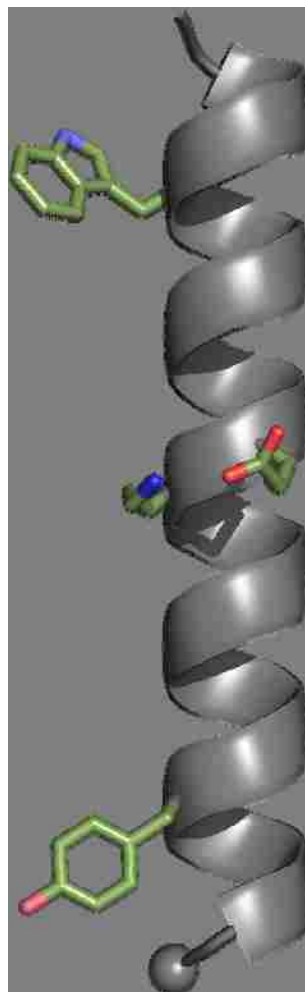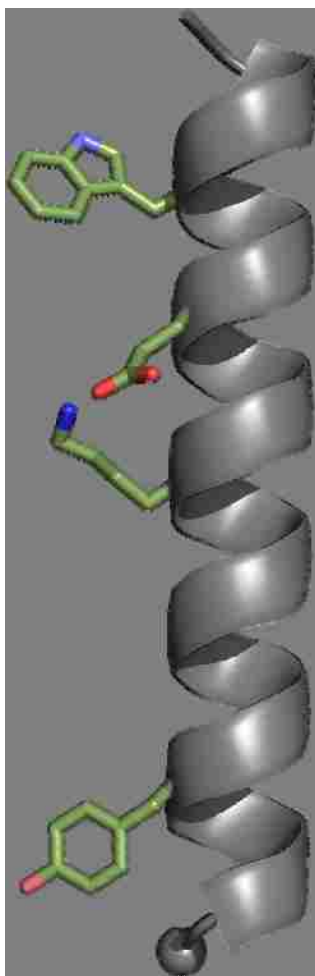
*Figure 2*. $^2$H NMR spectra of Y$^5$GWALP23 Lys-12 in DOPC and with an added counter-ion, Glu in multiple arrangements.
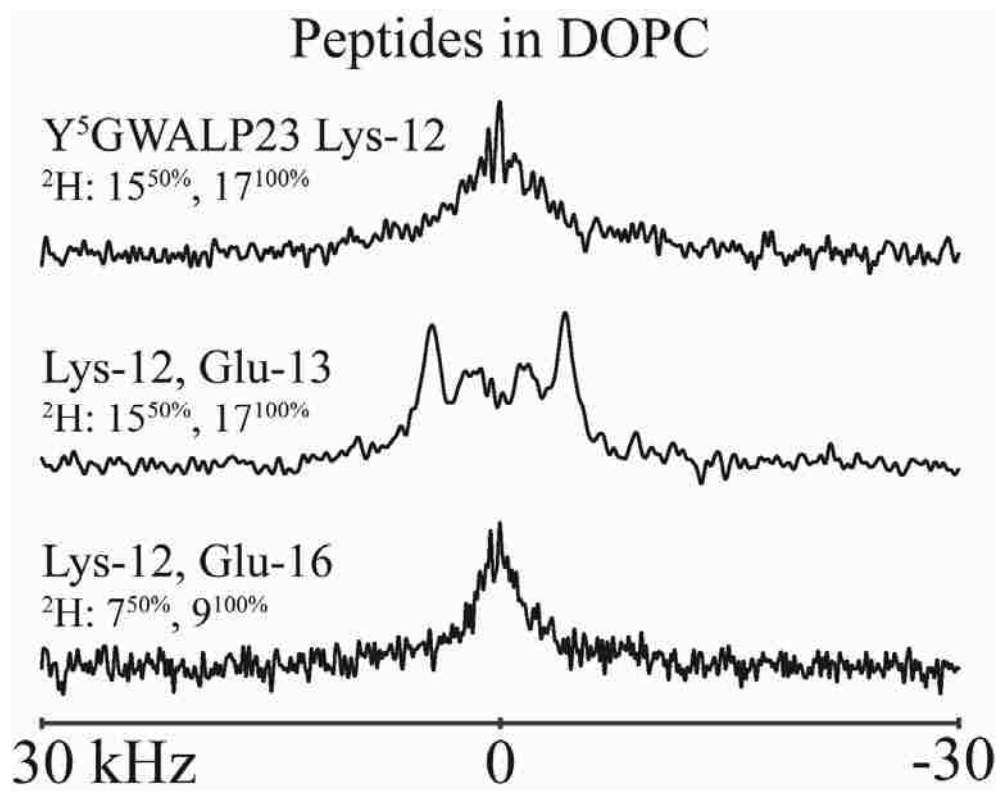
*Figure 3.* $^2$H NMR spectra of Y$^5$GWALP23 Lys-12 in DLPC and with an added counter-ion, Glu in multiple arrangements.



## Peptides in DLPC

Y$^5$GWALP23 Lys-12
$^2$H: 7$^{50\%}$, 9$^{100\%}$

Lys-12, Glu-13
$^2$H: 7$^{50\%}$, 9$^{100\%}$

Lys-12, Glu-16
$^2$H: 7$^{50\%}$, 9$^{100\%}$

30 kHz          0          -30
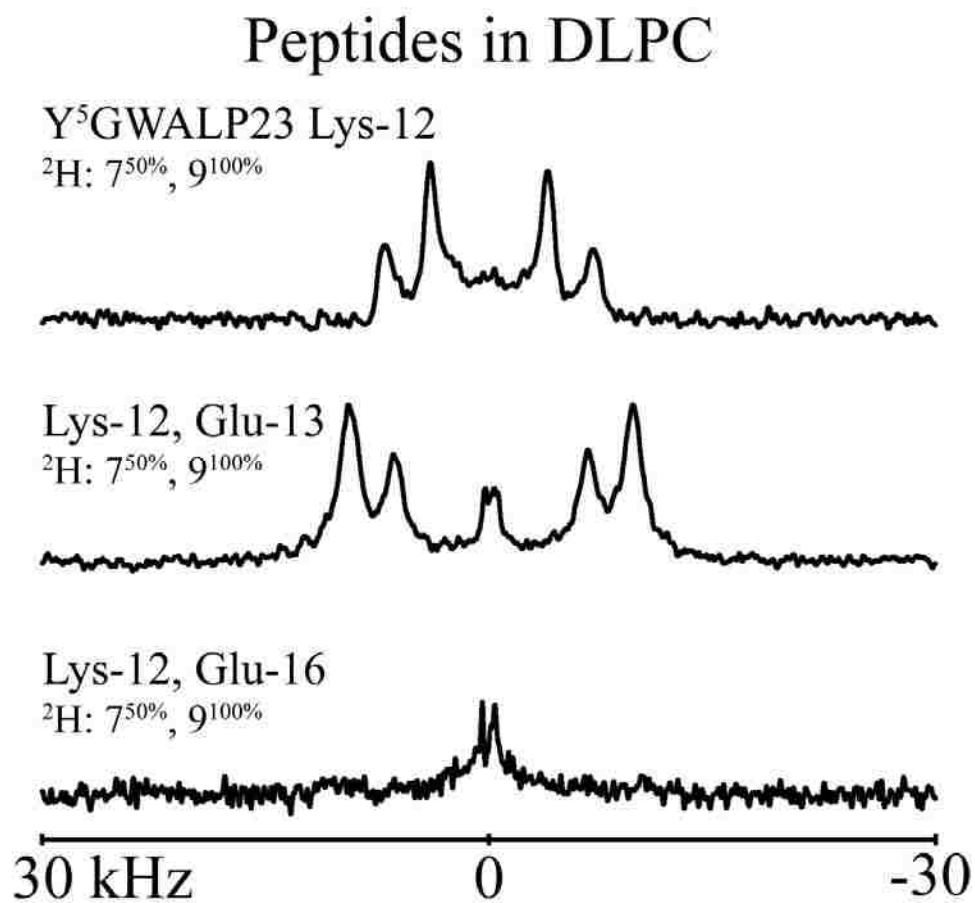
*Figure 4.* $^2$H NMR spectra of Y$^5$GWALP23 Lys-12, Glu-13 with two Ala-d$_4$ labels in DLPC displaying swapping of signal intensity between orientations leading to ambiguity of assignments.



Y$^5$GWALP23 Lys-12, Glu-13 in DLPC

$^2$H: 7$^{50\%}$, 9$^{100\%}$

β = 90°

β = 0°

40 kHz          0          -40
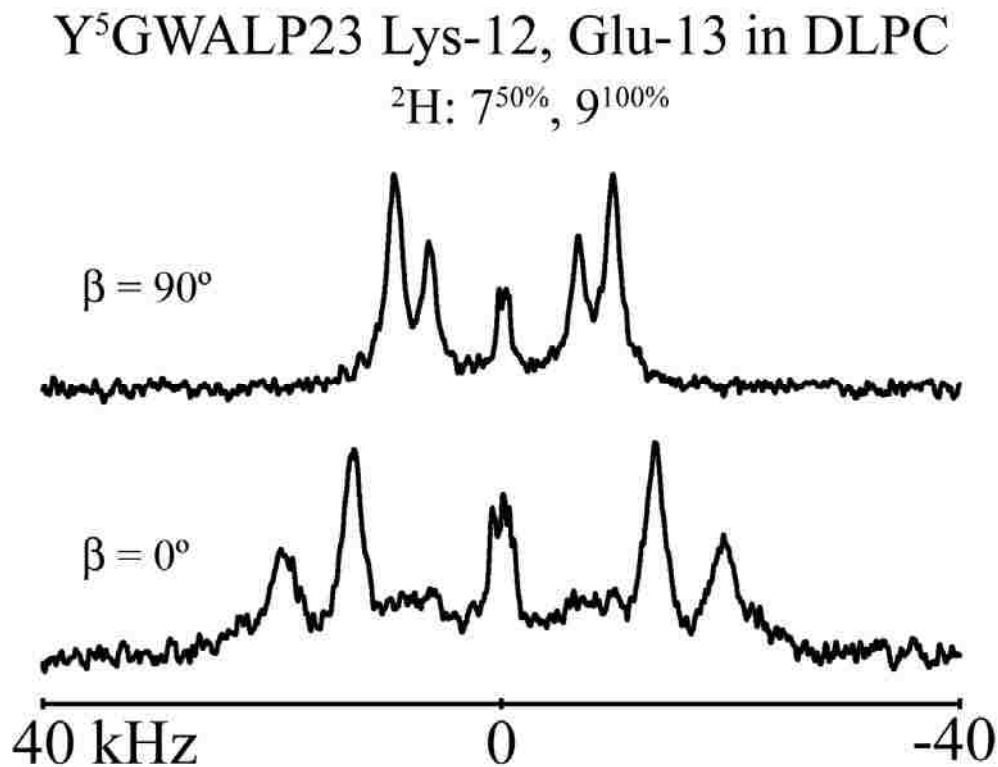
*Figure 5.* Quadrupolar wave plot from Variable-$S_{zz}$ analysis of Y[5]GWALP23 Lys-12, Glu-13 in DLPC[a] and DOPC
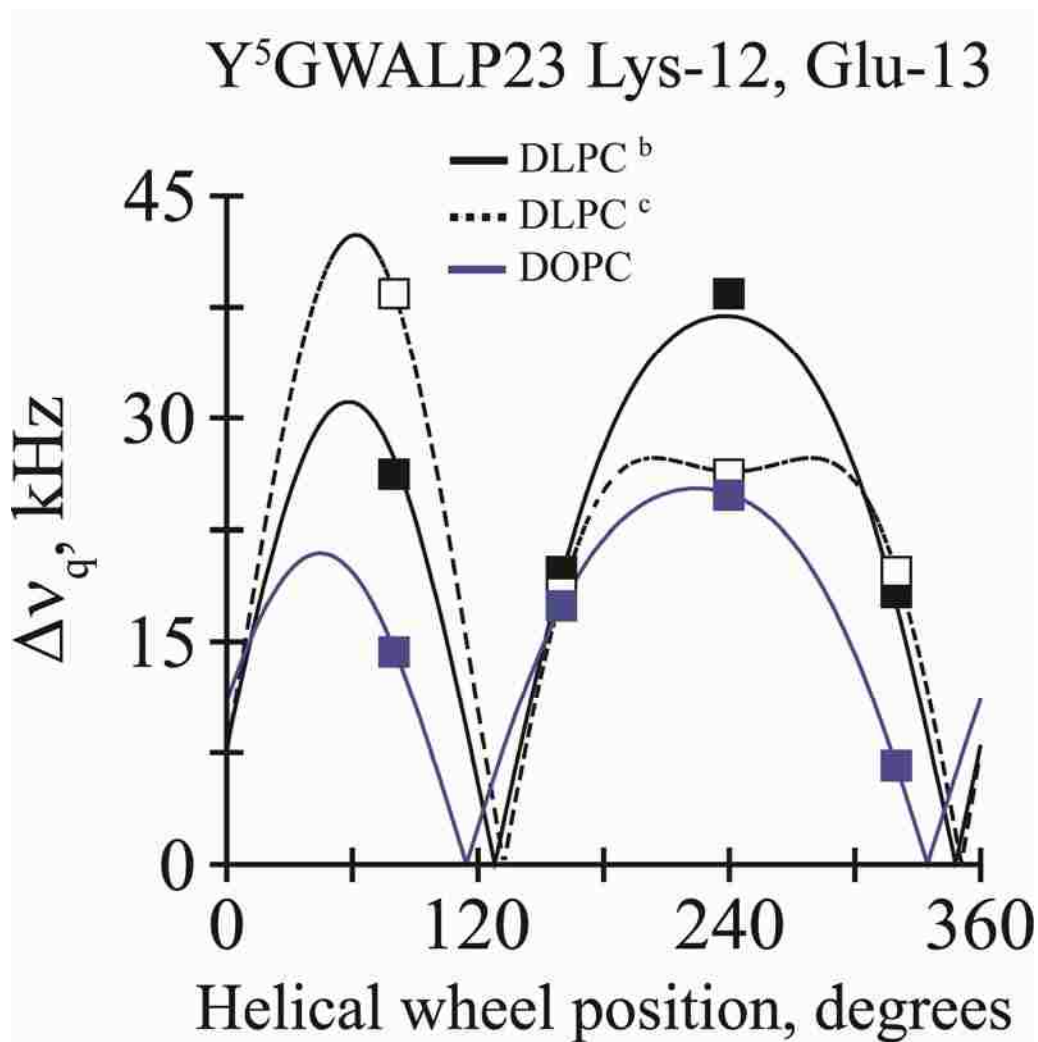
[a] Unable to discriminate Ala-7 and Ala-9 assignments in DLPC, both solutions are shown.

[b] Solution corresponds to $\tau = 19°$, $\rho = 282°$ and $S_{zz} = 1.0$

[c] Solution corresponds to $\tau = 37°$, $\rho = 285°$ and $S_{zz} = 0.65$

*Figure 6.* Quadrupolar wave plot from Variable-$S_{zz}$ analysis of $Y^5$GWALP23 Lys-14, Glu-15 (blue triangles) in DOPC (A) and DLPC (B) compared to $Y^5$GWALP23 Lys-14 (black squares).
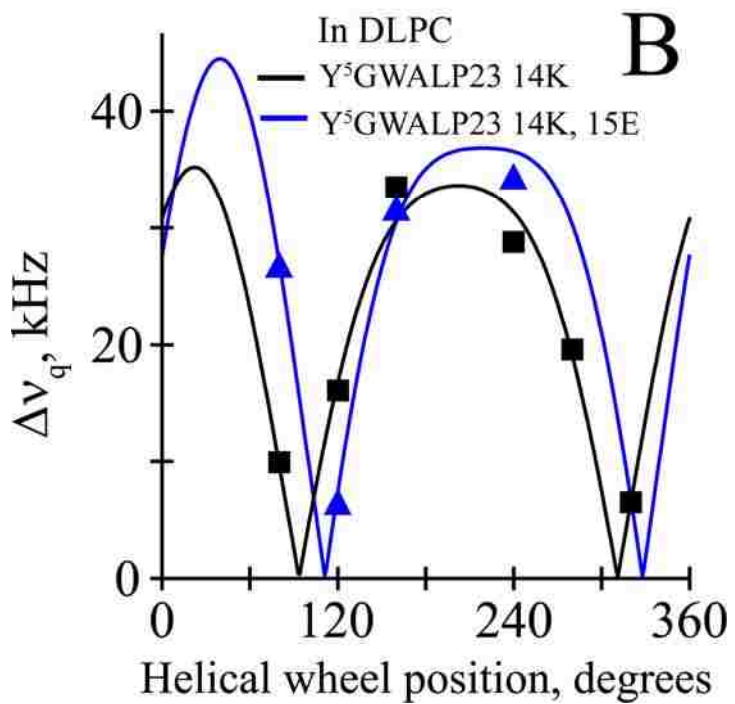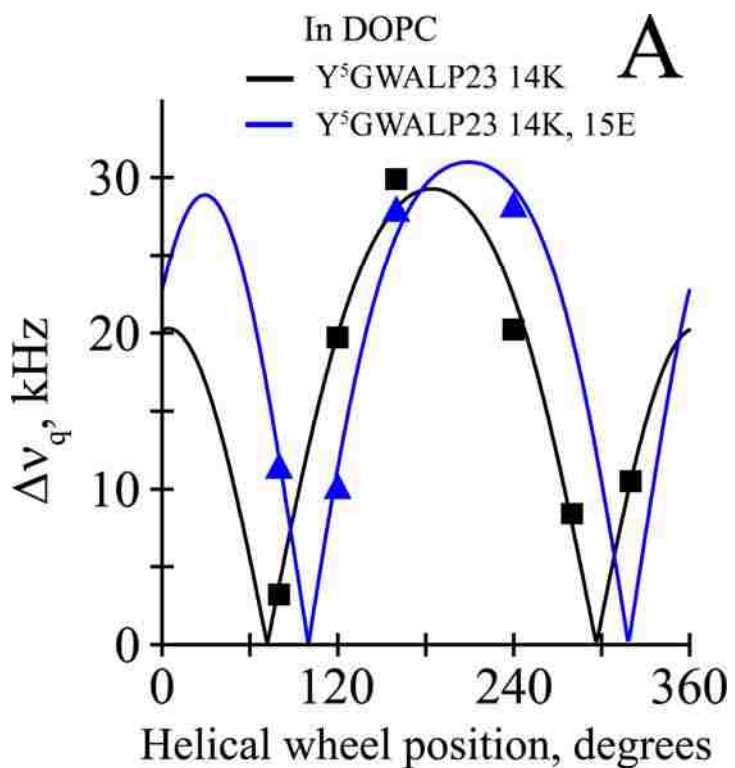
*Figure 7.* $^{2}$H NMR of Y$^{5}$GWALP23 Lys-12/14 with an *i* to (*i* + 1) Glu counter-ion in DOPC at a range of experiment pH values.
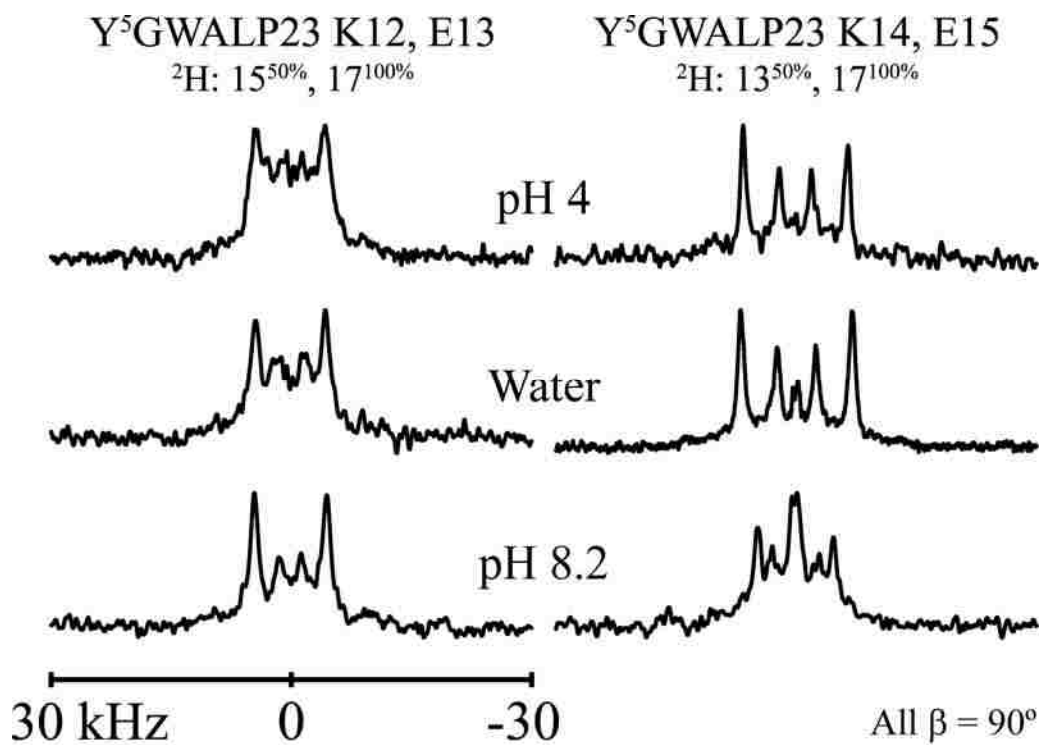
*Figure 8.* $^2$H NMR spectra ($\beta = 90°$ shown) of GWALP23 Arg-12 in DOPC and with an added Glu counter-ion in two locations. Samples prepared at high pH are shown in right column.
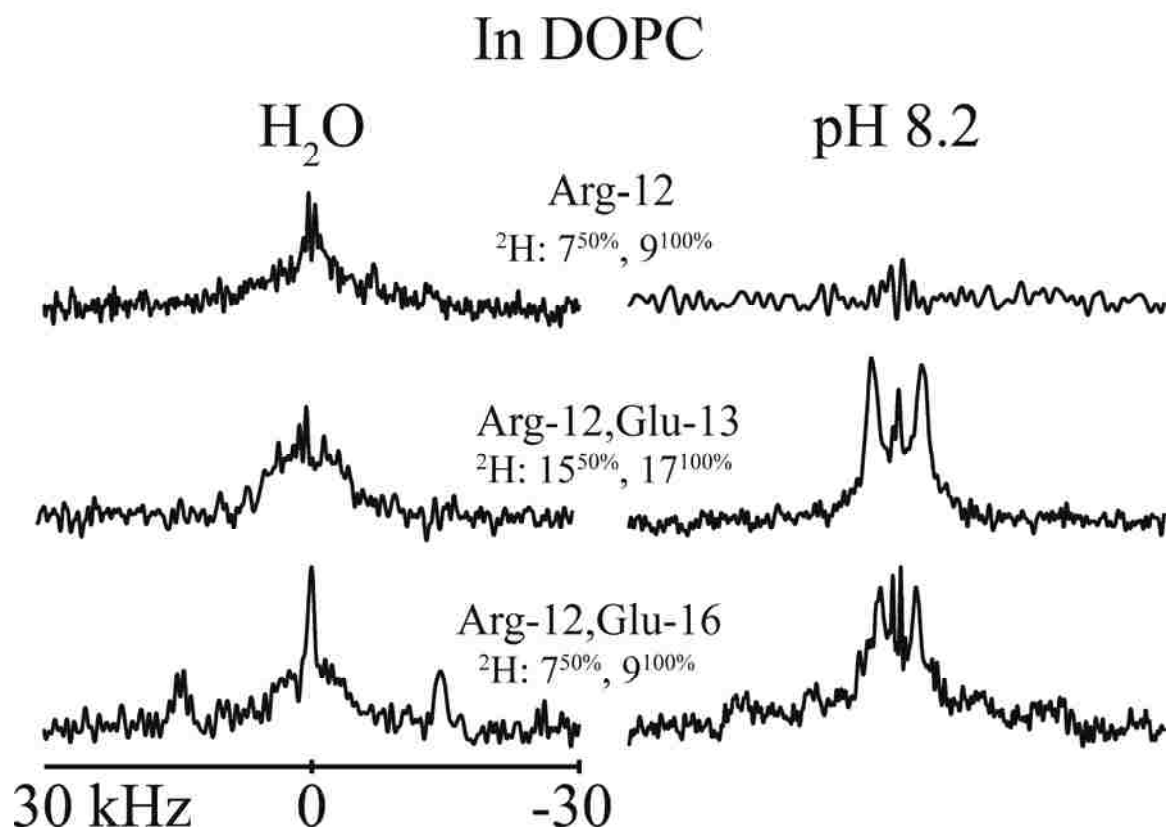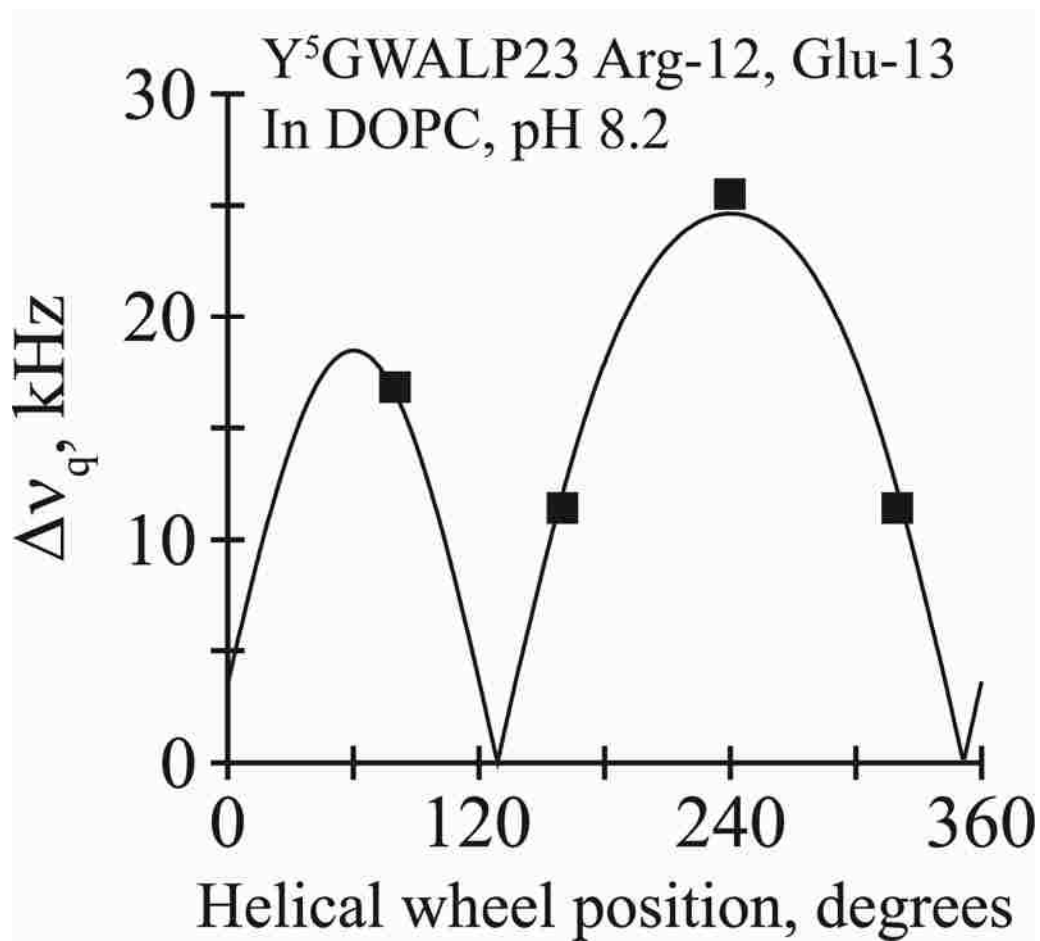
*Figure 9.* Quadrupolar wave plot from Variable-$S_{zz}$ analysis of $Y^5$GWALP23 Arg-12, Glu-13 in DOPC at pH 8.2.

## 5.10 Supporting Information

*Figure S1*. Peptide identity confirmation by MALDI-TOF Mass spectrometry of a $Y^5$GWALP23 Lys-12, Glu-13 peptide with two Ala-d$_4$ labels (50% and 100%).
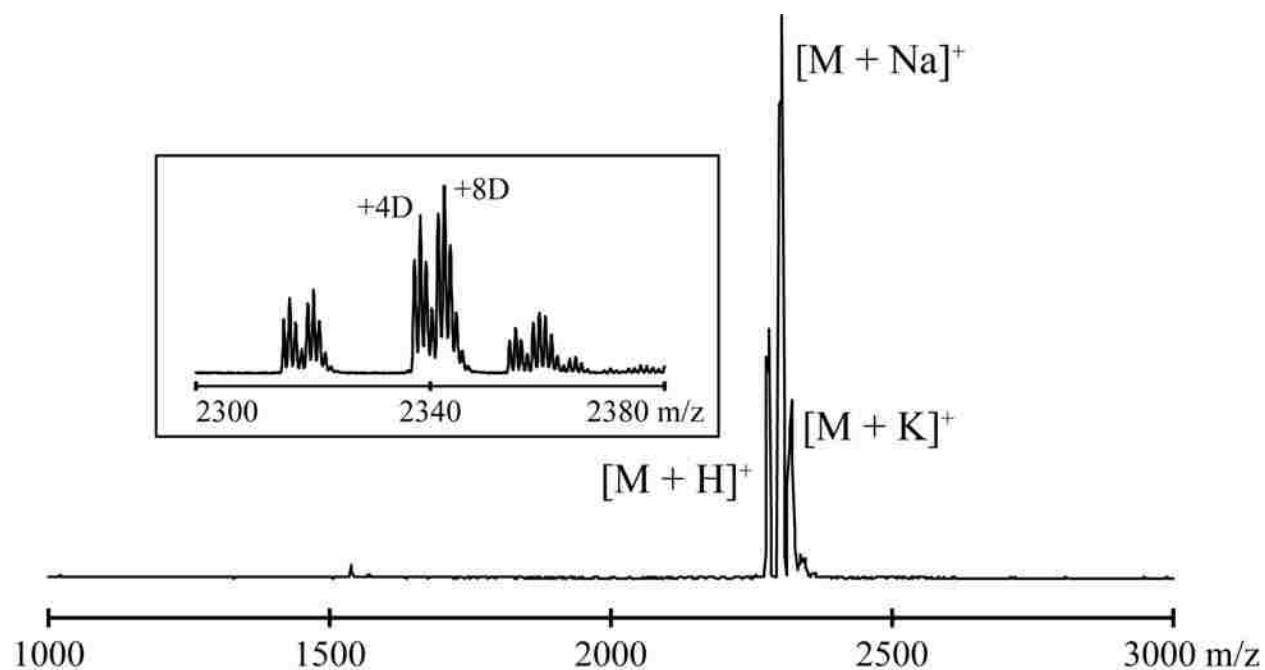
*Figure S2*. RP-HPLC analysis of Y⁵GWALP23 with ion-pairs. Elution time labeled (m:ss). Absorbance detection measured at 280 nm.
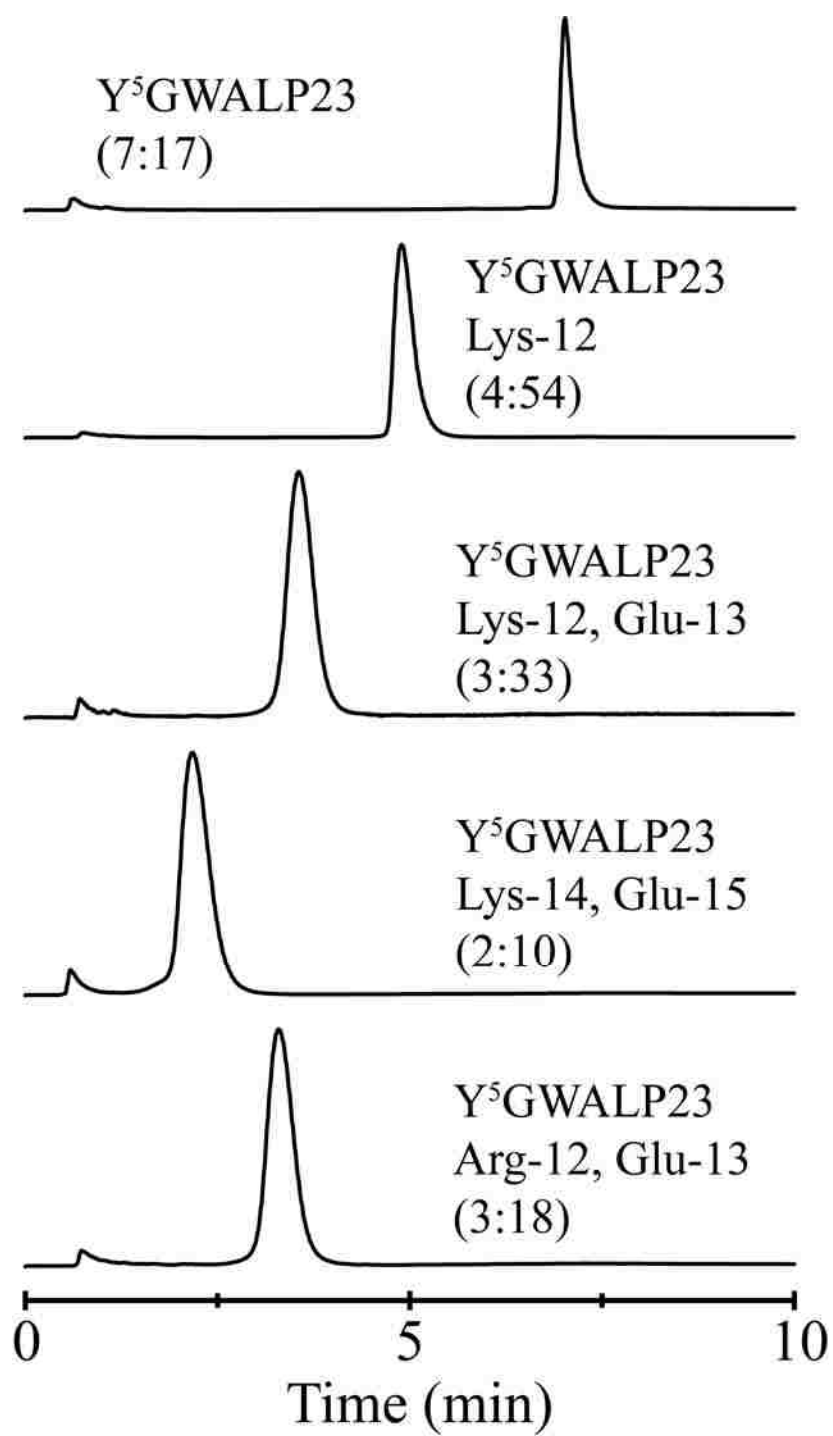
*Figure S3.* $^2$H NMR spectra of Y$^5$GWALP23 Glu-14 and Y$^5$GWALP23 Glu-12 in DLPC.



In DLPC; β = 90°

Y$^5$GWALP23 L14E

$^2$H: 7$^{50\%}$, 9$^{100\%}$

Y$^5$GWALP23 L12E

$^2$H: 7$^{50\%}$, 9$^{100\%}$
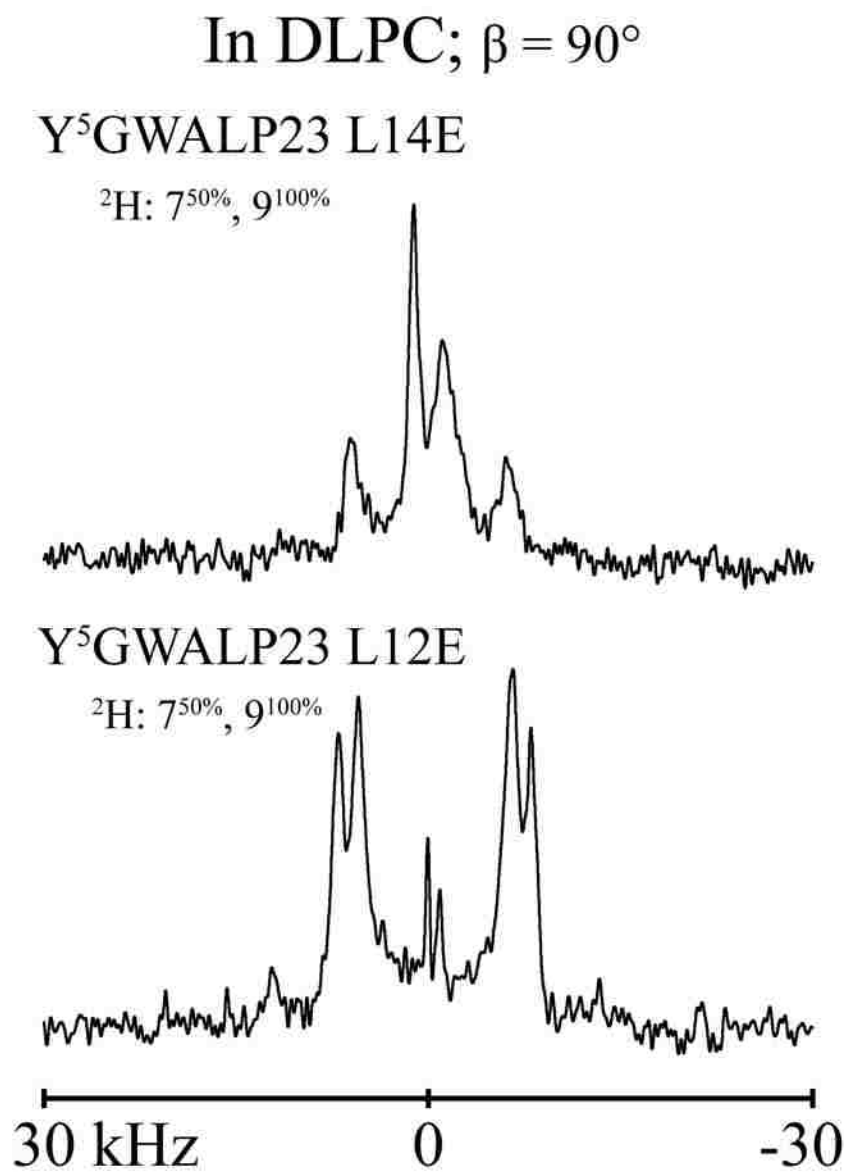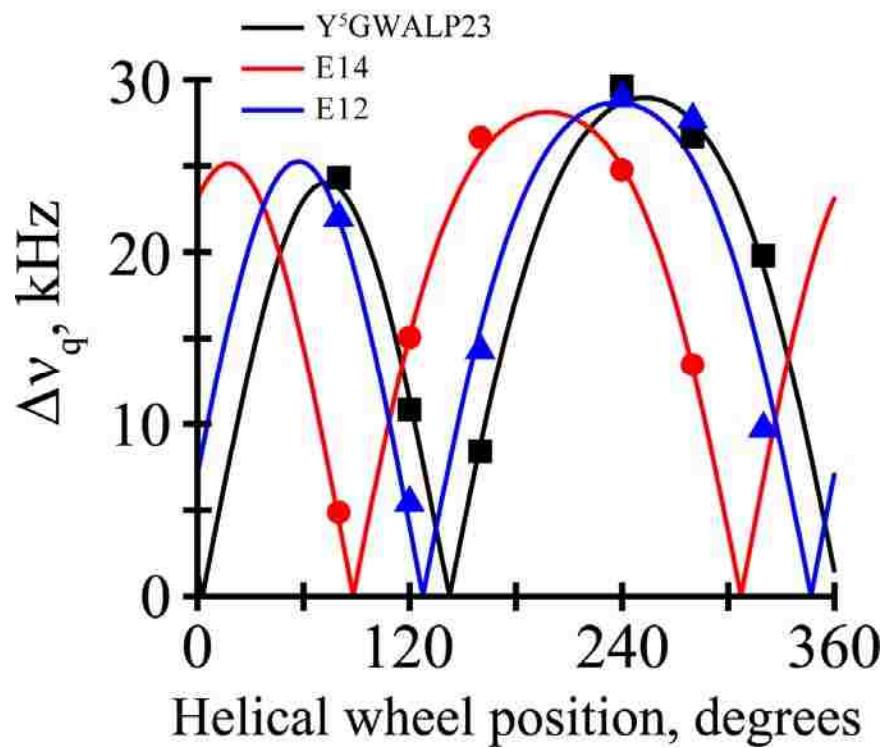
30 kHz      0      -30

*Figure S4.* Variable-S$_{zz}$ analysis of Y$^5$GWALP23 (black squares), L14E (red circles), and L12E (blue triangles) in DLPC.

**CONCLUSIONS**

Through the use of model membrane peptide systems, building off the designed GWALP23, we have characterized a number of important protein-lipid interactions largely through the use of solid-state $^2$H NMR spectroscopy. In membrane proteins, found in a complex heterogeneous lipid bilayer, these governing forces can be hidden at times in the larger protein-lipid system, with a number of protein-lipid as well as protein-protein interactions simultaneously in play. Nevertheless, by limiting the number of forces through model systems and systematically probing certain membrane protein properties, we have revealed some of the significant roles these individual interactions can have. Tryptophan and tyrosine were astonishingly nearly equivalent in their respective anchoring abilities of a transmembrane α-helix in a lipid bilayer, though small dissimilarities were observed (Chapter 2 and 3). GWALP23 and the tyrosine-containing analogues were found to exhibit nearly identical magnitudes of tilt in several lipid bilayers of various membrane thicknesses, as shown by solid-state $^2$H NMR as well as solid-state $^{15}$N NMR experiments. Small, but consistent shifts in the peptide's tilt direction were observed by single tryptophan to tyrosine replacement and were found to be terminally-dependent. Steady-state fluorescence experiments also demonstrated the asymmetric nature of the anchoring residues with the N-terminal anchor being buried further into the bilayer than the C-terminal. Through the use of a newly developed magnetically-oriented bicelle system (Chapter 1), additional orientational constraints were able to be obtained for analysis of model peptides in DLPC bilayers. GWALP23 served most useful as a host for a unique look at lysine buried in a lipid environment (in two locations) where it was observed that it would heavily modify the peptide's orientation in a range of bilayers to facilitate snorkeling of the charged ε-$NH_3^+$ group at position 14 (~ 3 Å from the peptide center) (Chapter 4). However, when lysine

was substituted for L12, corresponding to the center of the peptide, the peptide exhibited multiple low-intensity signals in DOPC that is indicative of multi-state behavior where the hydrophobic peptide appears to be unable to support submerging the highly polar $\varepsilon$-NH$_3^+$ into the bilayer.  In contrast, the Lys-12 peptide was found to incorporate well into DOPC bilayers at high pH when deprotonated, with a small tilt close to that of the host alone over the charged Lys$^+$-14 peptide.  Additionally, the titration of Lys-14 demonstrated a novel system for directly monitoring lysine pK$_a$ depression in the membrane with a $\sim$ 4 unit decrease going from water to DOPC.  The examination of ion-pair interactions illustrated the importance of the ionizable residue's identity and the coordinating counter-ion's placement on an $\alpha$-helix for optimal interaction (Chapter 5).  While an *i* to (*i* + 1) placement of glutamic acid was able to rescue Lys-12 in DOPC to adopt a well-oriented transmembrane configuration, an *i* to (*i* + 4) arrangement did not improve peptide stability in the bilayer and furthermore was detrimental to the peptide's orientation in the shorter DLPC bilayer where it had previously behaved.  Arginine-12 was also seen to be effected by a coordinated placement of glutamic acid at both *i* to (*i* + 1) and *i* to (*i* + 4) with small $^2$H NMR signals of low intensity being observed.  However, titration (migration of quadrupolar splittings) and improvement of the peptides' signal were observed at high pH where the glutamic acid is assumed fully deprotonated allowing a stabilizing ion-pair interaction to occur.  Furthermore, with both lysine and arginine containing peptides, an *i* to (*i* + 1) intra-helix arrangement was seen to improve peptide orientation over the alternative *i* to (*i* + 4) motif.